

# Future Climate Change and Urbanization Impact on Coastal Storm Surge Risk in the Pearl River Delta Region, China

Dissertation

zur Erlangung des Doktorgrades

an der Fakultät für Mathematik, Informatik und Naturwissenschaften

Fachbereich Geowissenschaften

der Universität Hamburg

vorgelegt von

Li Li

aus Heilongjiang, China

Hamburg, 2016

Als Dissertation angenommen vom Fachbereich Geowissenschaften  
der Universität Hamburg auf Grund der Gutachten  
von Prof. Dr. Jürgen Böhner  
und Prof. Dr. Gabriele Gönnert  
Hamburg, den 6. Juli 2016

Prof. Dr. Jürgen Böhner  
Leiter des Fachbereichs Geowissenschaften

## **Eidesstattliche Versicherung**

### **Declaration on oath**

Hiermit erkläre ich an Eides statt, dass ich die vorliegende Dissertationsschrift selbst verfasst und keine anderen als die angegebenen Quellen und Hilfsmittel benutzt habe.

I hereby declare, on oath, that I have written the present dissertation by my own and have not used other than the acknowledged resources and aids.

Li Li, Hamburg, den 27. April 2016

*'Time and tide wait for no man.'*

*David T. Pugh*

*I dedicate this work to my parents, for their constant support and  
unconditional love.*

*I love you all dearly.*

## Abstract

The Pearl River Delta (PRD) is one of the most rapidly developing coastal areas in China. Due to its low-lying topography and frequent typhoon attacks along the coast, coastal inundation by storm surges has become the major risk and the leading cause of death and injury affecting the PRD region. The impacts of climate change on river discharge (peak flows of the Pearl River), typhoon activities and rising sea levels, together with rapid socio-economic development are expected to further exacerbate this risk exposure. However, the internal coastal hydrodynamics and climate variability remain uncertain when it comes to the regional climatology of tropical cyclones with regional patterns. What is the hydrodynamic mechanism in the PRD estuary? How climate change influences the typhoon variability and coastal typhoon induced storm surges in the PRD region? What role does climate change play during the typhoon induced storm surge inundation? To what extent do climate change and urbanization contribute to coastal inundation changes and economic losses by typhoon induced storm surges in fastest-growing economies like the PRD region? The debate around these issues in this research context was explored.

Firstly, in order to explore the hydrodynamic mechanism in the PRD estuary, I applied two unstructured grid numerical hydrodynamic models, ANUGA and D-Flow Flexible Mesh, coupled with the ocean models ROMS and Delft3D WES, respectively. The upstream river discharge, topography, bathymetry and tidal component data were used for simulation. For the D-Flow Flexible Mesh, I have built up the D-Flow FM model for the Pearl River Delta, covering the domain between 15.54 - 23.94°N and 108.95 - 117.07°E. The domain includes the Pearl River distributaries and approximately 100 km of sea area. I simulated the hydrodynamic interaction process in wet and dry seasons in the years 1999, 2002 and 2009. I chose different roughness scenarios as the sensitive tests in order to calibrate the model performance. Afterwards, I compared the ability of two numerical hydrodynamic modelling suites to simulate the hydrodynamic process in the PRD region. Results from the new generation of numerical hydrodynamic model, D-Flow Flexible Mesh, are more encouraging; time series of tidal propagation was well reproduced. I found that temporal hydrodynamic processes distinctly control the upstream discharge distributions in different seasons. Frequent tidal activity during the wet season

increased the sub tidal discharge in the downstream deltaic region as well as the discharge upstream the Pearl River Delta.

Secondly, we investigated the North West Pacific Ocean climate change and its impacts on the extreme events, typhoons induced coastal storm surge risk. We used the new centre celled hydrodynamic numerical model (D-Flow Flexible Mesh) coupling with Wind Enhance Scheme (WES) model to explore how the typhoon induced storm surge influences the coastal region under different climate scenarios. I set up the climate projections according to the new Representative Concentration Pathways (RCP) scenarios, which present the future climate change conditions. The scenarios used were the basic scenario, RCP4.5 and RCP 8.5. The impacts of climate change in this study are supposed in three main factors: by river discharge, typhoons and sea level rise (SLR). I designed nine experiments based on three severe typhoon cases (Utor, Dujuan, Hagupit) under different climate scenarios. The results showed that the river discharges at upstream and downstream increased abundantly with a linear trend in the future climate change. The attributes of typhoon play an important role in affecting the storm tide elevations and coastal inundation under different climate conditions. The middle landfall typhoon reports a positive linear correlation between climate change and the maximum water level as well as the inundation area. The eastern landfall typhoon Utor has a higher risk under RCP 4.5 (0.8%) scenario compared to other scenarios. However, negative response happened under RCP 8.5 scenario. This research expands and improves the knowledge to understand the important mechanisms on the climatology of tropical cyclones in the Pearl River Delta region, and how the typhoon induced storm surge risk might change in the future in response to climate forcing.

Thirdly, a land use based approach was employed in the PRD region to estimate the economic losses of coastal inundation risk under climate change and urbanization scenarios. The peak water level and inundation extent of typhoon Dujuan under different climate scenarios from Chapter 3 were used to demonstrate the impacts of climate change on the coastal region. The land use data of the PRD region from 2000 and 2010 with five categories (urban and rural land, infrastructures, agricultural land, forest and grassland, water areas) was applied for the urbanization scenarios analysis. For each scenario, I calculated the coastal inundation economic losses

induced by typhoon under different climate scenarios using land use based method, absolute stage-damage function, under the Geographic Information System (GIS) environment. The results indicated that the economic losses of inundation area under RCP8.5 reported a 16.8% increase relative to the baseline scenario under the same land use scenario, but different land use categories displayed various changes under different scenarios. Growing urbanization contributed dramatically to economic losses compared to climate change, it made fast coastal growing areas more vulnerable to coastal storm surge risk.

In conclusion, we have developed a series of methodologies in this research, which improves the knowledge of regional climatology of tropical cyclones in the PRD region. The research findings provided support for climate change adaptation measures to the spatial planning, coastal management and protection of the Pearl River Delta region. However, several limitations lied in this research which provides opportunities for further study.



# Contents

Abstract.....	I
Figures.....	I
Tables .....	VII
Abbreviations .....	IX
1 Introduction .....	1
1.1 Problem statement .....	1
1.2 Objective and Research questions.....	3
1.2.1 Objective .....	3
1.2.2 Structure of the research.....	4
2 Numerical modelling of coastal hydrodynamics in the PRD.....	7
2.1 Study Area.....	8
2.2 Materials and methodologies.....	9
2.2.1 Model introduction.....	9
2.2.2 ANUGA Model Configuration .....	11
2.2.3 D-Flow Flexible Mesh Model Configuration.....	14
2.3 Results .....	18
2.3.1 ANUGA Results .....	18
2.3.2 Results of D-Flow Flexible Mesh Simulation .....	19
2.3.3 Discussion.....	24
2.4 Sensitive tests of friction roughness.....	26
2.4.1 Subtidal discharge division in the upstream region .....	27
2.4.2 Tidal propagation at the open sea.....	35
2.4.3 Discussion of sensitive tests .....	39

2.5 Conclusion.....	39
3 The Impacts of Climate Change on Storm Surges and Coastal Inundation in the Pearl River Delta Region.....	41
3.1 Climate Projections .....	41
3.1.1 Climate projections for the entire model settings.....	41
3.1.2 Climate projections for river discharge .....	42
3.1.3 Climate projections for tropical cyclones .....	44
3.1.4 Climate projections for sea level rise.....	46
3.2 Materials and Methodologies.....	47
3.2.1 Mesh Generation.....	47
3.2.2 Topography .....	49
3.2.3 Boundary conditions.....	50
3.3 Results .....	56
3.3.1 The Impacts of climate change on peak water levels at tidal gauge stations .....	57
3.3.2 The impacts of climate change on river discharge .....	62
3.3.3 Inundation extent during different typhoons under different climate scenarios.....	66
3.4 Discussions .....	73
3.4.1 The uncertainties.....	73
3.4.2 The difference of climate change impacts .....	73
3.5 Conclusion.....	92
3.5.1 River Discharge.....	93
3.5.2 Typhoon difference .....	94
3.5.3 Spatial difference .....	95
3.5.4 Outlook.....	95

4 Coastal inundation and economic losses under urbanization and climate change scenarios.....	97
4.1 Materials and Methodologies.....	98
4.1.1 Water level data .....	98
4.1.2 Land use data .....	99
4.1.3 Economic losses calculation .....	101
4.2 Results .....	103
4.2.1 Coastal inundation and economic losses under climate change scenarios .....	103
4.2.2 Coastal inundation and economic losses under urban development scenarios.....	110
4.3 Discussion.....	117
4.3.1 Coastal inundation and economic losses under climate change scenarios .....	118
4.3.2 Coastal inundation and economic losses under urban development scenarios.....	118
4.3.3 Uncertainty.....	119
4.4 Conclusion.....	119
5 Summary and outlook .....	121
5.1 Summary and Conclusion .....	121
5.2 Outlook.....	123
References.....	125
Appendix 1 .....	133
A. Governing Equations in D Flow Flexible Mesh.....	133
B. Brief Introduction of Wind Enhance Scheme (WES) .....	134
C. ANUGA model script examples .....	135
D. D-FLOW FM model set up script examples .....	138

D.1 Dry season of 2002.....	138
D.1.1 mdu file .....	138
C1.2 ext file .....	139
D.2 Typhoon scenarios: baseline scenario of Dujuan .....	141
D2.1 mdu file .....	141
C2.2 ext file .....	143
Appendix 2 About the Author .....	145
Acknowledgements .....	147

## Figures

Fig.1-1 Pearl River Delta (PRD), Research Area.....	1
Fig. 2-1 Map of the Pearl River System .....	9
Fig. 2-2 The flow chart of two modelling sets.....	11
Fig. 2-3 Digital Elevation Model of Pearl River Delta (height, depth, meters) .....	12
Fig. 2-4 Wave Height from ROMS model of Typhoon FANAPI in 2010 .....	13
Fig. 2-5 Mesh of the Pearl River Model .....	14
Fig. 2-6 Topography data of the PRD model .....	15
Fig. 2-7 The model setup and observations of the Pearl River Model .....	16
Fig. 2-8 The evolution in time of an inundation process .....	18
Fig. 2-9 Wave speed map from ANUGA model using SAGA GIS visualization .....	19
Fig. 2-10 The measurement and modeled daily river discharge at Makou station in the wet season of 1999 .....	20
Fig. 2-11 The input discharge (up) and modeled discharge (down) at Gaoyao and Shijiao station in the wet season of 1999.....	21
Fig. 2-12 The measurement and modeled daily discharge at Makou and Pinggang station in the dry season.....	22
Fig. 2-13 The measured and modeled water level at gauge stations in the wet season of 2002 .....	23
Fig. 2-14 The measured and modeled water level at gauge stations in the dry season of 2002.....	24
Fig. 2-15 Cross-section area for discharge calculation.....	25
Fig. 2-16 The modeled river discharge at Gaoyao station in July 1999 under different roughness scenarios .....	28
Fig. 2-17 The modeled river discharge at Shijiao station in August 1999 under different roughness scenarios.....	28
Fig. 2-18 The modeled hourly river discharge at Makou station in July 1999 under different roughness scenarios.....	29

Fig. 2-19 The boundary (up) and modeled river discharge (down) at Gaoyao station in December 1999 under different roughness scenarios .....	30
Fig. 2-20 The modeled river discharge at Gaoyao station in December 1999 under different roughness scenarios.....	31
Fig. 2-21 The boundary (up) and modeled river discharge (down) at Shijiao station in December 1999 under different roughness scenarios .....	32
Fig. 2-22 The modeled river discharge at Shijiao station in December 1999 under different roughness scenarios.....	32
Fig. 2-23 The measured and modeled river discharge at Makou in December 1999 under different roughness scenarios .....	33
Fig. 2-24 The measured and modeled hourly river discharge at Makou station in December 1999 under different roughness scenarios .....	33
Fig. 2-25 The measured and modeled hourly river discharge at Pinggang station in December 2009 under different roughness scenarios .....	34
Fig. 2-26 The measured and modeled daily river discharge at Pinggang station in December 2009 under different roughness scenarios .....	34
Fig. 2-27 The measured and modeled water level at the Shek Pik station in June 2002 under different roughness scenarios.....	35
Fig. 2-28 The measured and hourly modeled water level at the Quarry Bay station from August to September in 2002 under different roughness scenarios .....	36
Fig. 2-29 The measured and modeled water level at Kat_O station in October 2002 under different roughness scenarios .....	37
Fig. 2-30 The measured and modeled water level at Quarry Bay station from January to February in 2002 under different roughness scenarios.....	38
Fig. 2-31 The measured and daily modeled water level at Waglan station from January to February in 2002 under different roughness scenarios.....	38
Fig. 2-32 The measured and hourly modeled water level at the Shek Pik station from November to December in 2002 under different roughness scenarios .....	39
Fig. 3-1 Global average surface temperature change from 2006 to 2100 relative to 1986–2005 (IPCC, 2014).....	42
Fig. 3-2 Frequencies of typhoon in the PRD region after 1970.....	45

Fig. 3-3 Intensity changes of typhoon in the PRD region from 2001 to 2013.....	45
Fig. 3-4 D-FLOW FM model mesh network visualization from Google Earth in different scales .....	49
Fig. 3-5 The differences between DTM and DSM model .....	50
Fig. 3-6 Track of Utor: 1 - 8 July 2001 .....	52
Fig. 3-7 Track of Utor near Hong Kong.....	52
Fig. 3-8 Track of Dujuan: 29 August – 3 September 2003.....	54
Fig. 3-9 Track of Dujuan near Hong Kong.....	54
Fig. 3-10 Track of Hagupit on 19 – 25 September 2008.....	55
Fig. 3-11 Track of Hagupit near Hong Kong .....	55
Fig. 3-12 Location of all of the observation stations.....	57
Fig. 3-13 Simulated water level changes and peaks at gauge stations (Kat_O, Shek Pik, Waglan and Quarry Bay) during Dujuan under S0, RCP4.5 and RCP8.5.....	59
Fig. 3-14 Simulated water level changes and peaks at gauge stations (Kat_O, Shek Pik, Waglan and Quarry Bay) during Utor under S0, RCP4.5 and RCP8.5 .....	61
Fig. 3-15 Simulated water level changes and peaks at gauge stations (Kat_O, Shek Pik, Waglan and Quarry Bay) during Hagupit under S0, RCP4.5 and RCP8.....	62
Fig. 3-16 The hourly and daily river discharge during Dujuan at Makou station .....	64
Fig. 3-17 The hourly and daily river discharge during Dujuan at Pinggang station ...	64
Fig. 3-18 The hourly and daily river discharge during Utor at Makou station .....	64
Fig. 3-19 The hourly and daily river discharge during Utor at Pinggang station.....	65
Fig. 3-20 The hourly and daily river discharge during Hagupit at Makou station .....	65
Fig. 3-21 The hourly and daily river discharge during Hagupit at Pinggang station..	65
Fig. 3-22 Coastal inundation map during Dujuan under baseline scenario (S0) .....	67
Fig. 3-23 Coastal inundation map during Dujuan under RCP4.5 (S1) .....	67
Fig. 3-24 Coastal inundation map during Dujuan under RCP8.5 (S2) .....	68

Fig. 3-25 Coastal inundation map during Utor under baseline scenario S0 .....	69
Fig. 3-26 Coastal inundation map during Utor under RCP 4.5 (S1).....	69
Fig. 3-27 Coastal inundation map during Utor under RCP8.5 (S2).....	70
Fig. 3-28 Coastal inundation map during Hagupit under baseline scenario S0 .....	71
Fig. 3-29 Coastal inundation map during Hagupit under RCP4.5 (S1) .....	72
Fig. 3-30 Coastal inundation map during Hagupit under RCP8.5 (S2) .....	72
Fig.3-31 Wind speed at all of the gauge stations during Dujan under S0, RCP4.5 (S1) and RCP8.5 (S2).....	75
Fig. 3-32 Wind speed at all of the gauge stations during Utor under S0, RCP4.5 (S1) and RCP8.5 (S2) .....	76
Fig. 3-33 Wind speed at all gauge stations during Hagupit under S0, RCP4.5 (S1) and RCP8.5 (S2) .....	77
Fig. 3-34 Influence of the relative wind velocity on surges and water levels.....	78
Fig. 3-35 Influence of landfall locations on surges and wind set up in the semi-enclosed basins (Stoeten, 2013) .....	79
Fig. 3-36 Influence of inverted barometer effect on surges .....	80
Fig. 3-37 Air pressure at Kat_O station under baseline scenario S0, RCP4.5 (S1) and RCP8.5 (S2) .....	81
Fig. 3-38 Spatial distribution of atmosphere and wind speed during Dujan under S0 .....	82
Fig. 3-39 Spatial distribution of atmosphere and wind speed during Dujan under RCP4.5 (S1) .....	83
Fig. 3-40 Spatial distribution of atmosphere and wind speed during Dujan under RCP8.5 (S2) .....	84
Fig. 3-41 Spatial distribution of atmosphere and wind speed during Utor under S0 .	86
Fig. 3-42 Spatial distribution of atmosphere and wind speed during Utor under RCP4.5 (S1) .....	87
Fig. 3.-43 Spatial distribution of atmosphere and wind speed during Utor under RCP8.5 (S2) .....	88

Fig. 3-44 Air pressure at four gauge stations during Hagupit under S0, RCP4.5 (S1) and RCP8.5 (S2) .....	89
Fig. 3-45 Spatial distribution of atmosphere and wind speed during Hagupit under S0 .....	90
Fig. 3-46 Spatial distribution of atmosphere and wind speed during Hagupit under RCP4.5 (S1) .....	91
Fig. 3-47 Spatial distribution of atmosphere and wind speed during Hagupit under RCP8.5 (S2) .....	92
Fig. 4-1 Land use data in the year of 2000 (up) and 2010 (down) .....	100
Fig. 4-2 Land use area changes in the different categories from 2000 to 2010 .....	100
Fig. 4-3 Coastal inundation under the baseline scenario (S0) of the land use scenario 2000.....	103
Fig 4-4 Coastal inundation under RCP4.5 (S1) of the land use scenario 2000.....	104
Fig 4-5 Coastal inundation under RCP8.5 (S2) of the land use scenario 2000.....	104
Fig. 4-6 Urban region inundation area under different climate scenarios .....	105
Fig. 4-7 Forest and Grassland inundation area under different climate scenarios..	106
Fig. 4-8 Agricultural (Farmland) inundation area under different climate scenarios	107
Fig. 4-9 Inundated water areas under different climate scenarios .....	108
Fig. 4-10 The whole inundation area in the PRD under different climate scenarios	109
Fig. 4-11 Economic losses of coastal inundation under different climate scenarios	110
Fig. 4-12 Coastal inundation under the baseline scenario (S0) of the land use scenario 2000 .....	111
Fig. 4-13 Coastal inundation under the baseline scenario (S0) of the land use scenario 2010 .....	111
Fig. 4-14 Urban region inundation area under different land use scenarios .....	112
Fig. 4-15 Forest and grassland inundation area under different land use scenarios .....	113

Fig. 4-16 Agricultural (Farmland) inundation area under different land use scenarios ..... 114

Fig. 4-17 Inundated water areas under different land use scenarios ..... 115

Fig 4-18 The total inundation area of the land use in 2000 and 2010 ..... 116

Fig. 4-19 Economic losses of coastal inundation under different land use scenarios ..... 117

## Tables

Table 2-1 Timeline of the observation data and simulation .....	17
Table 2-2 Variation ratio of river discharge in the dry season at Makou and Sanshui (1956 -2006) .....	20
Table 3-1 Times and heights of the maximum sea level at tide stations during Dujuan .....	53
Table 3-2 Experiments under different climate scenarios .....	56
Table 4-1 Land use area per category in the year of 2000 and 2010 .....	100
Table 4-2 GDP in the PRD region in the year of 2000 and 2010 .....	101
Table 4-3 The economic value of each land use category.....	102
Table 4-4 The economic value (A) and (B) in the year of 2000 and 2010 .....	102
Table 4-5 Urban region inundation area under different climate scenarios .....	105
Table 4-6 Forest and Grassland inundation area under different climate scenarios	106
Table 4-7 Agricultural (Farmland) inundation area under different climate scenarios .....	107
Table 4-8 Inundated water areas under different climate scenarios .....	107
Table 4-9 The whole inundation area in the PRD under different climate scenarios	108
Table 4-10 Economic losses of coastal inundation under different climate scenarios .....	110
Table 4-11 Urban region inundation area under different land use scenarios .....	112
Table 4-12 Forest and grassland inundation area under different land use scenarios .....	113
Table 4-13 Agriculture (Farmland) inundation area under different land use scenarios .....	114
Table 4-14 Inundated water areas under different land use scenarios .....	114
Table 4-15 The total inundation area in the land use of 2000 and 2010 .....	115

Table 4-16 Economic losses of coastal inundation under different land use scenarios ..... 116

## Abbreviations

ANUGA	Australian National University and the Geoscience Australia
D-FLOW FM	D-Flow Flexible Mesh
D3D	Delft3D Flow model
DEM	Digital Elevation Model
DTM	Digital Terrain Model
GDP	Gross domestic product
mph	miles per hour
pdrop	pressure drops, air pressure minus standard air pressure
PRD	Pearl River Delta
PRE	Pearl River Estuary
PRD model	D-FLOW FM numerical hydrodynamic model of the Pearl River Delta
RCP	Representative Concentration Pathways
ROMS	Regional Ocean Modeling System
SAGA GIS	SAGA Geographic Information System
SLR	Sea Level Rise
WES	Delft3D Wind Enhance Scheme for cyclone modelling



# 1 Introduction

## 1.1 Problem statement

The Pearl River Delta (PRD), is located at the northern reach of the South China Sea (SCS), is one of the most rapidly developed and densely populated regions in China (Fig.1). After 20 years of accelerated economic and infrastructural development, the PRD region creates about 10% of Chinese gross domestic products and gathers 3% of the national population in an area which shares only 0.4% of the total states territory of the PR-China (FAN, ET AL. 2005; DU D.S., ET AL. 2010). Due to its low-lying topography and frequent typhoon attacks along its coast, coastal inundation from typhoon induced storm surges cause a severe loss of human life and infrastructural values every year in the PRD region. Changes in the Pearl River discharge (peak flows of the Pearl River), typhoon activities and sea level due to climate change, together with rapid socio economic development are expected further exacerbate this risk exposure.



Fig.1-1 Pearl River Delta (PRD), Research Area

There are some researches on the impacts of climate change on the Pearl River discharge (Liu et al., 2012; Zhang et al., 2008; Guan, 2010; Wu et al., 2014; Dan Yan

et al., 2015) and the sea level rising along the PRD coastal region (Chen, 1997; IPCC, 2007). Many researchers summarized the typhoon characteristic over the last 50 years to state the relationship between climate change and typhoon activities (Chang et al., 2008; Chao et al., 2012; Xiaoli Ding et al., 2004; ZHENGUO HUANG et al., 2004). However, when exploring the impacts of climate change on typhoon-induced storm surges and coastal inundation risk, the study to consider all of the three aspects together (river discharge, typhoon activities and sea level rise) as climate change scenarios hasn't conducted yet in the PRD region. Climate change is various on a global scale and regional scale, when it comes to spectacular low latitude region with the rapid urbanization, which factor will make the coastal region more vulnerable are not yet clear. Therefore, we should think about urbanization for a particular region before considering climate change. The typhoon-induced storm surges and coastal inundation risks in the PRD region need to be quantified under different climate change scenarios for providing sufficient information for coastal planners and decision makers.

At the same time, urbanization also plays an important role in increasing the storm surge induced coastal inundation risk worldwide. However, the research on quantifying the coastal inundation losses in the PRD region is very rare. From the city research scale, some researchers (Hao Zhang and Xiang-rong Wang, 2015) analysis the land use changes during rapidly urbanizing Foshan City of the PRD region using the Landsat TM and ETM+ imagery (1988-2003), and qualitative analysis the linkage between land use change and historical flood risk. Some researchers (Feng Liu et al., 2014) focus on the diverse human activities impacts on the hydrological responses such like river discharge, sediment concentration in the PRD region. Liang Yang (2015) investigated the Pearl River flood risk from both climate and urban responses point of view. He built an indicator system (15 indicators) to quantify the human activities impacts on flood vulnerability. Kang Lei et al. (2015) predicted the farmland losses due to the sea level rise and storm surge in the PRD region under the future climate change scenarios in 2030, 2050 and 2100, however, the impacts of land use change, the wind is not considered. The land used based flood risk assessment is already deeply explored in different scales in Europe. After reviewing the related researches, we could found that this is still a huge gap in China and in regional scale

like the PRD region. Therefore it is necessary to build up a quantitative methodology which fits China situation to analysis the urbanization response on coastal inundation risk.

Therefore, in rapidly developed areas such as the PRD region, climate change and urbanization, which one we should pay more attention from sustainable urban development perspectives? To what extent do the climate change and urbanization contribute to the coastal inundation changes and economic losses by typhoons? We need detailed information and improved methodologies for understanding the coastal inundation risk from typhoon induced storm surges in the PRD region.

## **1.2 Objective and Research questions**

### **1.2.1 Objective**

The objective of this research is to develop the methodologies mainly using the new generation of numerical hydrodynamic models, to understand the typhoon induced coastal storm surges and inundation risk in the PRD region under the impacts of climate change and urbanization. The results would facilitate the decision-making for sustainable urban development and climate change adaption.

In order to achieve the above objective, this study will answer the following research questions,

1. How the new generation of numerical hydrodynamic models works in the PRD region? How do the geographic data work under the new generation of hydrodynamic model using the GIS (Geographic Information System) tool? What are advantages and limitations of the applied methodologies and which aspects of improvements can be identified for future research?
2. How will future climate change affect coastal storm surge risks in the PRD region? What is the climatology of tropical cyclones in this region? Do the results contribute to the understanding of present and future coastal storm surge risks in the PRD region?
3. How will growing urbanization affect coastal storm surge inundation and economic losses in the PRD region? Compared to the impacts of climate change, which one will

be the main factor affecting coastal storm surge risks in the PRD region?

### **1.2.2 Structure of the research**

This research falls naturally into the following parts:

Chapter 1: a general introduction of the research

Chapter 2: Numerical modelling of the coastal hydrodynamics in the PRD

Chapter 3: The impacts of climate change on storm surges and coastal inundation in the Pearl River Delta region

Chapter 4: Coastal inundation and economic losses under urbanization and climate change scenarios

Chapter 5: Summary and outlook

The details of content are,

Chapter 1 is the general introduction of the research, including the problem statement, objective, research questions and brief introduction of each part of the content.

Chapter 2 is to apply different numerical hydrodynamic models for simulating the hydrodynamic process in the PRD. We examined the suitability of two unstructured grid numerical hydrodynamic models ANUGA (Australian National University and the Geoscience Australia) and D-Flow Flexible Mesh, and evaluated the D-FLOW FM model based on the sensitive test of different friction values. There are advantages of the D-FLOW FM model, the new generation of numerical hydrodynamic model, in simulating regions with complicated coastlines and this model is also more friendly for the land use mesh generation (used later in Chapter 3). This chapter is the basic numerical modelling part for the further simulation under different climate change scenarios in Chapter 3.

In Chapter 3, we combined theoretical and modelling studies to explore the potential impacts of future climate change on coastal typhoon induced storm surge and coastal inundation in the PRD region. The impacts of climate change were supposed in three

main factors in this research: by the river discharge, typhoons and sea level rise. Against this background, a typhoon induced storm surge simulation system was built for the PRD region. The system includes a typhoon model (Delft3D WES model) for generating the typhoon wind and pressure fields and a 2D numerical hydrodynamic model (DFLOW flexible mesh) for simulating the associated storm surge. Three typhoon cases in different landfall locations were used as the base cases in the storm surge simulation system. According to river discharge and typhoon intensity and sea level rise, different climate scenarios were set up for the modelling.

In Chapter 4 presented an estimation of the PRD regional economic exposure to coastal inundation risk under urbanization and climate change scenarios. The land use based method is used for impacts of urbanization on the PRD regional economic exposure to coastal inundation risk. The climate change scenarios based analysis is subject to typhoon case Dujuan from Chapter 3. Afterwards, we compared two results for damage estimation and found the different roles of urbanization and climate change in coastal inundation economic losses caused by typhoon in the PRD region. Finally, we can conclude the main threaten in this region when we make sustainable regional planning and coastal protection.

Chapter 5 is the summary and outlook of this research.



## **2 Numerical modelling of coastal hydrodynamics in the PRD**

This chapter built up the modelling chains for simulating the hydrodynamics in the PRD. The Pearl River is one of the most complicated river networks in the worldwide. The hydrodynamics are also complex due to the interaction between the multi-channel river upstream discharge and the tidal currents from the open sea. The upstream river runoff is discharged into the estuary by distributing its volume transport through eight river outlets. Due to nonlinear interaction between the river and the estuary, the freshwater discharge at the river outlet is a complex function of the upstream inflow, tides, and estuarine circulation as well as the structure of the river network.

A number of theoretical and numerical modelling studies have been conducted to examine the hydrodynamics in the PRE and adjacent coastal regions (Jiatang Hu et al. 2011; Chunyan Li, 2013; Lai, Z. et al., 2014; L. A. Wong et al., 2003). However, when it comes to the storm surge and coastal inundation impact studies, the complex hydrodynamic processes in the PRD are often ignored by previous studies, which will lead huge difference on the results accuracy. For example, either they mainly focused on the river discharge perspectives for flash flooding inundation risk assessment (Liu et al., 2012, Zhang et al., 2008) based on the tools like Geographic Information System or engineering measures (Zhang et al., 2013), or solely focused on the tidal wave propagation influence on the storm surge studies (Dronkers, 2005; Hunt, 1964; Godin, 1988; Prandle and Rahman, 1980; Jay, 1991; Friedrichs and Aubrey, 1994; Lanzoni and Seminara, 1998; Savenije, 2005).

As we can see in previous studies, the Pearl River is either simplified as several single-cell-wide straight channels or simply removed by specifying the inflow conditions at the locations of the river outlets. The river hydrodynamics in the estuary may include physical processes that are often ignored by previous studies of coastal tide influence. Particularly, in a tidal river-estuary system, the river plays an important role in energy and mass balances by storage of tidal water during the flood tide and persistent dissipation of tidal energy. Moreover, the multichannel river network in the Pearl River Estuary will produce more complex hydrodynamics with the differential

interaction of individual river channels. The physical factors include river discharge, bathymetry, tides, wind stress, and turbulent mixing (Lai, Z. et al., 2015).

Therefore, in order to explore the storm surges and coastal inundation further in this research, to understand hydrodynamic processes in the PRD is necessary and basic. Against this background, we aim to explore the relationship between the river discharge and typhoon tidal propagation employing different modelling suites. As traditional rectangular grids feature limited skill in adequately representing the complicated estuarine system, we applied the unstructured grid new generation modelling suites to simulate the delicate interaction between the marine system and complex estuaries network.

## **2.1 Study Area**

In the PRD, three main tributaries of the Pearl River (Western, Northern and Eastern), forming a complex network of estuaries, drain to the South China Sea at eight outlets (Yamen, Hutiaomen, Jitimen, and Modaomen, Hengmen, Hongqimen, Jiaomen, and Humen) (Fig.2-1). The Pearl River discharge in the wet season from April to September accounts for 80% of the annual total discharge and only 20% occurring in the dry season from October to March. Therefore the hydrological regime of the Pearl River is dominated by the East-Asian monsoon, which implying strong seasonal controls of discharge dynamics (Geertsema, 2013; Zhao, 1990).

The Pearl River Estuary includes three shoals (West Shoal, Middle Shoal, and East Shoal) and two deep longitudinal channels (West Channel and East Channel). The averaged depth of the Pearl River Estuary is only 5 m, with the bathymetry with more than 70 m in the open sea. To the north and west of the Pearl River Estuary is a delta, where river runoff from the Pearl River. The key physical processes of the Pearl River Estuary are mainly tides, river discharge, and winds. The mean tidal range is 1.0 m outside the mouth of the estuary and increases to 1.7 m in the upstream region. The mean residual current is counterclockwise with a stronger flood tidal flow on the east side of the estuary and a stronger ebb tidal flow on the west side of the estuary (Mao et al., 2004). The wind in this region is seasonally reversed with the northeasterly monsoon in winter and the southwesterly monsoon in summer. The outflow of the Pearl River forms multiple shallow, buoyant freshwater plumes, which have a direct

influence on the estuarine circulation and coastal ecological environment in the Pearl River Estuary and adjacent coastal area (Harrison et al., 2008).

The low topography, the remarkable increase of river discharge in the wet season, together with the typhoon influence makes the PRD highly vulnerable to storm surges and coastal inundation.

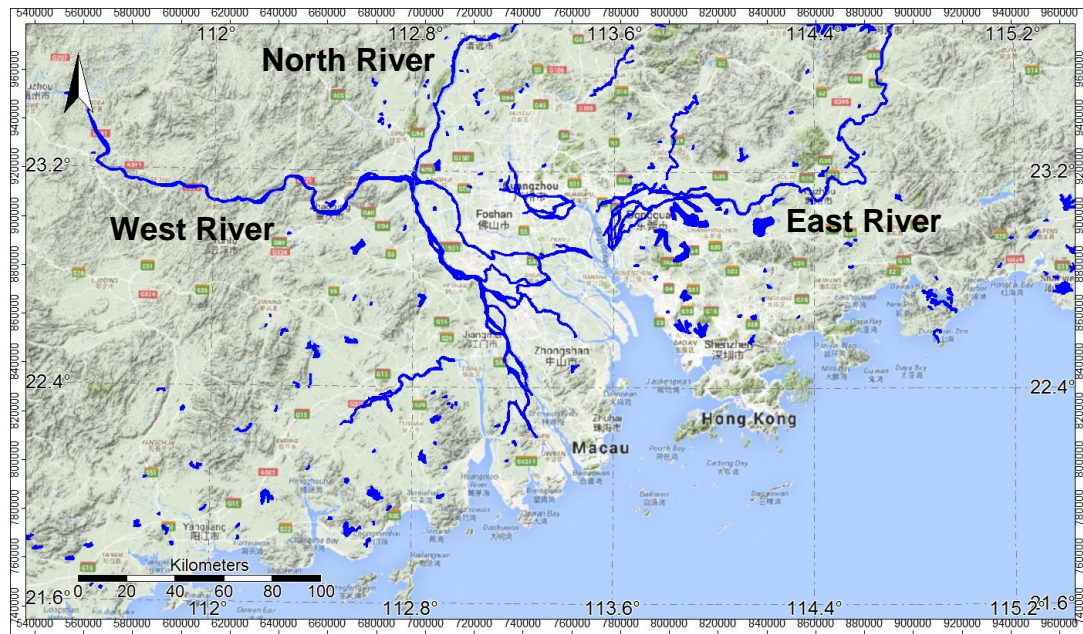


Fig. 2-1 Map of the Pearl River System

## 2.2 Materials and methodologies

### 2.2.1 Model introduction

In order to simulate both the river discharge and tidal propagation, we use hydrodynamic modelling suites, which simulates the river discharge in a traditional way but employ in addition the ocean component to accurately compute their storm surge boundary conditions, such as, wind forcing etc. These hydrodynamic modelling suites are ANUGA (Australian National University and the Geoscience Australia) and D-Flow Flexible Mesh, in which ANUGA is coupled with the ocean models of ROMS (Regional Ocean Modeling System). Though these modelling suites have been successfully applied over several regions in the world, these suites have not yet been applied in the PRD.

## ***ANUGA and ROMS***

The AUNGA is a finite volume hydrodynamic model with the unstructured grid, developed by the Australian National University and the Geoscience Australia. The model is well adapted to providing a robust solution to not only the ocean Inundation but also to the riverine flooding as well as the combination of both or the raised water levels (R. Van Drie., 2008). In contrast to the regular structured grid, the model employs a spatially varying triangular mesh, which is quite fit for discretization of interest area to simulate the inundation scope (when flooding brought by storm surge or tsunami enters and leaves an area). The AUNGA needs a separate ocean model to compute the forcing conditions for storm surge induced flooding since it cannot generate such forcing conditions by itself. For this purpose, an ocean model called ROMS (Regional Ocean Model System), developed at the Rutgers University, University of California Los Angeles, is coupled with the ANUGA model for the computation of boundary conditions.

The AUNGA model has successfully been applied in various parts of the world. For example, the model has been validated for the 1993 tsunami on Okushiri Island off Japan, for the wave tank tests at the University of Queensland (Baldock 2007), and the Tsunami run-up and inundation in the near field of Padang, West Sumatra (Schlurmann et al., 2010). In addition, ANUGA is applied for the accuracy and robustness assessment of the finite volume implementation for handling wet/dry and sub/supercritical flow transitions (Van Drie R et al., 2010).

## ***D-Flow Flexible Mesh***

The D-Flow Flexible Mesh is a new cell-centered 2D finite volume hydrodynamic modelling solution developed by Deltares (Delft, Netherlands), which employs an unstructured mesh and solves the shallow-water equations for a variety of forcing (Kernkamp 2011). The Flexible Mesh approach is an improved way to integrate different types of grids, required to represent a realistic and more reliable catchment flow patterns. For example, a rectangular grid can be used for the coarse resolution on the sea side, while for the coastal area and landside with the urban environments, transport infrastructure and large industries, the flexible mesh can be used. This approach was applied in the middle Yellow River to simulate flood hazard events

(Castro Gama, 2013). In D-Flow Flexible Mesh, the entire water system can be shown in 1D to 2D in depth, which results in a realistic picture of the entire catchment so that the impacts of measures can be calculated at each level. Geertsema (2013) modeled the river discharge and tidal propagation in the upstream and downstream regions using D-Flow Flexible Mesh but with limited ocean domain and without considering storm surge effects. Fig. 2-2 presented the flow chart of two model sets.

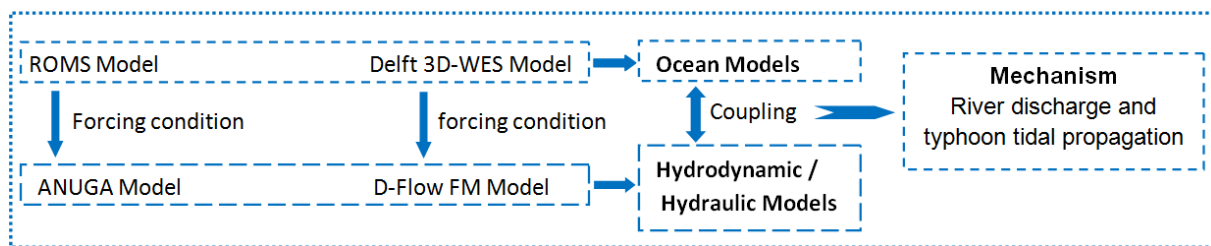


Fig. 2-2 The flow chart of two modelling sets

### 2.2.2 ANUGA Model Configuration

We set up the ANUGA model for the PRD, covering the domain between 15.54 - 23.94°N and 108.95 - 117.07 °E. The domain includes all distributaries of the Pearl River and approximately 100 km of offshore area.

#### ***Geostatic setup***

The high-resolution topographic information is very important for hydrodynamic modelling. For the ANUGA model, Digital Elevation Model is the input for mesh generation, so the resolution of the model grid corresponds to the resolution of the DEM. We used (ASTER) Global Digital Elevation Model (GDEM) with a horizontal resolution of 30\*30 meters for the land and the NOAA (National Oceanic and Atmospheric Administration) bathymetry data with 1 arc-minute resolution data for the oceanic bathymetry. We have projected the topographic and bathymetric data separately on UTM 50N WGS84, remapped them in a 100m resolution and then mosaicked them together to obtain the integrated PRD orographic coverage. The SAGA (System for Automated Geoscientific Analyses) open source geographic information system software originally developed at Goettingen University, Germany has been used for such processing. Fig. 2-3 shows the integrated orographic map of PRD generated from the ASTER GDEM and NOAA bathymetry data. As we can see,

the study area has a low-lying orography ranging from 0 to 200 meters above sea level, which exposes it to coastal natural hazards such as from storm surge.

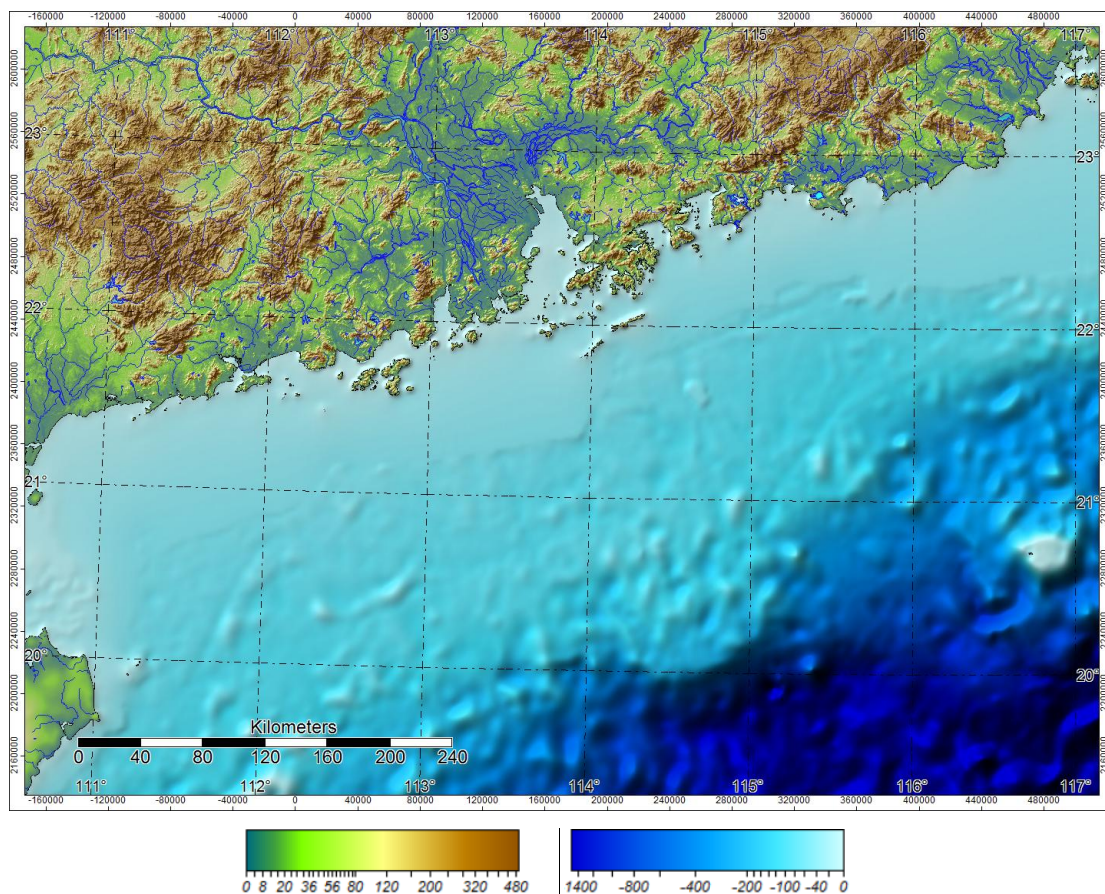


Fig. 2-3 Digital Elevation Model of Pearl River Delta (height, depth, meters)

### ***Boundary conditions***

We have setup two experiments, one with the ideal case scenario and other with the real case scenario. For an ideal case, we set the Dirchlet boundary as the onshore boundary, the time-dependent boundary as the offshore tide or storm surge scenario, the Transmissive Stage Zero Momentum boundary with continuing all values have been defined the neutral boundary. The initial conditions were all set to 0.0.

For the real case scenario, we again set the Dirchlet boundary as the onshore boundary. In order to generate storm surge boundary conditions for the ANUGA model, wave height and wave velocity have been computed by the ROMS ocean model ran by Hong Kong Technical University, China. The horizontal discretization of these data is 8 x 8 km (grid mesh resolution) and at 7 hourly time steps. Typhoon FANAPI in 2010 is used in this case. Fig. 2-4 shows the results from ROMS.

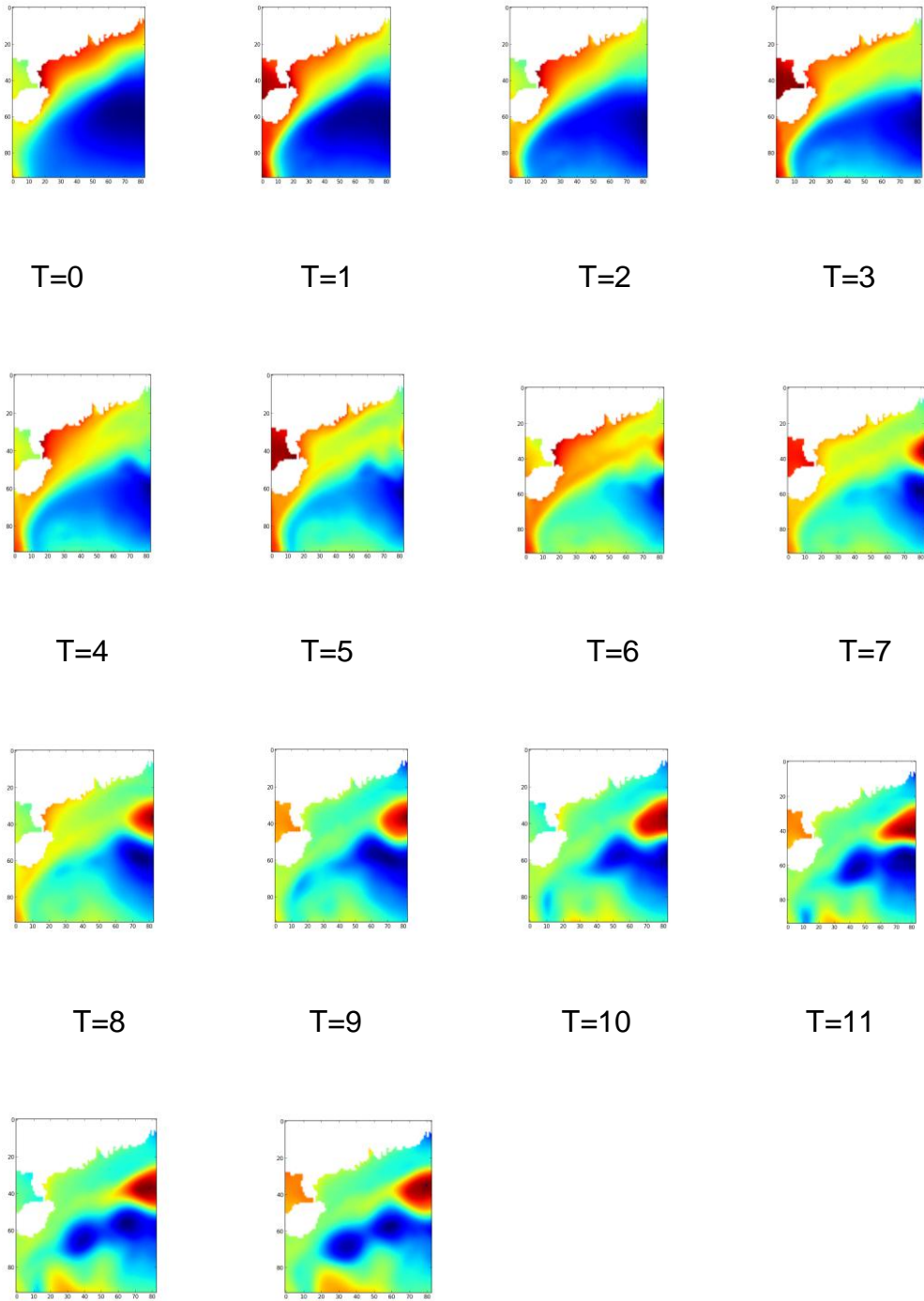


Fig. 2-4 Wave Height from ROMS model of Typhoon FANAPI in 2010

### 2.2.3 D-Flow Flexible Mesh Model Configuration

We set up the D-Flow model for the PRD, the research domain including a major axis of 50 km in the north-south direction and a width increasing approximately 100 km in the south from its mouth to the open sea.

The mesh network of the PRD model was combining the existing structure grid from the Delft 3D Flow model and unstructured grid using the D-FLOW FM model. As we can see from Fig.2-5, in order to speed up the computing time in the simulation, we used structure grid for the oceanic domain generated from Delft3D Flow model. The unstructured grid was used in the river channel and the connection between river and ocean. The entire mesh network is varying from meters along the coast and in river channel to kilometers at the open sea. There are 59752 nodes and 54917 elements in the PRD model.

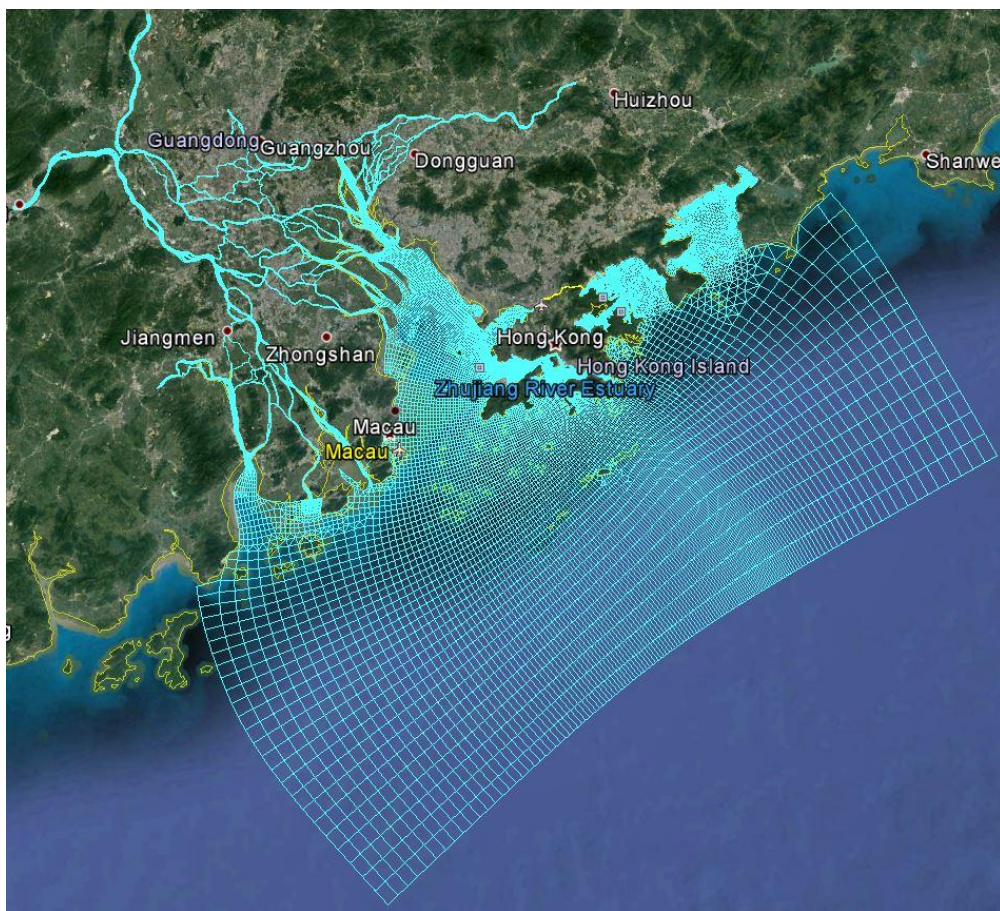


Fig. 2-5 Mesh of the Pearl River Model

The river bathymetry data was derived from Geertsema (2013) obtained in February 1999 and the ocean bathymetry from the local survey of Hong Kong. These two

datasets were interpolated by the D-Flow FM model to define its integrated bathymetry on an unstructured grid. The previously integrated (SRTM+NOAA ETOPO1 Data) topographic coverage on a 100-meter resolution has been used as the reference for calibrating the D-Flow FM model generated topography. The datum of all datasets is referenced relative to mean low low water level. Fig.2-6 shows the topography data setting of the PRD model.

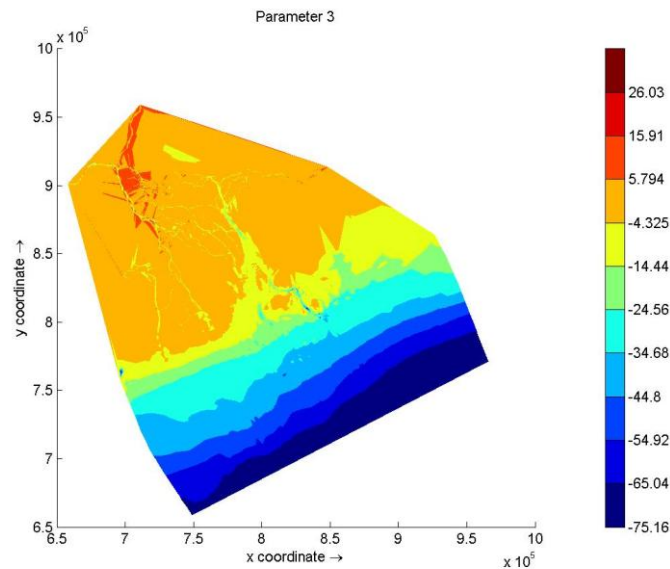


Fig. 2-6 Topography data of the PRD model

### ***Boundary conditions***

The model was simulated in the wet season and dry season separately, so we used river discharge in the upstream region from the dry and wet season of 1999 and 2002, and only dry season river discharge for 2009 as the boundary conditions at three gauging stations named Shijiao, Gaoyao and Boluo. All of the discharge data is monthly data with the minute's time resolution.

The tides in the PRD Estuary are irregular and semi-diurnal. The average tide range is between 0.86 and 1.6 meter, where the maximum tidal range is between 2.29 and 3.36 meters. We used the amplitudes and phases of 10 astronomic tidal components and a residual current as the open boundary conditions. The tide constituents are SA, O1, P1, K1, N2, M2, S2, K2, M4 and MS4. The residual current is A0. The diurnal constituents (K1 and O1) and the semi diurnal constituents (M2 and S2) are

the main tidal components for this region especially in HongKong (A.K.M.Ng et al., 1999).

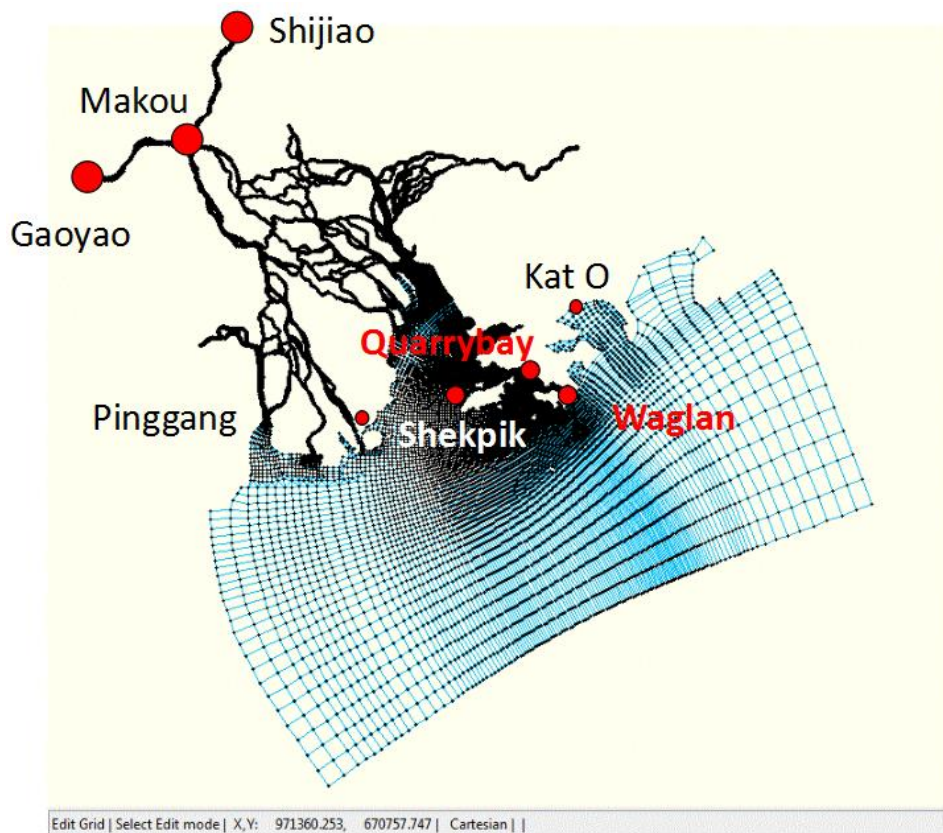


Fig. 2-7 The model setup and observations of the Pearl River Model

### **Observation data**

We have observatory data in station Makou, Pinggang, Kat\_O, Waglan, Shek Pik and Quarry Bay station from 1999, 2002 and 2009 year separately. Among them, Makou station and Pinggang station are used to calibrate the river discharge of the model, others located along Hong Kong coast, mainly for calibrate the tidal performance of the model.

Makou is located at the intersection of West River and North River in the upper stream of Pearl River. There are the measurement data in November, December and January in the dry season of 1999, and the measurement data in July in the wet season of 1999. Pinggang station is located at Modaomen channel of west bay of Pearl River Estuary. The river discharge is accounting for 28.3% total runoff into the sea of the Pearl River. The measurement data at Pinggang is from 1 October to 28 February 2009. The precipitation in 2009 is extremely less than average yearly discharge, thus

the discharge in Modaomen channel of Pearl River Estuary reduced heavily in the dry season as well (Jun Sun, 2012).

Kat\_O station, Waglan, Shek Pik and Quarry Bay station are the observations along Hongkong coast. Kat\_O station is in the Mirror Bay of Hongkong.

The tidal performance of the model is compared to tide level observations at these four stations for 2002 wet and dry season separately. Table 1 listed the period of the available data. The measurement data at Waglan station is from July 9 to 22 in the wet season, Shek Pik station is from June 11 to 25, Quarry station is from August 20 to September 3. For the dry season, Kat\_O station is from October 25 to 29, Waglan station is from January 29 to February 12 in 2002, Quarry Bay station is from January 22 to February 4 in 2002, Shek Pik station is from November 19 to December 3.

Table 2-1 Timeline of the observation data and simulation

1999 wet season	Observation(daily discharge)	Model(hourly discharge)	Description
<b>Makou</b>	July	July 09 to Sep 17 (70d)	Junction point between west river and north river for discharge calibration
<b>Gaoyao</b>	July	July 09 to Sep 17 (70d)	Control point of west river
<b>Shijiao</b>	July	July 09 to Sep 17 (70d)	Control point of north river

1999 dryseason	Observation(daily discharge)	Model(hourly discharge)	Description
<b>Makou</b>	December	Nov 21 to Jan 1 (70d)	Junction point between west river and north river for discharge calibration
<b>Gaoyao</b>	December	Nov 21 to Jan 1 (70d)	Control point of west river
<b>Shijiao</b>	December	Nov 21 to Jan 1 (70d)	Control point of north river

2009 dryseason	Observation(daily discharge)	Model(hourly discharge)	Description
<b>Pinggang</b>	Oct 1 _Feb 28	Dec 1 to Dec 31 (31d)	Modaomen Channel for discharge calibration

2002	Observation(hourly)	Model(hourly)	Description
------	---------------------	---------------	-------------

dryseason	discharge)	discharge)	
Waglan	Jan 29_Feb 12	Jan 12 to Feb 12 (32d)	Near Hongkong for tidal calibration
Shek Pik	Nov 19_Dec 3	Nov 9 to Dec 3 (25d)	Near Hongkong for tidal calibration
Quarry Bay	Jan 22_Feb 4	Jan 12 to Feb 12 (32d)	Near Hongkong for tidal calibration
Kat_O	Oct 25_Oct 29	Oct 15-19 (16d)	Mirs Bay for tidal calibration
2002 wetseason	Observation(hourly discharge)	Model(hourly discharge)	Description
Waglan	July 9_July 22	June 1 to July 31 (61d)	Near Hongkong for tidal calibration
Shek Pik	June 11_June 25	June 1 to July 31 (61d)	Near Hongkong for tidal calibration
Quarry Bay	Aug 20_Sep 3	Aug 10 to Sep 3 (24d)	Near Hongkong for tidal calibration

## 2.3 Results

### 2.3.1 ANUGA Results

The results show the visualization of various inundation scenarios in time series from ANUGA model viewer in Fig. 2-8. From these maps, we could see the inundation progress when timing changed, the southwest region was inundated obviously. We obtained the wave speed ASCII grid at 100 m<sup>2</sup> resolution, visualized using SAGA GIS as shown in Fig. 2-9. This was the first study case that the ANUGA model is one-way coupling with ROMS especially in PRD.

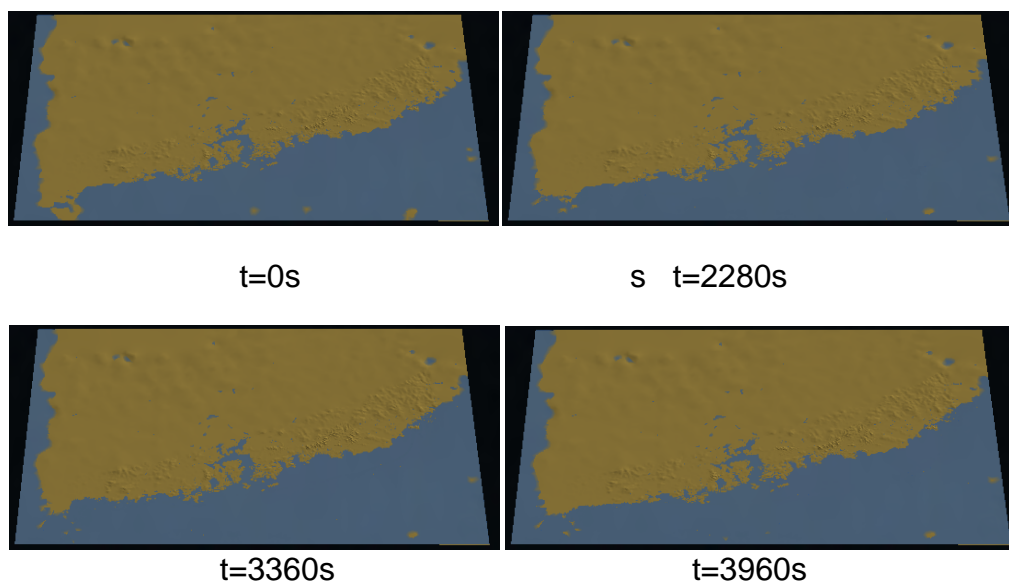


Fig. 2-8 The evolution in time of an inundation process

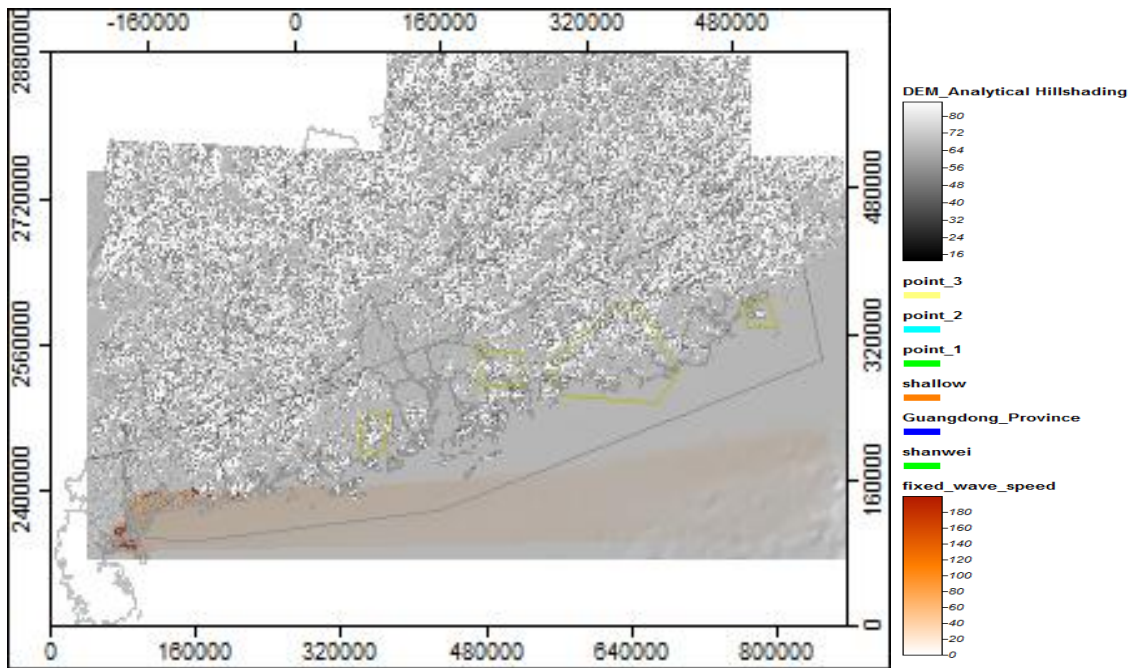


Fig. 2-9 Wave speed map from ANUGA model using SAGA GIS visualization

### 2.3.2 Results of D-Flow Flexible Mesh Simulation

#### *Subtidal discharge validation*

Makou station is located at the discharge division cross section between West River and North River. The modeled daily river discharge at Makou station in the wet season of 1999 is shown in Fig. 2-10. There was a difference on amplitudes and phases between model results and measurement data. The maxima modeled river discharge was over 15000 m<sup>3</sup>/s. In this part of simulation, we used the friction roughness 0.001, which can already result in a high flow. Even though it was lower than the observation, but the modeled discharge was within the range of the measured discharges.

The simplified mass balance equation could explain the difference,

$$Q_{in} = Q_{out} + \Delta S_{source} \quad ^1 \text{ (Nazaroff \& Alvarez-Cohen, 2001)}$$

$Q_{in}$  is the incoming discharge,  $Q_{out}$  is the outgoing discharge and  $\Delta S$  is the source term. The source term includes the exchange with the atmosphere or the sink water, it

<sup>1</sup> [http://www.cee.mtu.edu/~reh/courses/ce251/251\\_notes\\_dir/node3.html](http://www.cee.mtu.edu/~reh/courses/ce251/251_notes_dir/node3.html)

won't be considered due to lack of available information (Nazaroff & Alvarez-Cohen, 2001). Water enters the apex at Gaoyao and Shijiao and leaves at Makou (left branch) and right branch (Sanshui station, see Table 2-2). Therefore,

$$Q_{\text{gaoyao}} + Q_{\text{Shijiao}} = Q_{\text{makou}} + Q_{\text{right}}$$

As listed in table 2-2, Makou station contributes 83.5% stream flow in the dry season. We didn't model the river discharge at the right branch of the Pearl River. Fig. 2-11 shows the model from the input discharge locations all performed the mass balance from trend and magnitude at Gaoyao and Shijiao station. When the river flow comes to the apex, Makou station only has part of the entire input discharge. Therefore, the  $Q_{\text{makou}}$  should be less than the input discharge.

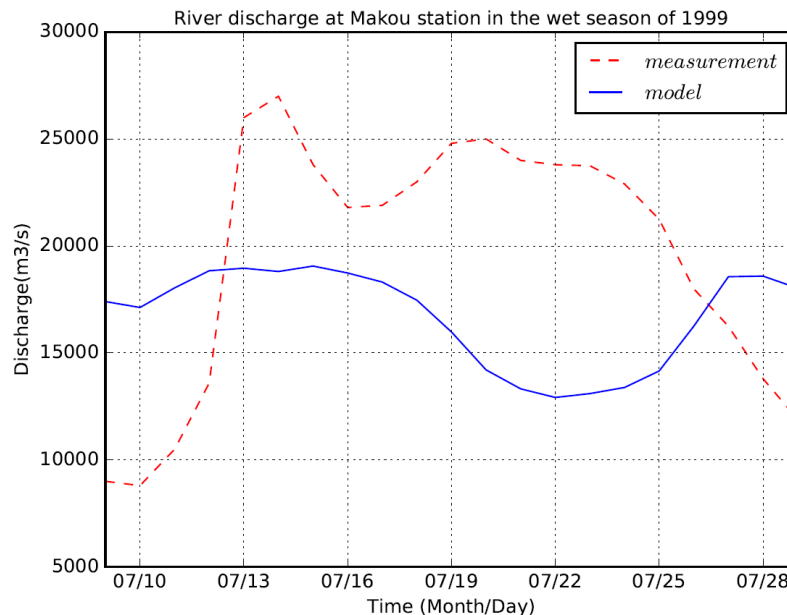


Fig. 2-10 The measurement and modeled daily river discharge at Makou station in the wet season of 1999

Table 2-2 Variation ratio of river discharge in the dry season at Makou and Sanshui (1956 -2006)

Time	Makou	Sanshui
1959-1969	93.4%	6.6%
1970-1979	92.6%	7.4%
1980-1989	90%	10%
1990-2003	83.5%	16.5%
2004-2006	81%	19%

( Joseph Hun-Wei Lee and Chiu-On Ng, 2011)

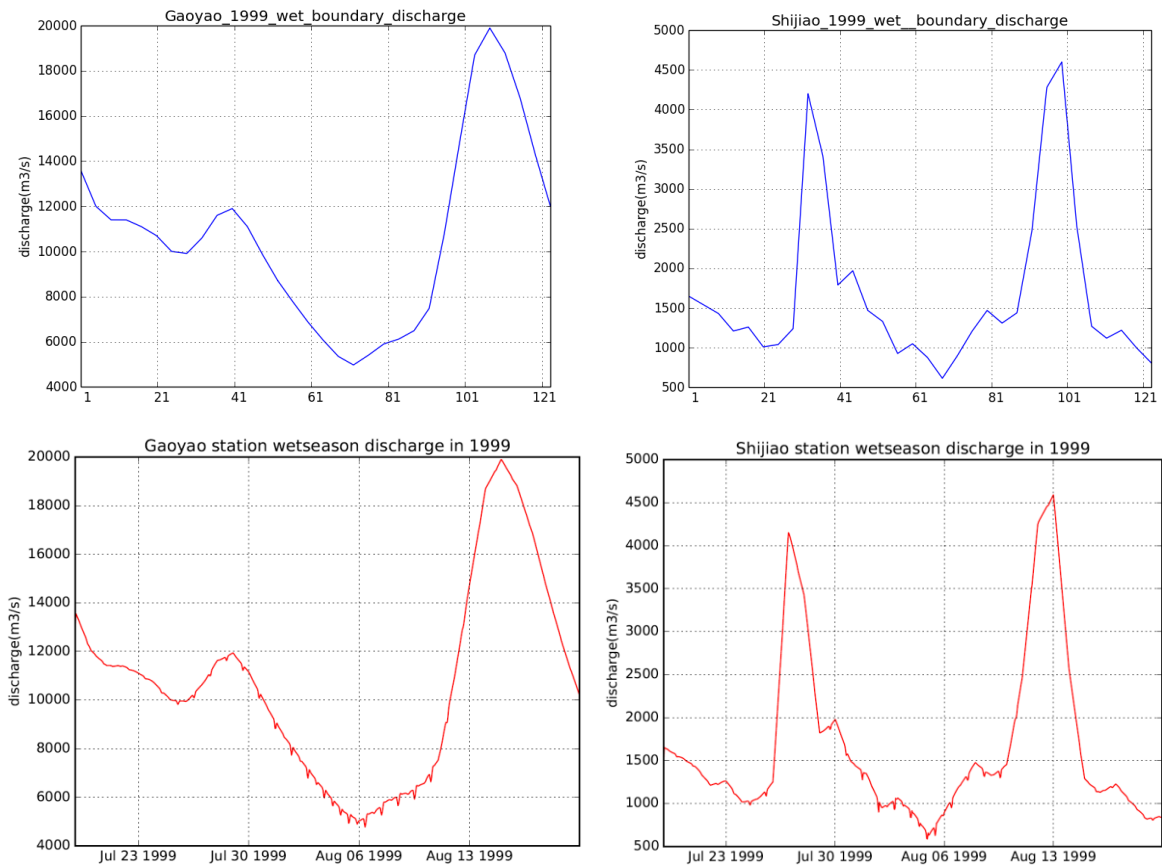


Fig. 2-11 The input discharge (up) and modeled discharge (down) at Gaoyao and Shijiao station in the wet season of 1999

Another reason, the changes in river discharge also depends on the cross section. Therefore the difference of cross section between modeled station and measurement station could also lead to the magnitude difference. Additionally, the possible reason for the amplitude difference might be because we re-adjusted the model warming up time. This could make the peak discharge amplitude differences between model and measurements.

### ***Subtidal discharge validation in the Dry season***

The hydrograph of daily river discharge from modeled data and measurement at Makou station (upstream) and Pinggang station (downstream) in the dry season is listed in the Fig.2-12. We could see that, there is a fine adjustment between model results and the measurement data at the Makou station in December. However, the modeled data of January has an approximately three days phase lag compared to the measurements.

At downstream Pinggang station, we compared the daily discharge of modeled data and measurement in December of 2009 as displayed in Fig.2-12. The higher high water level of modeled data is lower than the measurements. Since Pinggang station located at the estuary of Pearl River, there is an obvious tidal influence on the discharge is more obvious than upstream. The maxima discharge volume of modeled discharge was over 1500 m<sup>3</sup>/s, with 1000 to 1500 m<sup>3</sup>/s relative to the measurement.

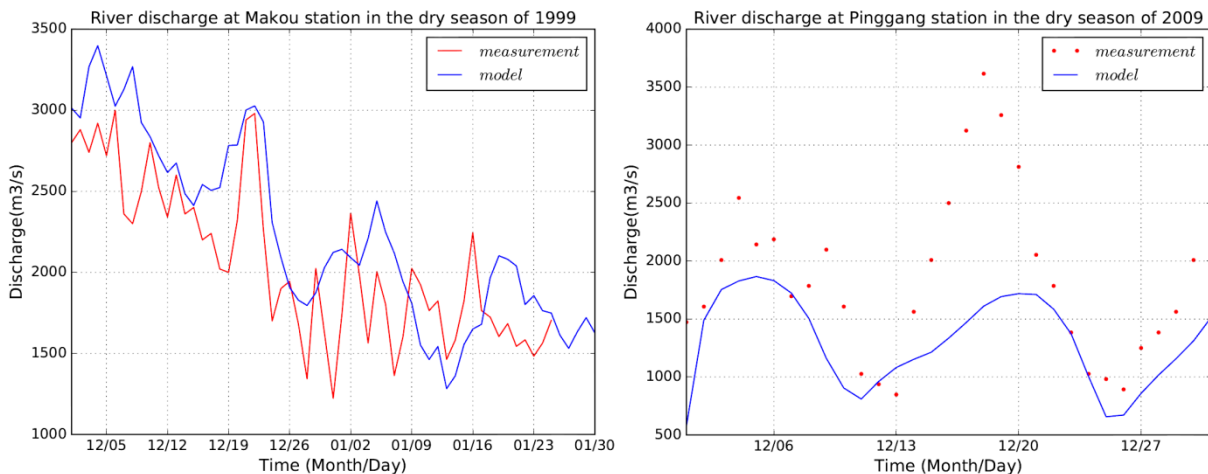


Fig. 2-12 The measurement and modeled daily discharge at Makou and Pinggang station in the dry season

### ***Tidal propagation analysis in the wet season***

We have three gauge stations, Waglan, Shek Pik and the Quarry Bay for the wet season tide propagation analysis. We could notice water levels of all stations had the same tidal period compared to the measurements. The amplitude during the high tide time and ebb tide time presented difference among all stations. The tidal range of modeled data of Shek Pik was larger than measurements. Waglan and Quarry Bay performed a similar tidal range relative to measurements although the higher high water and lower low water were lower than measurements. A maximum 0.5 meters difference existed at the both station at high and low water time. The lower high level among all stations remained more negative than measurements. Maybe the river discharge had less influence on tide levels during the wet season for the coastal area. Tidal amplitudes along the outer bay range around 2.5 meters as we can see at Shek Pik and Waglan, while the station inside of the bay (Quarry Bay) was much attenuated only with about 2 meters water level.

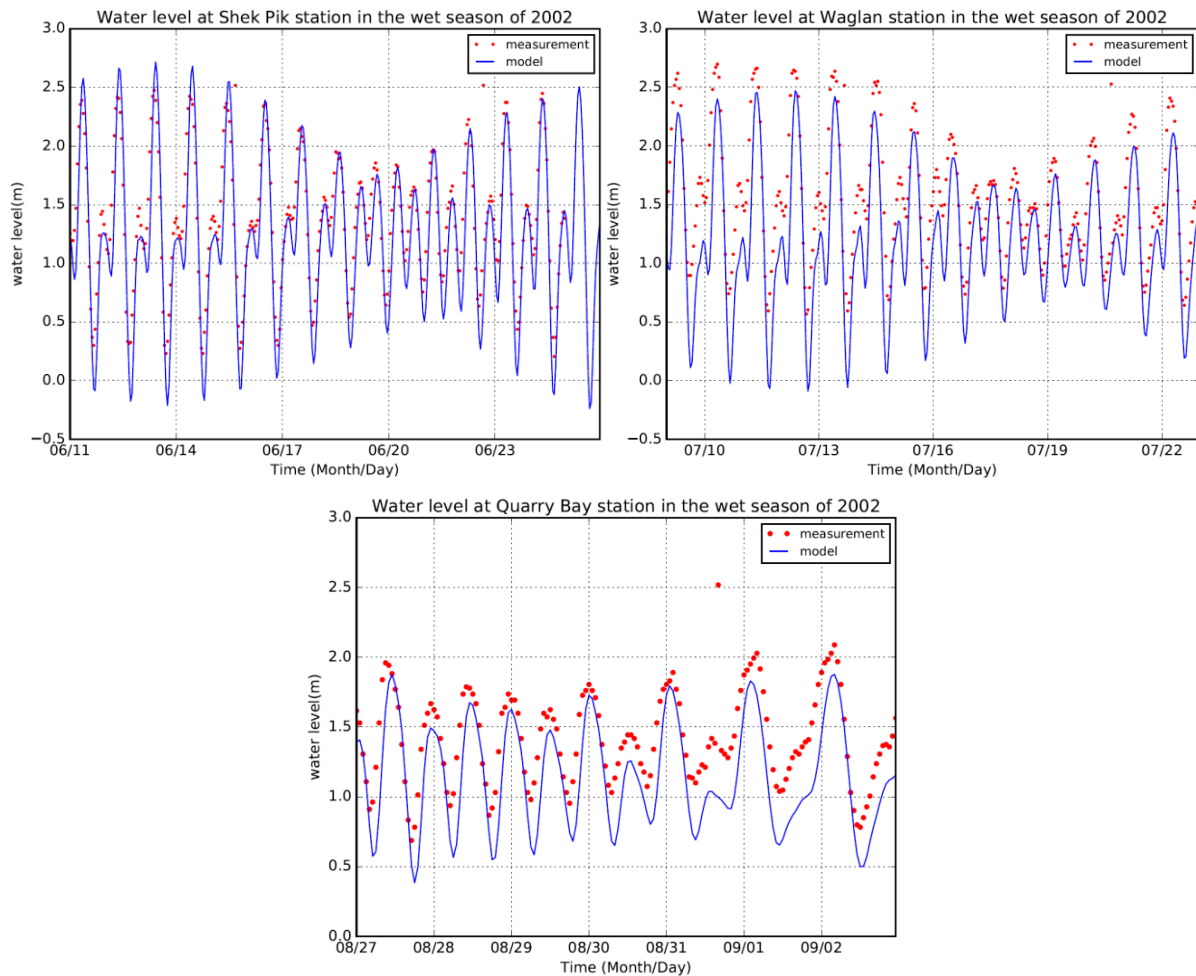


Fig. 2-13 The measured and modeled water level at gauge stations in the wet season of 2002

***Tidal propagation analysis in the dry season***

For the analysis of daily seasonal tidal propagation at the open sea, Kat\_O station in Mirs Bay of HongKong and Shek Pik station were selected. The observation data of Kat\_O station is the water level from 25 -29 October in hours. As we can see from the Fig. 2-14, the amplitude of modeled data was about 2 meters, which was higher than the observation data of 1.5 meters. The tidal range was larger than measurements and the difference was within 0.5 m. At Shek Pik station, the higher high water level was accorded well with measured data. The lower low water level and the lower high water level were much lower than measurements. We can conclude that the performance of the tidal gauge station was better than the discharge station. However, more observations are needed between the east bay and the western apex.

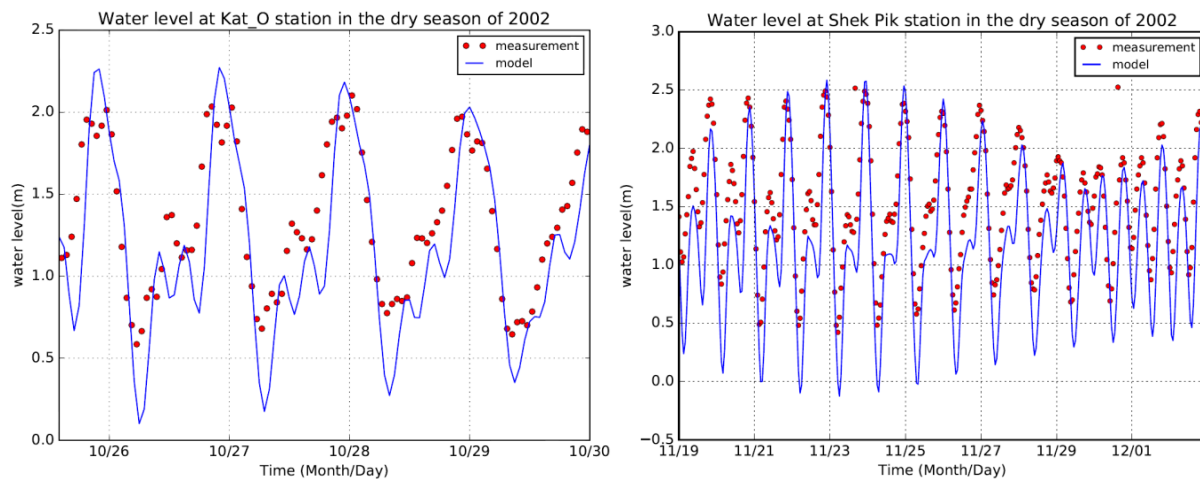


Fig. 2-14 The measured and modeled water level at gauge stations in the dry season of 2002

### 2.3.3 Discussion

We have set up two modelling suites to simulate the interaction between river system and ocean system in wet and dry season in the PRD, including the entire Pearl River distributaries and more than 100 km seaside region. As unstructured grid hydrodynamic models, ANUGA and D-Flow FM were both the first applications in such complicated river networks and over such a big domain. The D-Flow FM model can also combine the structural grid and unstructured grid together. This advanced flexible mesh generation methods offered a new sight of solution for the complicated coastlines according to various requirements.

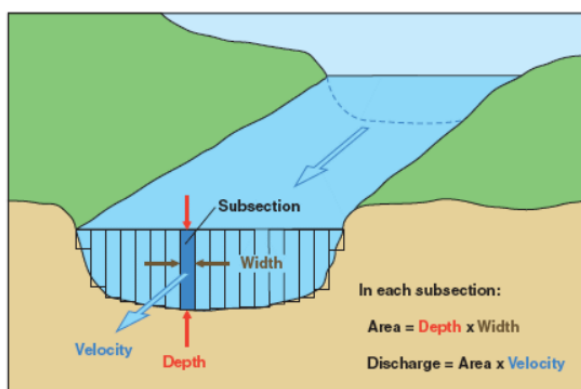
#### **ANUGA**

The ANUGA model performed in a fast and flexible way for the mesh generation. So far, the ideal case simulations performed well, which is a good case study for the flexible mesh application in the PRD. However, the real case simulation produced a weak one-way coupling process between ANUGA and ROMS. Further, constraints are the Boundary treatment of the ANUGA model, which needs to be covered comprising of forcing values such as time, latitude and longitude,  $u_{bar}$ ,  $v_{bar}$  (wave velocity in x-monument and y-monument) and wave height. There are distinct differences in the spatial resolution of the ROMS and ANUGA. Therefore, before starting the nesting, a suitable spatial refinement of the ocean model output is required, this may be achieved by e.g. thin-plate spline interpolation. The suitability of

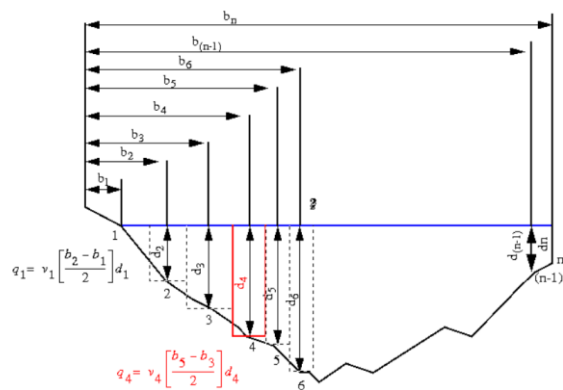
alternative interpolation and downscaling techniques, however, still needs to be evaluated.

### D-Flow Flexible Mesh

For the D-Flow Flexible Mesh model simulation, the difference of river discharge can be explained for several reasons. Firstly, the discharge depends on the cross section area and flow velocity, the location of the measure station and the observation verticals affect the discharge volume calculations (Fig.2-15). In our research, we cannot judge the model setting is exactly as same as the observations location. Thus it is possible there is a difference between the modeled data and river discharge. However, our model results were within the measurements discharge range.



Current-meter discharge measurements are made by determining the discharge in each subsection of a channel cross section and summing the subsection discharges to obtain a total discharge.



2

Explanation  
 1,2,3 .....n --Observation verticals  
 b<sub>1</sub>, b<sub>2</sub>, b<sub>3</sub>, .....b<sub>n</sub> --Distance from initial point to observation vertical  
 d<sub>1</sub>, d<sub>2</sub>, d<sub>3</sub>, .....d<sub>n</sub> ..Depth of water at observation vertical  
 Dashed lines --Boundaries of subsections

Fig. 2-15 Cross-section area for discharge calculation<sup>3</sup>

Secondly, the friction roughness plays an important role in the river discharge and tidal propagation. In this simulation, we used Manning coefficient 0.001 as the friction roughness. However, since D-FLOW FM model is the first application in the Pearl River, we will explore an optimal value in the part of sensitive tests.

<sup>2</sup> <http://ny.water.usgs.gov/pubs/posters/streamgagingposter.html>

<sup>3</sup> <http://geographyfieldwork.com/River%20Discharge%20Methodology.htm>

Moreover, the model is constrained by local data such as the bathymetry and the river discharge. A wrong reference level of the bathymetry results in a wrong cross section also results in the attenuated predicted effects of the water level, discharge and the tidal propagation in the context of the hydrodynamic model. This could be the reason of the low ranked fit agreements of all observations. The reference level needs to be adjusted first before the friction coefficient can be redetermined. The seasons can also affect the bathymetry, for instance, by larger sediment discharges during the wet season (Geertsema, 2013). Generally, high-quality validation data are rare; this is a shortcoming in the presented analysis, which fundamentally obstructs efforts to advance predictive modelling using the current setup.

Additionally, we also found that the discharge distributions depend strongly on temporal hydrodynamic processes distinctly in different seasons. In the East and West Bay, many lateral rivers drain to the Bays. River discharges can affect the tidal amplitude and the phase difference between high water slack and high water level or between low water slack and low water. In the other hand, the tides also affect the river discharge by the surge phenomenon. In the West Bay, the tidal propagation in the downstream was much influenced by the lateral river discharge during the wet season. In the East Bay, the tidal propagation in the downstream was less influenced by the lateral river discharge. In short, the wet season has more impact on the sub tidal discharge at upstream and in case of relatively high lateral river discharges in the downstream bays.

Therefore, based on the model performance, we will choose the D-Flow Flexible Mesh model for further application on storm surge simulation and coastal inundation research during typhoon period in the future climate change.

## **2.4 Sensitive tests of friction roughness**

Hydrodynamics involve a balance between gravity-driven flow and frictional resistance. Sensitivity analysis is widely accepted as a necessary part of good modelling practice (Jim W. Hall et al., 2009). For the inundation simulation, roughness is one of the most parameters of hydrodynamic models. Different hydrodynamic models have different performance on different roughness settings. And the roughness also varies in different river channels, topography, bathymetry, surface

roughness, land cover, river discharge and so on (Prabeer Kumar Parhi, 2013; R. Ramesh et al., 1997; HEC-RAS, 2008). Additionally, D-FLOW FM model is the first application in the PRD, in order to find the optimal roughness setting of this new hydrodynamic model in this particular region, we should evaluate the roughness coefficient (Manning's "n" value) for the Pearl River through simulation of hydrodynamics.

For this evaluation, we set up the PRD model by using different roughness scenarios in the wet season of 1999 and 2002, in the dry season of 2002 and 2009. The inundation plain has diverse landscape type, for example, crops, grassland and brush. Therefore, the Manning coefficient was designed by 0.01, 0.016, 0.023, 0.025, 0.027, 0.05 for the whole domain, and the floodplain and the river channel ('nc') were assumed to be spatially and also temporally invariant (M. Wood et al., 2016). We analysed the performance of the river discharge at upstream and the water level of tidal gauge stations under different roughness scenarios in the PRD model.

#### **2.4.1 Subtidal discharge division in the upstream region**

##### ***Wet season***

The results of upstream river discharge from three gauge stations (Gaoyao, Shijiao and Makou) under different roughness scenarios for wet season in the year of 1999 is showed from Fig. 2-16 to Fig.2-18. We can see a big difference on the river discharge under different roughness scenarios in these three stations. According to the definition of manning coefficient roughness, the higher value is, the lower flow speed is, and correspondingly the lower roughness will lead to the tidal period variation for the discharge. As we can see from the results when the roughness is as low as 1.0d (0.01), the tidal propagation shows a significant influence on the river discharge when the amplitude phrase is regular, the river discharge even has opposite direction flow due to the strong tidal influence. And the peak cycle period is around every 8 hours at Gaoyao and Shijiao station, but about 12 hours at Makou station. When the roughness was as high as 5.0d (0.05), there was almost no tidal influence at all. The river discharge trend was much smoother when roughness is 0.023. From the model results, the peak of the discharge was more than 120000 m<sup>3</sup>/s, the lowest level was

around 5000 m<sup>3</sup>/s. Additionally, the modelling results of the river discharge change trend had a close agreement with the input river discharge trend.

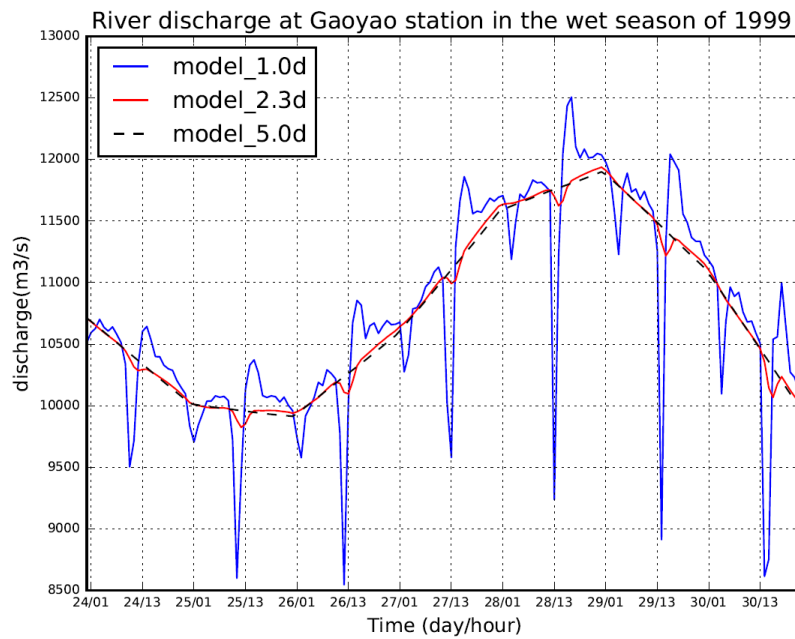


Fig. 2-16 The modeled river discharge at Gaoyao station in July 1999 under different roughness scenarios

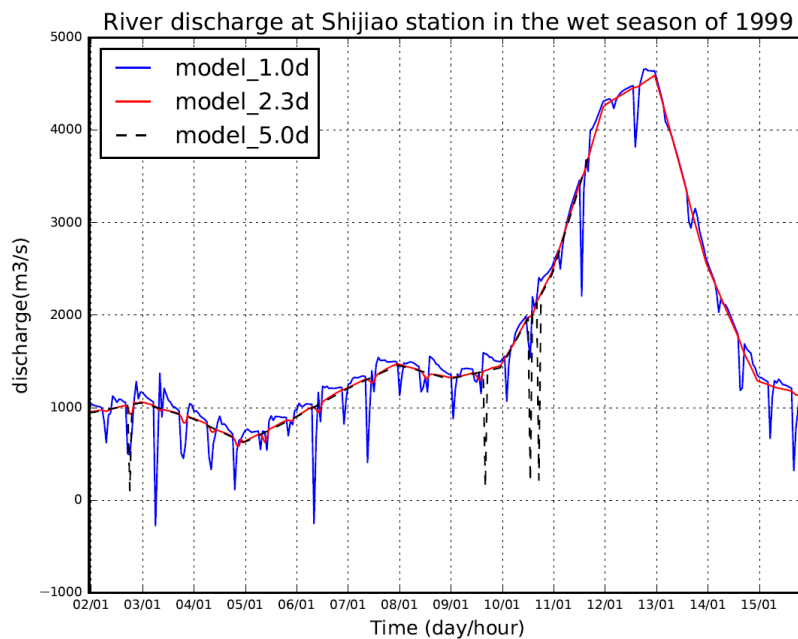


Fig. 2-17 The modeled river discharge at Shijiao station in August 1999 under different roughness scenarios

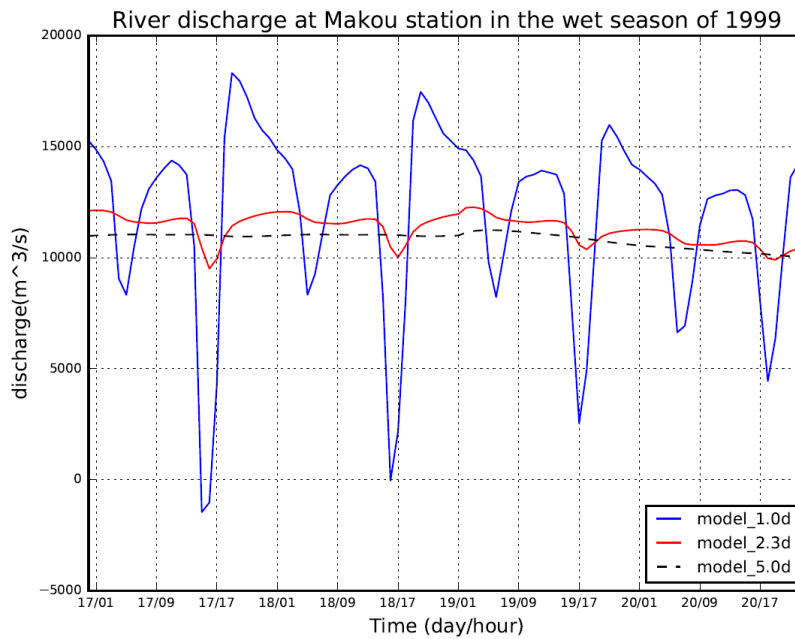


Fig. 2-18 The modeled hourly river discharge at Makou station in July 1999 under different roughness scenarios

### **Dry season**

For the dry season, we have four gauge stations, Gaoyao, Shijiao, Makou and Pinggang station for the sensitive test of roughness in the year of 1999 and 2009. The Gaoyao, Shijiao and Makou station are located at upstream of the Pearl River. The measurement data at the Makou station is the daily data without the tidal phenomena as we could see from the Fig.2-23 and Fig.2-24. In the dry season, the river discharge at upstream also showed the sensitive response to the tidal propagation under the low Manning coefficient roughness. Moreover, due to the lower river inflow volume in the winter time, the tidal forces had a greater influence on the discharge, especially more obvious at Shijiao and Makou station on the backward forcing under the lower roughness scenarios (Fig.2-19 to Fig.2-24). In addition, the lower roughness showed the higher flow volume at all gauge stations. The tidal phase at all stations is about 12 hours without any delay. On the contrast, there was almost no tidal effect on the river discharge when the roughness was extremely high like 0.05.

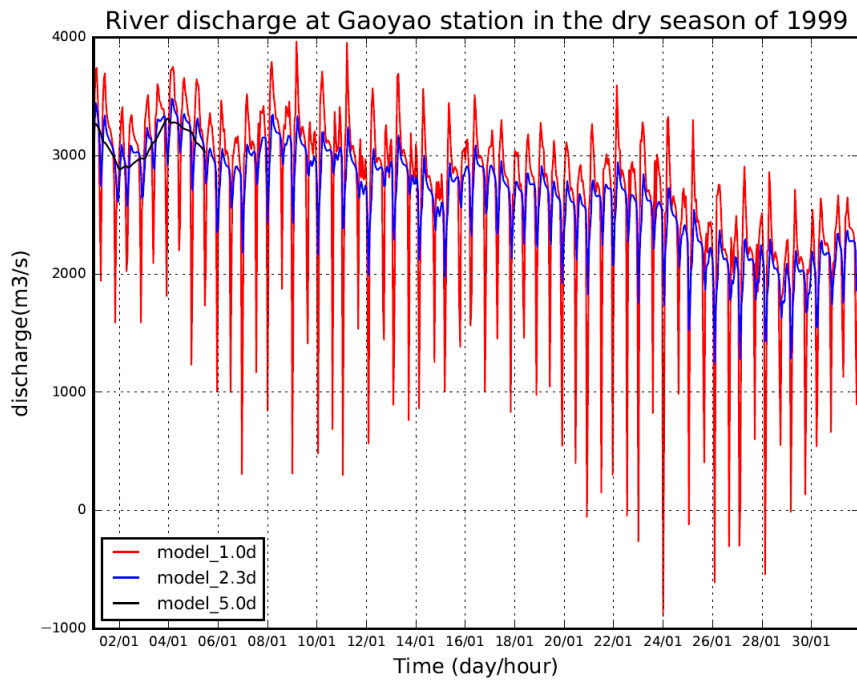
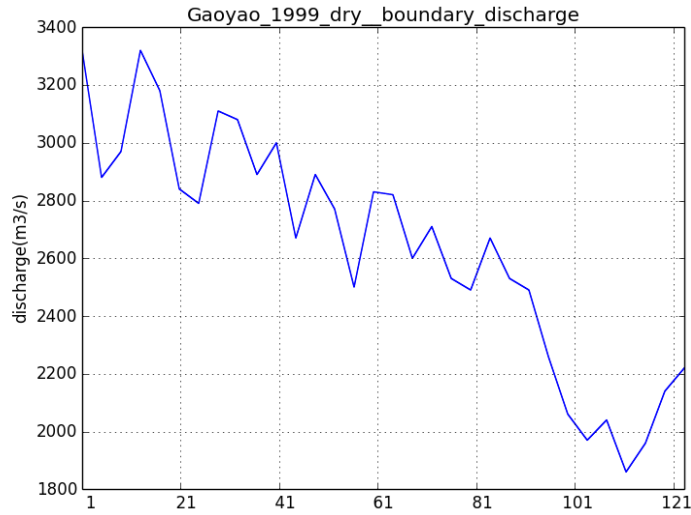


Fig. 2-19 The boundary (up) and modeled river discharge (down) at Gaoyao station in December 1999 under different roughness scenarios

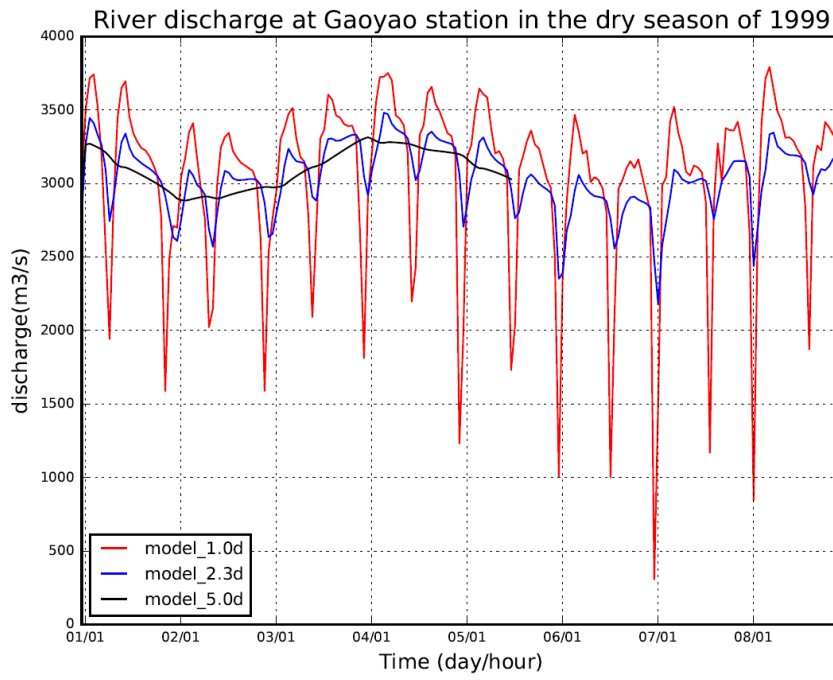
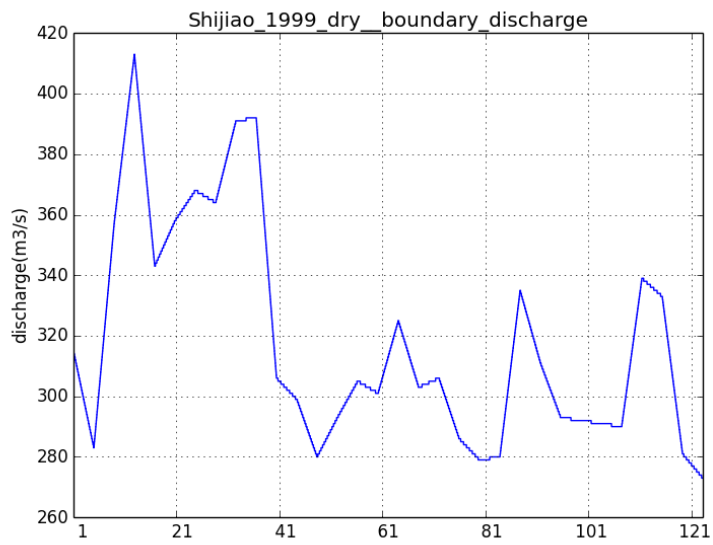


Fig. 2-20 The modeled river discharge at Gaoyao station in December 1999 under different roughness scenarios



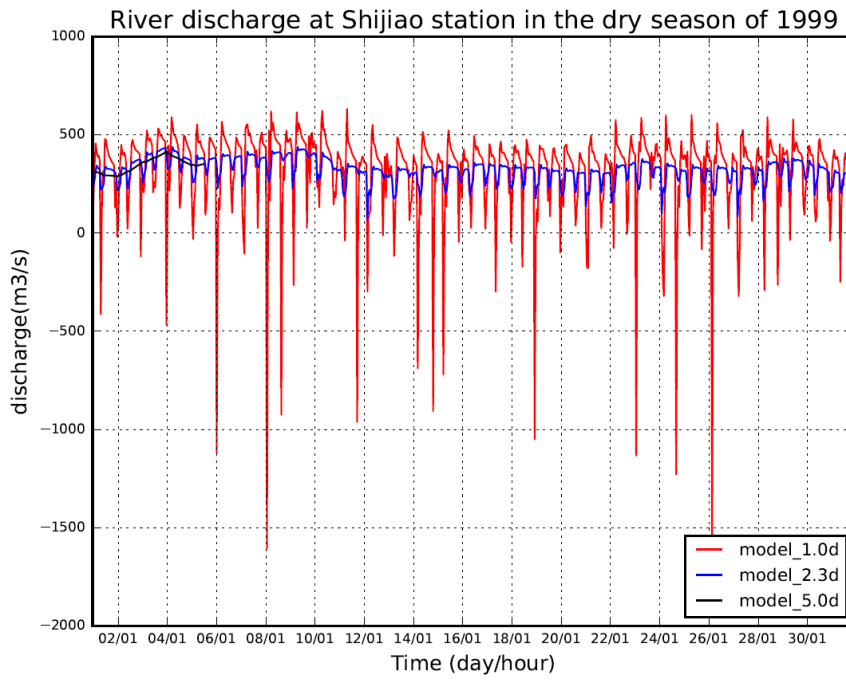


Fig. 2-21 The boundary (up) and modeled river discharge (down) at Shijiao station in December 1999 under different roughness scenarios

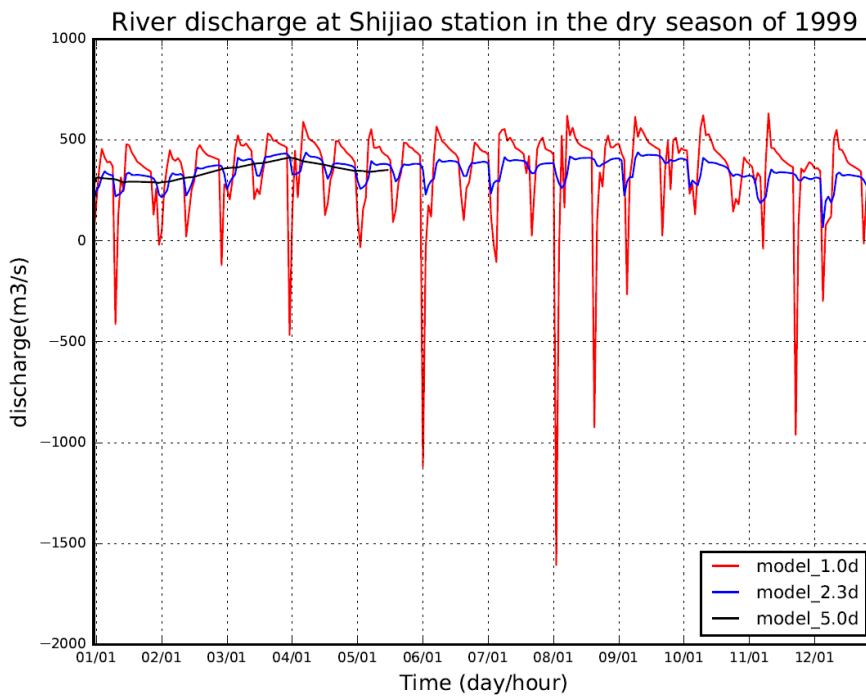


Fig. 2-22 The modeled river discharge at Shijiao station in December 1999 under different roughness scenarios

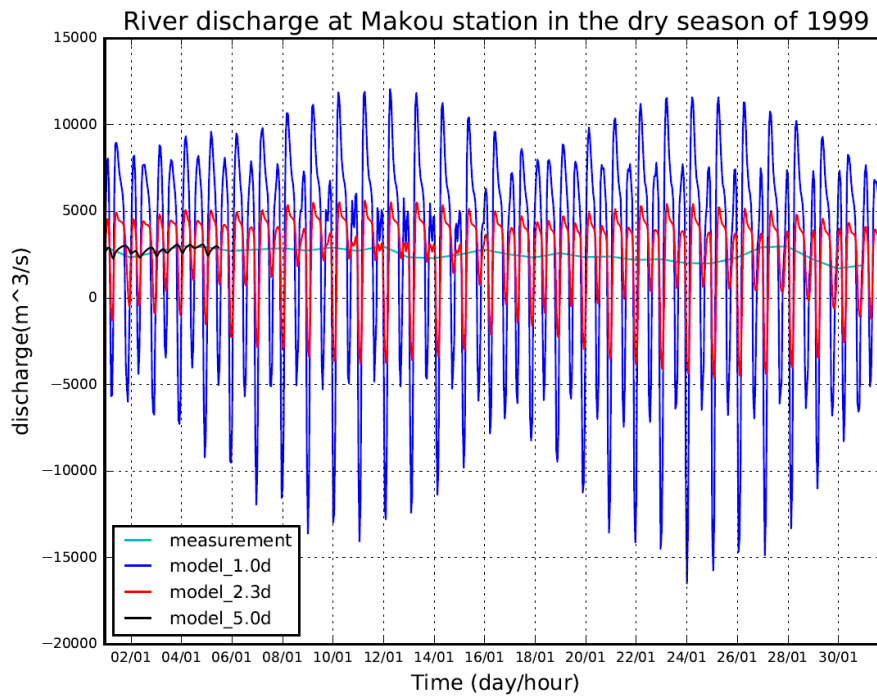


Fig. 2-23 The measured and modeled river discharge at Makou in December 1999 under different roughness scenarios

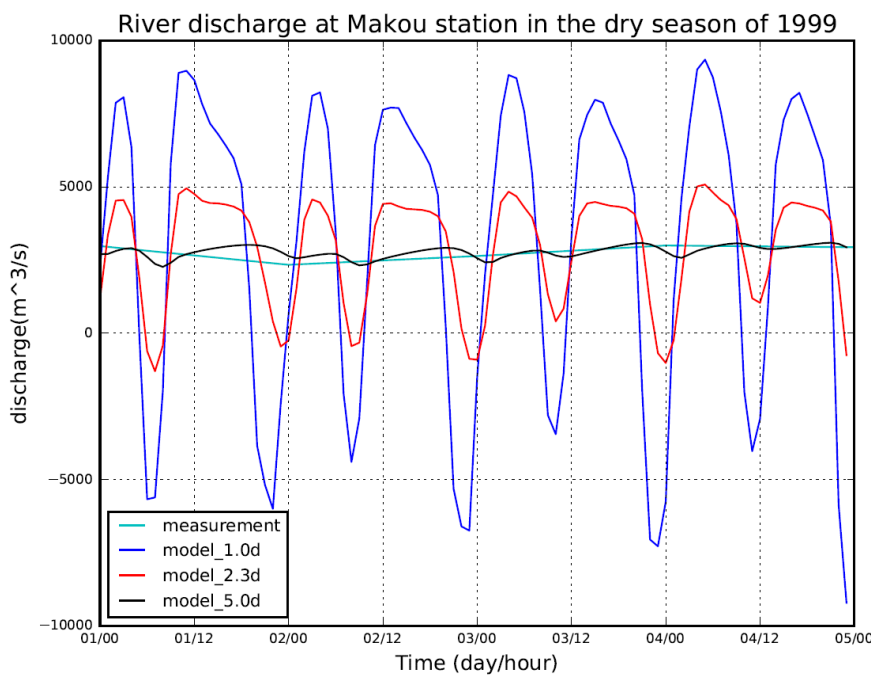


Fig. 2-24 The measured and modeled hourly river discharge at Makou station in December 1999 under different roughness scenarios

There are four months measurement data for the Pinggang station. December was selected to compare model results to measured data under different roughness scenarios as Fig. 2-25 and Fig. 2-26 showed. The measured data had the same trend as the modeled results. Since Pinggang station is located at the Pearl River

mouth, near Macao City, the influence from tidal is even greater than upstream even though at higher roughness scenarios. As same as in other stations, the tidal phrase is about 12 hours. The volume of the discharge at the 2.3d roughness scenarios had the better agreement with the measurement data.

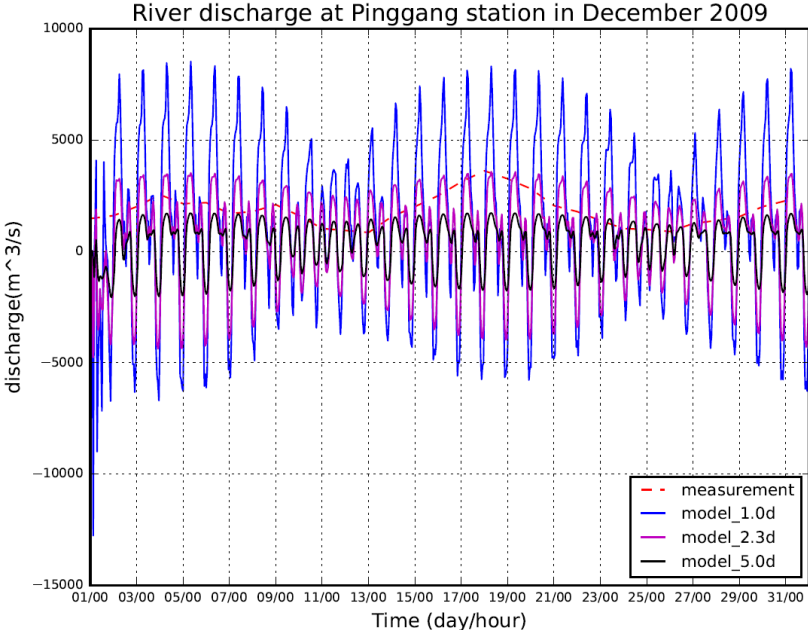


Fig. 2-25 The measured and modeled hourly river discharge at Pinggang station in December 2009 under different roughness scenarios

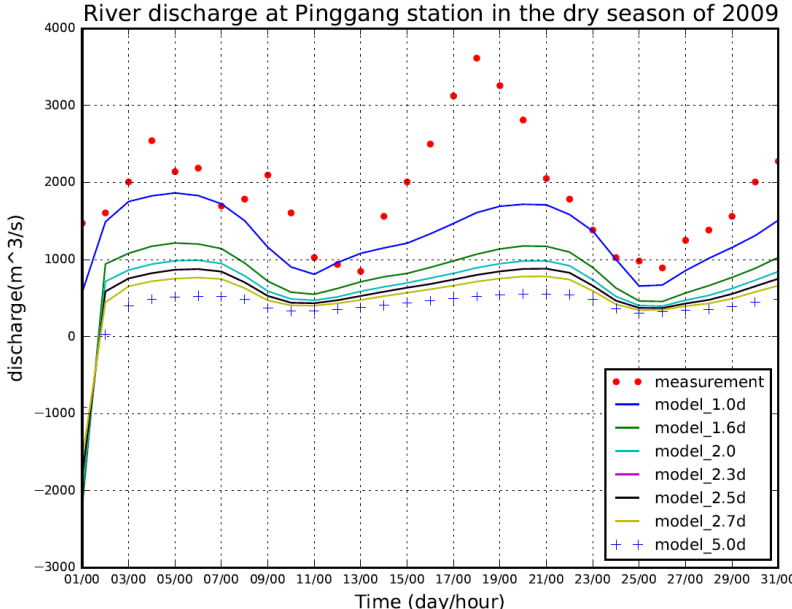


Fig. 2-26 The measured and modeled daily river discharge at Pinggang station in December 2009 under different roughness scenarios

## 2.4.2 Tidal propagation at the open sea

In order to confirm the model performance, a series of sensitive tests (calibration) for tidal calibration was done for this model. We have four gauge stations, Waglan station, Quarry Bay station, Kat\_O station and Shek Pik station for the calibration.

### **Wet Season**

There are three gauge stations which are Waglan station, Shek Pik station and the Quarry Bay station for the wet season sensitive tests in the year of 2002. We could see from Fig.27 and Fig.28, even though in different scenarios, there is a great difference in water level in all stations. There is the best uniformity with the measurement data at Shek Pik station, on the contrast, the comparison between observed data and measurement data is the Quarry Bay station. From the Waglan station, the lowest water level has differed with the measurement data. Therefore, we could get the conclusion that the river discharge has less influence on the water level during the wet season for the coastal area.

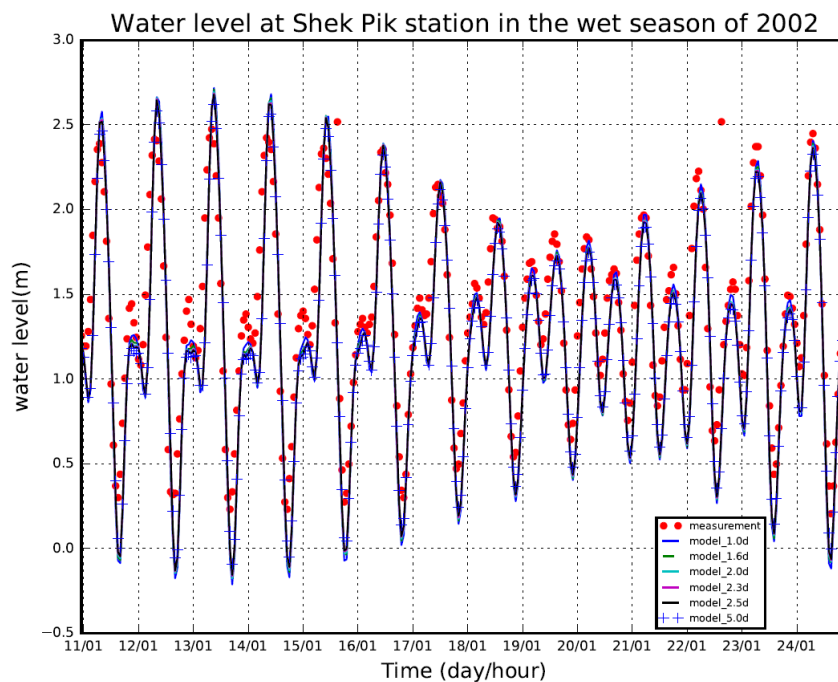


Fig. 2-27 The measured and modeled water level at the Shek Pik station in June 2002 under different roughness scenarios

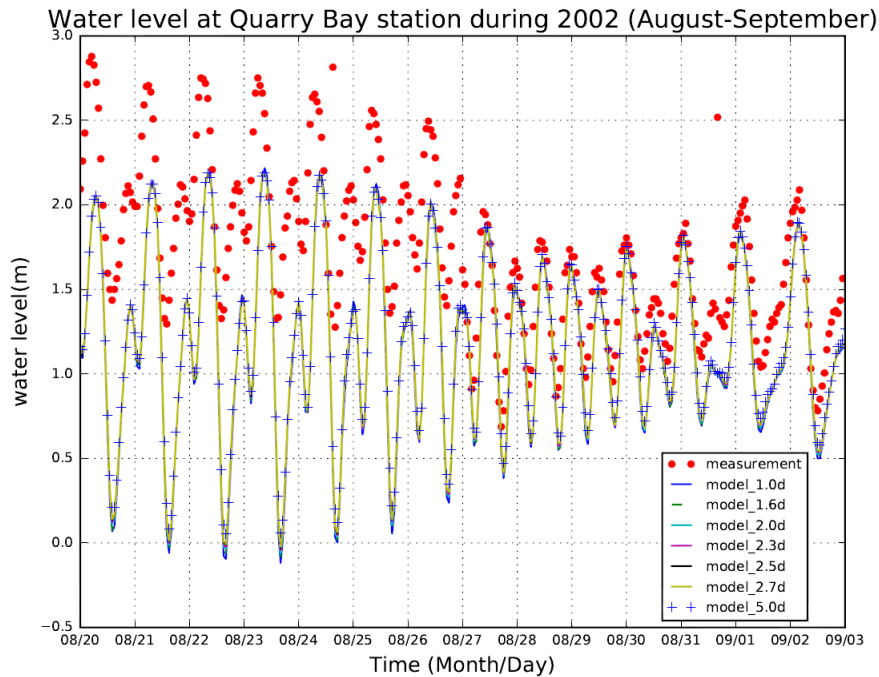


Fig. 2-28 The measured and hourly modeled water level at the Quarry Bay station from August to September in 2002 under different roughness scenarios

### **Dry Season**

We chose four tidal gauge stations, Waglan station, Shek Pik station, Quarry Bay station and Kat\_O station for the dry season model performance under different roughness scenarios in the year of 2002.

From the results, we could see the modeled tidal propagation showed greater amplification than the observation data in all stations (from Fig 2-29 to Fig 2-32). For example, there is no significant difference between the roughness 0.023 and 0.001 at Kat\_O station, which had a high consistency with the measurement data. However, compared to the observation data, the modeled data in roughness 0.05 is almost not acceptable. The tidal propagation has rarely effect on the water level in roughness 0.05 at this location. The peak water level of modeled data is about 2.0 meters, which is larger than the measurement data from 25 to 29 October at Kat\_O station.

There is a good coherence with the measurement data when the roughness value is 0.023 and 0.05 at Quarry Bay station (Fig.2-30), and there is almost no difference between roughness 0.023 and 0.05. When the roughness is 0.01, we could see the wave propagation speed is faster than other scenarios and observation data.

Waglan station almost has the same performance as other stations, the roughness 0.023 and 0.05 have the similar water level, and the phrase period is about 12 hours as we could see from Fig.2-31, which means the tidal effect is weaker when the roughness becomes higher. But when the roughness is lower, such as in 0.01, at the first few days from 29 January to 2 Feb, the modeled data has a good coordinate with the measurement data, even better than when the roughness are 0.023 and 0.05. However, in the latter days, after 2 February, the modeled result in 0.01 has a bad performance with the observed data. The emphasis is smaller than other scenarios, and the frequency is higher than other scenarios, too. Therefore, the modeled results of roughness 0.023 and 0.05 are more acceptable.

From Shek Pik station, there is barely a difference between different roughness scenarios. The results have good coordinates with the measurement data. In this case, as Shek Pik located in the main estuary of Pearl River, the river discharge has the limited influence on the water level.

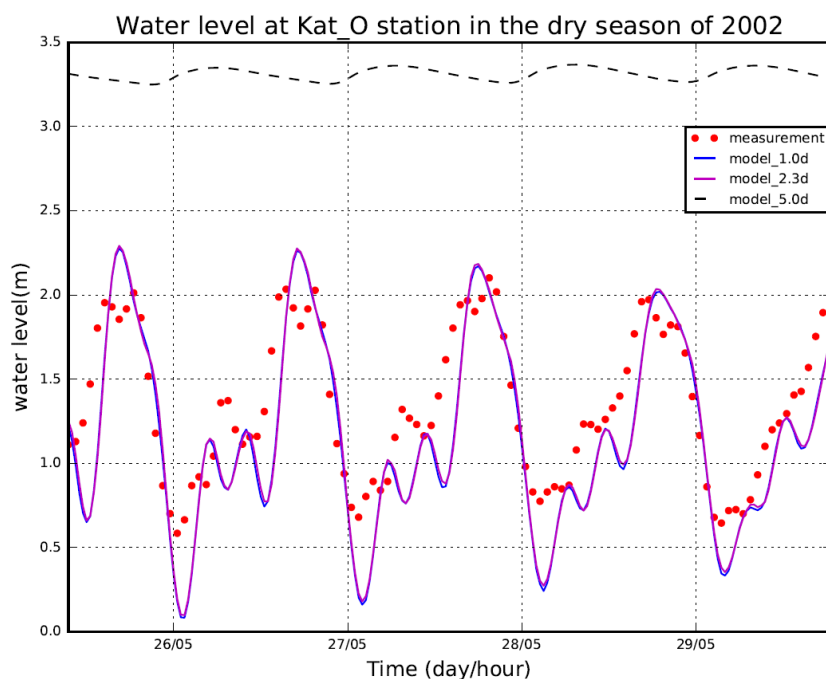


Fig. 2-29 The measured and modeled water level at Kat\_O station in October 2002 under different roughness scenarios

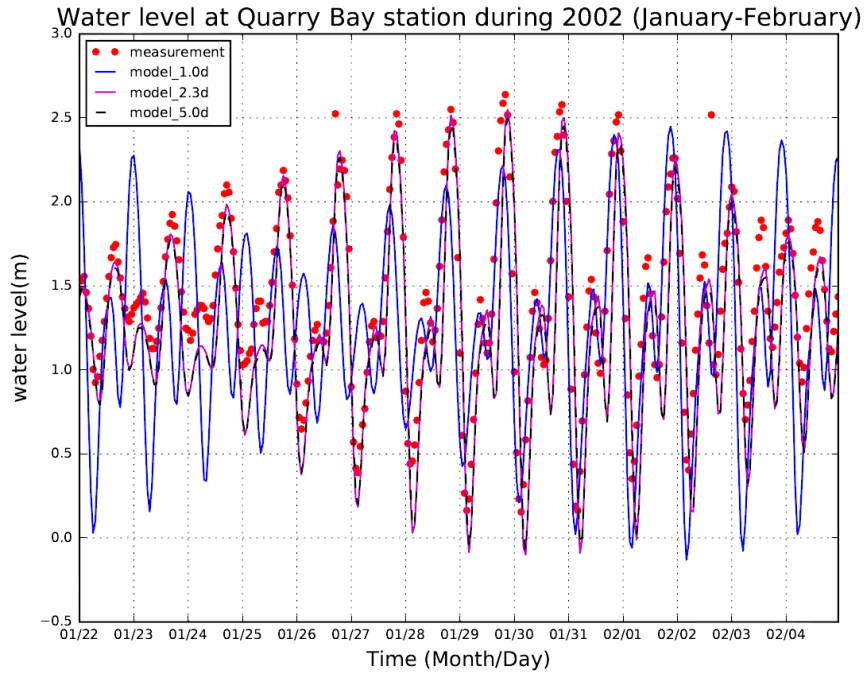


Fig. 2-30 The measured and modeled water level at Quarry Bay station from January to February in 2002 under different roughness scenarios

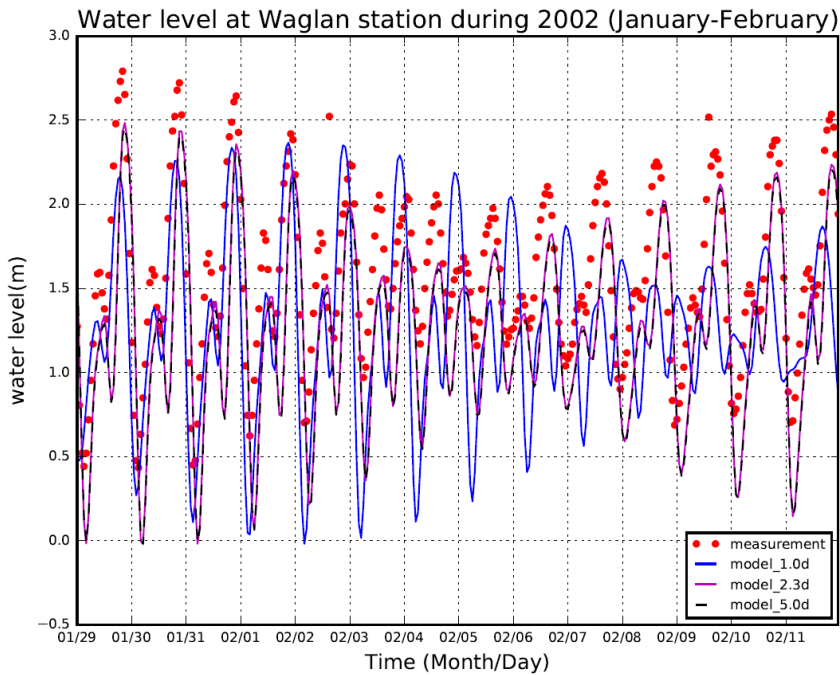


Fig. 2-31 The measured and daily modeled water level at Waglan station from January to February in 2002 under different roughness scenarios

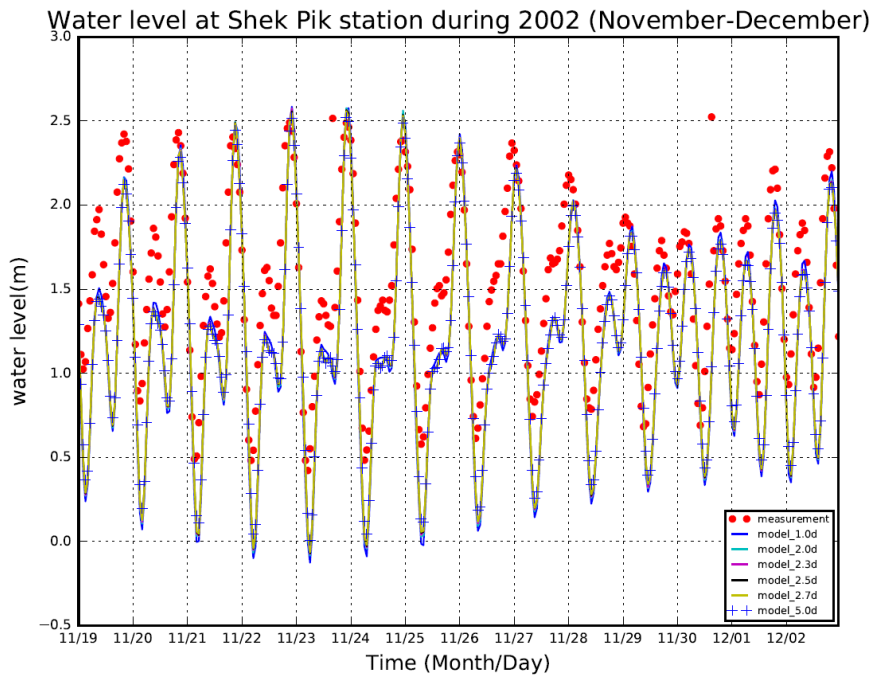


Fig. 2-32 The measured and hourly modeled water level at the Shek Pik station from November to December in 2002 under different roughness scenarios

### 2.4.3 Discussion of sensitive tests

Based on the calibration and validation of the PRD model, we could conclude that the relative appropriate Manning coefficient is 0.023. The Manning coefficient is highly sensitive in the region with discharge and tide propagation. The calibrated Manning's roughness coefficient of 0.023 also worked best for the estimation of peak river discharge and the maximum water level of tidal gauge station. The roughness coefficient, Manning's  $n$ , is highly sensitive at upstream with discharge in the winter dry season, is less sensitive in the coast region. The roughness coefficient is also less sensitive to the medium value, and more sensitive to the extreme high or low values. Additionally, the coefficient value is less sensitive to variations in the coastal extent.

### 2.5 Conclusion

This chapter introduced applications to simulate the coastal hydrodynamic process in the PRD by using numerical hydrodynamic models coupled with regional ocean models, resolving embayment tide dynamics, overtopping flows and overland flow along the coastal region. D-Flow Flexible Mesh provided a relatively better predict skill. Friction can cause a transition of energy among tidal species, as we chose D-

FLOW FM model as the further simulation on coastal inundation and climate scenarios study, we need to find a proper roughness for the D-FLOW FM model. Therefore we conducted a series of sensitive test analysis of roughness of D-FLOW FM model. A series of Manning's n coefficient varying from 0.01 to 0.05 was used as different roughness scenarios in the D-FLOW FM model. The simulation results demonstrated the relative optimal Manning coefficient for D-FLOW FM model is 0.023. However, we strongly suggested the roughness sensitive tests for the land mesh of D-FLOW FM model is necessary as well for the inundation plain study in the future.

## **3 The Impacts of Climate Change on Storm Surges and Coastal Inundation in the Pearl River Delta Region**

### **3.1 Climate Projections**

This Chapter investigated quantitative assessments of the potential impacts of climate change on typhoon induced coastal storm surges and coastal inundation. In this research, climate change is expected to affect the Pearl River Delta region by three main aspects, river discharge, tropical cyclones and the SLR (sea level rise). Therefore, we set up the climate projections for the hydrodynamic modeling based on these three aspects.

#### **3.1.1 Climate projections for the entire model settings**

We used the new Representative Concentration Pathways (RCP) scenarios to assess the impacts of storm surge on the coast under future climate change conditions in this study. The IPCC AR5 RCP 4.5 scenarios and RCP 8.5 scenarios are intended to apply in this research for the climate projections. RCP 4.5 represents a medium scenario in which the rate of radiative forcing is stabilizing till 2100. RCP 8.5 scenario represents a very high greenhouse gas emission until 2100. In order to keep the consistency of the climate projection, after compared to the IPCC report 4 and IPCC report 5, RCP 4.5 is parallel to the AR4 version B1 scenario when the global temperature will increase 2°C by 2100; RCP 8.5 is broadly comparable to the AR4 version A2 scenario when the global temperature will increase 4°C by 2100 (IPCC, 2014) (see Fig. 3-1).

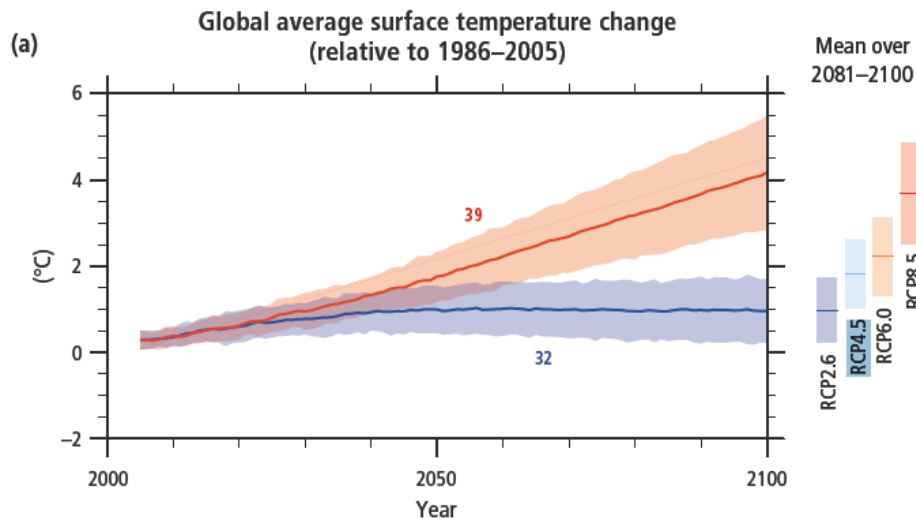


Fig. 3-1 Global average surface temperature change from 2006 to 2100 relative to 1986–2005 (IPCC, 2014)

### 3.1.2 Climate projections for river discharge

Few researches have yet been conducted on the impacts of climate change on the hydrology progress of the Pearl River. The research community believes that the annual discharge in the Pearl River showed the increasing trend (Zhang et al., 2008). For example, Liu lüliu et al. (2012) investigated the annual precipitation and runoff changes using the climate model NCAR-CCSM3\_0, MPI-ECHAM5 and CSIRO-MK3\_5. They found that the annual precipitation and runoff will increase maxima 15.5% under climate scenarios B1 by 2100, correspondingly increase maxima 26.4% under climate scenarios A2 by 2100, compared to the reference period of 1961-1990. The highest magnitudes can be found at the coast and delta. The increased runoff in the high flow season can bring larger floods and raise the flood frequency. However, this research didn't consider the influence of human activities on the river basin discharge changes (Liu et al., 2012).

Liu et al. used the similar approach to simulate the daily stream flow in Xijiang River (One of the three main tributaries of Pearl River using hydrological model HBV-D under the SRES A2, A1B and B1 driven by the same Global Climate Models). The results showed the high flow in wet season will increase around 15% under climate scenarios B1 till 2100, correspondingly approximately between 15% and 30% till 2100 under climate scenarios A2 (Liu et al., 2012).

Jianting Cao, Guoyu Ren and Tong Jiang stated that the annual average discharge of Pearl River downstream part would increase 23.4% under climate scenario SRES-A2 by 2100, will increase 20.8% under climate scenario SRES-B2 by 2100 compared to the baseline period (1956-2000). Luo yong et al. (2006) calculated the annual discharge under climate scenario SRES-A2 and SRES-B2 by using climate model under the hypothesis that there is consistency interrelation between river discharge and precipitation compared to the baseline scenario (1961-1990). He concluded that the annual discharge in downstream of Pearl River would increase from 7% to 10% in the middle of the 21st century and it would rise to 20% at the end of the 21st century under SRES-B2 ( Ren Guoyu, 2007).

Dan Yan et al. (2015) assessed the impacts of climate change on seasonal discharge and extreme flows using the VIS model forced by multiple climate models under the new IPCC scenarios RCP 4.5 and RCP8.5. They concluded that climate change could affect the timing and magnitude of high, low and mean flows in the Pearl River basin. The mean projected high flow would increase between 10% and 20% under RCP4.5, would increase ranging from 20% to 30% under RCP8.5 in the Pearl River downstream basin for 2079-2099 relative to 1979-1999.

There have been opposite research statements. Wu et al. (2014) found less increasing trends in high flow under the RCP4.5 scenarios in the Beijiang River Basin (Wu et al., 2014). Guan.(2010) analyzed the runoff of Luoding River Basin and Xinxin River Basin (part of Xijiang River) under different climate scenarios (SRES A1B, A2, B1) using Reliability Ensemble Averaging method. The results showed a decrease trend runoff in autumn and spring, and there is no significant change in winter and summer. However, she stated that the uncertainty of the method and global climate model in the special region contributed the negative results (Guan, 2010).

Therefore, we can conclude that the majority of researchers are more focused on the increasing trend of the river discharge in the PRD under the future climate change. Therefore, this research is based on two assumptions regarding the impacts of climate change on the river discharge of the Pearl River.

Firstly, I applied multiple scenarios (RCP4.5 and RCP8.5) in the future time frame until 2100 for the climate projection in this research. Since the extreme storms always

happen during July and August, we used high flow as river discharge in our modelling settings. The high flow in downstream discharge in the PRD will be 10% higher than the baseline (1999) under medium emission scenario RCP 4.5 by 2100, whereas it is likely to increase by 20 % the highest emission scenario RCP 8.5 by 2100.

Secondly, the river discharge for climate scenarios analysis is daily discharge data, while we used minutes discharge data for the numerical hydrodynamic model simulation. For the sake of clarification, the error between the 'daily discharge' and 'minute discharge' is thought to be negligible in this study.

### **3.1.3 Climate projections for tropical cyclones**

The storm surge is a long-period wave induced by extreme winds and air pressure gradients (FENG et al., 2014). Along the coast, the storm is often the greatest threat to life and property<sup>4</sup>. Coastal inundation risk caused by storm surges becomes the major risk and the leading cause of death and injury among natural disasters affecting the coastal region (UNDP/BCPR 2004).

The PRD region is a vulnerable region where suffers tropical cyclones every single year. Several researches have been conducted on the typhoon activities not only in northwest Pacific but also along the PRD region. However, it remains uncertainties especially in the individual basin scale like the PRD region. Most of the numerical simulations of typhoon intensities have the increasing trend, but the observation database set showed different results depends on the different dataset (Feng et al., 2014; Walsh et al., 2016; He et al., 2003). For example, the South China Sea region occurs a decreasing typhoon trend over the 60-yr time frame, but the eastern Asia shows an apparently increasing trend during the past 40 years (Walsh et al., 2016). Both the extreme intensity and the average intensity of typhoon affecting the Pearl River Delta have decreased throughout the analysis period, including the most recent decade (Chao et al., 2012). Some statistic analysis stated that the frequencies of strong storm surge during 1996-2005 were 2.5 times compared to 1949-1995 in the PRD region (Chang et al., 2008).

---

<sup>4</sup> <http://www.nhc.noaa.gov/surge/>

The data of typhoons affecting the PRD region were collected since the year of 1970. Then the frequencies and intensities of typhoon were summarized. The results showed in the Fig.3-2, there are three peak periods during last 40 years in PRD region for the frequency trend. One is from 1970 to 1980. The second is from 1993 to 2003. The other is from 2009 to 2013. The trends of typhoon intensity we could see from the Fig.3-3, the maximum pressure is higher exclusive in the year 2003 and 2008. Overall, given the available qualitative analysis on the observed data, the potential errors raised from past changes in observing capabilities (Knutson et al., 2010), the relationship between typhoon and climate change remains a challenge topics not only in the individual scale but also globally (Knutson et al., 2010).

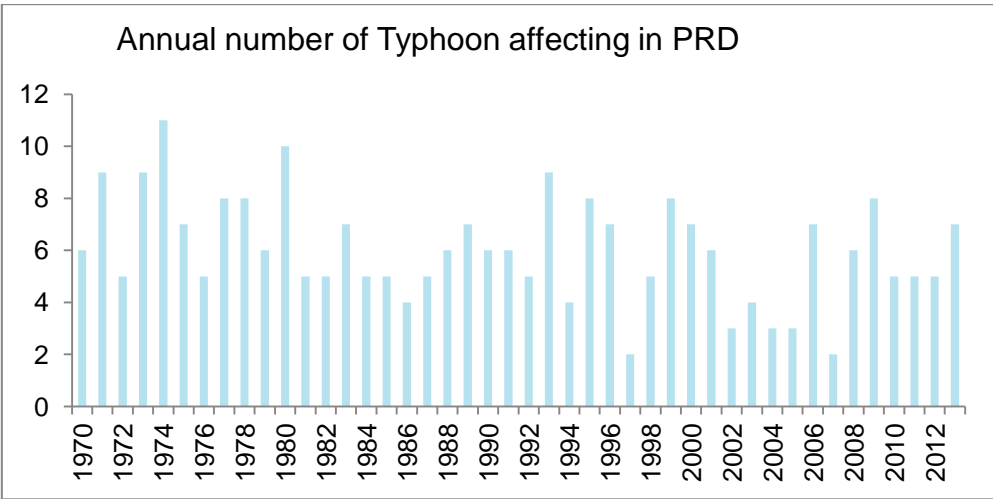


Fig. 3-2 Frequencies of typhoon in the PRD region after 1970

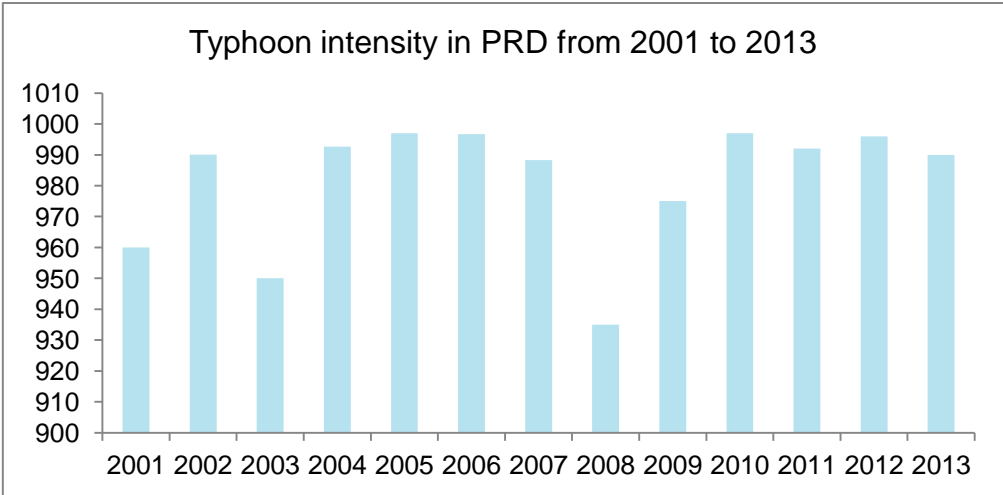


Fig. 3-3 Intensity changes of typhoon in the PRD region from 2001 to 2013

The climate theory of tropical cyclone formation remains elusive (Walsh et al., 2016). Researches show large differences among different modelling results and observation

studies for all of the typhoon parameters (typhoon frequency, tracks, intensity) related to climate change (Knutson et al., 2010). The mean sea level rise and the sea surface temperature (SST) rise are the two main factors related to climate change. Knutson et al. concluded that global mean tropical cyclone frequency would likely either decrease or remain essentially unchanged due to greenhouse warming based on existing modelling studies and limited existing observations (Knutson et al., 2010). However, the theoretical basis for relationships between climate and tropical cyclone intensity is well established (Walsh et al., 2016). Climate change is expected to affect tropical cyclones by increasing sea surface temperatures (SST) globally, a key factor that influences cyclone formation and behavior. The empirical relationship between the SST and typhoon intensity was used to calculate the change of typhoon wind fields in 2100 due to climate change, the results showed the typhoon intensity has a strong correlation with higher sea surface temperatures in the western Pacific (Kerry Emanuel, 1987, 2005, 2008). In addition, climate models continue to predict future increases in the intensities of the strongest storms (Walsh et al., 2016). Based on theories of potential intensity (Emanuel, 1987; Holland, 1997) and studies on higher resolution modeling, global maximum wind speed could increase by 2% to 20% over the 21st century (Knutson et al., 2010; Emanuel, 1987; Holland, 1997). According to IPCC report in 2007 and 2014, the SST will increase by 2.0°C to of 4.0°C at the end of 21 century (IPCC, 2007; IPCC, 2014). The maximum cyclone wind speed would be increased by 10% and 20% under an increase in SST by 2.0°C and 4.0°C, respectively (Emanuel, 1987).

Therefore, in this research, we set the climate projections based on maximum cyclone wind speed in order to represent the typhoons intensity increase due to the SST rise (Emanuel, 1987). The scenarios of the experiments are listed in Table 3-1. We used the same grid and open boundary conditions in all experiments for these future scenarios simulation to give insights into what might occur in the future.

#### **3.1.4 Climate projections for sea level rise**

Since the middle of the 19th century, sea level has risen about 0.17 m (Houghton et al., 2001; Miller and Douglas, 2004; Lombard et al., 2005; IPCC, 2007). It will likely contribute to an increase in storm surge risk along the coastal regions (Walsh et al.,

2016), although the regional differences exist due to various factors, including climate change (Knutson et al., 2010). Sea level rise has far-reaching impacts on low-lying coastal regions all over the world and can greatly increase the risks of coastal floods caused by storm surges (Morris et al., 2002; Nicholls, 2002; Rybczyk and Cahoon, 2002; Tian et al., 2010). Therefore it is very important to study the impacts of sea level rise on future typhoon induced coastal storm surge and inundation risk.

The State Oceanic Administration of China and the Intergovernmental Panel for Climate Change predicted the sea level rise in China would be between 22 cm and 88 cm by 2100 (Chen, 1997; IPCC, 2007). In this research, we used these statements as sea level settings in the modeling simulations.

Consequently, regarding to all of the researches on the impacts of future climate change on the PRD region, they either focus on the river discharge response under climate change, or focus on typhoon activities changes under climate change, or the SLR in the future climate change, but a research gap remains in considering all of the three aspects together to understand the influence and contribution of climate change impact on storm surges and coastal inundation in the PRD region. In this research, we aim to improve the knowledge in this field.

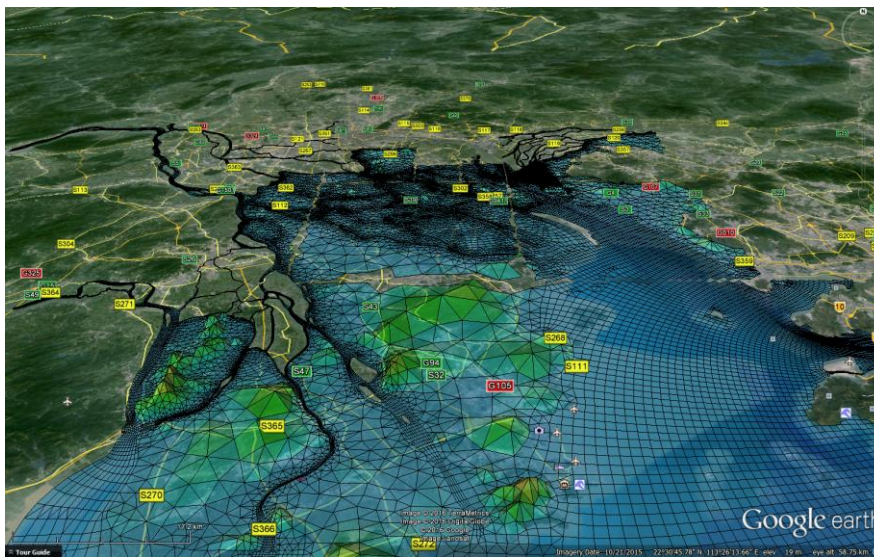
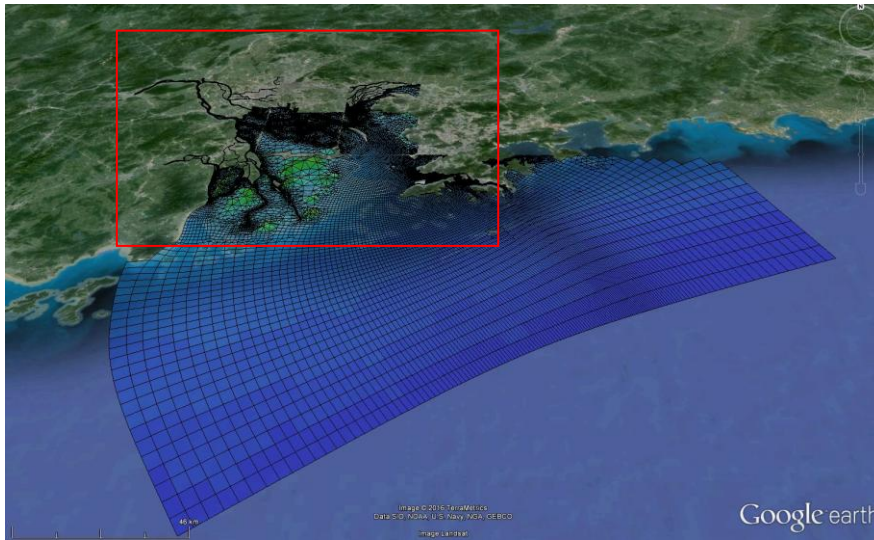
## **3.2 Materials and Methodologies**

The uncertainties and inaccuracies lie in climate models to predict storm surges caused by typhoons, so in this research, I used hydrodynamic modelling to predict the typhoon induced storm surges with climate projections we have concluded above. In order to guarantee the stability of the model, 10-15 days were used in the modelling configuration as a modelling warming period before the start of the typhoon.

### **3.2.1 Mesh Generation**

In order to explore the coastal inundation risk, I added the onshore land mesh on the PRD model from Chapter 2. The land mesh includes ten mega cities (Guangzhou, Shenzhen, Zhuhai, Macao, Zhongshan, Foshan, Zhaoqing, Jiangmen, Huizhou and Dongguan) which belong to the PRD economic zone within 30-meter contour line. There are totally 78296 nodes and 95437 elements for this newly generated model.

The mesh resolution is varying from meters at the inland to kilometers at the open sea (Fig.3-4).



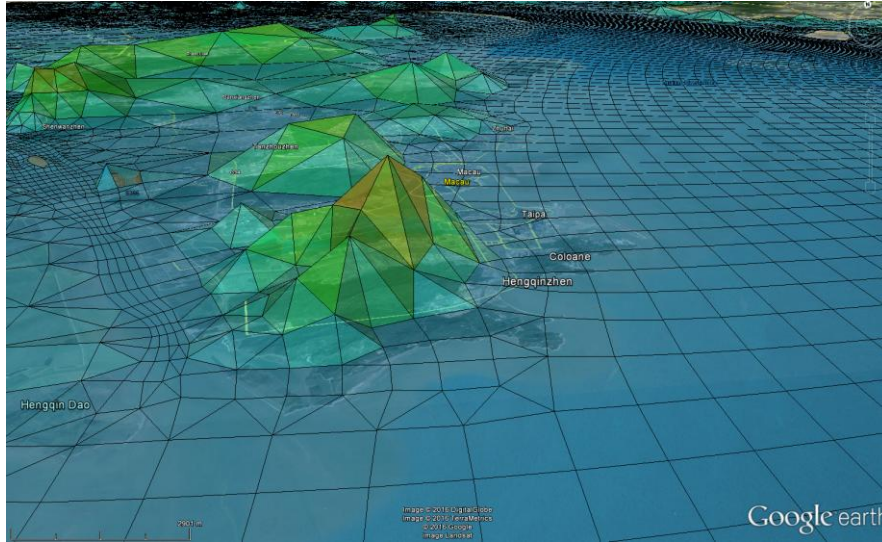


Fig. 3-4 D-FLOW FM model mesh network visualization from Google Earth in different scales

### 3.2.2 Topography

For the simulation of typhoon induced coastal storm surge and inundation risk, the Digital Terrain Model (DTM) data should be used for the land topography. Digital Elevation Model (DEM) obtained from SRTM data is a subset of DTM and the most fundamental component of DTM (Fig.3-5). It did not indicate “bare-earth” surface or Digital Terrain Model (DTM), the actual height cannot be reflected in areas where land covered by the noise like tree canopy and/or buildings in urban regions (Zandbergen, 2008). Therefore we adjusted the overestimated elevations of SRTM DEM data to match with the real elevation of terrain because this study area is located in the low part of the Pearl River basin. In our research, the DTM data from Google Earth is used for the land geomorphologic map. At the same time, places used for elevation collaboration must have bare surface or existing sparse and low trees like paddy field, bare soil, thus the SRTM DEM data from 2000 year was selected for calibration. The results show the confidence on the Google Earth elevation data, but the resolution is various, then the sample file is interpolated in the DFLOW Flexible mesh modelling.

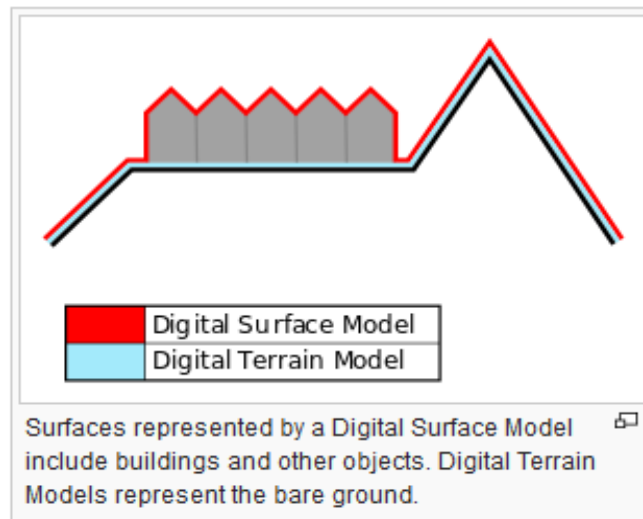


Fig. 3-5 The differences between DTM and DSM model <sup>5</sup>

### 3.2.3 Boundary conditions

#### *River Discharge*

In this research, we applied the wet season river discharge in the year of 1999 as the baseline scenarios (S0). As the discussion above, the river discharge of RCP4.5 (S1) scenario by 2100 will be 10% higher than the baseline scenarios (S0), correspondingly, there will be 20% higher than the baseline scenarios (S0) under the RCP8.5 (S2) scenario. The time resolution is minutes in two month period.

#### *Typhoon forcing*

In this research, we used the 'Wind Enhance Scheme' (WES, initially developed by the UK Met Office for cyclone modelling) to generate tropical cyclone surface wind fields and central air pressure. This numerical model is based upon Holland (1980), including the typhoon parameters such as the typhoon track, the maximum wind speed ( $V_{max}$ ), the central pressure and radius to maximum winds (Deltares, 2016).

Based on this model, we selected three typhoons from different landfall locations in different years which had significant influence and huge economic losses along the PRD coast. They are typhoon Utor in 2001 in the east direction, typhoon Dujan in 2003 in the middle, typhoon Haugupit in 2008 in the west direction. The typhoon track

<sup>5</sup> [https://en.wikipedia.org/wiki/Digital\\_elevation\\_model](https://en.wikipedia.org/wiki/Digital_elevation_model)

file consists of the location (lat, lon) of the typhoon centre, the maximum wind speed ( $V_{\max}$ , m/s) and pressure drop (Pdrop) of the centre (millibar) with the 6 hours time resolution. For the baseline scenarios (S0), the track data of Utor and Dujuan was from Wenzhou Typhoon Website <sup>[32]</sup>, Hapugit was from HongKong Observatory in 2008. The standard air pressure is either 101300 pa or 100000 pa. I used 101300 pa to calculate the Pdrop for typhoon Dujuan. In order to keep all pdrop values in a positive value, I used 100000 pa to calculate the Pdrop for typhoon Utor and Hagupit and then deleted the negative ones at the genesis location or dissipated points of typhoon.

For the future climate scenarios, as we discussed above, the increase of maximum wind speed represents the increase of typhoon intensity under climate change. The theory function is based on Emanuel's reversible ascent formulation of potential intensity theory.

$$V_{\max} = 3.447(1010 - P_0)^{0.644}$$

Vmax is maximum wind speed, P0 is central pressure. In this function, the relationship between the central pressure and the maximum wind speed is based on an analysis of 28 years of maximum wind measurements made at the coastal and island stations in the northwestern Pacific (Atkinson and Holliday, 1977). The forward speed of the typhoon center can be calculated according to the typhoon path. As the assumption we introduced above, the Vmax under RCP 4.5 is 10% higher than the baseline scenario (S0), then I calculated the corresponding P0. The same method was applied to the RCP8.5 scenario. In the following parts, the characters of three typhoon cases as forcing conditions were introduced.

### **Description of Utor (1 - 8 July 2001)**

Typhoon Utor entered the South China Sea and approached the coast of Guangdong on 5 July, then made landfall near Shanwei (Eastern PRD) and then tracked generally westwards across Guangdong. Utor affected the PRD region over 40 hours after landfall. The winds subsided and Utor weakened into a lower storm at 11.20 am on 6 July. Utor circulation was extensive, its radius reaching some 1 000 km. Utor is coupled with the astronomical high tide, inducing the extremely high storm tide at

many measurement stations such as 3.6 metres at Tsim Bei Tsui and 3.4 metres at Quarry Bay at around 9 to 10 a.m. It caused 25 cases of flooding. For example, in Hongkong, Tai\_0, some villages along Deep Bay, numerous places in the northwestern New Territories, Kennedy Town Praya, Lau Fau Shan and Sheung Wan suffered the most severe flood in the last 40 to 50 years during Utor. When it crossed Guangdong, over 4 000 houses were damaged, 7.58 km<sup>2</sup> of farmland were submerged, 5 km<sup>2</sup> of fishponds were destroyed and 23 persons were dead. The direct economic losses were about 2.4 billion RMB (326.8 million Euros) (HongKong Observatory, 2001).



Fig. 3-6 Track of Utor: 1 - 8 July 2001

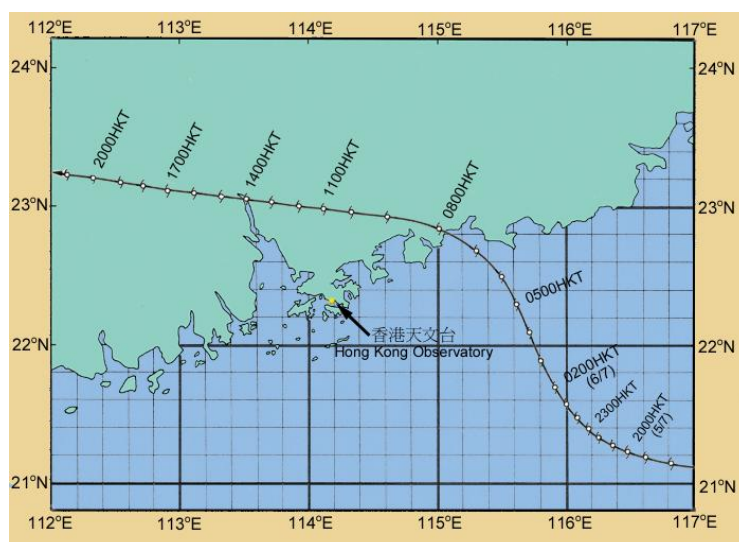


Fig. 3-7 Track of Utor near Hong Kong

### Description of Dujuan (29 August - 3 September 2003)

Dujuan headed into the South China Sea on the early morning of 2 September and made landfall in the middle of the PRD region. Dujuan with the strong northwesterly winds crossed the north of Hong Kong and then moved forward to Shenzhen at around 22:00 pm on September 2. It weakened rapidly into a tropical storm on the morning of September 3 and dissipated over Guangxi afterward. Dujuan is double eyes structured typhoon with the diameter of the inner and outer eyes about 20 km and 100 km respectively. During the approach of Dujuan, huge casualty happened in Guangdong and Hongkong. There are 40 people dead and about 1 000 injured in Guangdong and 24 people injured in Hongkong. Power supplies were suspended in 90 % of the area in Shenzhen. Almost 400 flights were either cancelled or delayed at Hongkong airport. The direct economic loss was approximately 2.3 billion RMB (313.2 million Euros) (HongKong Observatory, 2003). Table 3-1 gives the maxima sea level at tide gauge stations during Dujuan.

Table 3-1 Times and heights of the maximum sea level at tide stations during Dujuan

Station	Maximum sea level (above chart datum)		
	Height (m)	Date/Month	Time
Quarry Bay	2.59	2/9	22:40
Shek Pik	2.63	2/9	23:37
Tai Po Kau	3.54	2/9	22:08
Tsim Bei Tsui	3.12	3/9	01:22

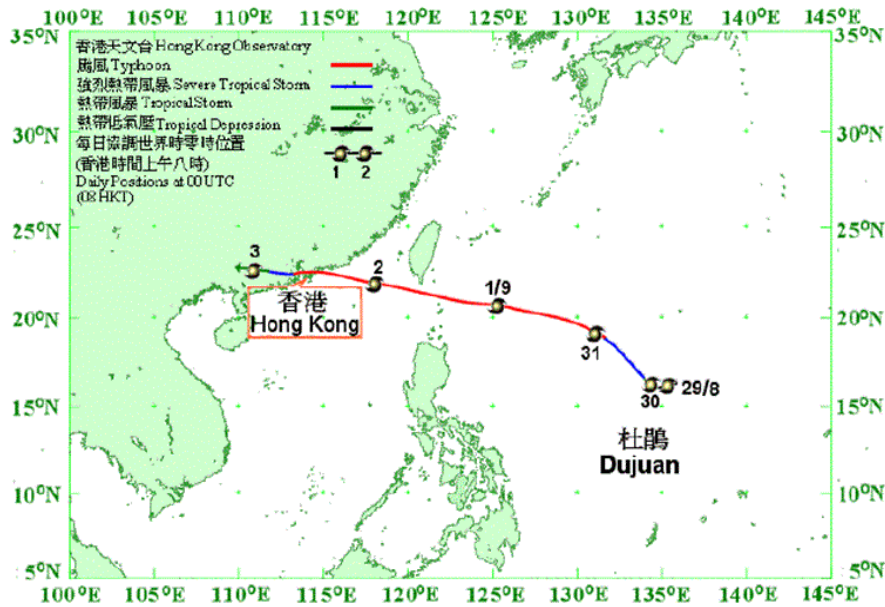


Fig. 3-8 Track of Dujuan: 29 August – 3 September 2003

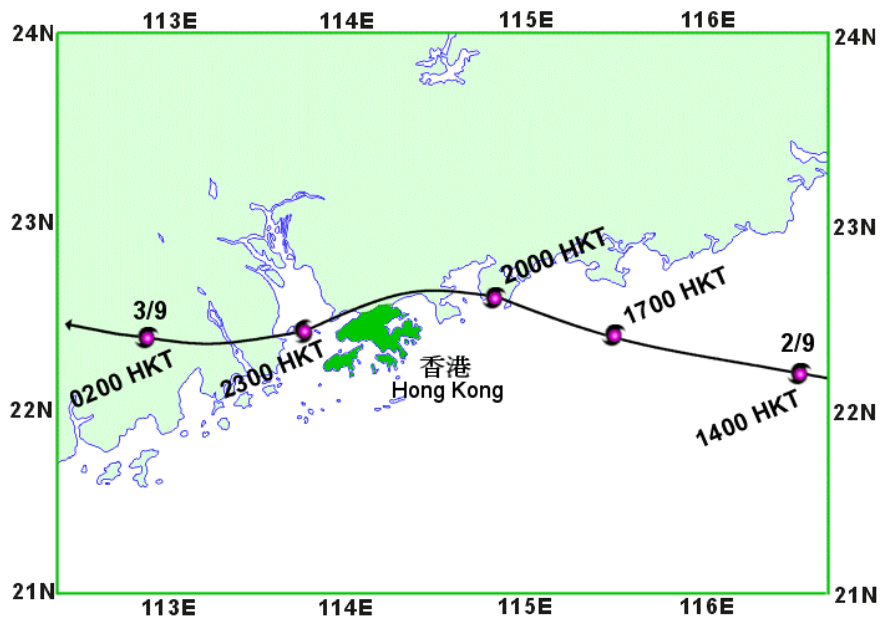


Fig. 3-9 Track of Dujuan near Hong Kong

### Description of Hagupit (19 – 25 September 2008)

Hagupit was the most intense typhoon affected the PRD region and caused a huge economic loss around 5.8 billion RMB (789.9 million Euros) in the year of 2008. It approached southwest of Hong Kong around 10 p.m. on September 23, then made landfall in western Guangdong on the morning of September 24. Finally, it subsided as a tropical depression on the morning of September 25 in Guangxi. The maxima

wind force circle radius is about 50-80 km. The combined effect of storm surges and high tides induced floods and damages along the coastal areas. 16 flooding cases were reported in Hongkong, including Tai O, Peng Chau, Tuen Mun, Sham Tseng, Sai Kung, Yau Tong, Lei Yue Mun and Chai Wan. The maximum sea level even reached 3.53 metres at Quarry Bay and 3.77 metres at Tai Po Kau in Hongkong during the passage of Hagupit. Several popular beaches along the bay and islands were suffered severely damaged. The worst weather condition made over 400 flights at the Hong Kong International Airport cancelled or delayed. Hagupit led to about 8.5 million people affected and at least 58 people injured, over 14 000 houses were destroyed (HongKong Observatory, 2008).

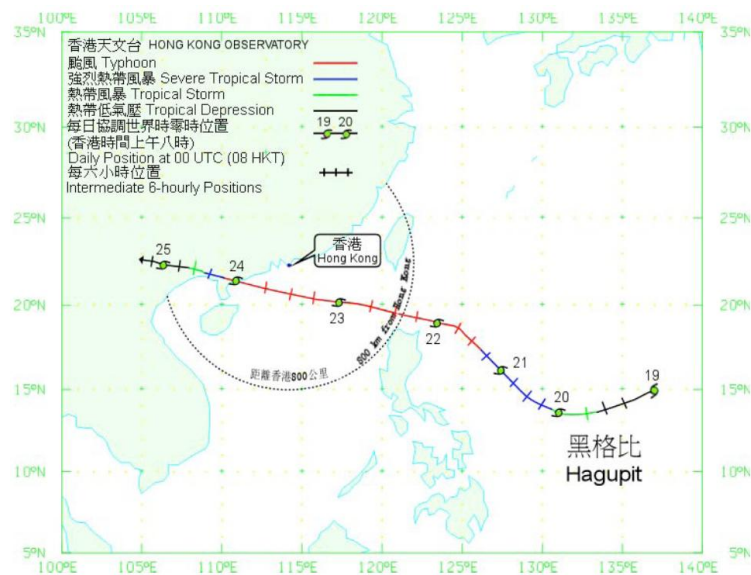


Fig. 3-10 Track of Hagupit on 19 – 25 September 2008

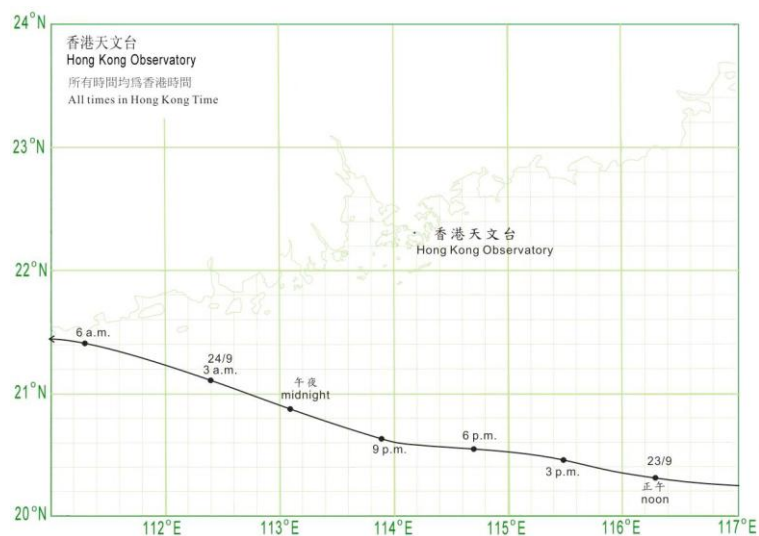


Fig. 3-11 Track of Hagupit near Hong Kong

### **Sea level rise and tidal current data**

Except for the typhoon forcing condition, we need to set up the open boundary for the modelling. In this Chapter, we used the same tidal current data of the PRD model in Chapter 2 as the open boundary condition. They are the amplitudes and phases of 10 major tide constituents, SA, O1, P1, K1, N2, M2, S2, K2, M4, MS4 and a residual current A0.

Sea level prediction results from the State Oceanic Administration of China and the Intergovernmental Panel for Climate Change were used as initial conditions. That is 22cm sea level rising when the temperature is rising to 2°C comparable with the medium emission scenario RCP4.5; 88cm sea level rising when the temperature is rising to 4°C comparable with the extreme emission scenario RCP8.5 by2100 (Chen, 1997; IPCC, 2007, IPCC,2014). To sum up, all scenarios are listed in table 3-2.

Table 3-2 Experiments under different climate scenarios

Climate scenarios	Modelling setting up
Baseline scenarios (S0)	Typhoon in baseline scenarios (S0)
2°C / RCP 4.5/ A1B (S1)	10% rise in typhoon and river discharge + 0.22 SLR (S1)
4 °C / RCP 8.5/ A2 (S2)	20% rise in typhoon and river discharge + 0.88 SLR (S2)

### **3.3 Results**

In chapter 4, I designed and carried on 9 experiments based on three typhoon cases (Utor, Dujan, Hagupit) in order to explore the impacts of future climate change (river discharge, typhoons and SLR) on the coastal storm surges and inundation extent in the PRD region. We used four tide gauge stations, Kat\_O, Waglan, Quarry Bay and Shek Pik station to study the storm tide changes during different typhoons under different climate condition. Another two stations at upstream, Makou and Pinggang station was used for analyzing the river discharge changes in these three typhoon cases under different climate scenarios. Fig.3-12 shows the location of all stations.

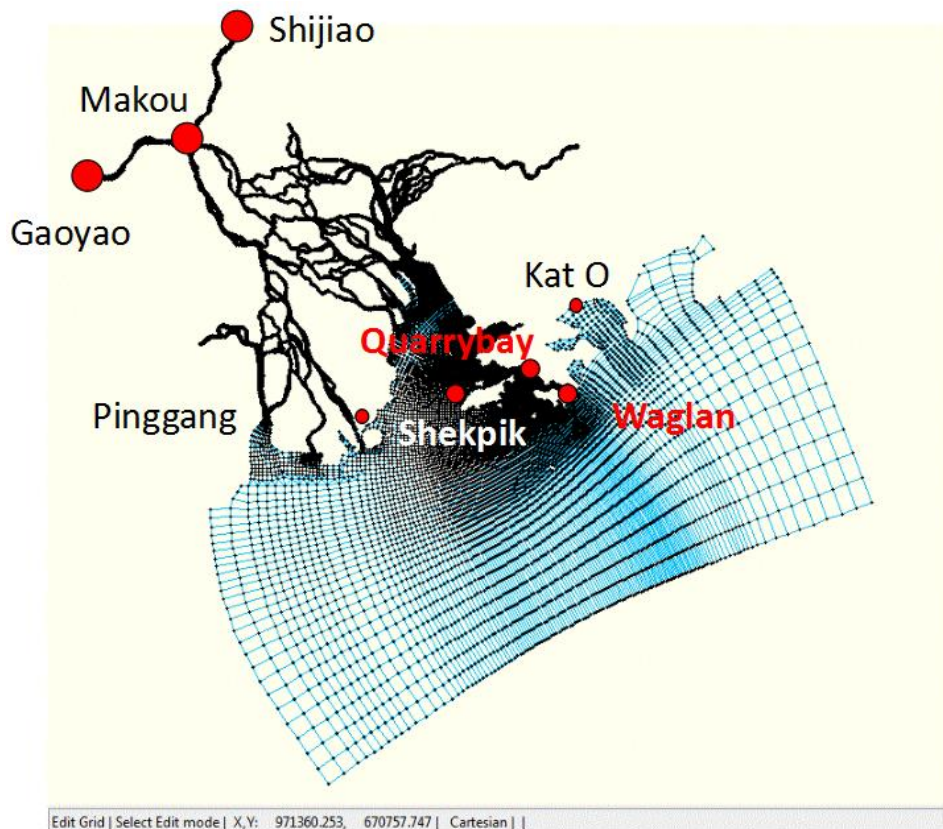


Fig. 3-12 Location of all of the observation stations

Two concepts are needed to be clarified before showing the results. The storm tide is different from storm surge. Comparing to the storm tide, the storm surges are more sensitive to climate change because we set up the climate projections for river discharge, tropical cyclones and sea level rise. In this research, we didn't subtract the storm surge elevations from the entire storm tides. The results from hydrodynamic modellings contain storm surges and tides.

### 3.3.1 The Impacts of climate change on peak water levels at tidal gauge stations

I have concluded the impacts of climate change on peak water levels at tidal gauge stations from three typhoons cases individually.

#### *Dujuan*

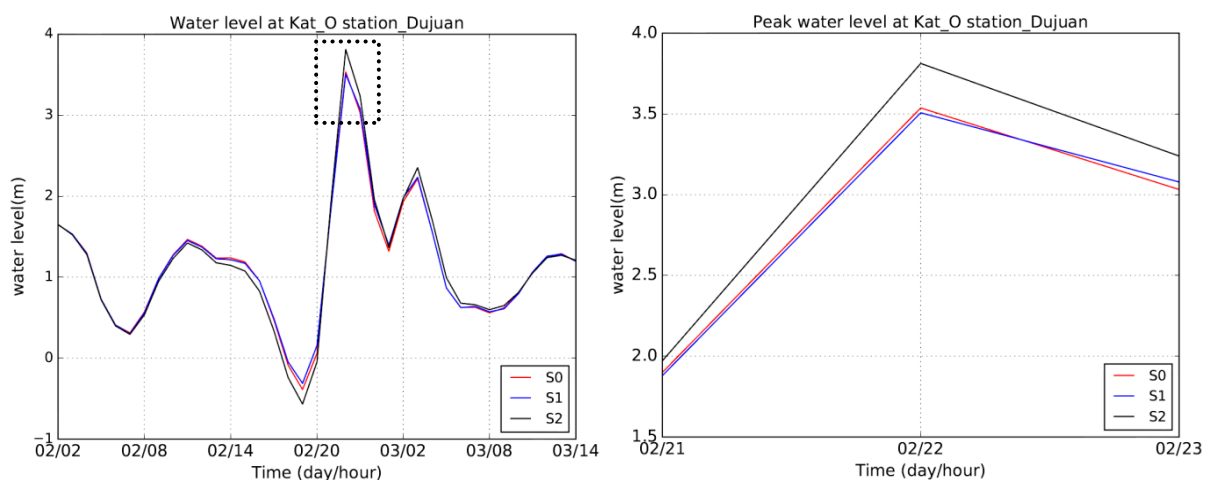
The results from Dujuan showed that the increased river discharge, typhoon intensity and SLR affected the peak water levels, but the changes were different in different locations and different climate scenarios.

The climate scenario RCP 8.5 (S2) resulted in an absolute water level rise during Dujuan at all pilot stations, and the maximum rise happened when the water level reached the peak (Fig.3-13). The peak water level at Kat\_O station of RCP 8.5 (S2) scenario dramatically increased by 30cm (the peak level, 3.815m), 8% higher than baseline scenario S0. Both Shek Pik and Quarry Bay station of RCP 8.5 (S2) scenario increased to around 2.5m, almost 4% higher than baseline scenario S0. The peak water level at Waglan station is the lowest one (2.3 m), with an increase by 2% compared to S0.

However, as we can see from Fig.3-13, the impacts of the climate scenario RCP 4.5 (S1) on increasing peak water level is not as significant as RCP 8.5 (S2). The peak water level at the Shek Pik station increased by 5.5cm in the scenario RCP 4.5 (S1) compared S0, by 2cm at Quarry Bay station and by 1.4cm at Waglan station. At Kat\_O station, the peak water level declined by 3.6cm under the scenario RCP 4.5 (S1) compared to S0.

Additionally, the duration of the peak surge in the RCP 8.5 (S2) was likely to increase with hours. This important finding indicated that substantial impacts could increase the flood duration risk along the coast.

Therefore, it can be concluded that the peak water elevation would increase at a maximum 8% due to climate change in the PRD region. When there is a typhoon with the intensity and track attributes similar to Dujuan, in the future climate change may increase peak surge elevation.



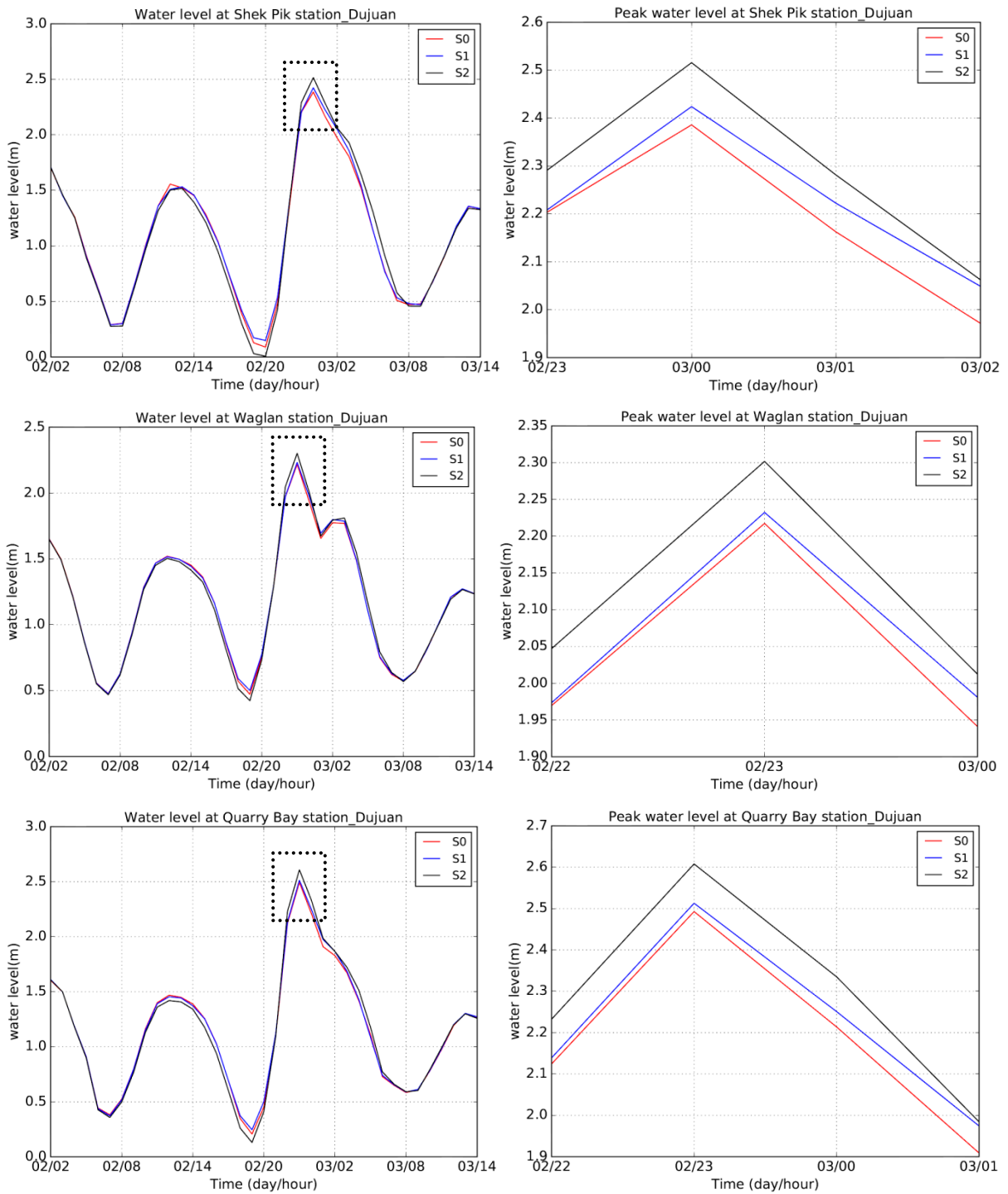


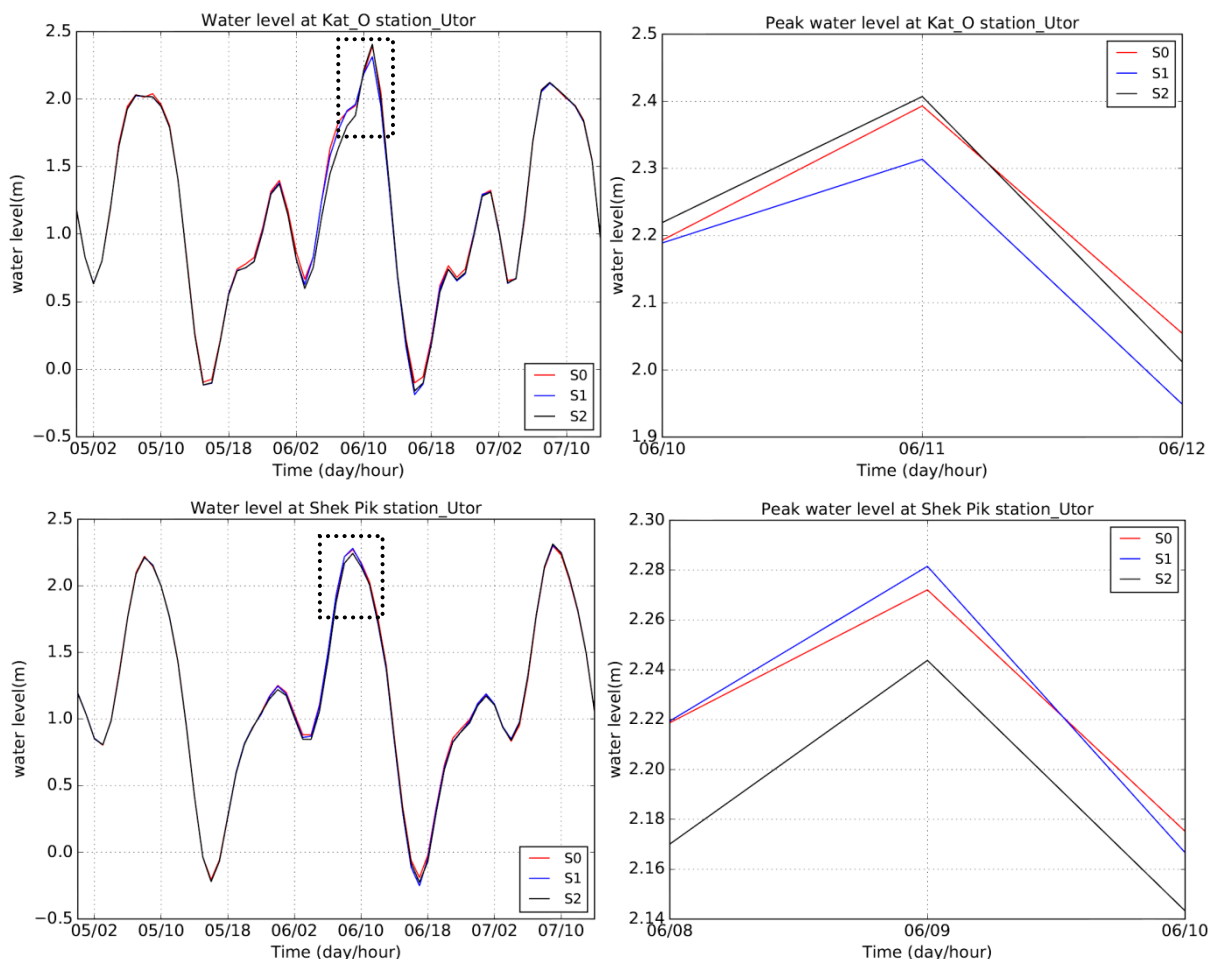
Fig. 3-13 Simulated water level changes and peaks at gauge stations (Kat\_O, Shek Pik, Waglan and Quarry Bay) during Dujuan under S0, RCP4.5 and RCP8.5

**Utor**

Compared to the moving track of Dujuan, Utor tracked even eastwards across the PRD region. The following figure (Fig.3-14) presents the increased typhoon intensity, river discharge and SLR affected the maximum water level at the four stations during

Utor. The results of peak water level during Utor displayed a varied trend under different climate scenarios. The peak water level also happened at Kat\_O station. Under RCP8.5 (S2) scenario, the peak water level was 1.2cm (5%) higher than baseline scenario S0 at Kat\_O station. All other three stations had a negative trend at the extreme climate scenario RCP8.5 (S2). For the climate scenario RCP4.5 (S1), there was a 1.4cm increase of the peak water level at Shek Pik station, other three gauge stations also represented decreasing trends. At Kat\_O station, the peak level declined by 8 cm considerably.

Therefore, when typhoons have attributes similar to Utor and make western landfall, climate change could result in a decreased trend of the peak water level due to the relative position of pilot stations and typhoon tracking. The details will be explored later in the discussion.



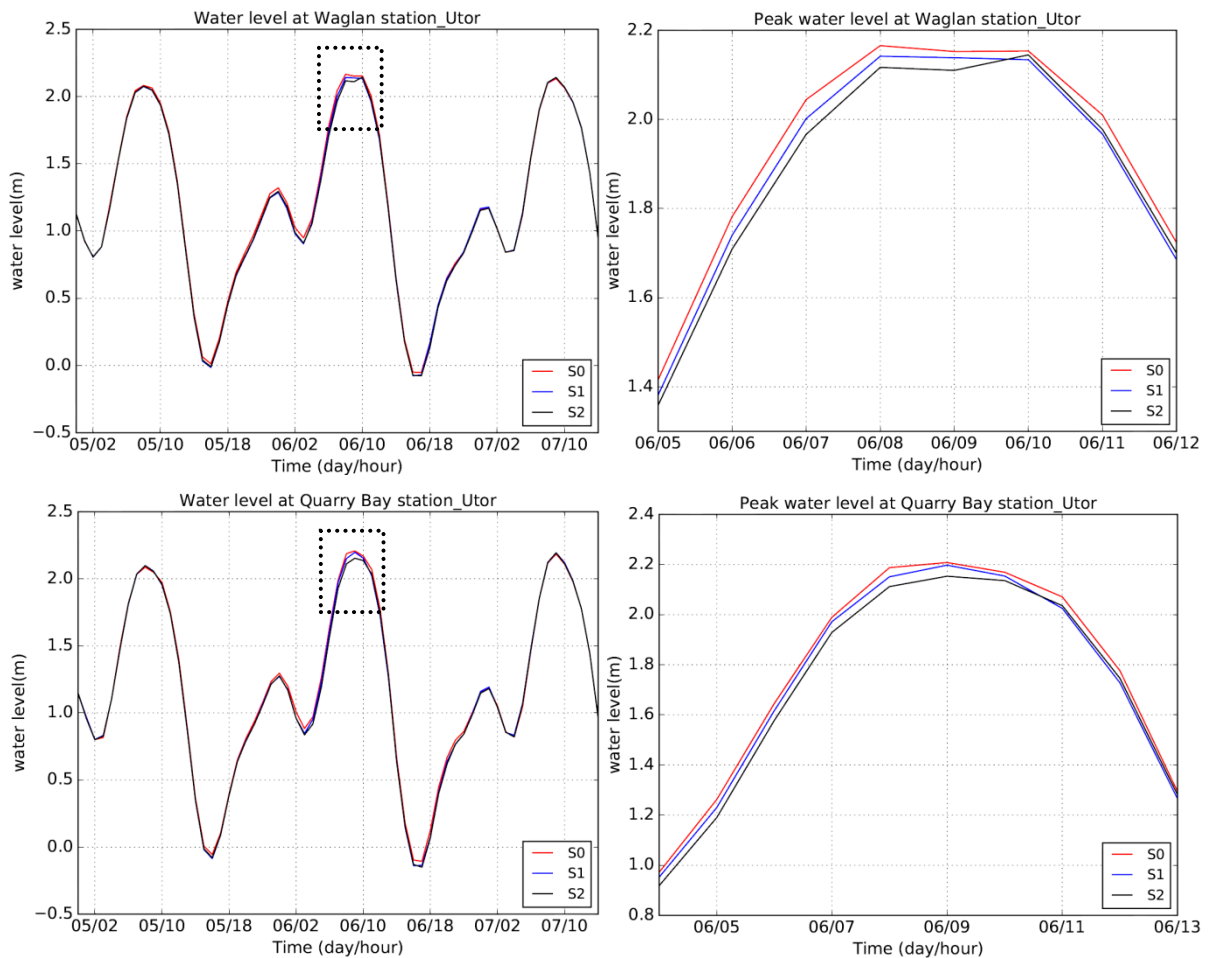


Fig. 3-14 Simulated water level changes and peaks at gauge stations (Kat\_O, Shek Pik, Waglan and Quarry Bay) during Utor under S0, RCP4.5 and RCP8.5

**Hagupit**

Fig.3-15 indicated that the extreme climate scenario RCP 8.5 (S2) caused the maximum water level to achieve a higher elevation. The peak water level occurred at Kat\_O station with a depth at 3.5 meters. However, we can see that the maximum water level under scenario RCP 8.5 (S2) showed an increasing trend in all of the tide stations, but with a different the rising rate at different locations. A considerable amount of 20cm increase remained at Shek Pik station, 8cm increasing at Quarry Bay station and 3 cm rising at Kat\_O station under RCP 8.5 (S2) scenario. That revealed that the water level could cause an increase ranging from 1.5% to 8% under RCP 8.5 scenario. At Waglan station, the RCP 8.5 (S2) scenario showed a decrease at the beginning and then changed to an increasing trend, fairly 8cm rising at 18:00 on

September 23 after the Hagupit passed Hongkong. S1 scenario (RCP 4.5) again indicated a decreasing trend at all stations compared to baseline scenario S0.

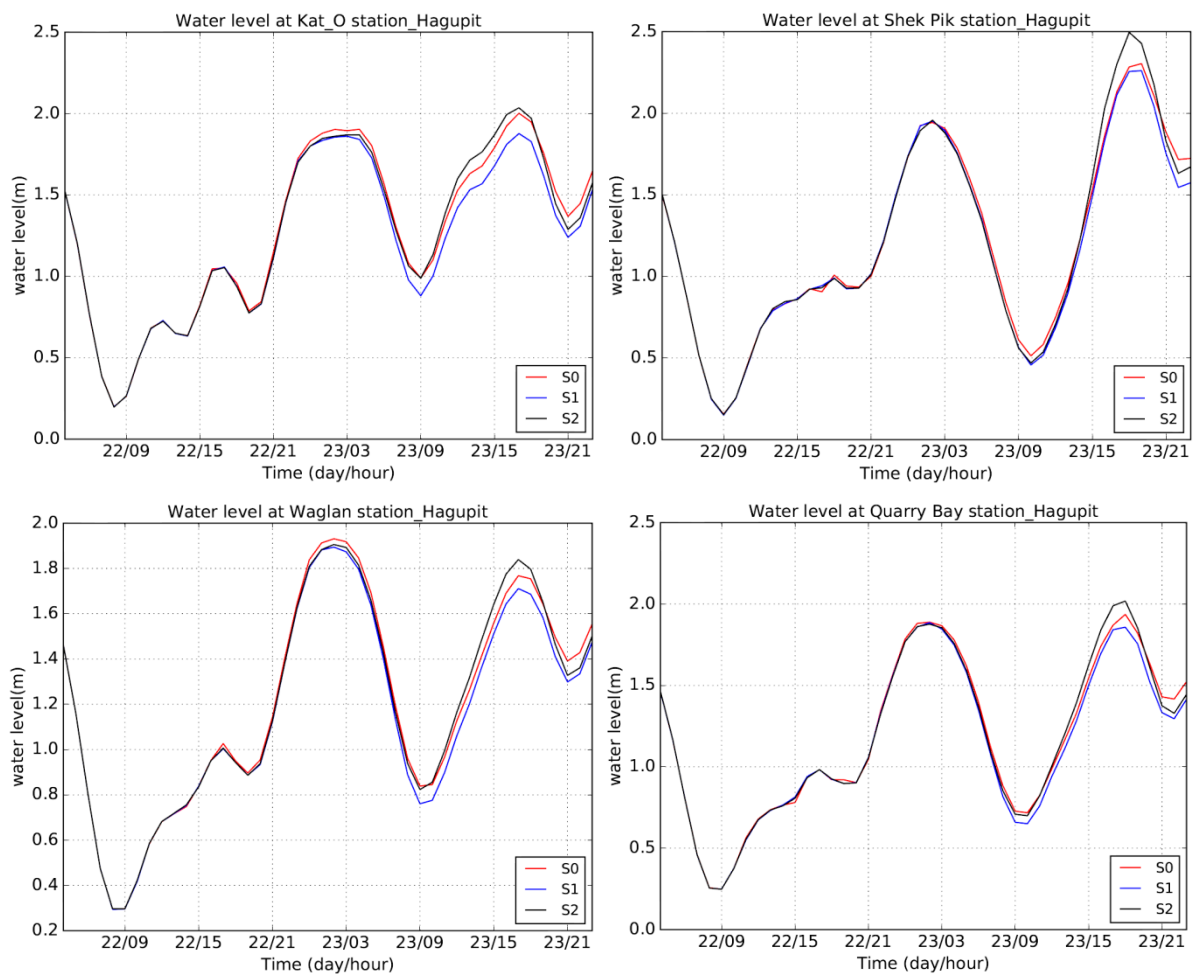


Fig. 3-15 Simulated water level changes and peaks at gauge stations (Kat\_O, Shek Pik, Waglan and Quarry Bay) during Hagupit under S0, RCP4.5 and RCP8.

### 3.3.2 The impacts of climate change on river discharge

From Fig.3-16 to Fig.3-21 revealed that the river discharge at both Makou station (upper stream) and Pinggang station (downstream) increased dramatically with a linear trend from baseline scenario (S0) to RCP 8.5 (S2) scenario during all typhoons. During the typhoon passages, when storm tides were coupled with the intensive rainfall, there will be a significant increase in river discharge. For example, the river discharge of Makou station during Dujuan started to rise dramatically after September 2nd 5 pm. At the same time, the river discharge of Pinggang station started to increase abundantly from September 2nd 11 am.

Moreover, because Pinggang station is located at the mouth of the PRD estuary, the hourly river discharge showed an obvious surge phenomenon following a Gaussian distribution during the typhoon. The hourly river discharges at Makou station also presented a typhoon oscillation as we noticed from all of the typhoon cases. The difference is, Utor and Hagupit are closer to a regular Gaussian distribution at Makou station.

Additionally, the daily river discharge at upstream and downstream experienced an increased variation in different typhoon cases under climate change. At Makou station (located in the upstream), the maxima daily river discharge happened during the middle landfall typhoon Dujuan, with about 16000 m<sup>3</sup>/s under the baseline scenario (S0) and over 19000 m<sup>3</sup>/s under RCP8.5 (S2). The increase reached up to 28.5% under RCP4.5 (S1) and 35.7% under RCP8.5 (S2) compared to S0. The eastern landfall typhoon Utor and western landfall typhoon Hagupit showed a similar daily river discharge increase in the future climate change. For the east landfall typhoon Utor, the maximum daily river discharge at Makou station was about 7900 m<sup>3</sup>/s under RCP8.5 (S2) with a 20% rise compared to S0, correspondingly around 7250 m<sup>3</sup>/s under RCP4.5 (S1) with 11.5% relative to S0. For the western landfall typhoon Hagupit, there was 11.8% increase under RCP4.5 (S1) and 20.3% increase under RCP8.5 (S2) on daily river discharge at Makou station. However, the magnitude is the lowest one among all of the three typhoon cases, the maxima discharge during Hagupit was only 5900 m<sup>3</sup>/s under RCP4.5 (S1) scenario and 7100 m<sup>3</sup>/s under RCP8.5 (S2) scenario.

The maxima daily river discharge of Dujuan at downstream Pinggang station was around 5200 m<sup>3</sup>/s under S0. Then it raised to about 6400 m<sup>3</sup>/s under RCP8.5 (S2). A 5.6% rise under RCP4.5 (S1) and 20.7% rise under RCP8.5 (S2) occurred during middle landfall at Dujuan. Both Utor and Hagupit showed dramatically increases during typhoon approaching under all climate scenarios, then with a speedy decline, which presents an obvious surge phenomenon during typhoon period. This phenomenon in the downstream was apparently more sensitive than upstream. Both typhoon cases have an amount of daily river discharge of 1750 m<sup>3</sup>/s under RCP4.5 (S1) scenario and 2150 m<sup>3</sup>/s under RCP8.5 (S2) scenario at Pinggang station.

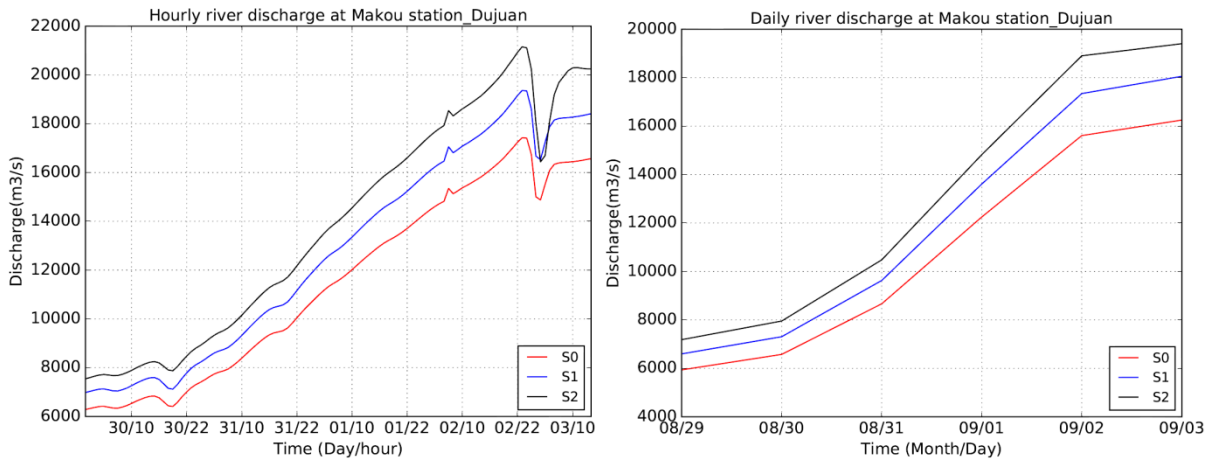


Fig. 3-16 The hourly and daily river discharge during Dujuan at Makou station

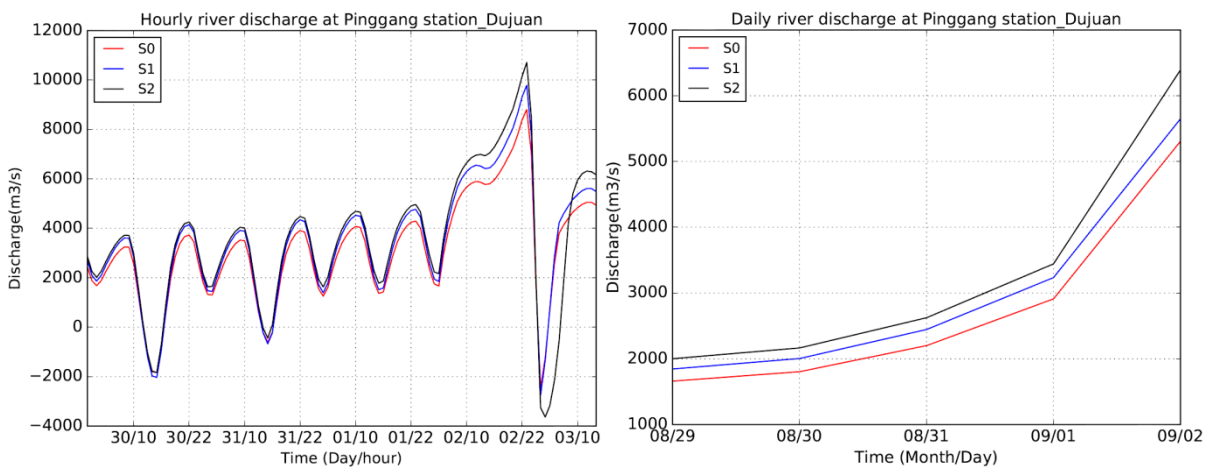


Fig. 3-17 The hourly and daily river discharge during Dujuan at Pinggang station

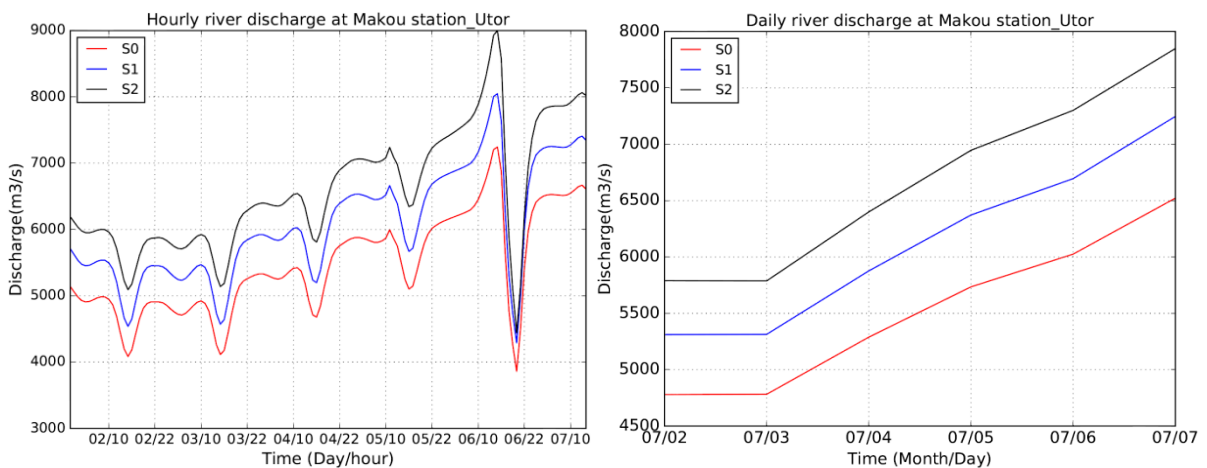


Fig. 3-18 The hourly and daily river discharge during Utor at Makou station

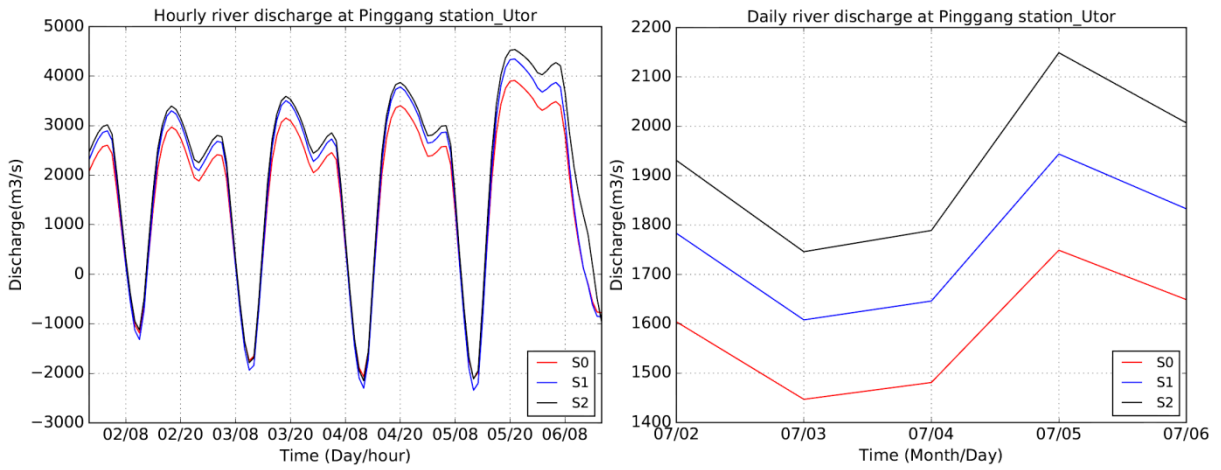


Fig. 3-19 The hourly and daily river discharge during Utor at Pinggang station

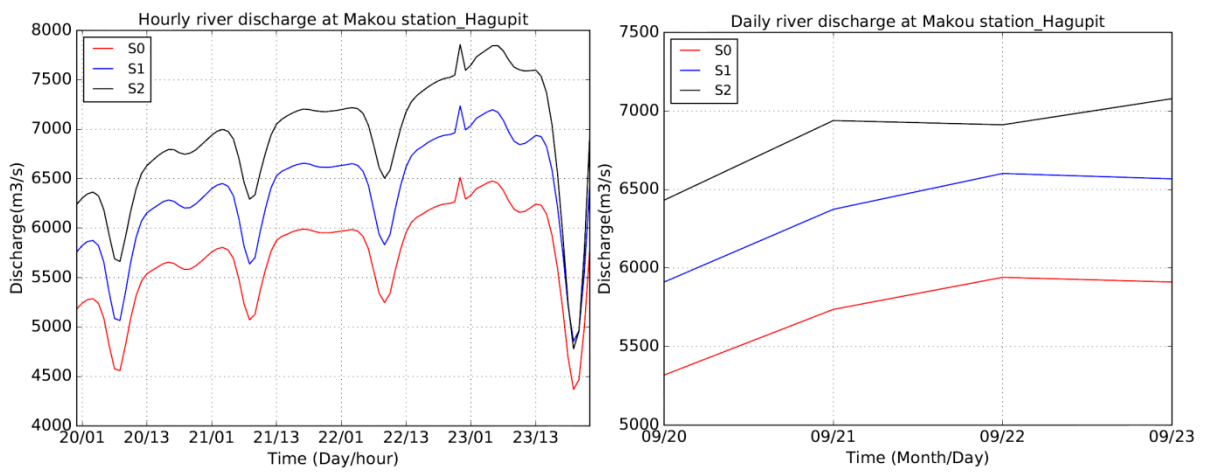


Fig. 3-20 The hourly and daily river discharge during Hagupit at Makou station

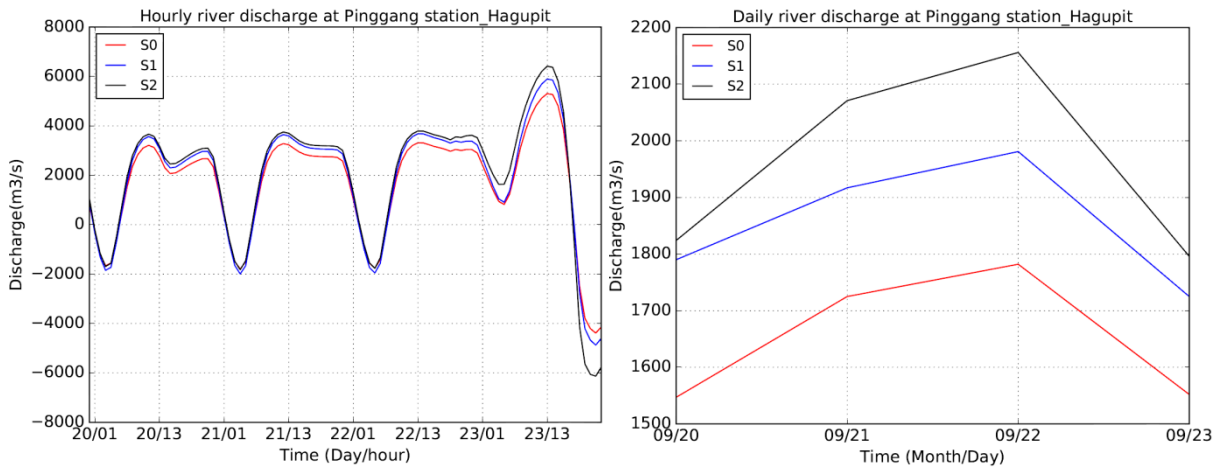


Fig. 3-21 The hourly and daily river discharge during Hagupit at Pinggang station

### **3.3.3 Inundation extent during different typhoons under different climate scenarios**

As we discussed above, the water level varied at different locations with different typhoons under different scenarios. Because there were only a few pilot points, this was not enough to reveal the overall impacts of climate change. Therefore, this part we analyzed the inundation extent during Dujuan and Utor under different scenarios.

#### ***Dujuan***

Fig. 3-22 and Fig. 3-24 showed inundation changes during Dujuan under the baseline scenario, RCP 4.5 and RCP 8.5 scenario. The maximum water level during Dujuan was ranging from -1.866858 to 4.9 meters under baseline scenario S0, from -1.804642 to 6.7 meters under RCP 4.5 scenario, and from -2.479342 to 7.2 meters under RCP 8.5 scenario. The inundation extent varied under three scenarios at several locations. With the changes of climate condition, we could see the water level at upstream increased obviously (the red frame A). This indicated that the upstream could be more and more vulnerable when the climate condition changed during typhoon cases like Dujuan. Another important finding was that the inundation extent of the eastern river part (the red frame B) had an obvious expansion from S0 to RCP 8.5 (S2). The third observation was, there was a considerable increase of the water level from the north of the eastern bay of the PRD region (the red frame C) remained under RCP 8.5 scenario. Because this region is located in the upside of the storm wind direction, both the storm wind speed and the storm forward speed resulted in substantial surge changes. The fourth apparent inundated region was the western bay of the PRD region (the red frame D), especially under the RCP 8.5(S2) scenario. The results showed that in the future under climate change, the most vulnerable regions are the southeast of Zhaoqing city (the Gaoyao, Dinghua Districts), the north of Dongguan city, the bay between Shenzhen and Hongkong, the south of Huizhou city, the middle east of Foshan city and also Zhongshan city.

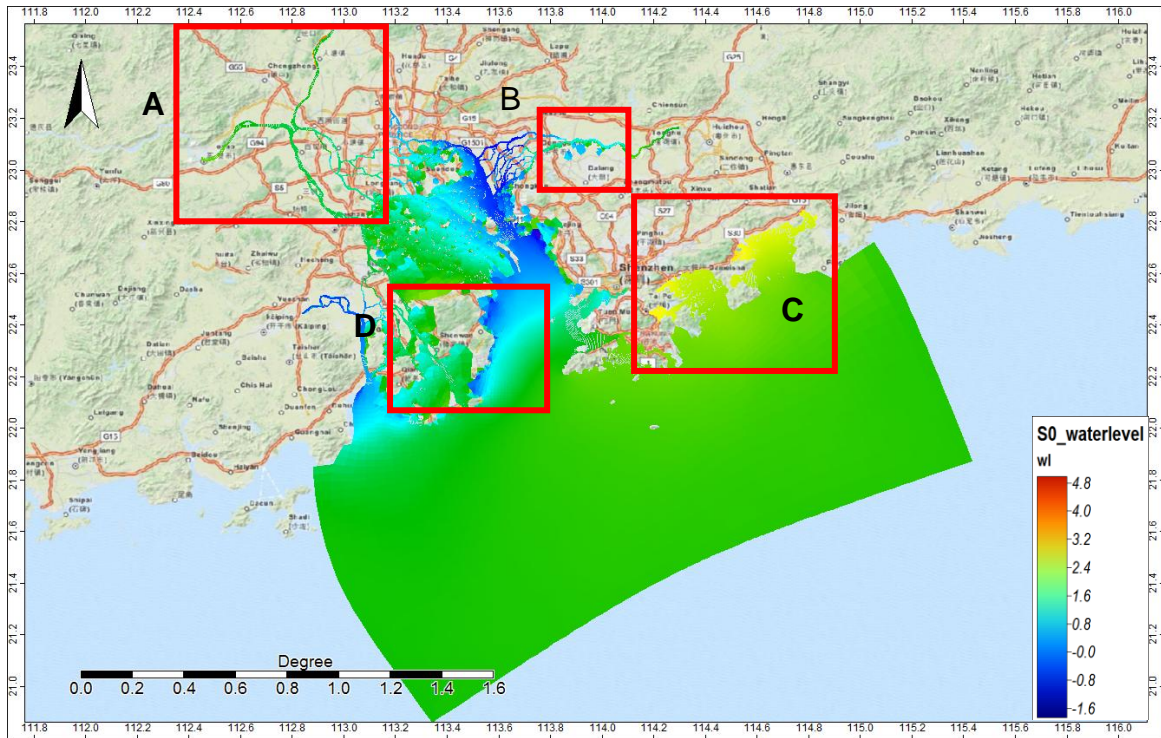


Fig. 3-22 Coastal inundation map during Dujuan under baseline scenario (S0)

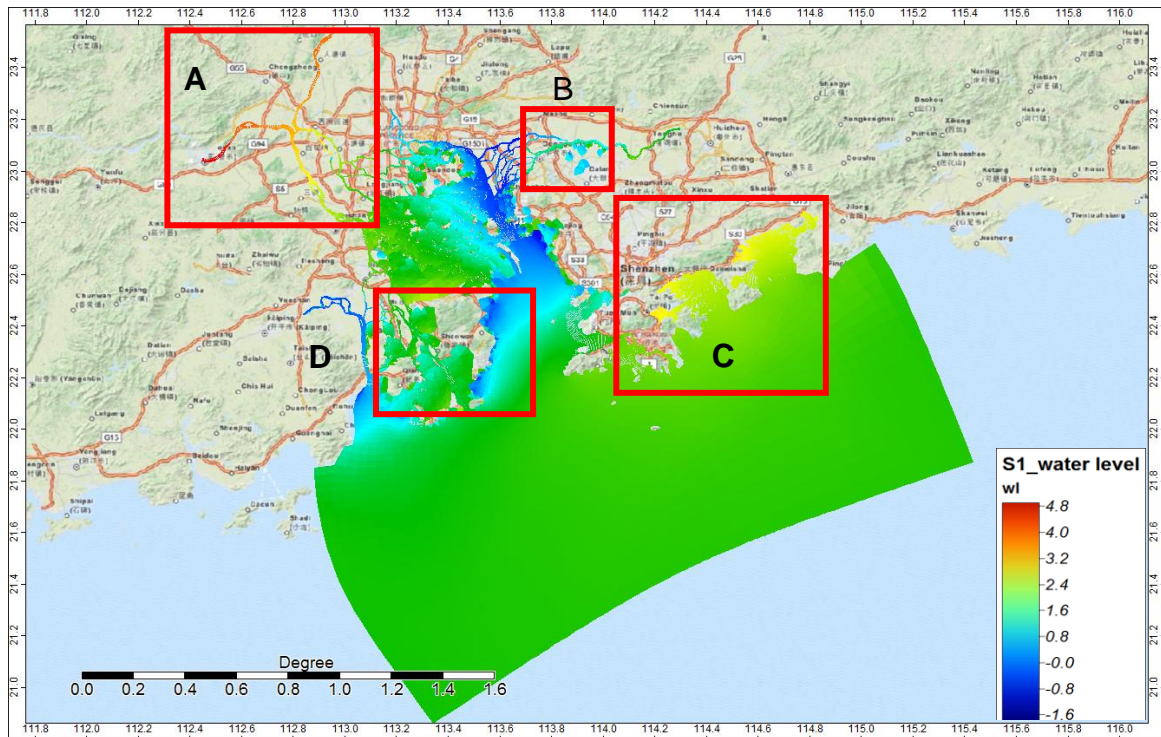


Fig. 3-23 Coastal inundation map during Dujuan under RCP4.5 (S1)

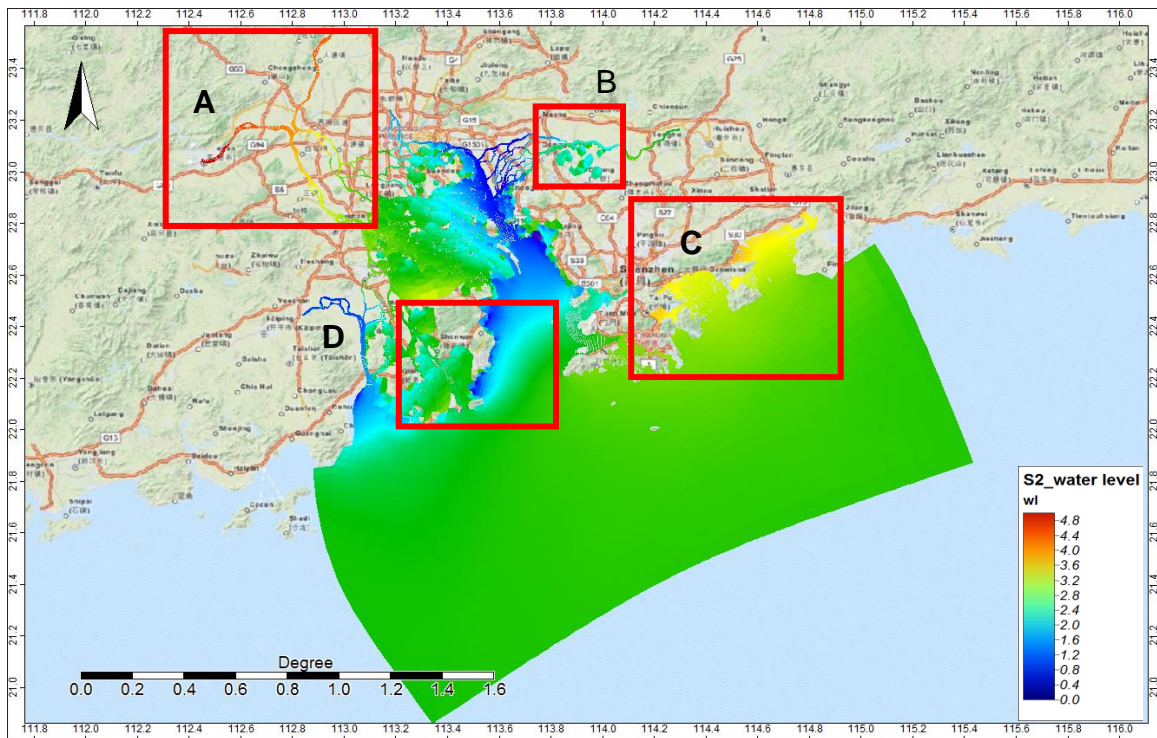


Fig. 3-24 Coastal inundation map during Dujuan under RCP8.5 (S2)

### **Utor**

When we discussed the water level changes at all pilot locations in the last part, we found the water level changes were barely noticeable under climate change scenarios at some locations during Utor. However, when it came to the spatial inundation extent changes of water level in the entire PRD region, we can find that it was visible that the water level of RCP 4.5 scenario (S1) was much higher than the baseline scenario (S0). We observed from Fig.3-25 to Fig.3-27, the maximum water level during Utor was varying from -0.18303 to 4.94 meters under S0, from 0.049558 to 4.98 meters under RCP 4.5 (S1) and from 0.0059 to 4.98 meters under RCP 8.5 (S2). That is why there were visible spatial changes of inundation extents from S to RCP 4.5 scenario (S1), but not apparently from RCP 4.5 (S1) to RCP 8.5 (S2) scenario.

Spatially, the most vulnerable region was the upstream part, the eastern river bank, the easternmost part of the eastern bay and the south western bay. The inundated area revealed that, the southeast of Zhaoqing city, like Gaoyao, Dinghua District, the north of Dongguan city, the bay between Shenzhen and Hongkong, the south of Huizhou city, the east of Foshan city and Zhongshan city, the entire Zhuhai city and Makau, were the most vulnerable region in the future climate change. When there is a

typhoon with the intensity and track attributes similar with Utor, the surges were also dramatically rising at the mouth of the PRD estuary.

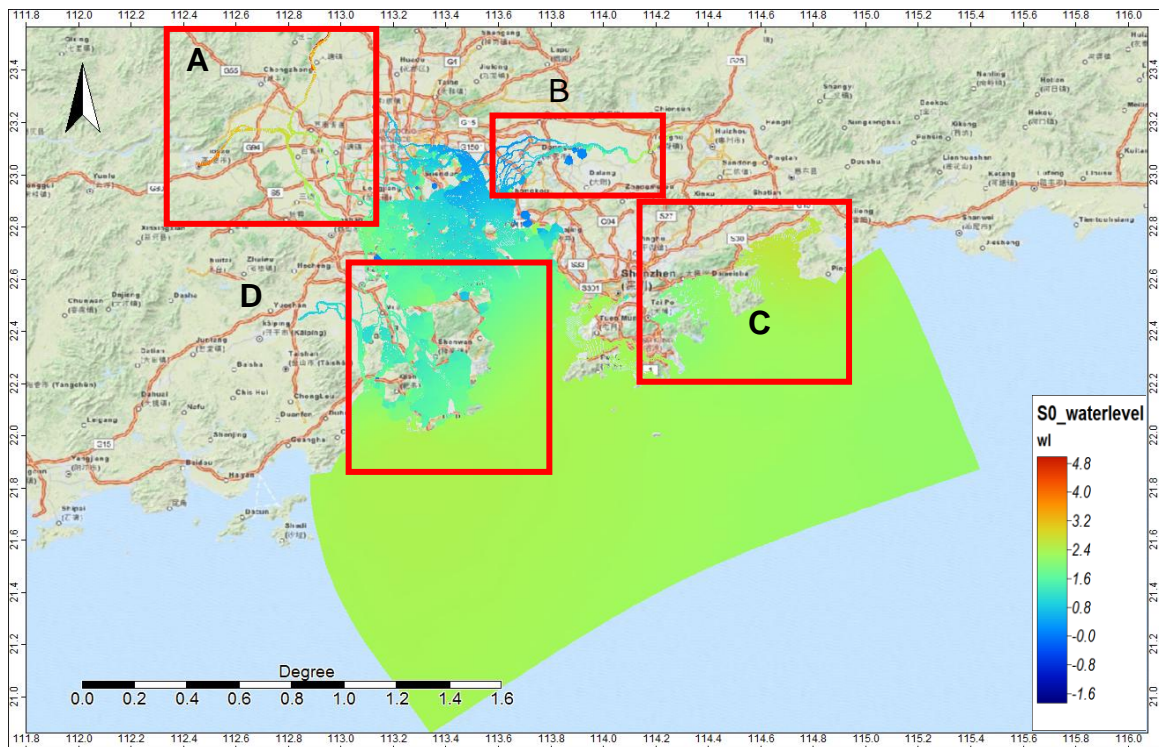


Fig. 3-25 Coastal inundation map during Utor under baseline scenario S0

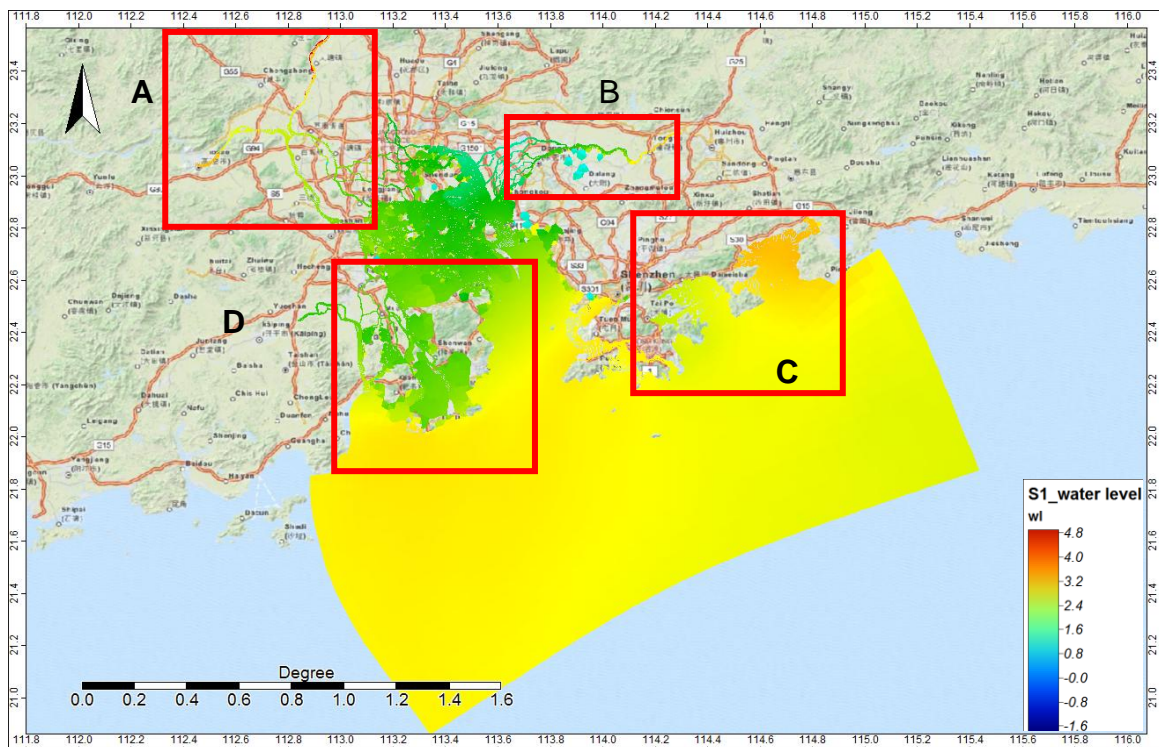


Fig. 3-26 Coastal inundation map during Utor under RCP 4.5 (S1)

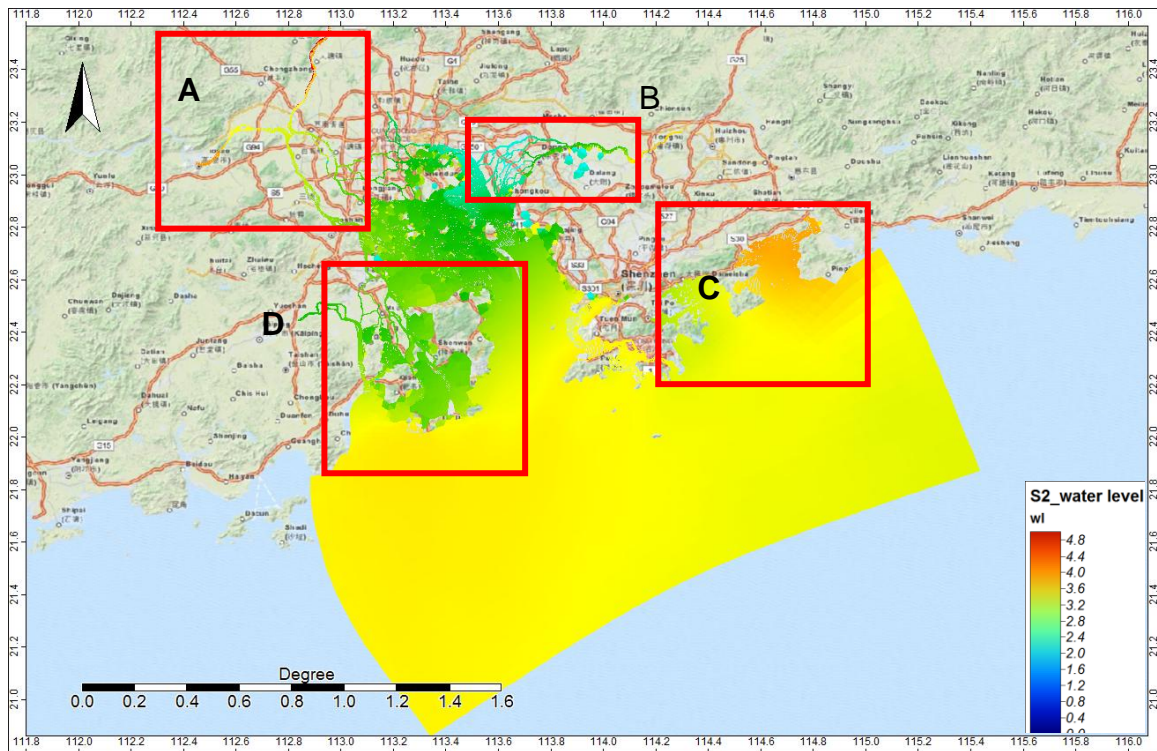


Fig. 3-27 Coastal inundation map during Utor under RCP8.5 (S2)

Typhoon induced inundation changes obtained from this study under different climate scenarios could assist with surge defense facilities along the PRD coastline.

### **Hagupit**

The following figures (see from Fig.3-28 to Fig.3-30) demonstrated the inundation changes during Hagupit under different climate scenarios. The maximum water level during Hagupit was ranging from -1.188593 to 4.943017 meters under baseline scenario S0, from -1.215827 to 4.987389 meters under RCP 4.5 scenario (S1), and from -1.659675 to 4.98739 meters under RCP 8.5 scenario. Regionally, the maximum water level in the east bay of the PRD region increased apparently from RCP 4.5 scenario (S1) to RCP 8.5 scenario (S2). This meant the city like Zhuhai, Macao, Zhongshan, middle east of Foshan and southwest of Guangzhou had higher inundation risks under extreme climate conditions like RCP 8.5 scenario (S2). Another obvious inundated region was along the east river ('B'), the inundation extent under RCP 8.5 scenario (S2) was dramatically larger than other scenarios. Correspondingly, the finding indicated that the north east of Dongguan city would have a higher risk under RCP 8.5 scenario (S2). Additionally, in the east bay region like Hongkong east

region, south east of Shenzhen, south of Shanwei, the water level was accelerating gradually from baseline scenario (S0) to RCP 8.5 scenario (S2). Therefore, it was believed that the climate adaption strategy of coastal protection along this region should be given increasing attention. Overall, the results highlighted that the maximum water level increased slightly by 0.8% under RCP 4.5 scenario (S1), but the inundation extents were more obvious under RCP 8.5 scenario (S2) than other scenarios

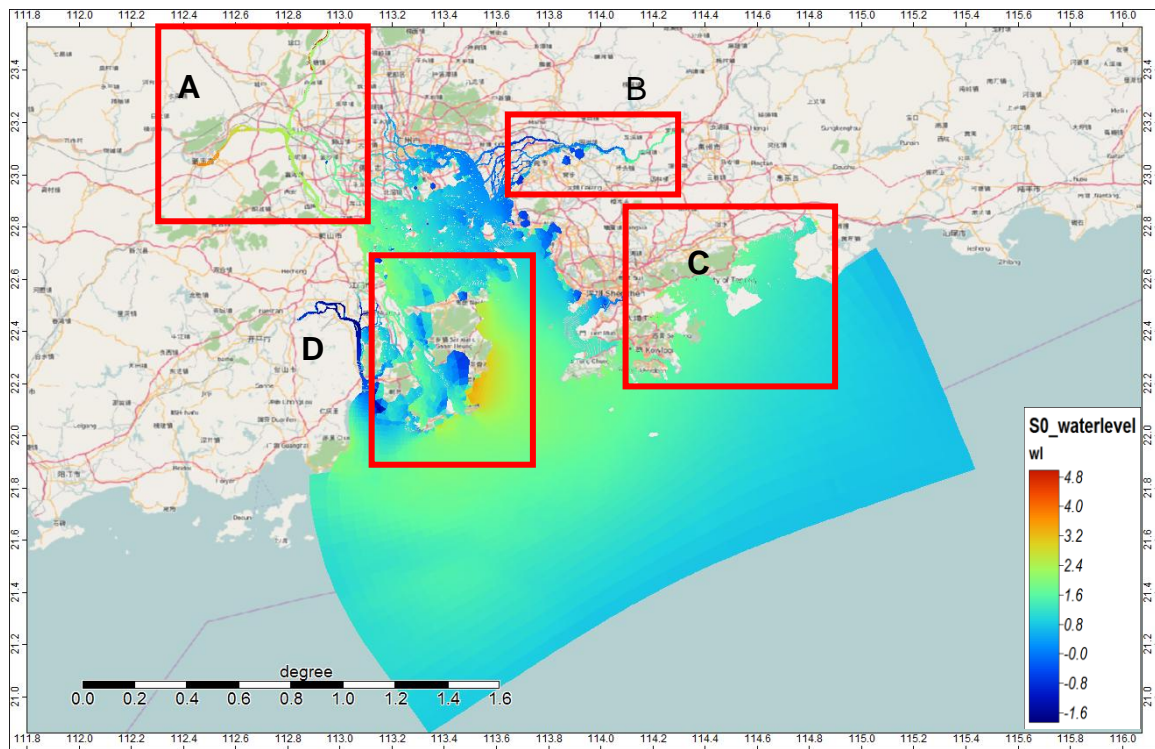


Fig. 3-28 Coastal inundation map during Hagupit under baseline scenario S0

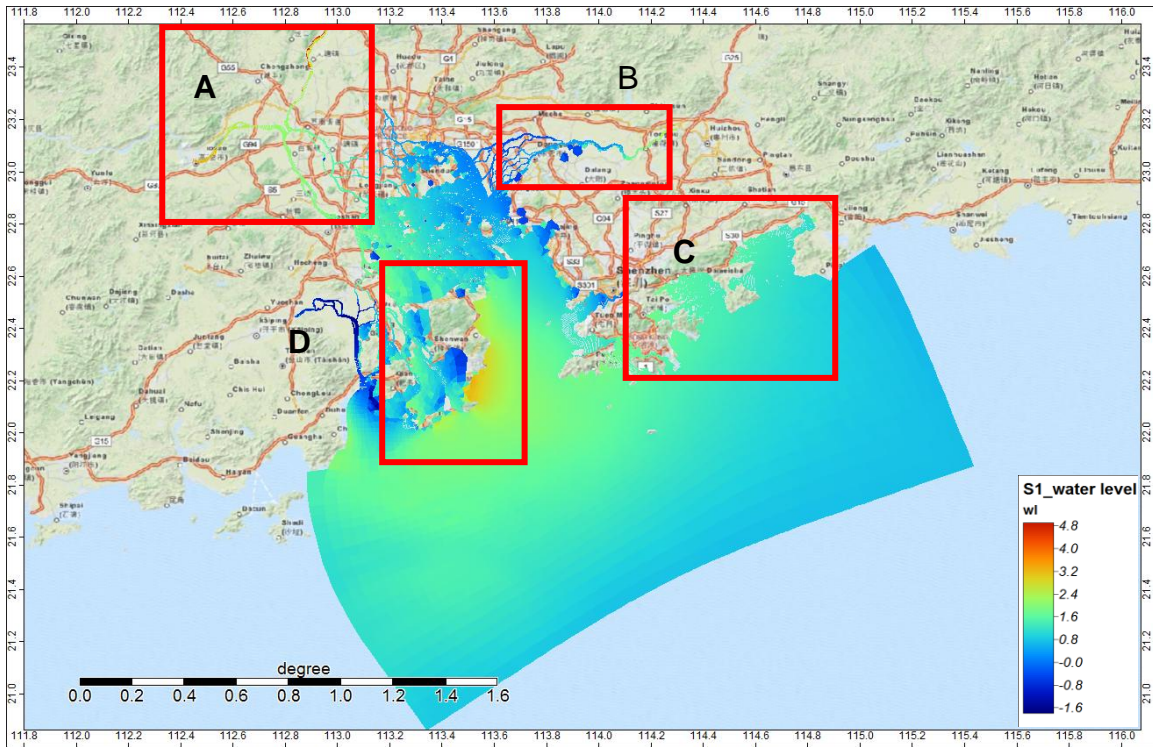


Fig. 3-29 Coastal inundation map during Hagupit under RCP4.5 (S1)

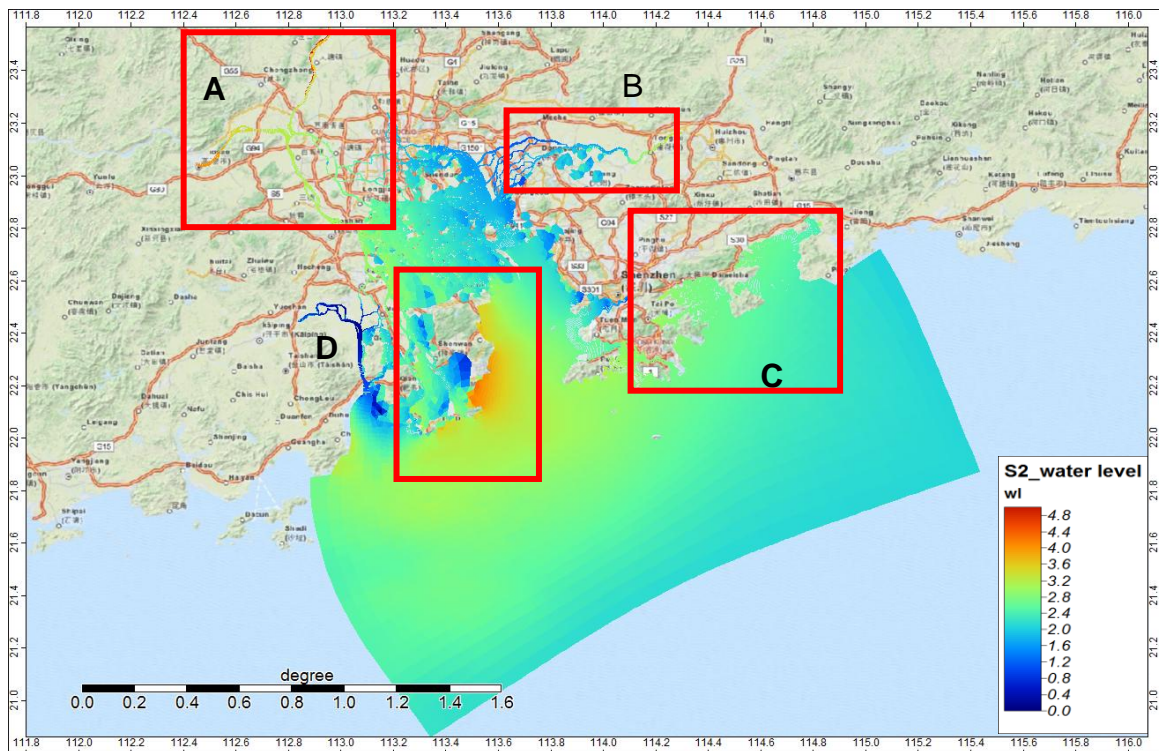


Fig. 3-30 Coastal inundation map during Hagupit under RCP8.5 (S2)

## **3.4 Discussions**

### **3.4.1 The uncertainties**

The main goal of this research is to identify typhoon induced storm surges and inundation changes in the future climate change. The first main uncertainty remains in the climate change model projections of future tropical cyclones (Teng et al., 2012). There are three main uncertainties in these climate projections.

The first uncertainty is how the tropical climate could change in different research scales, and the second lies in the implications of these changes for tropical cyclone activities (Knutson et al., 2010). For example, the projections of increase in tropical SSTs and related variables during the 21st century are substantial differences between global climate models and regional-scale models, which induced the progressive differences during the downscaled regional projections of typhoon activities in a given region (Knutson et al., 2010). This research was based on regional scale, and the PRD region is with its own attribute. The third one is an uncertain relationship between tropical cyclones and internal climate variability like SST distribution. This also reduces our confidence on studying typhoon intensity changes due to climate change (Knutson et al., 2010). However, in our research, we made the assumption that typhoon intensity would accelerate if the SSTs increase according to previous researches in the western North Pacific Ocean (Knutson et al., 1987, 2005, 2008, 2010; Emanuel, 1987; Holland, 1997).

### **3.4.2 The difference of climate change impacts**

In the results section, we found that the impacts of climate change on the peak water levels were different at different locations and different typhoon cases. Except for the climate projection uncertainties, the complex mechanism of internal variability of each typhoon could enhance the difference. A relatively small shift of storm track or changes of genesis location can lead to a relatively huge difference of peak water levels as well as a result in different inundation extents along the coast (Knutson, 2008; Bender, 2010). The tropical cyclone internal variability, such as the wind speed (intensity), the wind flow angle (the tropical cyclone approach angle), the forward speed and the air pressure (inverted barometer effect) can also affect the water levels

and inundation extents during typhoon period. In our research, the wind forcing model (WES) required the pdrop as the air pressure parameter. The standard air pressure is either 101300 pa or 100000 pa, in order to keep all pdrop values in a positive value, the negative ones at the genesis location points of Utor were deleted. These changes of genesis location may lead to a different performance between the model results and the measurement data at pilot locations. Therefore, the storm surge changes at coast resulted from complex interactions among coastal geometry, bathymetry, wind and pressure forcing (Rego and Li, 2010). A slight variation of the typhoon track, propagation speed or wind speed intensity can have a significant impact on the local extreme hydrodynamic conditions. We have discussed the internal variability (wind speed, wind direction and air pressure) of each typhoon to understand the difference of climate change impacts in the next part.

### ***Wind speed***

The wind speed is one of the most important factors that influence the water level changes. We will discuss the effects of wind speed on the water level changes of three typhoon cases in the following part.

### **Dujuan**

As listed in Fig.3-31, it provides the wind speed at the peak water level time at four gauge stations during Dujuan. We can see the wind speed at Shek Pik, Waglan and Quarry Bay station under climate scenarios had a linear agreement with water levels. That means maxima water level occurred at the highest wind speed time at these three stations during Dujuan. Even though a linear increase of the wind speed trend happened at Kat\_O station under RCP8.5 (S2) like other three stations, the peak water level at Kat\_O station under RCP4.5 (S1) was declining as given in the Fig.3-31. The negative correlation remained between the water level and the wind speed under RCP 4.5 scenario (S1) at Kat\_O. That means, even though the wind speed is one of the main factors to affect the water levels, there might be still another factor could contribute to the changes in water levels. We have discussed this point in the following part.

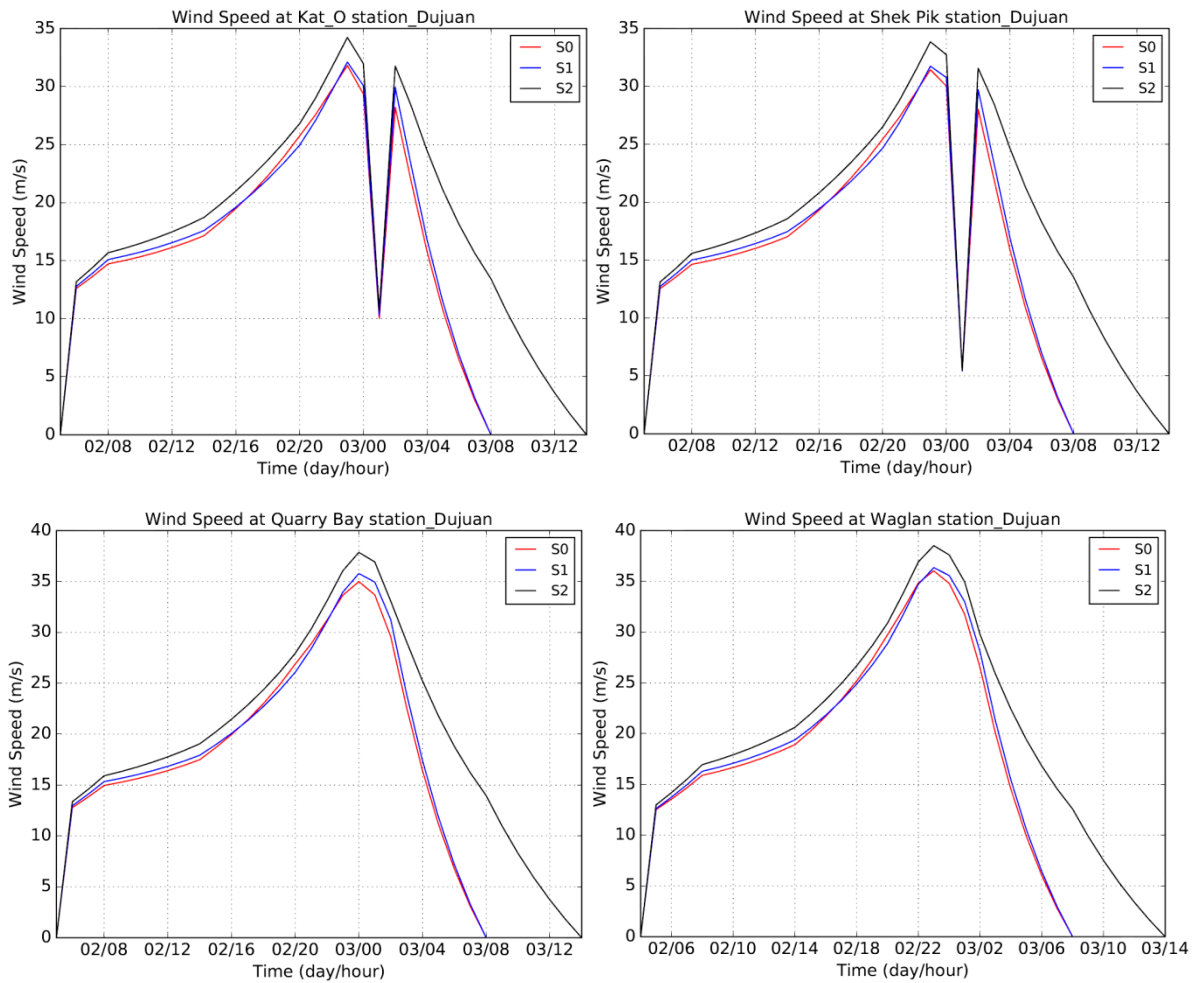


Fig.3-31 Wind speed at all of the gauge stations during Dujuan under S0, RCP4.5 (S1) and RCP8.5 (S2)

### Utor

Utor yielded different trends, the strong wind speed leads to a declining trend of the water levels at these four stations, as reported in the Fig.3-32. These results enhanced the point, the wind speed is not only the factor for water level rising, and other factors could be more sensitive in this spectacular case.

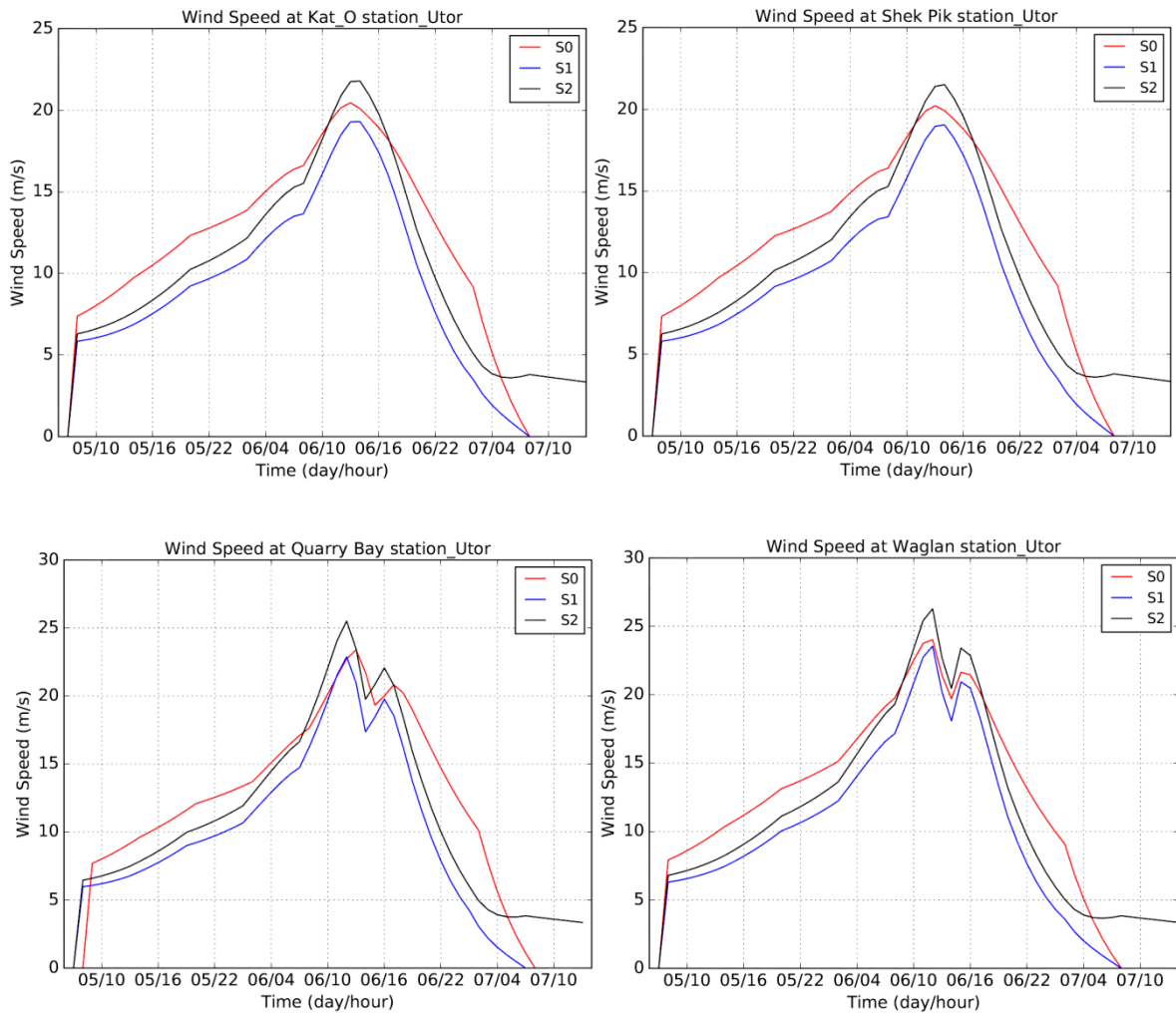


Fig. 3-32 Wind speed at all of the gauge stations during Utor under S0, RCP4.5 (S1) and RCP8.5 (S2)

### Hagupit

The wind speed during Hagupit also presented a linear correction with the water levels at all of the gauge stations under different climate scenarios (see in Fig.3-33). The speedy wind added to a higher water level during Hagupit passage. The wind direction of Hagupit was southeastward, which could bring the water from ocean to inland. In this case, we could conclude that the water level of the western landfall typhoon is clearly sensitive to wind speed.

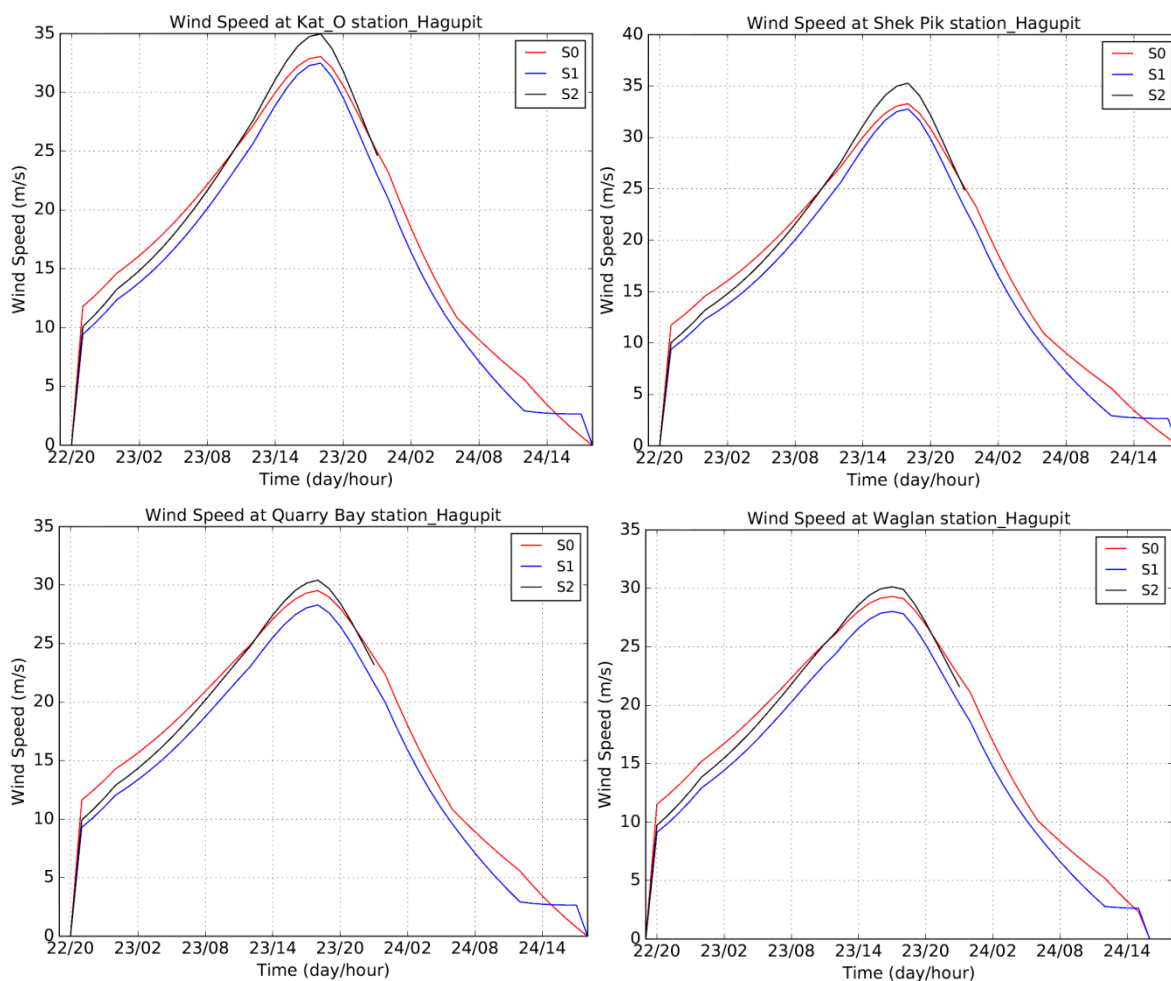


Fig. 3-33 Wind speed at all gauge stations during Hagupit under S0, RCP4.5 (S1) and RCP8.5 (S2)

Additionally, among all three typhoon cases, the highest wind speed happened during Dujuan, almost over 35 m/s at all stations. It is also evident that the water level gave the largest increase compared to other typhoons.

### ***Wind flow angle and inverted barometer effect***

Storm surge changes along the coast are complex interactions among coastal geometry, bathymetry, wind and pressure forcing (Regos and Li, 2010). Within one typhoon process, the wind direction of a storm affects the relative wind velocity and the water level at different locations along the coast in a different way. Fig.3-34 presented an example that how the relative velocity of wind of a storm affects the water levels. In this figure, we have three locations along the coast ('A,' 'B,' 'C'), when the typhoon is approaching the coast, the water level changes are different because

the direction and the relative velocity of the wind are different in a storm. The 'A' location has suffered the wind speed of the storm (100mph) and the storm forward speed (20m/s), so the storm surge at 'A' location is the highest one among three locations. 'B' location is affected by the typhoon moving speed 20m/s and slightly winds speed of typhoon (100mph) from the north direction so that the storm surge will increase, but not as high as 'A' location. The water level at 'C' location is negatively affected by the typhoon wind speed. However, it is positively affected by the typhoon moving speed (20m/s). The water level of 'C' station is the lowest one among three locations. Therefore, we can see the water level changes vary along coast even in the same storm progress. The slow moving storms can produce an increase in coastal inundation volume but decrease peak surges, while faster moving storms generate a higher peak surge, but less duration stays inland (Rego and Li, 2009.) This can supply a reasonable interpretation for the different water level changes in the same typhoon under different climate scenarios.

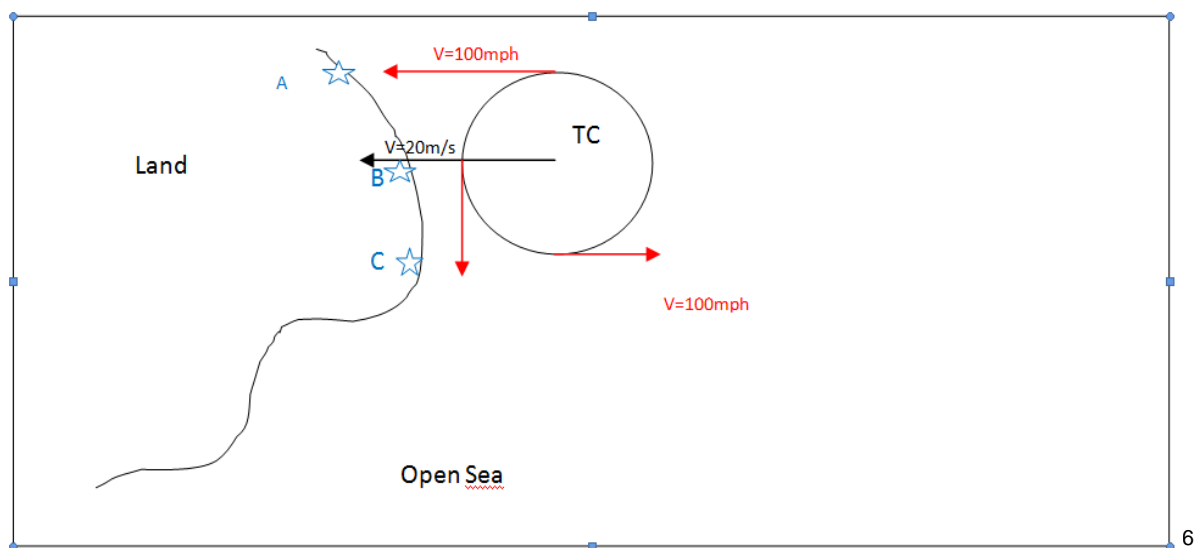


Fig. 3-34 Influence of the relative wind velocity on surges and water levels

The PRD region is a kind of semi-enclosed bay, the mechanisms inflow, overflow, wind set-up and wave set-up all influence the storm surge (Shen, Wang, Sisson, & Gong, 2006). The factor, including the angle and location of typhoon landfall, also

<sup>6</sup> <https://www.youtube.com/watch?v=EosrJcGHvrY>

affect the storm surge height and inundation extents. Fig.3-35 shows the influence of landfall location on surge and wind set up in the semi-enclosed basins.

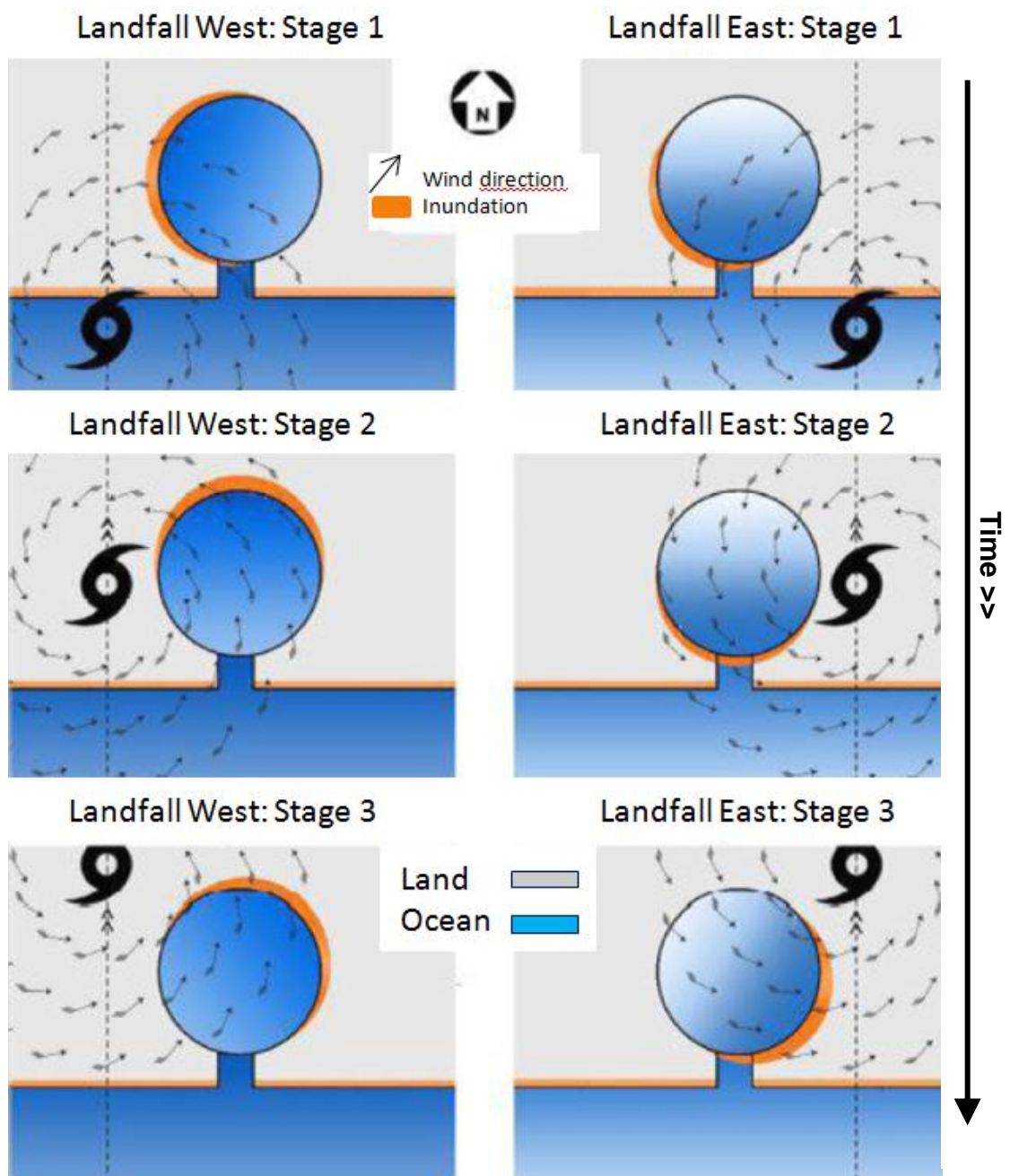


Fig. 3-35 Influence of landfall locations on surges and wind set up in the semi-enclosed basins (Stoeten, 2013)

Moreover, the air pressure, which is inverted barometer effect, can lead to a water level difference. A low core pressure can contribute to around 5% of the total surge lifting (National Weather Service, 2014). 1 mbar drop in air pressure can result in 10mm water level rise (Rego and Li, 2010).

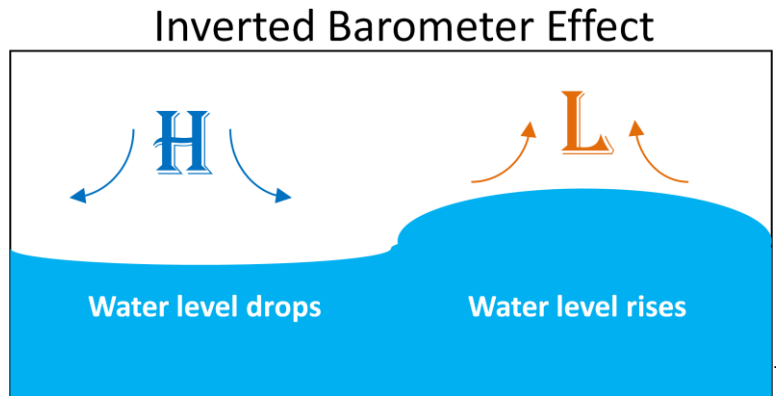


Fig. 3-36 Influence of inverted barometer effect on surges

During periods of high pressure, the water level tends to be lower than normal. During periods of low pressure, the water level tends to be higher than normal.

As discussed above, we will analyze the reasons for storm surges and inundation changes in three typhoon cases under climate change from air pressure and forward wind direction. From Fig.3-37 to Fig.3-39 represents the centre air pressure and wind speed of all of the three typhoon cases at peak water level time under different climate scenarios. As we could see, Dujuan made landfall in the Middle West, Utor is in the East, and Hagupit is in the West.

In the following part, we will discuss the wind flow angle and inverted barometer effect on the three typhoon cases.

### Dujuan

The changes of peak water level during Dujuan at gauge stations showed a positive sensitivity under future climate change scenarios, except Kat\_O showing a slight declining trend in RCP 4.5 (S1) as we discussed in the results section. The future climate change that is increasing the typhoon intensity, river discharge and SLR, can lead to a higher water level at individual stations. This can be illustrated from Fig.3-37 to Fig.3-40. We can see that Waglan, Shek Pik and Quarry Bay station are located almost in the low air pressure centre and the downside of the wind direction of Dujuan (like the 'A' position in Fig.3-34). Therefore, both the low air pressure and the wind

<sup>7</sup> <http://www.oc.nps.edu/nom/day1/partc.html>

direction of typhoon can lead to an increase in water levels in this case. This phenomenon followed the same pattern as the wind speed trend with the wind speed trend discussed in section 4.1.1. However, the peak water level at Kat\_O station was declining at RCP 4.5 scenario (S1) even though the wind speed of RCP 4.5 scenario (S1) was slightly higher than the baseline scenario S0. This could be explained by air pressure differences. As presented in the Fig.3-37, the air pressure at Kat\_O of RCP 4.5 scenario (S1) was dramatically higher than S0, the marked air pressure changes were possible to lead a lower water level with barely increased wind speed.

When all other conditions, such as the increasing magnitude, the relative position between the typhoon and pilot stations remain unchanged, then the difference of drop air pressure could result in the water level difference. In this case, the peak water level at Kat\_O station could show a decreasing trend in this specific situation.

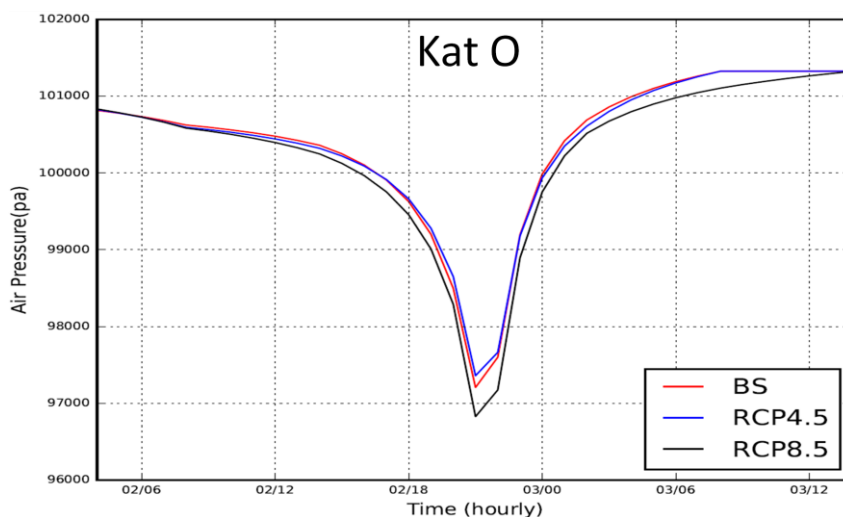


Fig. 3-37 Air pressure at Kat\_O station under baseline scenario S0, RCP4.5 (S1) and RCP8.5 (S2)

The atmosphere distribution of Dujan also displayed a close resemblance with the spatial distribution of inundation area as we can see from Fig.3-38 to Fig.3-40. The typhoon low-pressure centre is enclosed in the east bay and the south of the east river.

The east bay and the south of the east river are located at the typhoon low-pressure centre and the downside of the typhoon wind direction, so the water level in these two regions increased obviously under climate change. We can notice that the inundated

area changes from S0 to RCP 8.5 (S2). This indicated a higher flood risk in this region. The upstream and the north of the west bay are already far away from the typhoon centre, but they are located at the downside of the typhoon wind direction. These can contribute to a water level increase apparently.

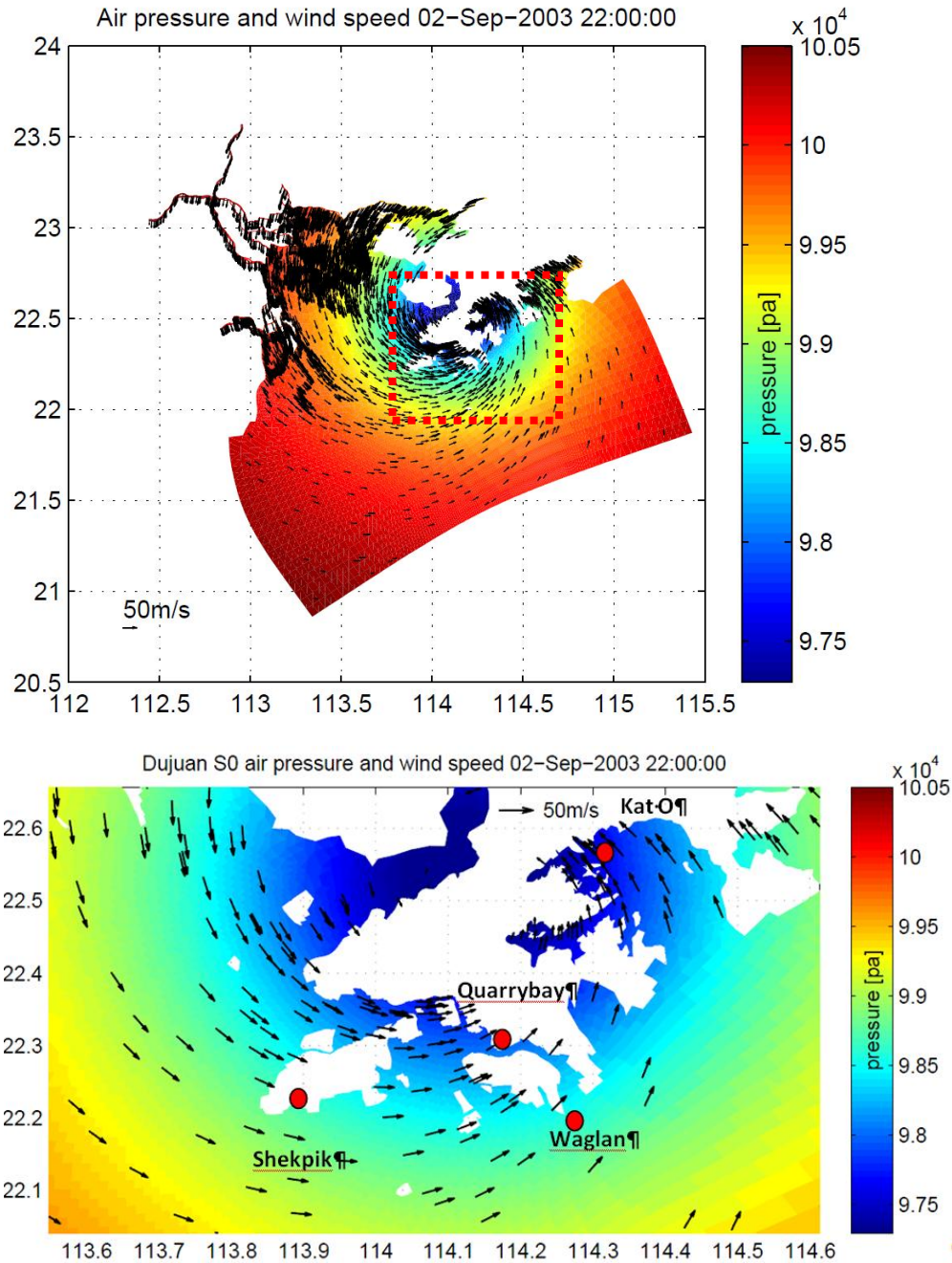


Fig. 3-38 Spatial distribution of atmosphere and wind speed during Dujuan under S0

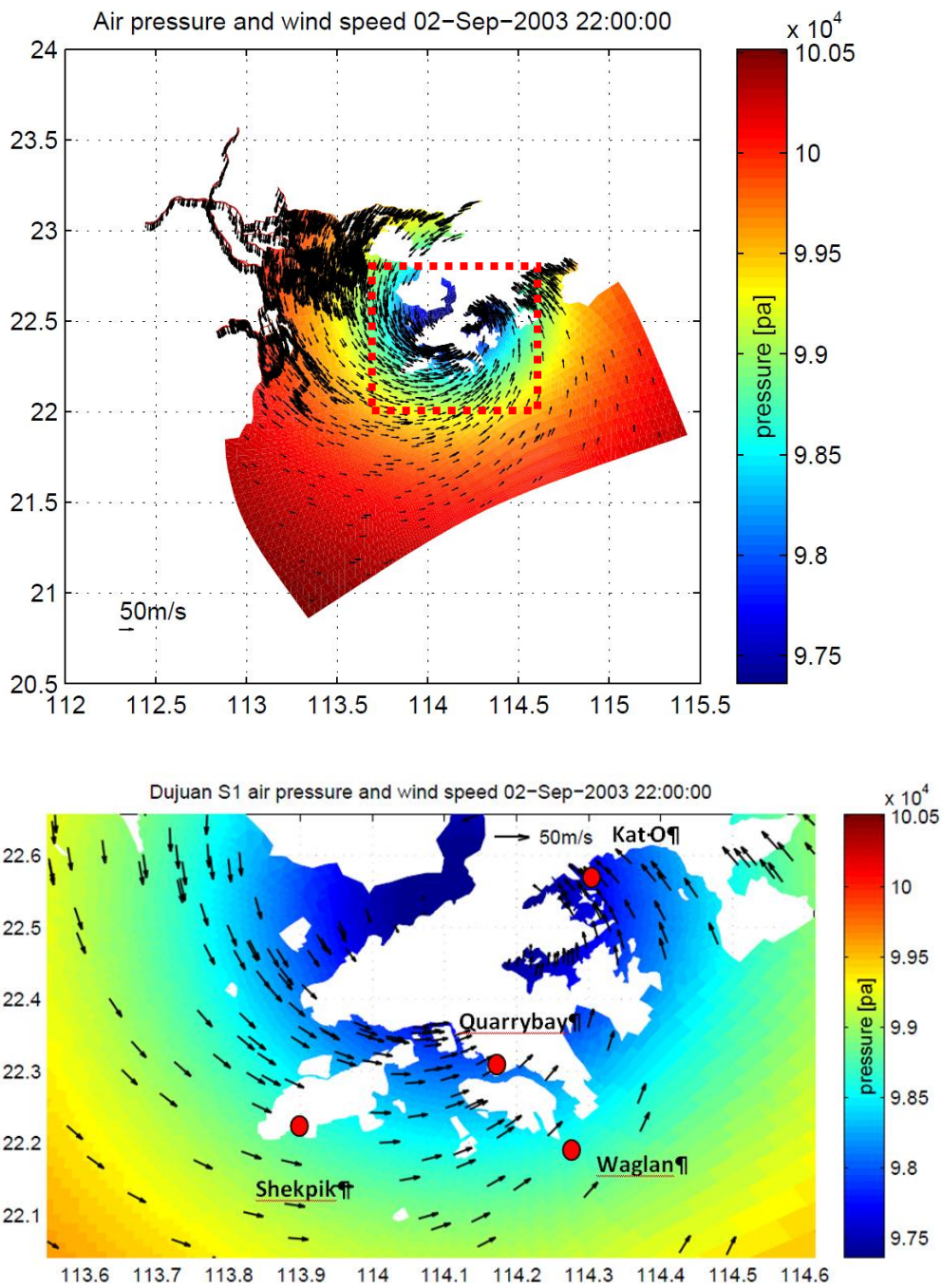


Fig. 3-39 Spatial distribution of atmosphere and wind speed during Dujan under RCP4.5 (S1)

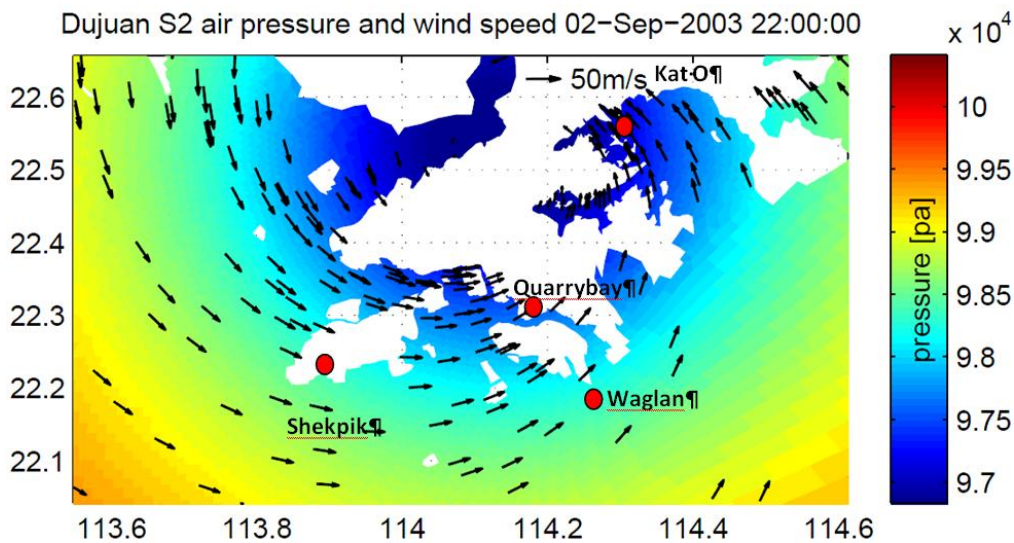
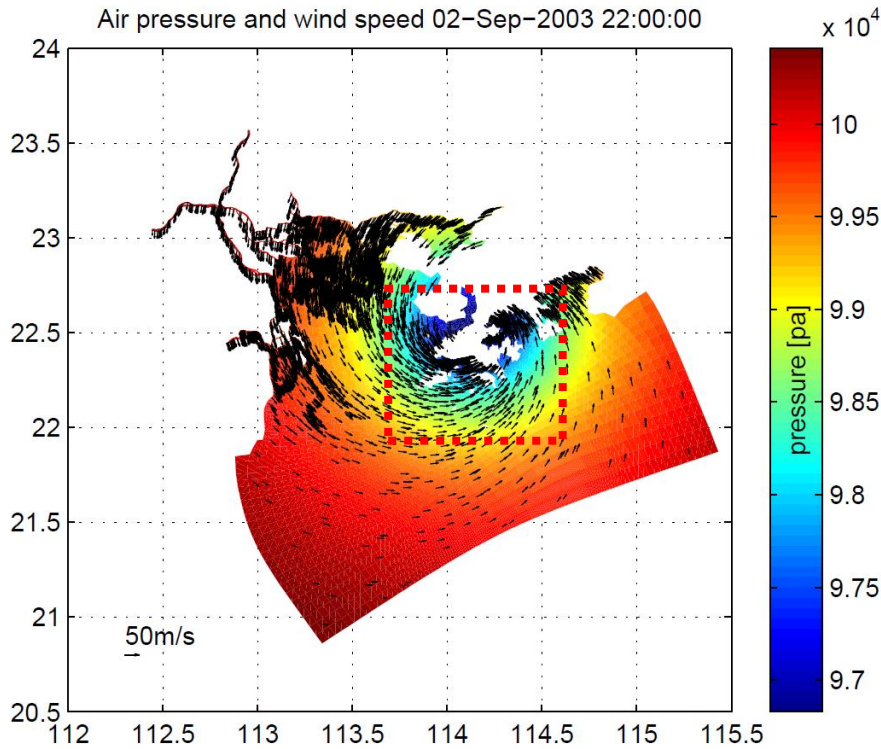


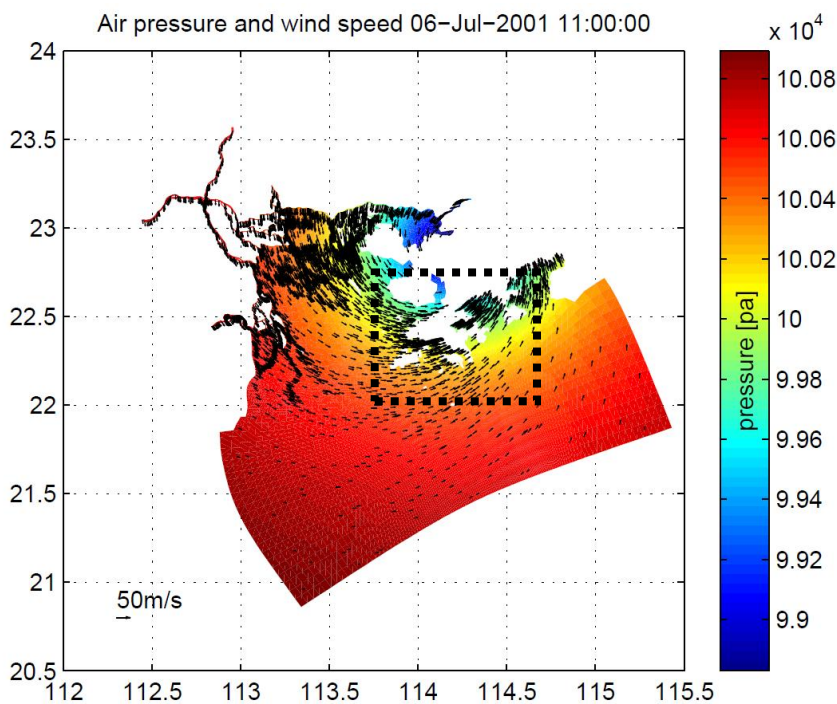
Fig. 3-40 Spatial distribution of atmosphere and wind speed during Dujan under RCP8.5 (S2)

### Utor

Utor made landfall at the east side of the PRD region. The changes of peak water levels at all gauge stations showed a negative trend when the climate scenario changes (typhoon intensity, river discharge and the SLR). We can notice from the

Fig.3.41 to Fig.3-43, there was a wind flow angle between typhoon track and the coastline (the typhoon approach angle). Different typhoon approach angles lead to different storm surge behavior. Generally, the wind flow angle has opposite effects on flooded volumes and peak surge elevations (Jelesnianski, 1965). The wind during Utor blew westerly, which forced water from land to the ocean in this particular situation. That is why the water level is even lower at the individual stations than the baseline scenario (S0) when the wind speed is increasing in the future climate conditions during Utor.

The spatial distribution of air pressure during Utor also revealed the inundation changes as discussed in the results section. The four major inundation areas were upstream, the easternmost part of the east bay, the east river bank and the south west of the west bay. We found all of them are located at the downside of typhoon wind direction and closed to the typhoon low-pressure centre. That's why there was an obvious consequence of rising water levels in those regions.



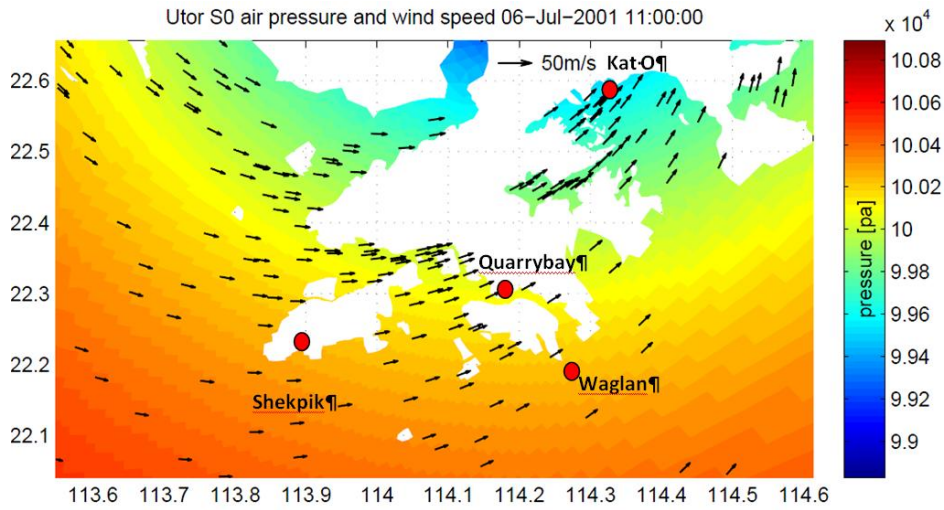
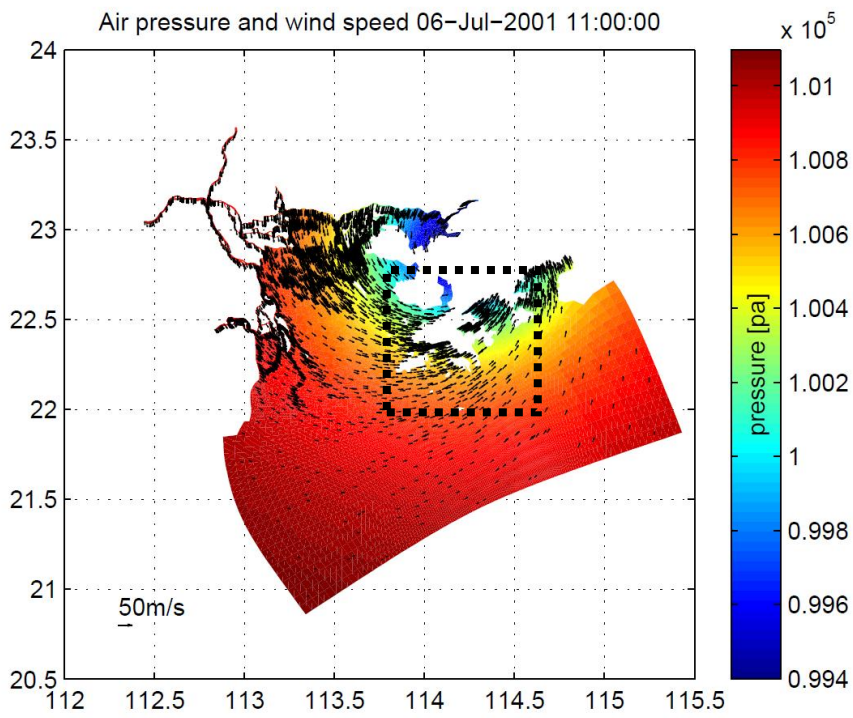


Fig. 3-41 Spatial distribution of atmosphere and wind speed during Utor under S0



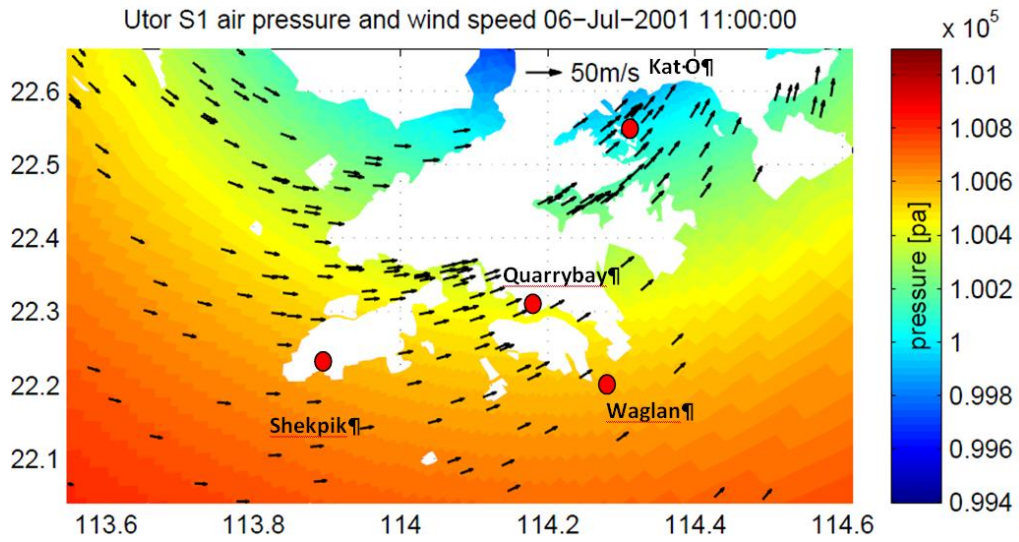
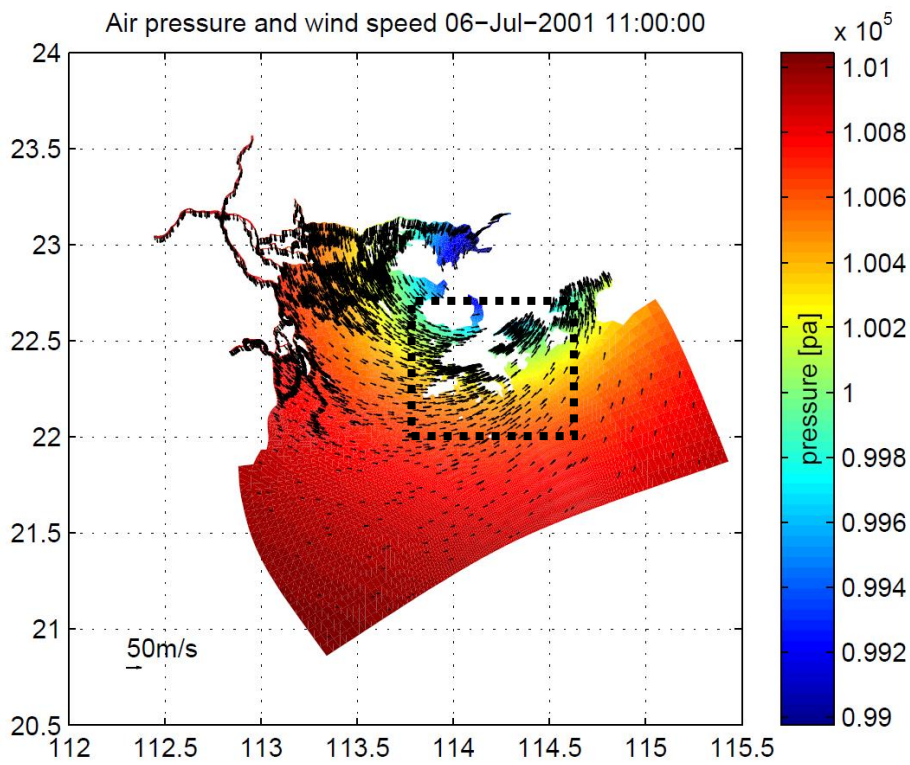


Fig. 3-42 Spatial distribution of atmosphere and wind speed during Utor under RCP4.5 (S1)



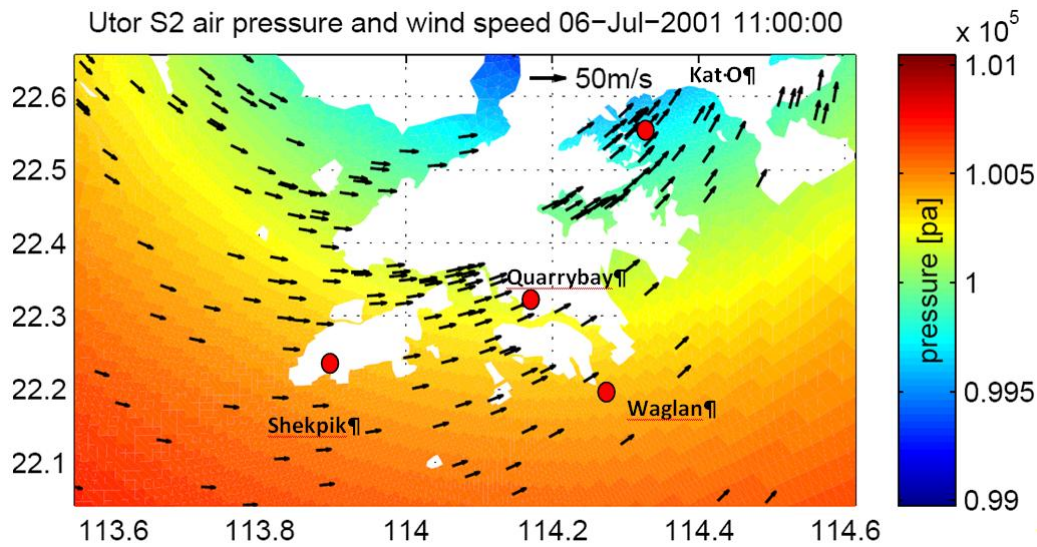
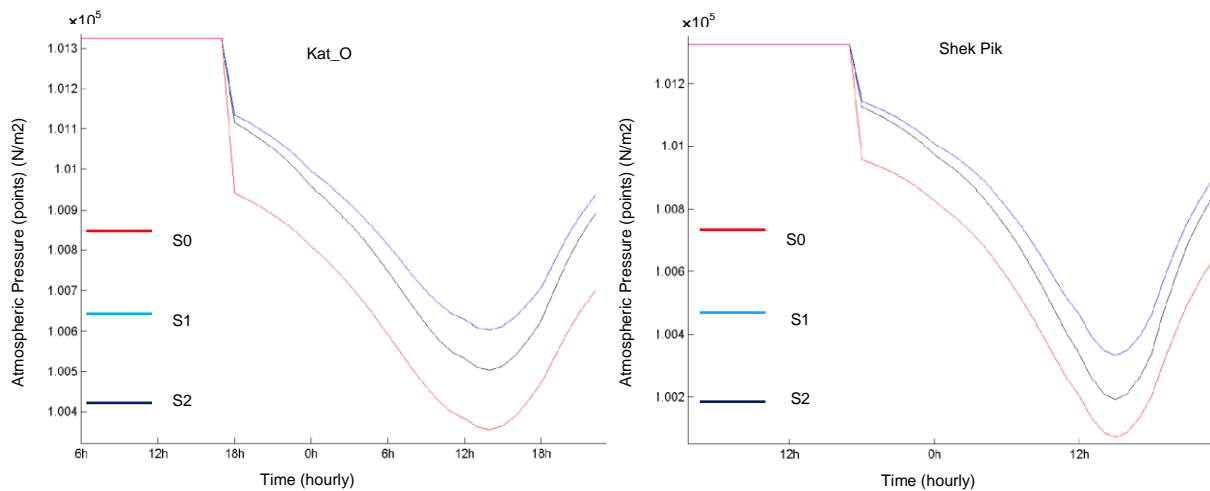


Fig. 3.-43 Spatial distribution of atmosphere and wind speed during Utor under RCP8.5 (S2)

### Hagupit

Changes of the maximum water level and coastal inundation at different gauge stations under different climate scenarios can be explained by the fact that the air pressure and wind flow direction have a significant impact on water levels (Fig.3-44 to Fig.3-47). The air pressure at four gauge stations during Hagupit had a negative linear correlation with water level changes. Because the lower air pressure results in a higher water level, and the positive linear correlation exists between wind speed and water level. The air pressure and wind speed trend could contribute to the water level changes of west landfall typhoon. We can identify that the water level changes of west landfall typhoon were more dependent on air pressure and wind speed changes rather than other factors.



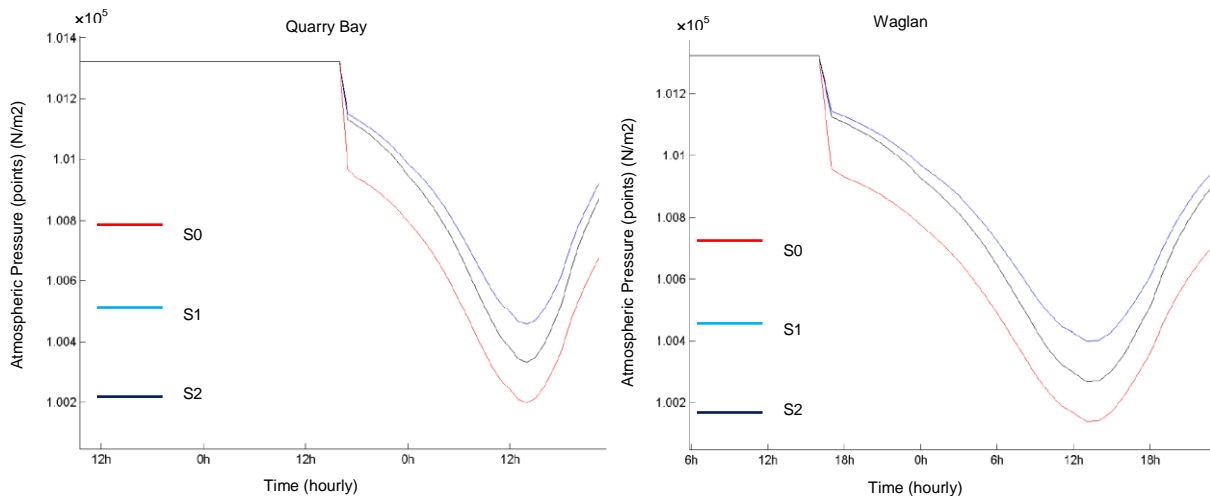


Fig. 3-44 Air pressure at four gauge stations during Hagupit under S0, RCP4.5 (S1) and RCP8.5 (S2)

The spatial distribution of air pressure and wind flow direction during Hagupit provided a good explanation for the inundation changes. Hagupit made landfall in the western part of the PRD region as we can see from Fig.3-45 to Fig.3-47. The estuary is located in the downwind direction of the typhoon, this combined with the effects of the forward speed of the typhoon, means that Hagupit can have a greater impact on the east bay, west bay and estuary. However, because the east bay is more closed to the air pressure centre, it suffered the highest risk compared to other regions.

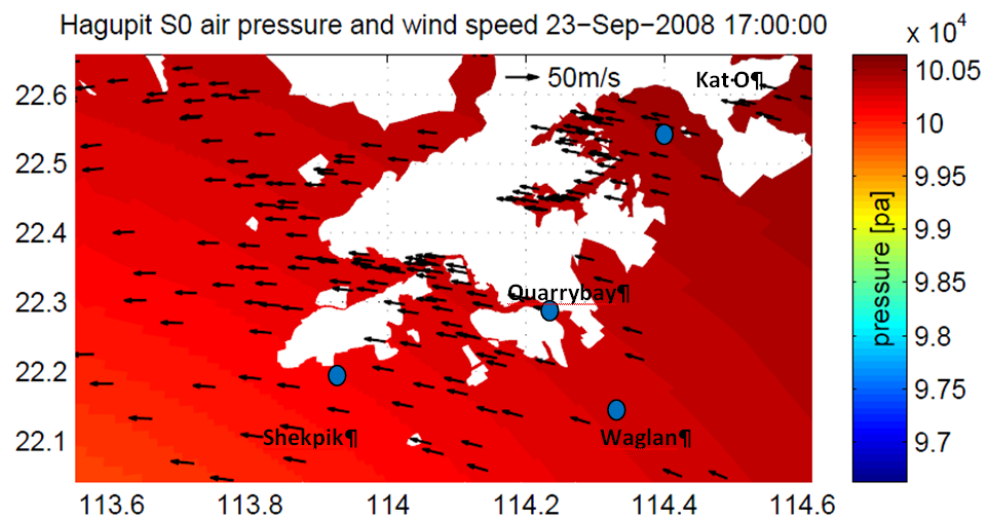
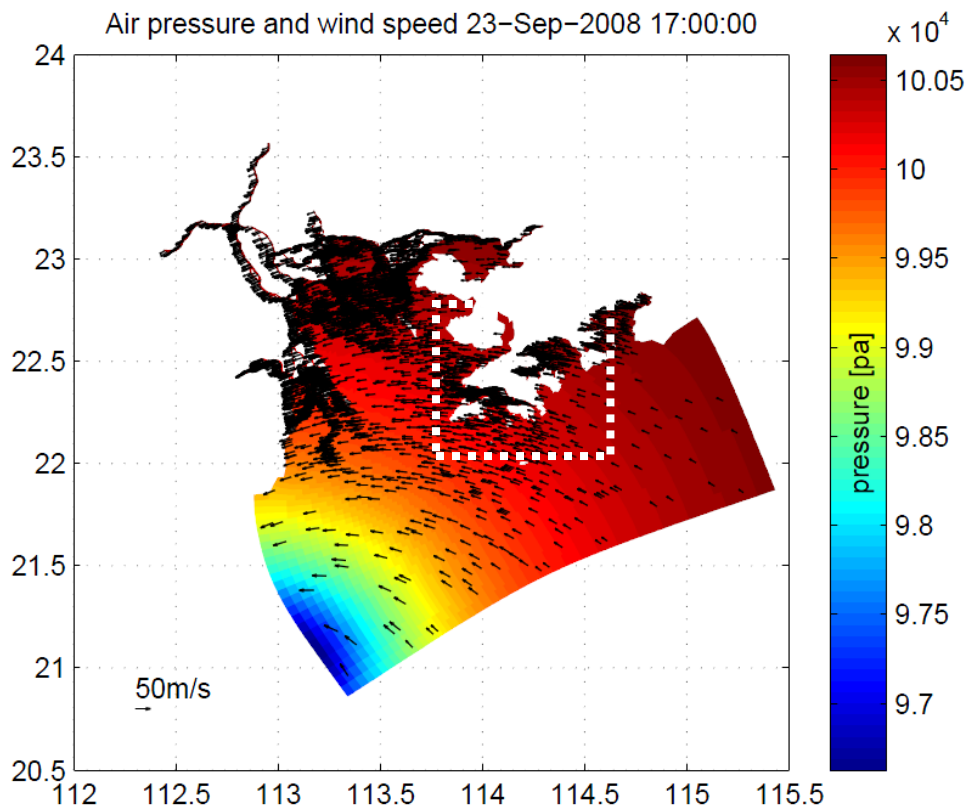


Fig. 3-45 Spatial distribution of atmosphere and wind speed during Hagupit under S0

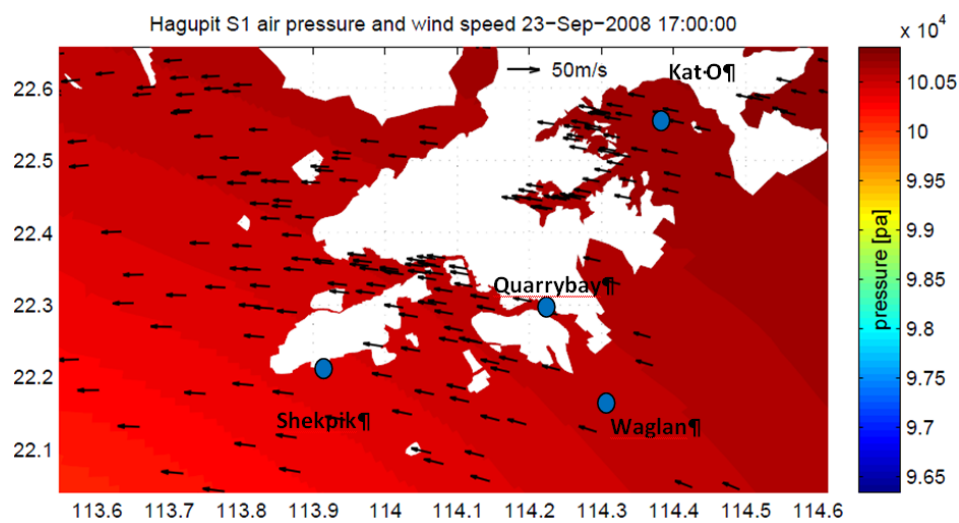
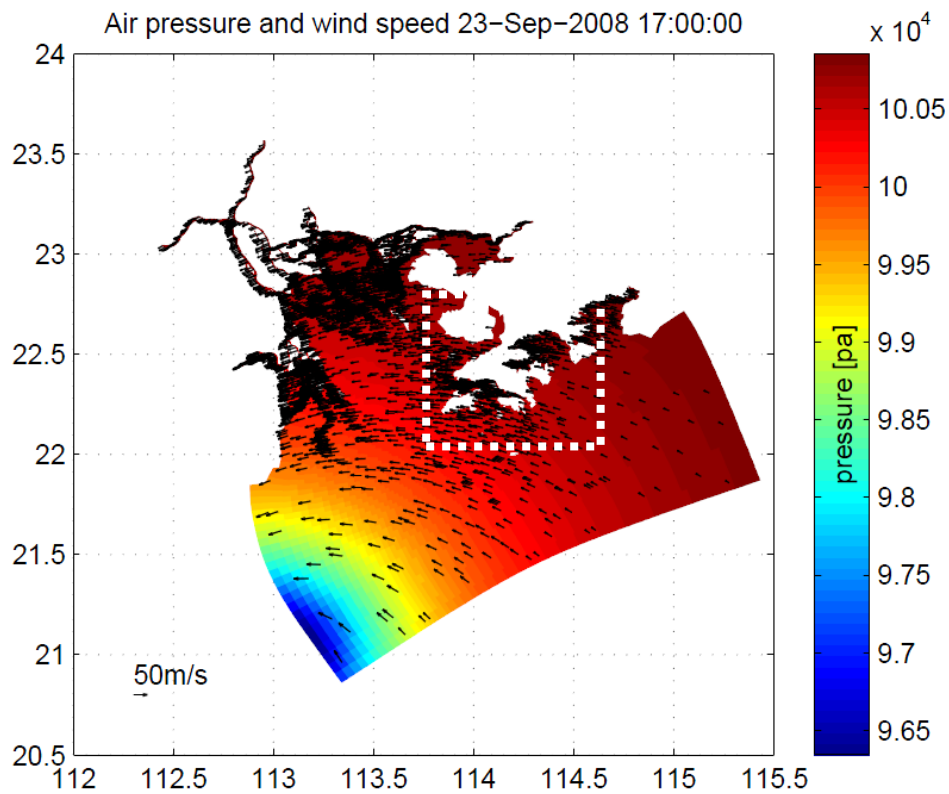


Fig. 3.-46 Spatial distribution of atmosphere and wind speed during Hagupit under RCP4.5 (S1)

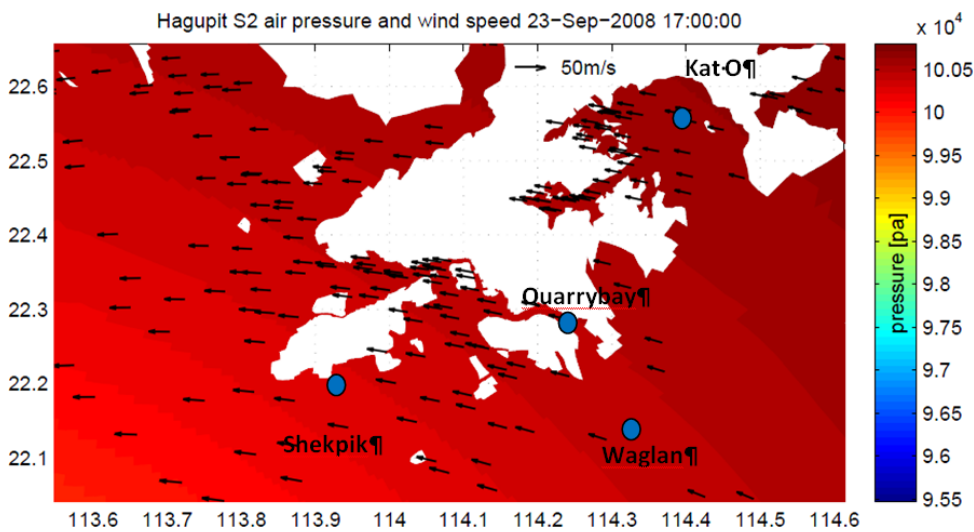
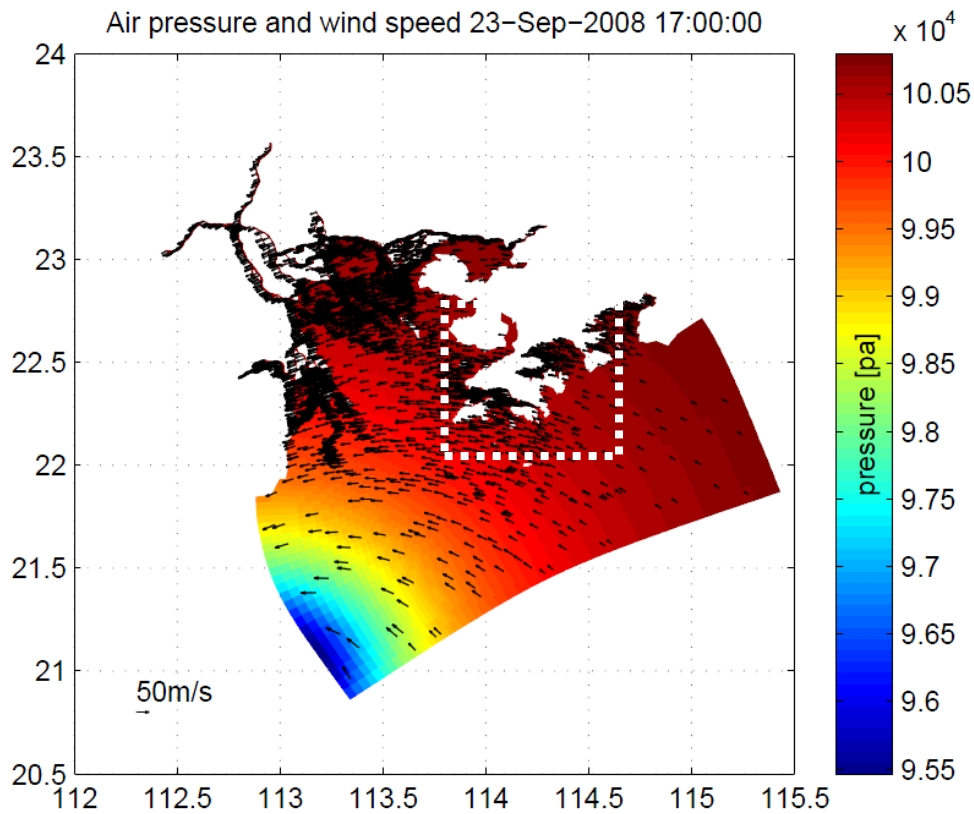


Fig. 3-47 Spatial distribution of atmosphere and wind speed during Hagupit under RCP8.5 (S2)

### 3.5 Conclusion

In this chapter, based theoretical study on the climatology, ocean physics and coastal dynamics, we presented a typhoon induced storm surge simulation framework to explore the impact of climate change on typhoon induced storm surges and coastal inundation in the PRD region. A 2D hydrodynamic model (DFLOW flexible mesh) was

forced with a typhoon model (Delft WES model) under different climate scenarios to quantify the associated storm surge and coastal inundation in the PRD region. We used typhoon Utor in 2001, typhoon Dujuan in 2003 and Hapugit in 2008 as the base case scenarios in the storm surge simulation system. We set up the model for different climate scenarios (RCP 4.5 and RCP 8.5) according to river discharge, typhoon intensity and SLR. We selected six stations for analyzing the impact of climate change on river discharge and typhoon induced storm surges. The upper stream station Makou and the downstream station Pinggang were used for analysis the river discharge change under climate scenarios. Four tidal stations, Kat\_O, Quarry Bay, Shek Pik and Waglan station were chosen for the storm surge study. All stations are located at the estuary along Hongkong coast.

The results showed that the anticipated temperature is increasing and sea level rise under RCP 4.5 and RCP 8.5 scenario could affect river discharge, typhoon induced storm tide elevations and inundation in the PRD region. However, the impacts presented the various spatial attributes under different climate scenarios and different typhoon attributes.

### **3.5.1 River Discharge**

The river discharge at upstream and downstream increased abundantly with a linear trend in the future climate change. Extreme climate condition RCP 8.5 scenario had a higher threat compared to the RCP4.5 scenario. The middle landfall typhoon made the largest increase in daily river discharge in the upstream regions, ranging from 28.5% under RCP4.5 (S1) to 35.7% under RCP8.5 (S2) relative to the baseline scenario (S0). Although the increased magnitude of river discharge during Utor and Hagupit was different, the growth rate almost remained the same. The lowest rise occurs during Hagupit. In the lower reaches of the Pearl River, the hourly river discharge has an apparent storm surge oscillation which indicates the strongly influence by the typhoon. The variation of river discharge during typhoon passage is likely to increase the flood frequencies and intensity. These changes could especially have an impact on the Delta which is one of the leading economic regions and major manufacturing centers of China (D.Yan et al., 2015).

### 3.5.2 Typhoon difference

The different landfall locations of typhoon play an important role in affecting the storm tide elevations and coastal inundation under different climate conditions.

The middle landfall typhoon, Dujuan, had the largest effect on water level changes under climate scenarios. Storm-surge magnitude (the magnitude of the overall storm tide elevation) during the middle landfall typhoon was increasing under RCP 4.5 and RCP 8.5 scenarios. Maximum water level during typhoon attributes similar with Dujuan would increase from 36.7% (RCP4.5) to 46.9% (RCP8.5) by 2100 due to climate change in the PRD region. The most vulnerable region was upstream, the north of the east bay and the south of the east river. Climate change had had a more complex response to water level changes and inundation during the eastern landfall typhoon Utor. The maxima storm elevation of Utor changed apparently, with an increase of 0.8% under RCP4.5 (S1) scenario by 2100. However, the difference between RCP4.5 scenario (S1) and RCP8.5 scenario (S2) is not significant due to the complicated storm tide-surge mechanisms. Under each scenario, there were not only the wind speed and air pressure of typhoon, but also the wind flow angle can result in the water level and inundation changes at particular locations in the PRD region. As the eastern landfall typhoon, the easternmost part of the east bay, the east river bank and the south west of west bay suffered the highest flood risk in those regions.

The western landfall typhoon, Hagupit, showed the water level changes had a positive linear correlation with the wind speed and a negative linear correlation with the air pressure. The maximum water level increased by 0.8% under RCP 4.5 scenario (S1) by 2100, but inundation extents were more obvious under RCP 8.5 scenario (S2) than other scenarios. The western landfall typhoon can affect the east of west bay and east river bank more significantly than other regions especially under RCP 8.5 scenario (S2).

Therefore, we can conclude that landfall locations of typhoons may account for variations in coastal storm tides and coastal inundation. Firstly, the middle landfall typhoon Dujuan is more sensitive to climate change, and it had the greatest threats in the PRD region among all of the three typhoons. There were positive linear correlations between climate projections, the maximum water level and the inundation

extents increased. Secondly, the eastern landfall typhoon Utor existed a higher risk under RCP 4.5 (S1) scenario compared to other scenarios. Due to the wind flow angle function, when the typhoon intensity, river discharge and SLR increasing, negative response happened under RCP 8.5 (S2) scenario during Utor. Thirdly, RCP 8.5 (S2) scenario, the extreme climate condition, had the most danger to the PRD region for the western landfall typhoon Hagupit.

### **3.5.3 Spatial difference**

The uneven spatial and temporal distribution of maximum storm surge elevations in the future climate change during all of the three typhoons in the PRD region revealed that the south of east river constantly was the most vulnerable region in a different level of risk. Climate change was projected to affect not only the downstream (the west bay and east bay) but also the upstream in a different level of risk under different typhoon cases. This finding was coincident with most researches on the PRD geomorphology study, the north Guangdong, north Shenzhen city is less impacted by typhoon induced storm surges compared to the Zhuhai, Zhongshan, Macao region due to the complicated topography at the estuary. Therefore, the climate adaption measurements such as marine defense facilities along the PRD coast should consider the regional differences in different typhoon attributes.

### **3.5.4 Outlook**

This research provided new insight into the coastal risk analysis induced by typhoons in the future climate change but still with many limitations.

Firstly, it must be stressed that this research is not intended to predict the actual inter-annual variability, but only discusses the extreme changes of storm tides and coastal inundation caused by climate change. It is expected that some extreme storms may cause extremely large surges and risks around the PRD area in the future. However, we should conduct more case studies in the future to increase our confidence. Because there are too many other factors could affect the climate response including typhoon intensity, bathymetry, and wind flow angles. This can lead to a significant difference in the results (Knutson et al, 2008; Bender et al., 2010).

Secondly, many studies contested that finer resolution models hopefully will increase the future projections accuracy of tropical cyclone intensity of very intense cyclones, however, in this research, based on the flexible mesh model attribution, the modelling could have the potential advantage to increase the quality of result with the complex coastline region.

Thirdly, a detectable change in tropical cyclone-related rainfall has not been established by this study, which could be revealed in the future. The satellite data assimilation in this spectacular model application still remains blank in the PRD region. Moreover, a substantial and complete database will improve the numerical model results qualities. For example, in Europe, the relative comprehensive database and shared system provide an efficient and advanced coastal research environment. Therefore, the database establishment not only in the PRD region also in the entire coastal region in China is extremely necessary to improve the research in the similar field. Additionally, we also provide specific recommendations on building up a climatology theory on coastal research, enhancing the climate-relevant observational activities, and modelling of tropical cyclones related regional climate change in the future (Knutson et al., 2010) along the China coast.

## 4 Coastal inundation and economic losses under urbanization and climate change scenarios

The fast developing coastal area such like the PRD region is more vulnerable for the storm surge inundation risk as we discussed in the previous chapters. The fast urbanization will also increase the coastal inundation risk in this developed coastal region. Among the climate change and the urbanization, which one is the critical driver of coastal inundation changes and economic losses by typhoon induced storm surge in a particular region? To what extent do the climate change and urbanization contribute to the coastal inundation changes and economic losses by the typhoon? Should we pay more attention to the urbanization before we talk about climate change? All these questions are left unclear.

Some researches on the land use exposure and vulnerability flood risk assessments have already been conducted in the different regions of China. However, the PRD region has not received as much attention. An example of flood damage estimation analysis for the downtown of Shanghai is a good reference for the coastal risk research<sup>8</sup>, which concluded that the damage function is the most sensitive factor on flood damage estimation. The research on the flood risk assessments under climate change is even rare in the PRD region. Liang Yang et al. (2015) applied the climate model in the PRD region to exam the climate- flood risks (flood frequency and flood vulnerability) and urban responses. Another modelling study on the impacts of land use change on hydrological processes was carried out in Shenzhen city (one big city in the PRD region) (ZHENG Jing. et al., 2009). Those researches provided a valuable reference. However, they are barely to investigate the coastal inundation changes and economic losses induced by typhoons under different land use scenarios and climate change scenarios in the PRD region.

This chapter will explore the role of urbanization and climate change in the coastal inundation and economic losses caused by typhoons on a large scale (PRD). For each scenario, I assessed the economic losses using land use database combined

---

<sup>8</sup> Q. Ke, S.N. Jonkman, P. H. A. J. M. van Gelder and T. Rijcken. Flood damage estimation for downtown Shanghai – sensitivity analysis.

with coastal inundation extent map and economic data. Since the PRD region is one of the fastest-growing regions in China, the land use experiences huge changes every single year. I used the land use changes to represent the urbanization changes process in the PRD region. The peak water level and extent of typhoon Dujuan under different climate scenarios from Chapter 3 are used to demonstrate the climate impacts on the coastal region. The study area includes nine cities in the PRD region and Macao. This land use based appraisal of present and future economic losses of coastal inundation can provide information to support climate change adaptation strategies, disaster risk reduction and sustainable urban planning, and also validates hydrodynamic simulation models (De Roo et al., 2001, Van der Sande C,2003).

#### **4.1 Materials and Methodologies**

I used land use based approaches and absolute stage-damage function to calculate coastal inundation area changes and economic losses induced by typhoons under different climate scenarios. In the mesoscale estimation, land use based approach is one of the common methods to assess the economic losses in a region or a city. The stage-damage function is a widely accepted concept for illustrating the correlations between flood characteristics (such as water depth, velocity, flood duration, etc.) and damage extent (being shown either by the absolute damage values or relative damage ratio) (KeQian, Van Der Sande, 2001). Therefore, the land use based approaches and stage-damage function will be introduced in this chapter but in a slightly different way from the flood risk assessment.

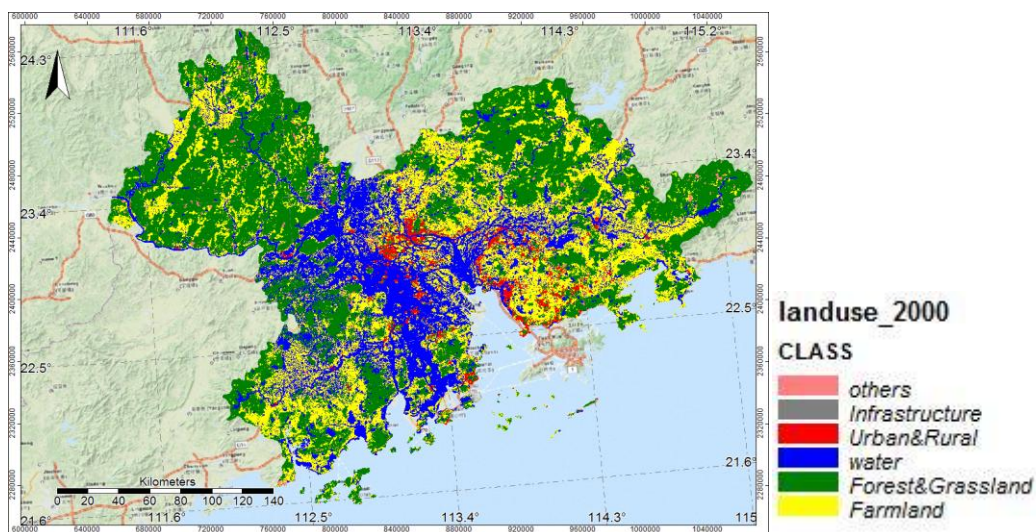
##### **4.1.1 Water level data**

It should be specified that the definition of flood is broader than the definition of coastal inundation. In this research, I consider the coastal inundation risk induced by typhoon induced storm surges, the inland flooding and rainfall effects are not included. The water level and extent are the most important aspects for direct losses on a large scale (Green et al., 1994).The peak water level and extent data of Dujuan in different climate scenarios are from Chapter 3.

#### 4.1.2 Land use data

The process of urbanization plays an important role in influencing the local hydrologic system and altering hydrologic characteristics (Montz, 2000). The land use data in the year of 2000 and 2010 were employed to present the urban development scenarios. In this research, the dataset originally from the Landsat TM imagine with a resolution of 30\*30 meters was used. This data was corrected using the SPOT scenes based on field investigation and visual judgment in the Geographic Information System (GIS). The final dataset comprises six land use categories those are urban and rural land, agricultural land, forest and grass land, water areas, infrastructure and others. The water areas in this land use classification also include the Fishpond areas. All land use categories are applied to the absolute stage-damage function calculation.

The detailed land use information as shown from Fig.4-1, it is obvious that the area per land use category changed dramatically in the PRD region from 2000 to 2010 especially for urban and rural land. The fast urbanization development during these ten years in the PRD region could be represented by the expansion of urban, rural area and infrastructure transportation area. Among them, the urban and rural area increased by 30%, ranging from 5775.5 km<sup>2</sup> to 7520.2 km<sup>2</sup>.The infrastructure transportation area even grew by 58%. On the contrast, a decline in agricultural land (farmland) exceeding 10%, which was from 12797.5 km<sup>2</sup> to 11606.2 km<sup>2</sup>. Forest and grassland were with a decrease of 285 km<sup>2</sup>.The water areas also marked almost 4% decrease (Table 4-1, Fig.4-2).



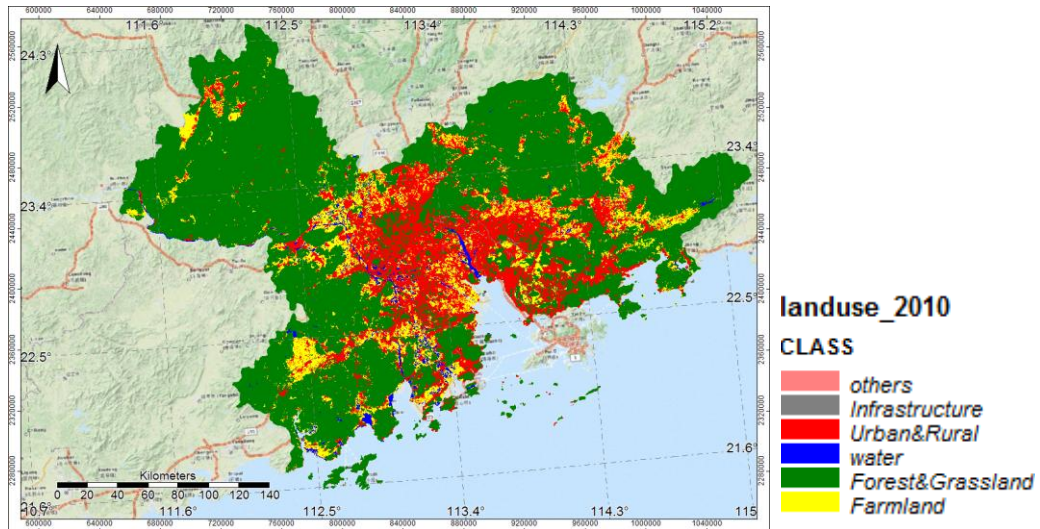


Fig. 4-1 Land use data in the year of 2000 (up) and 2010 (down)

Table 4-1 Land use area per category in the year of 2000 and 2010

Class/Year	2000 (unit km <sup>2</sup> )	2010 (unit km <sup>2</sup> )
Urban and Rural land	5775,546467	7520,234463
Infrastructure	43,30839093	68,49826747
Forest and Grassland	29784,813	29499,55819
Agricultural land (Farmland)	12797,51717	11606,23477
Water areas	4840,119636	4656,219806
Total	53442,16777	53447,7159

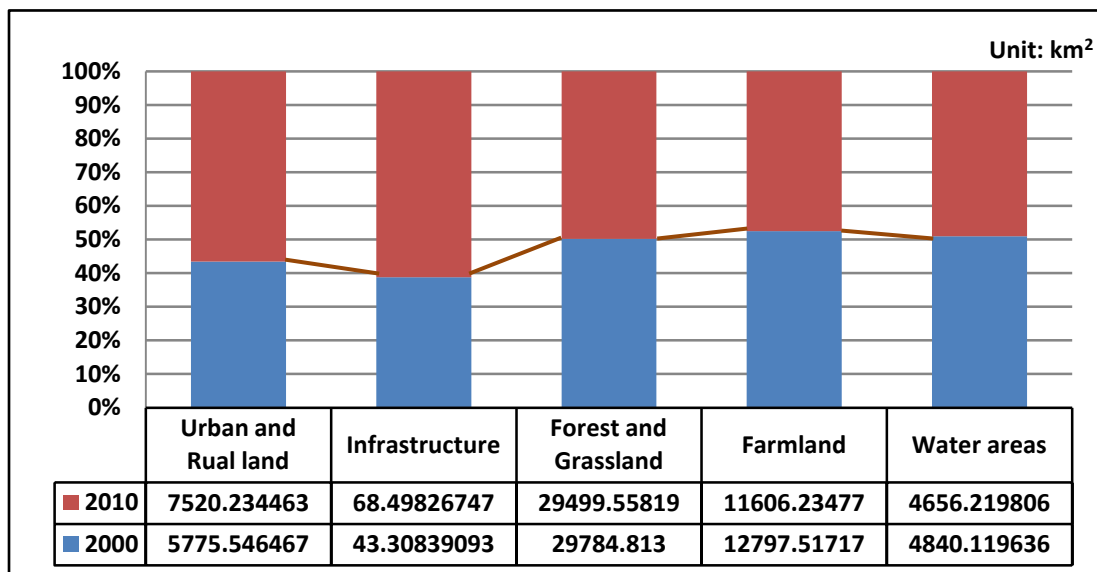


Fig. 4-2 Land use area changes in the different categories from 2000 to 2010

The water level data and land use data were progressed in the SAGA GIS environment.

#### 4.1.3 Economic losses calculation

Economic losses in this research are calculated by the absolute stage-damage function, where have three components: different land used classes, typhoon induced water levels and economic value per square kilometer (ICPR, 2002). The maximum fixed damage values are based on the average price per km<sup>2</sup> GDP of the three main industries. That is the Primary Industry, the Secondary and the Tertiary Industry. We used GDP data in the PRD region in the years of 2000 and 2010 and correspondingly the land use data from 2000 and 2010.

It is emphasized that the PRD economic data is not including the Macao economic data, however, my research domain in the hydrodynamic modelling including Macao, therefore I added the GDP in Macao to the GDP value of PRD. Primary Industry and Secondary Industry are rarely found in Macao, the economy of Macao is predominantly Tertiary Industry. Therefore we made the assumption that the GDP of Macao mainly goes to Secondary and Tertiary Industry in this research. Table 4-2 shows the detailed data.

Table 4-2 GDP in the PRD region in the year of 2000 and 2010

PRD (include Macao) unit (million EURO)	2000	2010
Gross domestic product (GDP)	120356,6501	539469,4548
Primary Industry	6263,196376	11070,43255
Secondary and Tertiary Industry	114090,0645	528422,1823

Note: I collected the PRD GDP data of 2000 according to the Interim Regulation on the Division of Urban and Rural Areas in Statistics promulgated by the National Bureau of Statistics. The rate is based on 26.04.2016: 1 Chinese RMB Yuan = 0,1367 Euro; 1 Macao Pataca (MOP) = 0,11 Euro. The inflation is ignored here.

White outlined this basic methodology of stage-damage function in 1945 (White, 1945) and the stage damage curve is used to represent the relation between inundation depth and economic cost for a land use class. The economic value of the each land use category has to be known to calculate the damage. We defined the value of each

land use category: the urban and rural land use along with the Infrastructure are belonging to Primary Industry, the other land use classes (forest and grassland, farmland and water areas) are categorized to Secondary and Tertiary Industry (see Table 4-3).

Table 4-3 The economic value of each land use category

Land use category	GDP
Urban and Rural area	The Primary Industry
Infrastructure	
Forest and Grassland	The Secondary and Tertiary Industry
Farmland	
Water Areas	

After the calculation, the economic value of the Secondary and Tertiary Industry per km<sup>2</sup> (A) and the value of the Primary Industry per km<sup>2</sup> (B) are listed in Table 4-4.

Table 4-4 The economic value (A) and (B) in the year of 2000 and 2010

Unit (million EURO/km <sup>2</sup> )	2000	2010
$A(Q_{\text{Secondary+TertiaryIndustry}}/\text{land use area}_{\text{Urban\&Rual+Infrastructure}})$	19,60696173	69,63246711
$B(Q_{\text{PrimaryIndustry}}/\text{land use area}_{\text{(forest\&grassland, farmland, water areas)}})$	0,132072392	0,158806563

The principle of economic losses calculation is as follows,

$$\text{Loss\_Q}_{\text{Secondary +TertiaryIndustry}} = A * \text{Inundation area}_{\text{(Urban\&Rual + Infrastructure)}}$$

$$\text{Loss\_Q}_{\text{PrimaryIndustry}} = B * \text{Inundation area}_{\text{(Forest\&Grassland, Farmland, water)}}$$

$$\text{Loss\_total} = \text{Loss\_Q}_{\text{PrimaryIndustry}} + \text{Loss\_Q}_{\text{Secondary +TertiaryIndustry}}$$

A linear absolute stage-damage curve based on the stage-damage function is finally built up according to the economic losses and a range of water depth (1-5 meters in this research).

## 4.2 Results

In this section, I analyzed the results of the coastal inundation area changes and economic losses under different climate change scenarios and different land use scenarios.

### 4.2.1 Coastal inundation and economic losses under climate change scenarios

#### *Coastal Inundation*

In this part, I calculated the economic losses of coastal inundation under different climate scenarios. The land use scenario in 2000 and the water level of Dujuan from different climate scenarios were applied here. The GDP in 2000 in the PRD region including Macao was used for the economic losses calculations. The infrastructure transportation area is much less than other land use categories, I combined the infrastructure transportation category to urban and rural category when calculating the inundation area. From Fig.4-3 to Fig.4-5 presents the coastal inundation under climate scenario S0, RCP4.5 (S1) and RCP8.5 (S2).

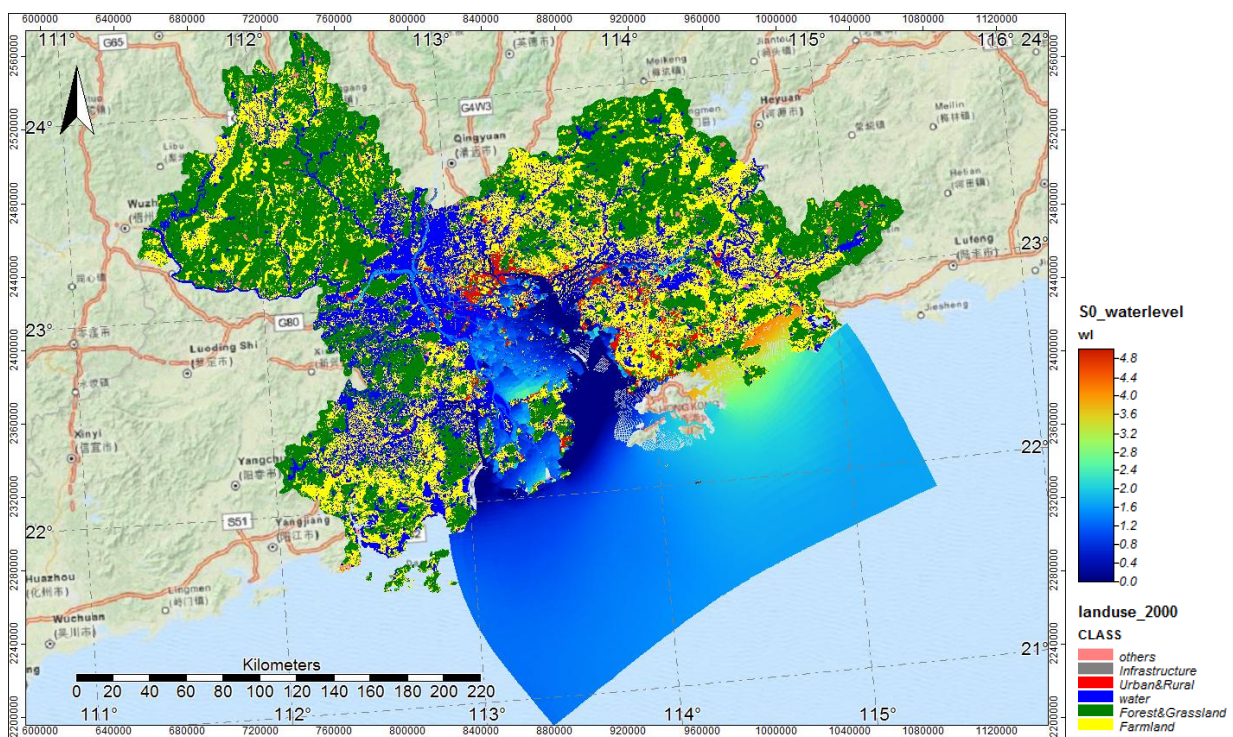


Fig. 4-3 Coastal inundation under the baseline scenario (S0) of the land use scenario 2000

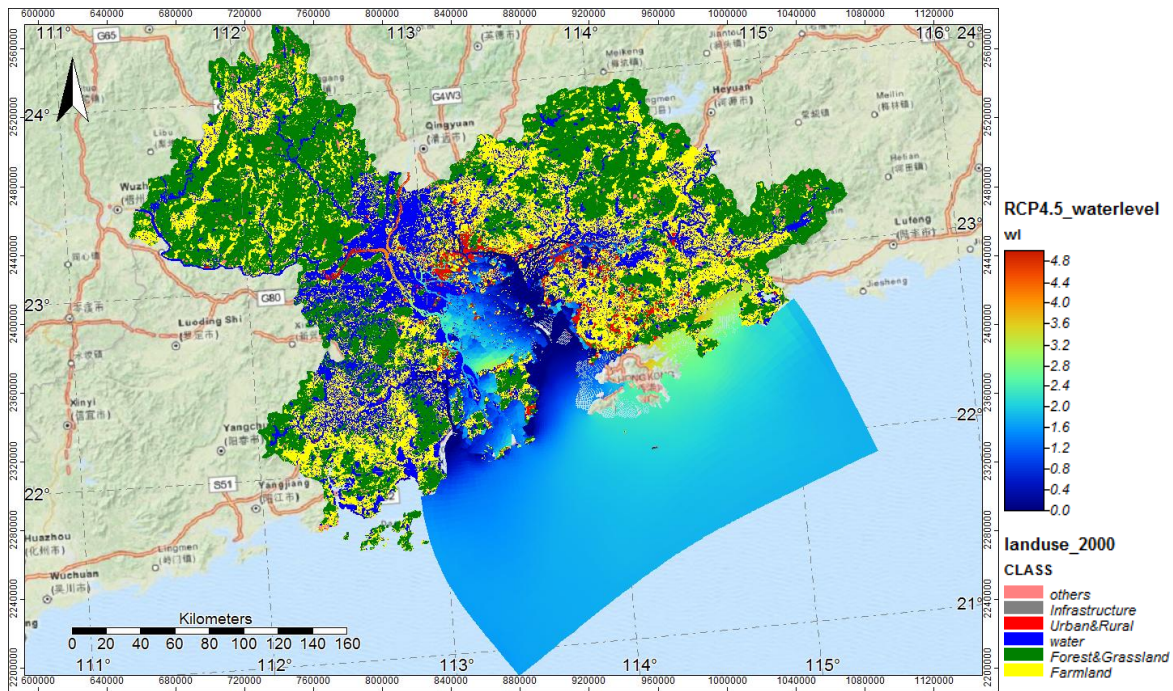


Fig 4-4 Coastal inundation under RCP4.5 (S1) of the land use scenario 2000

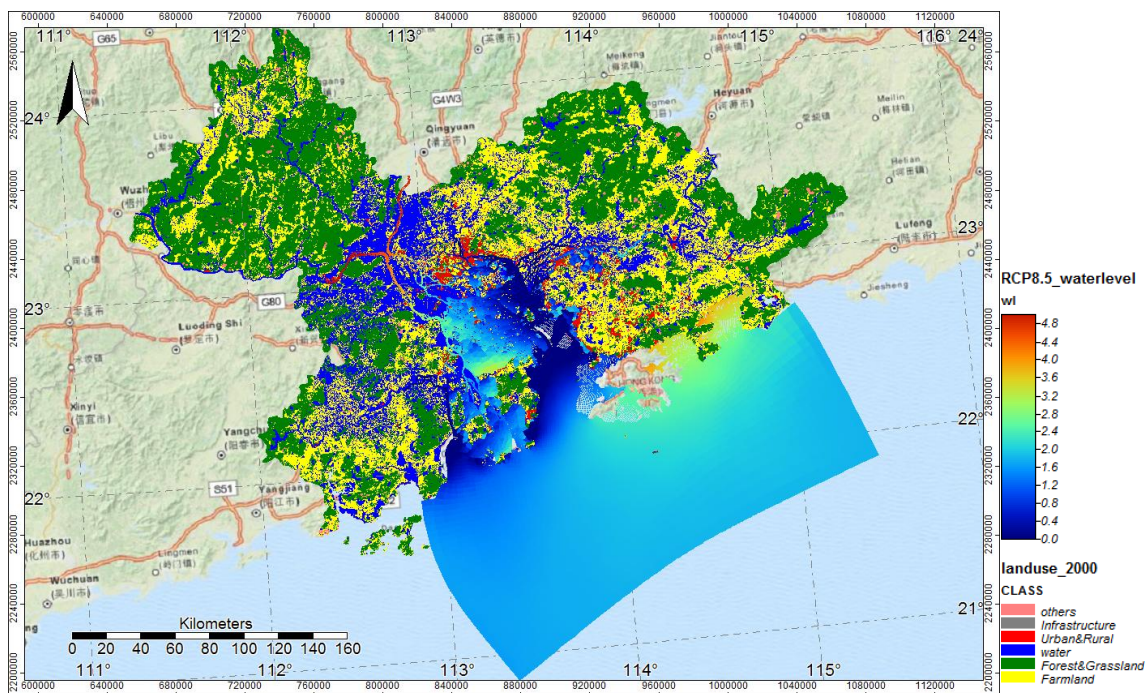


Fig 4-5 Coastal inundation under RCP8.5 (S2) of the land use scenario 2000

In the table 4-5 and Fig.4-6, we can see that the inundation area of the urban region under baseline scenario (S0) and the RCP8.5 scenario is larger than RCP4.5 scenario when the inundation water level is 1 meter high. When the inundation water level goes to 2 meters high, the inundation area in all three scenarios accelerates dramatically.

The total inundation area of the urban region shows a linear increase in climate change conditions. The maxima inundation area under RCP 8.5 will be 993,6 km<sup>2</sup> with a 17% increase compared to the baseline scenario S0. However, the increased inundation area slows down under scenario S0 and RCP 4.5 when the water level is higher than 3 meters. When it goes to more than 4 meters (including 4 meters), the increased inundation area under RCP 8.5 is not obvious as well.

Table 4-5 Urban region inundation area under different climate scenarios

Water level (m)	Inundation Area (km <sup>2</sup> )		
	S0	RCP4.5(S1)	RCP8.5(S2)
1	356,6238645	288,334582	390,9150677
2	781,8779906	747,4895326	846,4893468
3	846,8923649	871,1745699	968,4443995
4	847,8422091	875,2155918	990,9109841
5	848,3037281	877,5828239	993,5737505

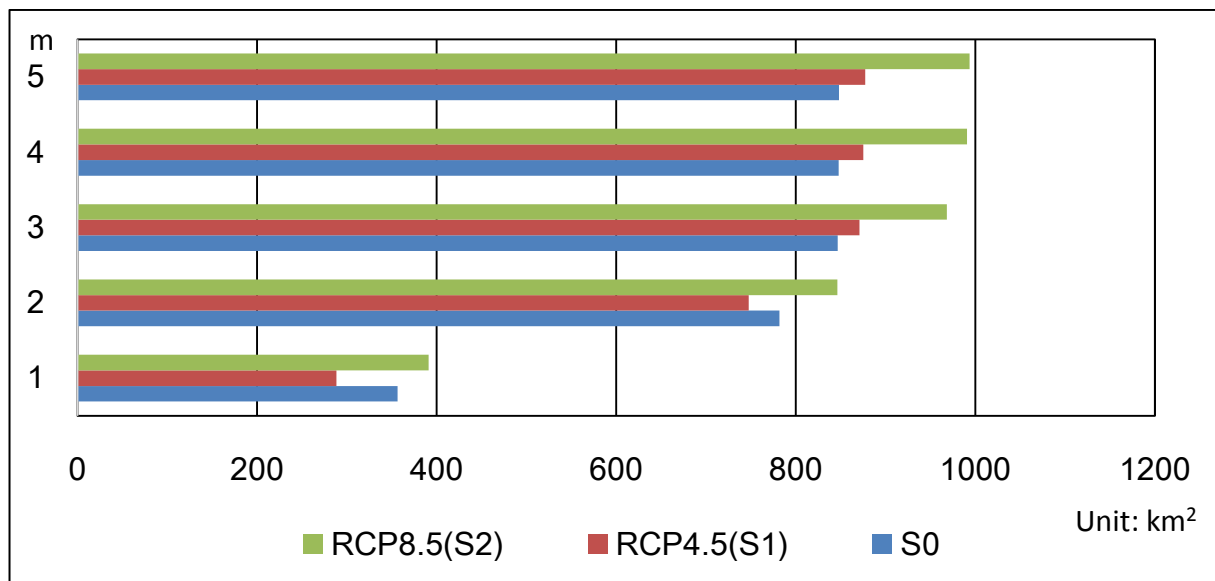


Fig. 4-6 Urban region inundation area under different climate scenarios

The inundation area of Forest and Grassland is much lower than urban region under the climate change. We can notice that the RCP4.5 (S1) scenario gave the largest inundation extents about 352,7 km<sup>2</sup> among all scenarios. When the water level is 1 meters high, the baseline scenarios (S0) displayed a significant increase extents

than other scenarios. The inundation area of Forest and Grassland occurs as an increasing linear trend along with climate conditions changes.

Table 4-6 Forest and Grassland inundation area under different climate scenarios

Water level (m)	Inundation Area (km <sup>2</sup> )		
	S0	RCP4.5(S1)	RCP8.5(S2)
1	144,1447468	99,01776318	97,0570973
2	293,4997556	296,5118605	281,5246729
3	318,8472202	347,7498791	335,3965687
4	321,3222524	350,7036946	343,0582506
5	323,4599818	352,7176302	345,2416173

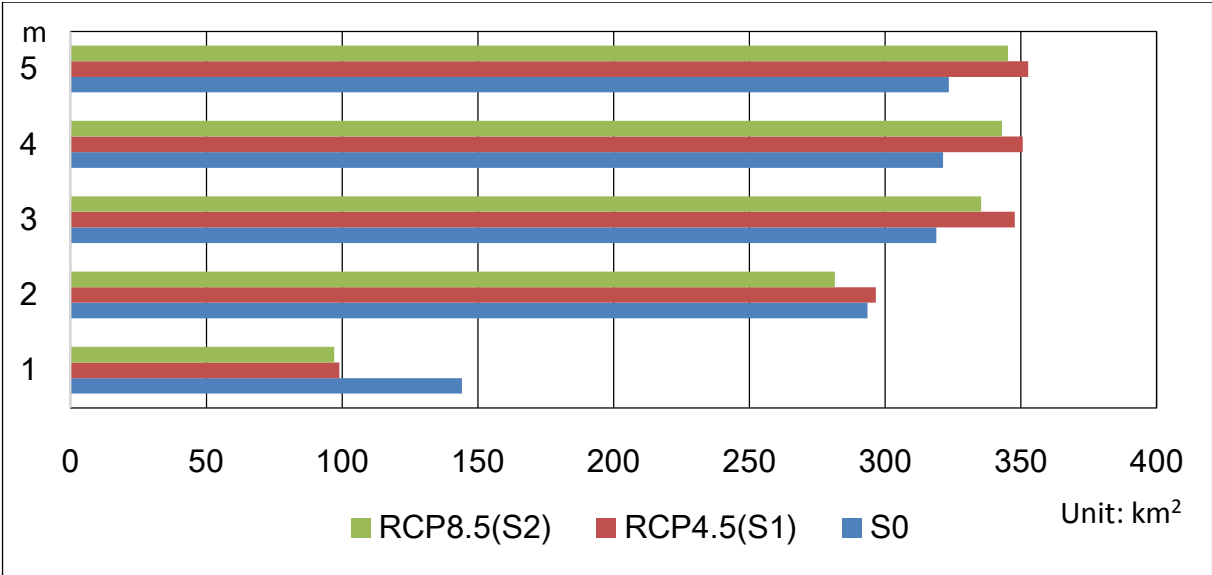


Fig. 4-7 Forest and Grassland inundation area under different climate scenarios

It is apparent that both agricultural land and water region exhibited a huge inundation in all climate conditions. As same as the forest and grassland, the most enormous increase lies in the RCP4.5 (S1) scenario. The inundation extent of agricultural land (farmland) is 1170 km<sup>2</sup> under RCP4.5 (S1), the water region is 1328 km<sup>2</sup>. The water region includes the fish pond. We also can notice that even the water level only increase 1 meter high, agricultural land is the most vulnerable region for the coastal inundation. For example, the minimum inundation area is around 504 km<sup>2</sup>, which is much larger compared to the other land use categories.

Table 4-7 Agricultural (Farmland) inundation area under different climate scenarios

Water Level (m)	Inundation Area (km <sup>2</sup> )		
	S0	RCP4.5(S1)	RCP8.5(S2)
1	591,9472397	515,5476417	504,2171778
2	1104,348954	1048,482378	1012,383866
3	1143,505951	1147,75014	1126,679785
4	1148,035772	1159,108263	1141,305622
5	1149,658895	1170,012902	1154,269436

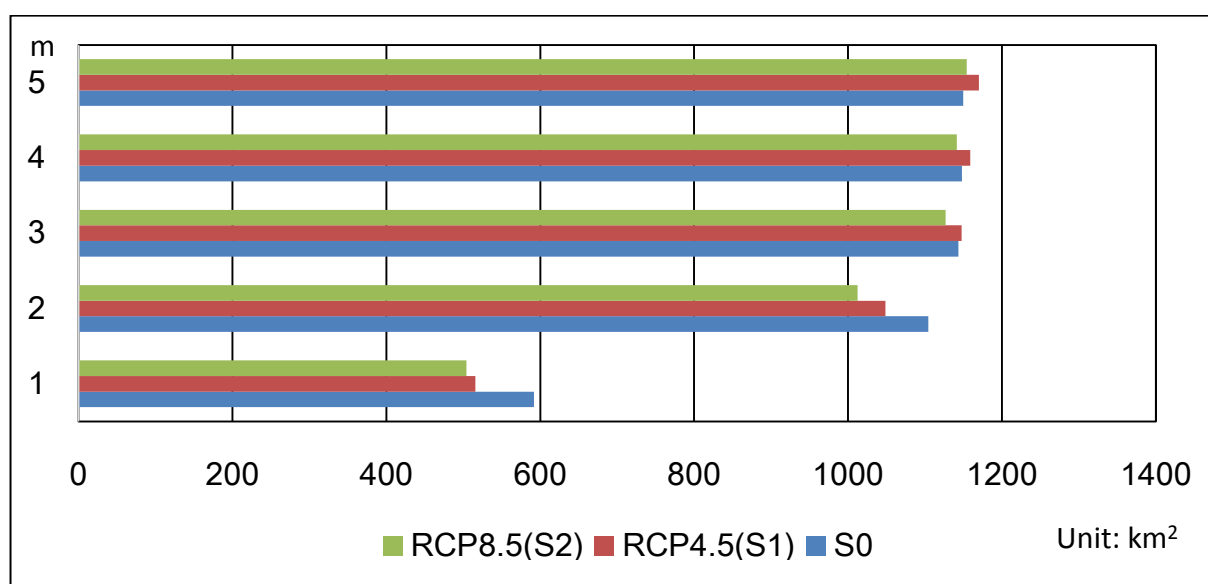


Fig. 4-8 Agricultural (Farmland) inundation area under different climate scenarios

Table 4-8 Inundated water areas under different climate scenarios

Water level (m)	Inundation Area (km <sup>2</sup> )		
	S0	RCP4.5(S1)	RCP8.5(S2)
1	505,2073289	349,5477557	356,3594868
2	1208,544972	989,6610095	945,0707214
3	1247,072573	1196,585133	1173,08326
4	1249,84914	1251,238237	1229,434977
5	1251,472263	1328,134785	1321,523148

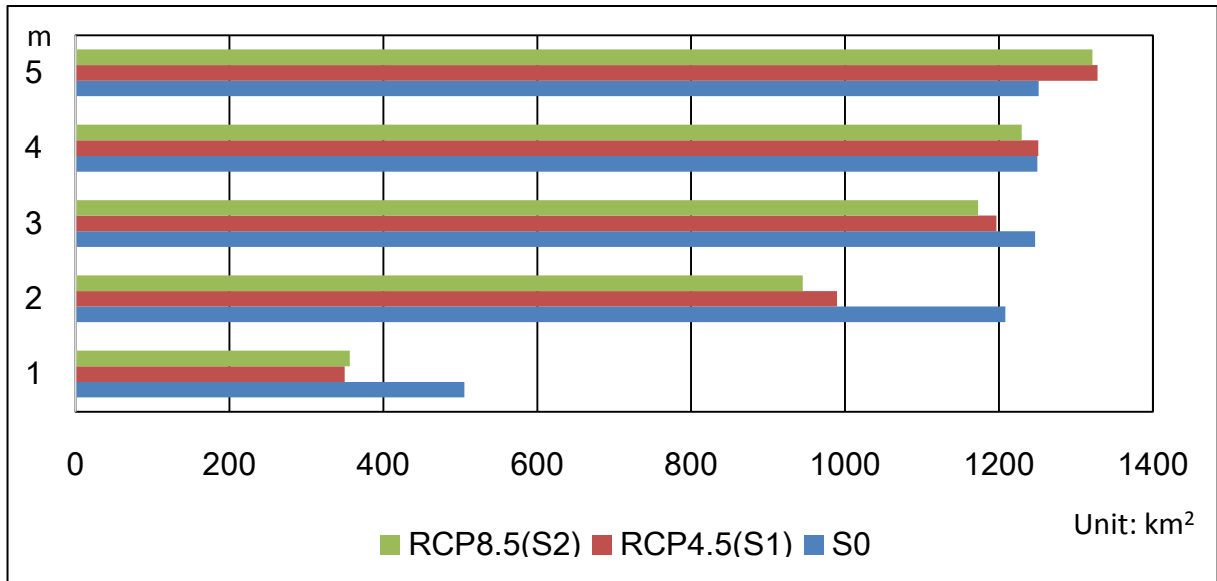


Fig. 4-9 Inundated water areas under different climate scenarios

Therefore we could infer that under the land use scenario 2000, agricultural land (farmland) would have the highest risk of typhoon induced storm surges. The Urban region can also suffer a higher threaten, but the forest and grassland are much less inundated during Dujuan under different climate scenarios. Additionally, the urban region is higher vulnerable under RCP8.5 (S2) scenario, other land use categories are more affected under RCP4.5 (S1).

Table 4-9 and Fig.4-10 provide the whole inundation area during Dujuan in the PRD region in all scenarios, we can see that the inundation area increase from the baseline scenario to RCP 8.5. The growth is around 3.8%. The results show that inundation changes have a linear relationship with climate condition changes, which closely resemblances the results in Chapter 3.

Table 4-9 The whole inundation area in the PRD under different climate scenarios

Water Level (m)	Inundation Area (km <sup>2</sup> )		
	S0	RCP4.5 (S1)	RCP8.5 (S2)
1	1597,92318	1252,447743	1348,54883
2	3388,271673	3082,144781	3085,468607
3	3556,318109	3563,259721	3603,604013
4	3567,049374	3636,265786	3704,709834
5	3572,007661	3728,448141	3814,597346

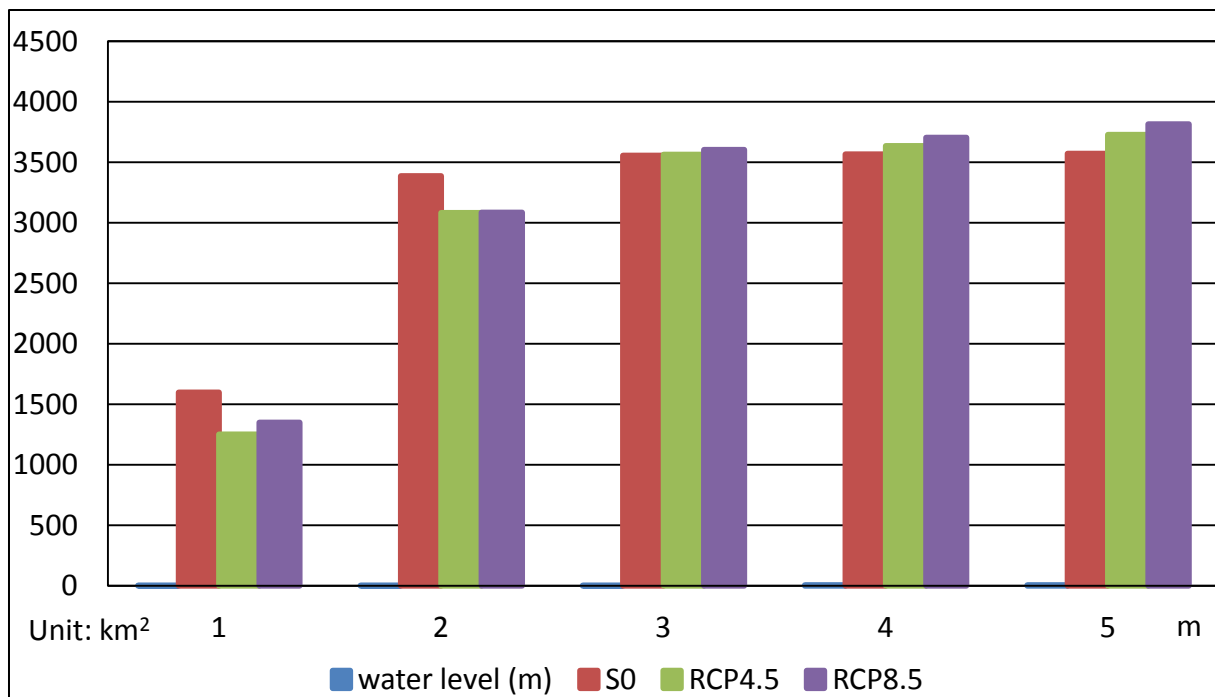


Fig. 4-10 The whole inundation area in the PRD under different climate scenarios

### Economic losses

Table 4-10 and Fig.4-11 list the economic losses (Million Euro) of Dujan coastal inundation under different climate scenarios. We can see that the losses of RCP8.5 are absolutely higher than other scenarios with around 19853 million Euros, which has a 16.8% increase compared to the baseline scenario S0. However, the RCP4.5 gives the lowest economic losses among all scenarios. As discussed before, we found that agricultural land (farmland), forest and grassland, water areas remain at the highest inundation risk during RCP4.5. All of these land use categories are belonging to the Primary Industry, and the Primary Industry only accounts for 0,132072392 Euro/km<sup>2</sup>. Even though the inundation areas of these land use categories are larger than that of urban regions, the economic losses are much lower. We can see that the economic losses from coastal inundation under different climate scenarios at the same water level demonstrated an increasing linear trend that was interrupted by a decrease under the RCP4.5 scenario. Therefore, we could make a preliminary judgment that the economic losses of coastal inundation highly depend on the land use scenarios.

Table 4-10 Economic losses of coastal inundation under different climate scenarios

Water Level (m)	Economic Losses (million Euro)		
	S0	RCP4.5	RCP8.5
1	7156,251831	5780,697845	7791,133752
2	15674,48448	10372,52	16892,79157
3	16962,82652	12844,81442	19336,28411
4	16982,74194	12933,15496	19787,17164
5	16992,38482	12991,43128	19853,33529

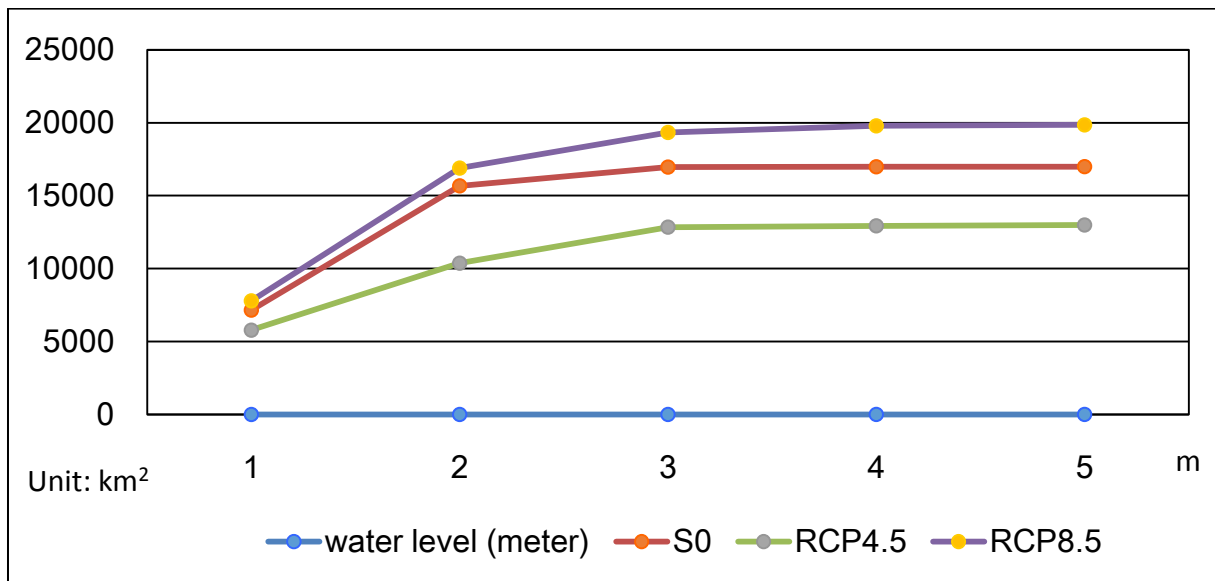


Fig. 4-11 Economic losses of coastal inundation under different climate scenarios

#### 4.2.2 Coastal inundation and economic losses under urban development scenarios

In this research, land use changes were used to present the urban development scenarios. This part examined the coastal inundation and economic losses during Dujan in the baseline scenario S0 under different land use scenarios in the year of 2000 and 2010. The GDP from 2000 and 2010 in the PRD region, including Macao, were used for economic loss calculations. As explained in the data section, the land use changed significantly from 2000 to 2010 especially in the urban region, which increased the inundation risk. The Fig.4-12 and Fig.4-13 show how much area in the PRD region was inundated and the economic losses during the same typhoon under the different land use scenarios.

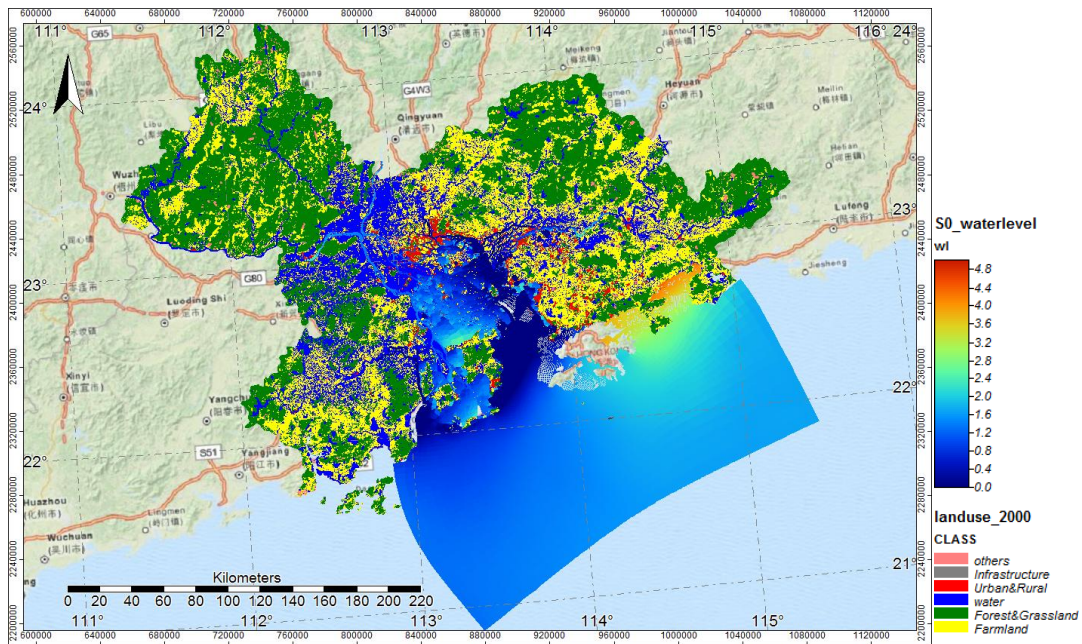


Fig. 4-12 Coastal inundation under the baseline scenario (S0) of the land use scenario 2000

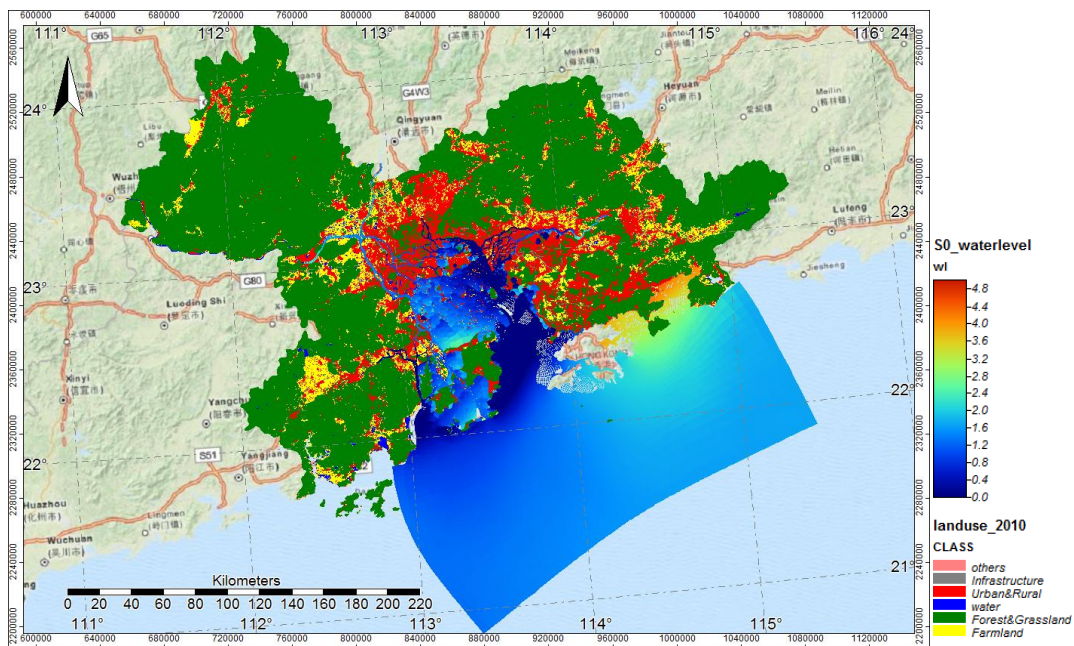


Fig. 4-13 Coastal inundation under the baseline scenario (S0) of the land use scenario 2010

### ***Urban-Rural Land and Infrastructure***

As we can see from table 4-11 and Fig.4-14, the urban region inundation area in 2010 was almost 30% higher than in the year of 2000 in the same typhoon scenario. The inundation extent was also linearly increased when the water level raised. The

inundation area in 2010 was about 1168.6 km<sup>2</sup> when the water level reached 5 meters.

Table 4-11 Urban region inundation area under different land use scenarios

Urban region Water level (m)	Land use area (km <sup>2</sup> )	
	2000	2010
1	356,6238645	492,0548508
2	781,8779906	1086,784055
3	846,8923649	1166,471099
4	847,8422091	1167,837994
5	848,3037281	1168,591458

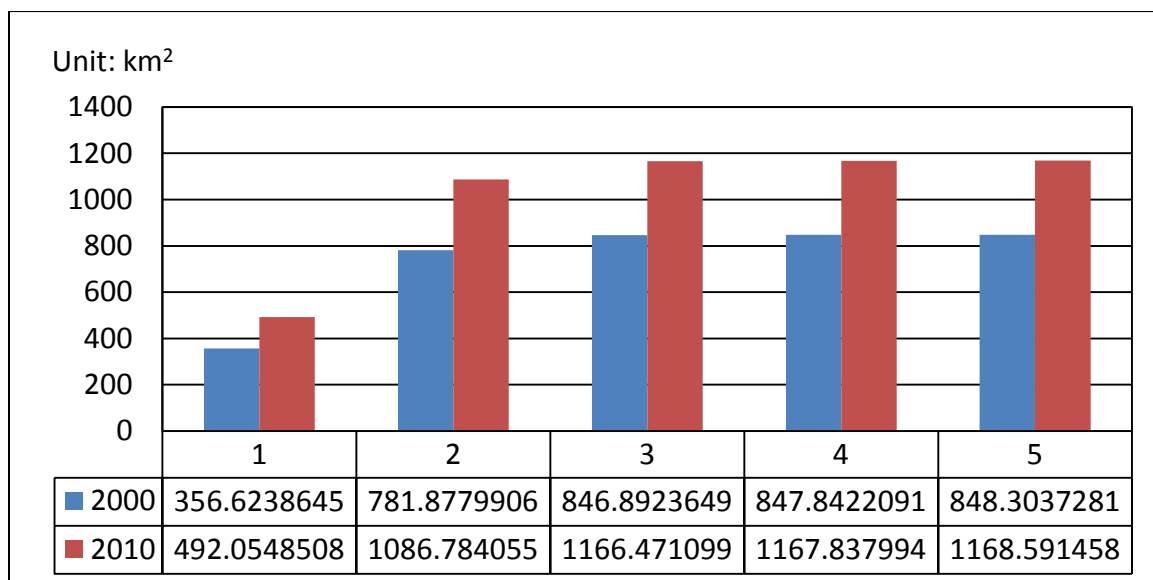


Fig. 4-14 Urban region inundation area under different land use scenarios

### **Forest and Grasslands**

The land area of forest and grasslands decreased from 2000 to 2010. Compared to the inundation area of urban regions, forest and grasslands also showed much lower inundation extents. The maximum inundation area in 2010 was declined by 3.7% relative to the year of 2000. The main reason for this declination is that forest and grasslands have been reduced by urban expansion, correspondingly the coastal inundation areas of forest and grasslands have also been reduced.

Table 4-12 Forest and grassland inundation area under different land use scenarios

Water level (m)	Inundation area (km <sup>2</sup> )	
	2000	2010
1	144,1447468	135,3843449
2	293,4997556	283,6686356
3	318,8472202	308,6164987
4	321,3222524	310,6549589
5	323,4599818	311,2708873

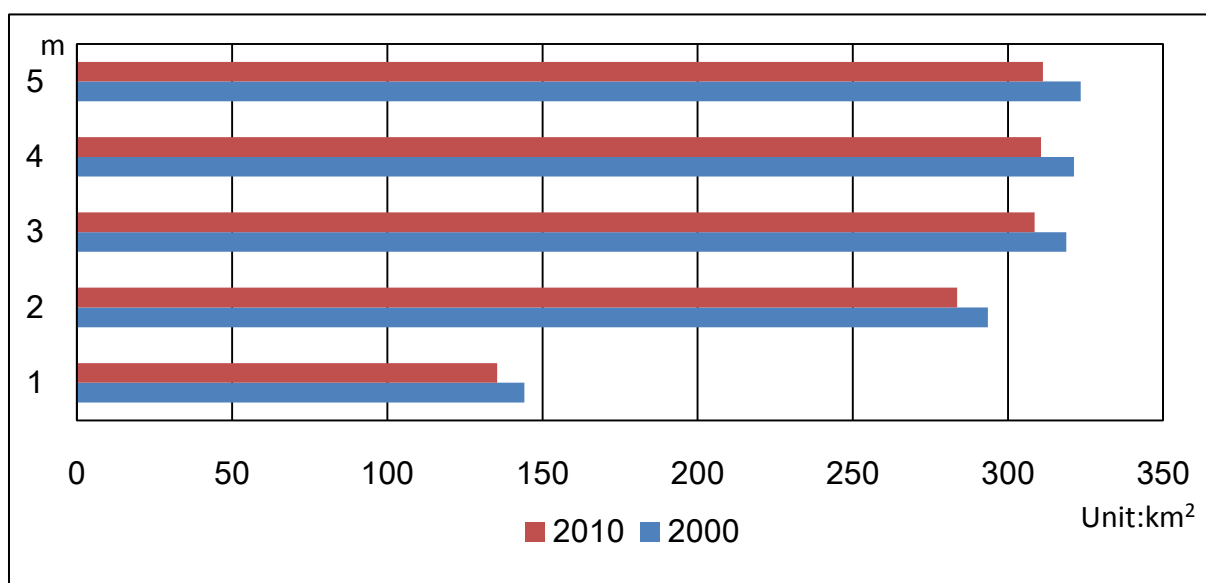


Fig. 4-15 Forest and grassland inundation area under different land use scenarios

### ***Agricultural Land (Farmland)***

The agricultural land (farmland) and water areas present a similar trend as forest and grassland. The inundation areas in both land use categories provide a decreased tendency. The total decrease amounts of the agricultural (farmland) inundation are 208 km<sup>2</sup> from 2000 to 2010. A slight decrease occurs in the inundated water area ranging from 1251.4 km<sup>2</sup> to 1217 km<sup>2</sup>. When the water level increased from 1 meter to 2 meters, the inundation of the agricultural land (farmland) and water areas doubled. However, the inundation increased slowly by a relatively small amount when the water level rose to 3 meters and beyond, under both land use scenarios (2000 and 2010).

Table 4-13 Agriculture (Farmland) inundation area under different land use scenarios

Water level (m)	Inundation area (km <sup>2</sup> )	
	2000	2010
1	591,9472397	493,9720434
2	1104,348954	905,3608934
3	1143,505951	935,5980603
4	1148,035772	939,9115108
5	1149,658895	941,843757

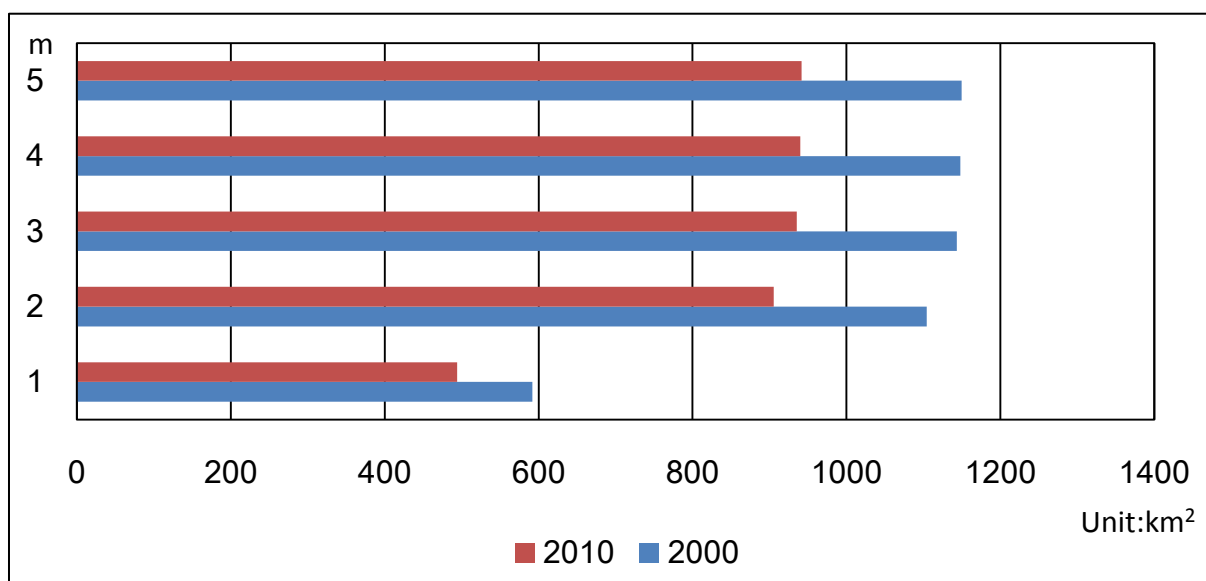


Fig. 4-16 Agricultural (Farmland) inundation area under different land use scenarios

Table 4-14 Inundated water areas under different land use scenarios

Water level (m)	Inundation area (km <sup>2</sup> )	
	2000	2010
1	505,2073289	477,7112584
2	1208,544972	1176,56419
3	1247,072573	1210,931103
4	1249,84914	1213,825753
5	1251,472263	1217,026456

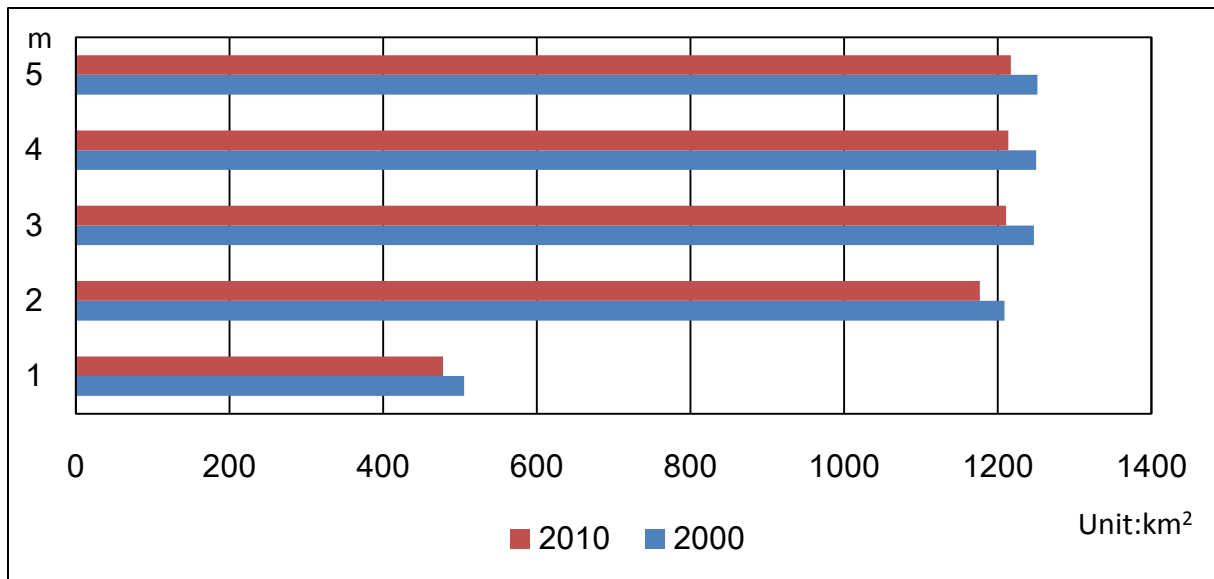


Fig. 4-17 Inundated water areas under different land use scenarios

Table 4-15 and Fig.4-18 present the total inundation area of land use in 2000 and 2010 under the same typhoon scenario. We can notice that the similar increasing trend exists in 2000 and 2010. The inundation area of 2010 is slightly higher than the year of 2000 with an increase of 67 km<sup>2</sup>. The inundation area in both years have an abundantly increase when the water level is rising from 1 meters to 2 meters, then the growth stays changes barely after the water level raised to 3 meters high.

Table 4-15 The total inundation area in the land use of 2000 and 2010

Water Level (m)	Inundation Area (km <sup>2</sup> )	
	2000	2010
1	1597,92318	1599,122498
2	3388,271673	3452,377774
3	3556,318109	3621,616761
4	3567,049374	3632,230217
5	3572,007661	3638,732558

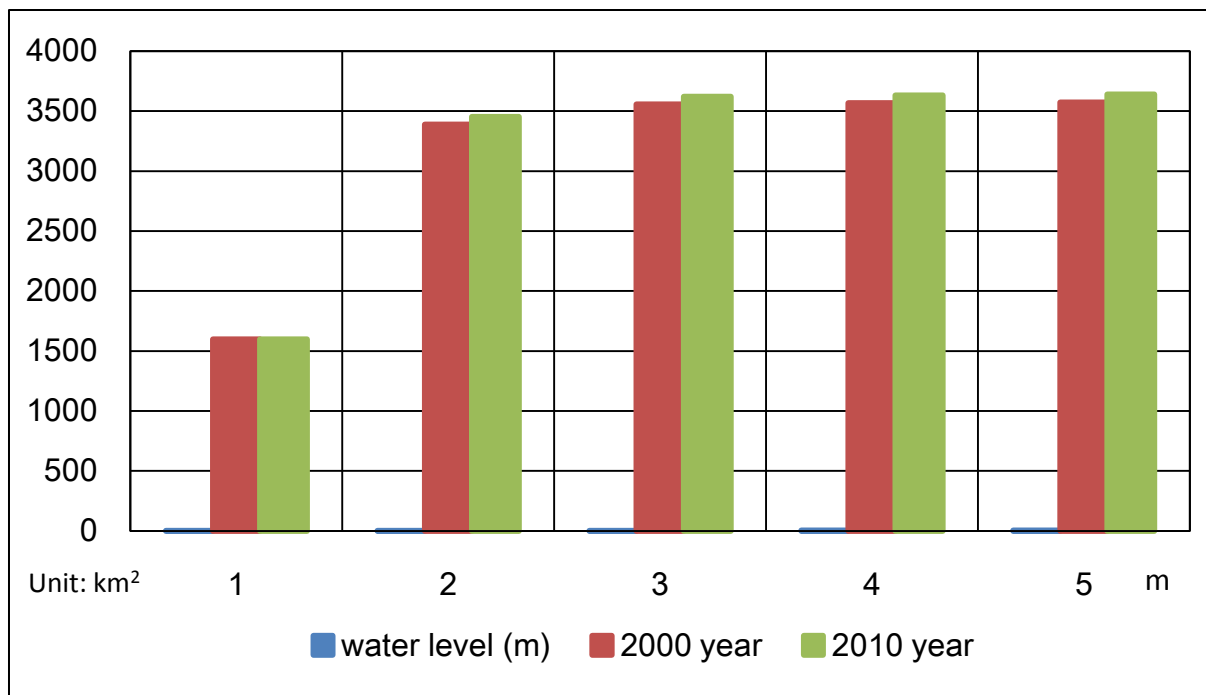


Fig 4-18 The total inundation area of the land use in 2000 and 2010

### **Economic losses**

Consistent with the remarkable increase in urban regions from 2000 to 2010, the economic losses of coastal inundation in 2010 were great, almost four times higher than the year of 2000 under the same typhoon scenarios. When the water level approached to 5 meters, the maximum economic losses were approximately 81764.7 million Euros. However, economic losses grew speedy when the water level ranged from 1 meter to 2 meters. After 2 meters, the economic losses increased slightly.

Table 4-16 Economic losses of coastal inundation under different land use scenarios

Water Level (m)	Economic Losses (million Euro)	
	2000 year	2010 year
1	7156,251831	34438,80282
2	15674,48448	76051,12678
3	16962,82652	81614,15368
4	16982,74194	81710,80238
5	16992,38482	81764,73631

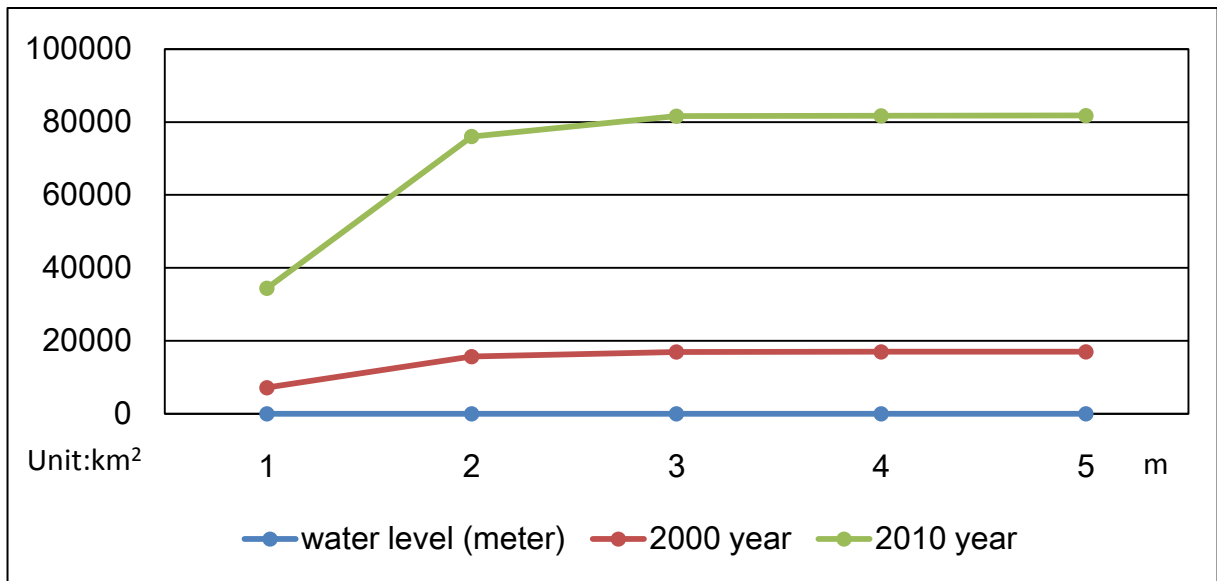


Fig. 4-19 Economic losses of coastal inundation under different land use scenarios

Consequently, the economic losses of coastal inundation under the different climate scenarios show an uncertainty change. In extreme climate conditions, the economic losses increase absolutely. However, there is no doubt that a dramatical increase of economic losses happens after land use changes. Therefore, we can confirm the conclusion in the 3.1 section, the economic losses of coastal inundation depend significantly on land use changes in the fast growing area such like the PRD region.

### 4.3 Discussion

In this chapter, I explored the coastal inundation area and economic losses changes induced by typhoon under different climate scenarios and land use scenarios in the PRD region. The water levels of Typhoon Dujuan under the baseline scenario (S0), RCP4.5 and RCP8.5 scenario from Chapter 3 were used in this chapter. We used the land use data of the PRD region from 2000 and 2010 with basic five categories (Urban-rural Land, Infrastructures, Agricultural Land, Forest and Grassland, Water Areas) for land use scenarios analysis. The GDP of the Primary Industry, the Secondary and Tertiary Industry from the year of 2000 and 2010 in the PRD region (including Macao) are applied for economic losses calculation.

#### **4.3.1 Coastal inundation and economic losses under climate change scenarios**

The inundation area increased from the baseline scenario (S0) to RCP 8.5 under the same land use scenario 2000. Among all five land use categories, the inundation area of agricultural land (farmland), water areas and urban regions are larger than forest and grassland under climate change scenarios. The coastal inundation of urban region remains the largest extents under RCP8.5 (S2), the biggest extents of other land use categories occur under the moderate emission scenario RCP4.5 (S1). Even though the inundation areas show an increasing trend under climate change, the economic losses gave different results. The agricultural (farmland) land as well as the water areas contribute to a huge inundation ratios under the land use scenario 2000, due to the lower economic product (mainly the Primary Industry) than the urban region (mainly the Secondary and Tertiary Industry), the economic losses show a lower level correspondingly. However, the economic losses under RCP8.5 report a 16.8% increase relative to the baseline scenario S0.

#### **4.3.2 Coastal inundation and economic losses under urban development scenarios**

The total inundated area in the year of 2000 and 2010 showed slight changes, that's because a huge increase lies in the urban inundated area but decline trend happens in other land use categories. The inundated urban areas expand sharply around 320 km<sup>2</sup> from 2000 to 2010, but a decrease of 208 km<sup>2</sup> remains in the agricultural (farmland) land. However, the economic losses gave a dramatically increased (almost 4 times) from 2000 to 2010 because the urban expansion contributes more economic growth.

In a word, the results demonstrate that, in the fast growing area like the PRD, the economic losses of coastal inundation are more sensitive to land use changes than climate change. The dramatically urban land expansion occurred in the last ten years, which made this region even more vulnerable to climate change.

### **4.3.3 Uncertainties**

The accuracy of economic losses calculation highly depends on hydrodynamic modelling results (water depth and inundation extents) and the land use data. One of the uncertainties lies in hydrodynamic modelling simulations such as the boundary condition data and the model ability. An improved data sets for hydrodynamic modelling analysis are recommended for the further research on the coastal inundation changes and economic losses assessment. Another uncertainty is the land use data accuracy. The land use data in this research is originally from the Landsat TM image with a resolution of 30\*30 meters. The correction of the classification of the land use data was used the SPOT scenes based on field investigation and visual judgment. The field investigation and visual judgment could lead to error manually, which remains the uncertainty. Therefore, the main purpose of this research is to use the land use based approaches to assess the economic losses of typhoon induced storm surge risks. The methodologies could be improved with the higher quality available dataset in the future.

### **4.4 Conclusion**

Chapter 4 provided methodologies for the absolute coastal inundation economic losses calculation and assessment. Even though the flexible mesh hydrodynamic model from the Chapter 3 gave a better solution for the mesh generation, we could choose the mesh resolution according to our requirements. We could make a higher fine resolution mesh as same as the land use data, in this case the high-performance computers are required. The resolution difference of this two dataset will affect the accuracy of the economic calculation. Therefore, we strongly recommend applying a higher performance computer cluster with improved mesh resolution when using the same methodology in the future. The coastal inundation risk is significantly important in different research scales. The microscale research such as tangible and intangible assessments should be encouraged in the future as well. Thirdly, there is no doubt that the detailed economic data will be helpful for a more precise economic evaluation.



## **5 Summary and outlook**

### **5.1 Summary and Conclusion**

In this research, we have explored climate change and urbanization impact in the fast economic growing region, the Pearl River Delta of China. Both from a theoretical and practical point of view, this research gives a new sight for the typhoon induced coastal storm surges, inundation changes and economic losses study under climate change and urbanization scenarios. We have concluded all of the research results in this chapter to answer three main questions as mentioned in Chapter 1.

#### **Research Question part 1 on numerical hydrodynamic modellings**

We applied two unstructured grid hydrodynamic models, ANUGA and D-Flow FM to simulate the interaction between river system and ocean system in the PRD region. They gave the difference performance ability. The new generation numerical hydrodynamic modelling, D-Flow Flexible Mesh, provides a relatively better predict skill. We built up the PRD model based on D-Flow Flexible Mesh model. The PRD model covers an area about 150 km in the north-south direction and a width increasing approximately 100 km in the south from its mouth to the open sea with 59752 nodes and 54917 elements. The model simulated the Pearl River discharge and tide propagation in the wet and dry season. The results show the fine agreement with the measurement data at the gauge stations. Additionally, due to the limited application experience of D-FLOW FM model in the PRD region and roughness is one of the most sensitive parameters of hydrodynamic models, we carried out the sensitive roughness test for the PRD model in order to find the optimal roughness setting. The model results indicate the Manning coefficient 0.023 would be the optimal choice for the further application of the PRD model.

#### **Research Question part 2: The impacts of climate change on the PRD region**

In order to understand the potential future climate change impact on the coastal typhoon storm surges and coastal inundation in the PRD region, we developed a storm surge simulation framework based theoretical study on the climatology, ocean physics and coastal dynamics. This framework contains a 2D hydrodynamic model

(D-FLOW flexible mesh) was forced with a typhoon model (Delft WES model) under different climate scenarios (basic, RCP4.5, RCP8.5) to quantify the associated storm surge and coastal inundation in the PRD region. Three typhoon cases (Dujuan, Utor and Hapugit) with different attributions in different years were selected for the simulation. Six measurement stations were used for analyzing the impacts of climate change on river discharge and typhoon induced storm tides. The simulation results showed that the impacts of climate change present various spatial attributes under different climate scenarios and different typhoon attributes. The river discharge had an increasing linear trend in the future climate change. However, the typhoons have a complex impact on climate change at all of the gauge stations. Firstly, the results show that the landfall locations of typhoons may account for variations in coastal storm tide dynamics and coastal inundation extents. The middle landfall typhoon is more sensitive to climate change with the greatest threaten upon the PRD region among all three typhoons. The western landfall typhoon has the linear correlation between typhoon intensity and water level changes. Due to the wind flow angle function, the eastern landfall typhoon has a complicated response to climate change, a higher risk occurs under RCP 4.5 (S1).

The uneven spatial and temporal distribution of coastal inundation in the future climate change during typhoon make East river, upstream North river, west and east bay more vulnerable.

**Research Question part 3: To what extent do the climate change and urbanization contribute to coastal inundation changes and economic losses by the typhoon?**

I chose land use based approaches and absolute stage-damage function to calculate coastal inundation area changes and economic losses induced by typhoon under different climate scenarios on a mesoscale in the PRD region. I used the land use change process to present the urbanization changes. The peak water level and inundation extent of typhoon Dujuan under different climate scenarios were used to demonstrate the climate impacts on the PRD region. The research results indicated that the total inundation areas induced by typhoon showed an increasing linear trend in the future climate change even under the same land use scenario, the coastal inundation of urban region remains the largest extents under RCP8.5 (S2). However,

huge economic losses happened when the urbanization scenario changed dramatically even though climate conditions remain unchanged. The economic losses also depend on different land use categories. These results gave a hint that, in the rapid developed mid-latitudes regions, economic losses of the typhoon induced coastal inundation are more sensitive to the land use changes than climate change. The dramatically urban land expansion made this region even vulnerable for climate change.

## **5.2 Outlook**

This research provided methodologies on typhoon induced coastal storm surge risk under climate change and urbanization, which improved understanding of the causes and impacts of coastal inundation risk in the PRD region. Due to the author's ability and limitations of other objective conditions, those research limitations remain mainly in following aspects,

Firstly, during research data availability limitations always exist. Real case studies have a higher requirement for the accessibility and quality of data. With the fast development of (in the fields of) science and technology in China, numerical models, and the ability of modellers are not an obstacle in this field of research. However, a lack of data limits the numerical model development and application. For example, Europe has the rich research and practical experience on the coastal inundation risk related studies. Not only because they have the sophisticated modelling approaches, but also has the accessibility of the high-quality dataset given a better platform for numerical modelling development, validation, calibration and application. The coastal storm surge risk research including the flood risk research still remains a long way to progress compared to the other region in the world. This highlights the reason for a strong recommendation on the database development firstly.

Secondly, uncertainty lies in all numerical modelling researches. One of the main uncertainties comes from climate projections. The assumptions behind climate projections may not necessarily hold in reality. The modelling configuration such as bathymetry and boundary conditions can also result in completely different model performances. The D-FLOW FM model, which is a part of new generation of hydrodynamic models, has numerous potential development opportunities and

application prospects not only in the PRD region but also in China. An intensive sensitive model evaluation work can test and avoid the uncertainty to some extent. However, the time is also expensive for a large scale modelling application.

Thirdly, the influences of inland flooding and rainfall are not considered for the simulation during the typhoon process, this probability for a given event is outside of the scope of this study. However, inland flooding and rainfall represent another important dimension of flood forecasting and deserve further investigation. Additionally, coastal altimetry study remains grossly underexploited. The validation and calibration with the satellite and radar data are strongly recommended for coastal storm surge risk research in the future.

## References

- A. K. M. Ng, A. Roelfzema and L.J.M.Hulsen.1999.Three dimensional water quality and hydrodynamic modelling in Hong Kong, Part One.Concept and model set-up. Environmental Hydrodynamics.
- Atkinson, G. D., and Holliday, C. R., 1977. Tropical cyclone minimum sea level pressure-maximum sustained wind relationship for western north pacific. *Monthly Weather Review*, 105: 421-427.
- A. De Roo, M. Odijk, G. Schmuck, E. Koster, A. Lucieer.2001. Assessing the effects of land use changes on floods in the meuse and Oder catchment. *Physics and Chemistry of the Earth, Part B: Hydrology, Oceans and Atmosphere*.26, (7–8), 2001:593–599. doi:10.1016/S1464-1909(01)00054-5
- Baldock, T. E., Barnes, M. P., Guard, P. A., Hie, Thomas, Hanslow, D., Ranasinghe, R., Gray, D., Nielsen, O. 2007 "Modelling tsunami inundation on coastlines with characteristic form", 16th Australasian Fluid Mechanics Conference (AFMC), published by School of Engineering, The University of Queensland.Availability:<[http://espace.library.uq.edu.au/eserv/UQ:121035/Baldock\\_afmc\\_16\\_07.pdf](http://espace.library.uq.edu.au/eserv/UQ:121035/Baldock_afmc_16_07.pdf)> ISBN 978-1-86499-894-8.
- Bender, M.A., Knutson, T. R., Tuleya, R. E., Sirutis, J. J., Vecchi, G. A., Garner, S. T., and Held, I. M., 2010. Modeled impact of anthropogenic warming of the frequency of intense Atlantic hurricanes. *Science* (2010).
- Chunyan Li. 2013.Subtidal water flux through a multiple-inlet system: Observations before and during a cold front event and numerical experiments. *JOURNAL OF GEOPHYSICAL RESEARCH: OCEANS*, VOL. 118, 1877–1892, doi:10.1002/jgrc.20149, 2013.
- Chester P. JELESNIANSKI.1965. A NUMERICAL CALCULATION OF STORM TIDES INDUCED BY A TROPICAL STORM IMPINGING ON A CONTINENTAL SHELF. *MONTHLY WEATHER REVIEW*,93 (6).
- Chao Qingchen and Chao Jiping. 2012. Statistical Features of Tropical Cyclones Affecting China and Its Key Economic Zones. *J. Meteor. Res.*, 26(6): 758-772.
- Chang, J.-X., C.-F. Huang, and X.-L. Liu, 2008: Geographical distribution and risk assessment of typhoon storm surge disasters in coastal regions of Guangdong province in 1949-2005. *Journal of Basic Science and Engineering*

- (in Chinese), 16(3), 393-402.
- Chen, J., 1997. The impact of sea level rise on China's coastal areas and its disaster hazard evaluation. *Journal of Coastal Research*, 13: 925-930.
- David T. Pugh.(1987).Tides, Currents, and Water Levels. John Wiley & Sons Ltd , ISBN 0 471 91505 X
- Deltares. (2016). WES: User Manual (Tech. Rep.).
- D. Yan et al. 2015.Hydrological response to climate change: The Pearl River, China under different RCP scenarios. *Journal of Hydrology: Regional Studies* 4 (2015) 228–245.
- DRONKERS, J. 2005. Dynamics of coastal systems, Hackensack, WORLD SCIENTIFIC PUBLISHING COMPANY.
- Emanuel, K.A. 1987.The dependence of hurricane intensity on climate. *Nature*, 326, 483-485 (1987).
- Elisabetta Genovese. A methodological approach to land use-based flood damage assessment in urban areas: Prague case study (2006). EUR - Scientific and Technical Research series; ISSN 1018-5593.
- FENG et al. 2014.Numerical Prediction of Storm Surge in the Qingdao Area under the Impact of Climate Change *J. Ocean Univ. China (Oceanic and Coastal Sea Research)* 2014 13: 539-551
- Feng Liu, Lirong Yuan, Qingshu Yang, Suying Ou, Lili Xie, Xin Cui. 2014. Hydrological responses to the combined influence of diverse human activities in the Pearl River delta, China. *Catena* 113 (2014) 41–55.
- FRIEDRICHS, C. T. & AUBREY, D. G. 1994. Tidal propagation in strongly convergent channels. *Journal of Geophysical Research-Oceans*, 99, 3321-3336.
- GODIN, G. 1988. Tides. Centro de Investigacion Cientifica y de Educaion Superior de Ensada, 290 pp.
- Guan, Q. (2010). A study of change for runoff and simulation under different scenarios at Xijiang River-take Luoding River Basin and Xinxin River Basin as examples. Master Thesis.
- Guangdong Statistical Yearbook 2011.
- <http://www.gdstats.gov.cn/tjnj/2011/table/20/c20-03-1.htm>
- Green C. et al. (1994), "Vulnerability refined: analysing full flood impacts" (Chapter

- 3). In: Penning-Rowsell, E., Fordham, M. (eds.), *Floods across Europe (EUROflood): hazard assessment, modelling and management*, London, pp. 32-68.
- He Haiyan, Jian Maoqiu, Song Lili, Weiqin (2003). Some climatic features of the tropical cyclones landed onto GUANGDONG province during the recent 50 years. *Scientia Meteorologica Sinica* 23(4): 401-409.
- Holland, G.J. 1997. The maximum potential intensity of tropical cyclones. *J. Atmos. Sci.*, 54, 2519-2541 (1997).
- Holland, G., 1980. "An Analytical Model of the Wind and Pressure Profiles in Hurricanes." *Monthly Weather Review*. 108: 1212-1218.
- Hong Kong Observatory ., 2003. *Tropical Cyclones in 2003* [B], Hong Kong.
- Hong Kong Observatory ., 2001. *Tropical Cyclones in 2001* [B], Hong Kong.
- Hong Kong Observatory., 2008. *Tropical cyclones in 2008*. [B], Hong Kong.
- Harrison, P. J., K. Yin, J. H. W. Lee, J. Gan and H. Liu. 2008. Physical-biological coupling in the Pearl River Estuary, *Cont. Shelf Res.*, 28(12),1405–1415.
- Hao Zhang, Weichun. M., Xiang-rong Wang. 2008. Rapid Urbanization and Implications for Flood Risk Management in Hinterland of the PRD Foshan. *Sensors* 8: 2223-2239.
- Hao Zhang & Xiang-rong Wang. 2007. Land-use dynamics and flood risk in the hinterland of the Pearl River Delta: The case of Foshan City, *International Journal of Sustainable Development & World Ecology*, 14:5, 485-492, DOI: 10.1080/13504500709469747.
- HEC-RAS, 2008. "User Manual," US Army Corps of Engineers, Hydrologic Engineering Center, Davis Version 4.0, 2008.
- HUNT, J. N. 1964. Tidal oscillations in estuaries. *Geophysical Journal of the Royal Astronomical Society*, 8, 440-455.
- IPCC, 2007: *Climate Change 2007: The Physical Science Basis*. Contribution of Working Group I to the Fourth Assessment Report of the Intergovernmental Panel on Climate Change. S. Solomon, D. Qin, M. Manning, Z. Chen, M. Marquis, K. B. Averyt, M. Tignor, and H. L. Miller (eds.). Cambridge University Press, Cambridge, United Kingdom and New York, NY, USA, 996 pp. (2007).
- IPCC 2014: *Synthesis Report*. "Climate change 2014: Impacts, adaptation, and vulnerability. part a. global and sectoral aspects. contribution of working group

- ii to the fifth assessment report of the intergovernmental panel on climate change (IPCC).” Technical report, Field, C. B., V. R. Barros, D. J. Dokken, K. J. Mach, M. D. Mastrandrea, T. E. Bilir, M. Chatterjee, K. L. Ebi, Y. O. Estrada, R. C. Genova, B. Girma, E. S. Kissel, A. N. Levy, S. MacCracken, P. R. Mastrandrea and L. L. White, eds., Cambridge University Press, Cambridge and New York.
- ICPR (2002), International commission for the protection of the Rhine, “Non-structural flood plain management: Measures and their effectiveness”, Koblenz. [http://www.iksr.org/GB/bilder/pdf/rz\\_iksr\\_engl.pdf](http://www.iksr.org/GB/bilder/pdf/rz_iksr_engl.pdf)
- Joseph Hun-Wei Lee, Chiu-On Ng.2011.Asian and Pacific Coasts 2011. World Scientific, 24.11.2011
- Jim W. Hall, Shawn A. Boyce, Yueling Wang, Richard J. Dawson, Stefano Tarantola and Andrea Saltelli.2009. Sensitivity Analysis for Hydrodynamic Models. JOURNAL OF HYDRODYNAMIC ENGINEERING. 2009, 959-969. DOI:10.1061/\_ASCE\_HY.1943-7900.0000098
- Jiatang Hu, Shiyu Li , Bingxu Geng.2011. Modelling the mass flux budgets of water and suspended sediments for the river network and estuary in the Pearl River Delta, China. Journal of Marine Systems 88 (2011) 252–266.
- J.H.W. Lee, A.W. Jayawardena and Z.Y. Wang. Environmental Hydrodynamics.1998 PROCEEDINGS OF THE SECOND INTERNATIONAL SYMPOSIUM ON ENVIRONMENTAL HYDRODYNAMICS/HONG KONG/CHINA/16-18 DECEMBER 1998.
- Knutson, Thomas R. et al. 2010.“Tropical Cyclones and Climate Change.” Nature Geosci 3.3: 157-163.
- Kerry Emanuel. 2005. Increasing destructiveness of tropical cyclones over the past 30 years.Nature.letters. 436: 686-688. doi:10.1038/nature03906
- Knutson, T. R., Sirutis, J. J., Garner, S. T., Vecchi, G. A., & Held, I. Simulated reduction in Atlantic hurricane frequency under twenty-first-century warming conditions. Nature Geoscience, 1(6), 359-364 (2008).
- KERNKAMP, H.W.J., VAN DAM, A., STELLING, G.S., DE GOEDE, E.D. 2011. Efficient scheme for the shallow water equations on unstructured grids with application to the Continental Shelf. Ocean Dyn., 61, 1175-1188.
- Kang Lei, Ma Li, Liu Yi.2015. Loss evaluation of farmland caused by sea level rise

- and storm surge in the Pearl River Delta region under global climate change. *ACTA GEOGRAPHICA SINICA*. (2015), Vol.70, No.9: 1375-1389. DOI: 10.11821/dlxb201509002.
- Jun Sun, Yigang Wang, Guoping Chen, Hongyan Shen, Chi Zhang et al. 2012. Technical Research on 2D numerical modelling development on salt tide dynamic monitoring and prediction between Sixianzhi and Modaomen channel in Pearl river estuary, report 6. Hohai University, 2012.
- Lai, Z., R. Ma, G. Gao, C. Chen, and R. C. Beardsley. 2015. Impact of multichannel river network on the plume dynamics in the Pearl River estuary, *J. Geophys. Res. Oceans*, 120, 5766–5789, doi:10.1002/2014JC010490.
- L. A. Wong, J. C. Chen, H. Xue, L. X. Dong, J. L. Su, and G. Heinke. 2003. *JOURNAL OF GEOPHYSICAL RESEARCH*, VOL. 108, NO. C5, 3156, doi:10.1029/2002JC001451, 2003
- LANZONI, S. & SEMINARA, G. (1998). On tide propagation in convergent estuaries. *Journal of Geophysical Research-Oceans*, 103, 30793-30812.
- Liu, H., Y. Lu, et al. 2012. "GIS Approach of Inundation Analysis In The Dongjiang(East River) Drainage Area." *Procedia Environmental Sciences* 12: 1063-1070.
- Liang Yang • Juergen Scheffran • Huapeng Qin , Qinglong You. 2015. Climate-related flood risks and urban responses in the Pearl River Delta, China. *Reg Environ Change* (2015) 15:379–391. DOI 10.1007/s10113-014-0651-7.
- Liu, L.L., Jiang, T., XU, J.G., LUO, Y., 2012. Research on the hydrological processes using multi-GCMs and multi-scenarios in the Xijiang River basin. *J. Hydraul. Eng.* 43 (12), 1413–1421 (in Chinese).
- Morris, J. T., P. V. Sundareshwar, C. T. Nietch, B. Kjerfve, and D. R. Cahoon (2002), Responses of coastal wetlands to rising sea level, *Ecology*, 83, 2869- 2877, doi:10.1890/0012-9658(2002)083[2869:ROCWTR]2.0.CO;2.
- Mao, Q., P. Shi, K. Yin, J. Gan, and Y. Qi. 2004. Tides and tidal currents in the Pearl River Estuary, *Cont. Shelf Res.*, 24(16), 1797–1808.
- M.CASTRO GAMA, I.POPESCU, A.MYNETT, L. SHENGYANG, AND A.VAN DAM, 2013. Modelling extreme flood hazard events on the middle Yellow River using DFLOW-flexible mesh approach. *Natural Hazards and Earth System Science*, 1, 6061-609.

- M. Wood , R. Hostache , J. Neal, T. Wagener , L. Giustarini , M. Chini , G. Corato , P. Matgen & P.Bates.2016. Calibration of channel depth and friction parameters in the LISFLOOD-FP hydrodynamic model using medium resolution SAR data. *Hydrol. Earth Syst. Sci. Discuss.*, doi:10.5194/hess-2015-511, 2016.
- National Weather Service. 2014. National Hurricane Center. Retrieved 2014-10-01, from <http://www.nhc.noaa.gov/>
- Prabeer Kumar Parhi, 2013. HEC-RAS Model for Mannig's Roughness: A Case Study. *Open Journal of Modern Hydrology*, 2013, 3, 97-101.
- PRANDLE, D. & RAHMAN, M. 1980. tidal response in estuaries. *Journal of Physical Oceanography*, 10, 1552-1573.
- Q. Ke, S.N. Jonkman, P. H. A. J. M. van Gelder and T. Rijcken. Flood damage estimation for downtown Shanghai – sensitivity analysis.
- R. Ramesh, B. Datta, S. Bhallamudi and A. Narayana. 2000. "Optimal Estimation of Roughness in Open-Channel Flows," *Journal of Hydrodynamic Engineering*, Vol. 126, No. 4, 1997, pp. 299-303. doi:10.1061/(ASCE)0733-9429(2000)126:4(299)
- R. Van Drie., M.Simon., I. Schymitek. 2008. 2D Hydrodynamic Modelling over A Wide Range of Applications with Anuga. *Engineers Australia, 9th National Conference on Hydrodynamics in Water Engineers, Australia.*
- Ren Guoyu. *Climate change and China's water resources.*2007. China Meteorological Press.
- Rego, J. a. L., & Li, C. 2010, September. Storm surge propagation in Galveston Bay during Hurricane Ike. *Journal of Marine Systems*, 82(4), 265–279. doi: 10.1016/j.jmarsys.2010.06.001
- Rego, J. a. L., & Li, C. 2009. On the importance of the forward speed of hurricanes in storm surge forecasting: A numerical study. *Geophysical Research Letters*, 36(7), 1–5. doi: 10.1029/2008GL036953
- RYBCZYK, J.M. ANDD. R. CAHOON. 2002. Estimating the potential for submergence for two wetlands in the Mississippi River delta. *Estuaries* 25:985–998.
- Stoeten, K. J. 2013. Hurricane Surge Risk Reduction for Galveston Bay (Tech. Rep.). Delft: Master Thesis: Delft University of Technology.
- SAVENIJE, H. H. G. 2005. *Salinity and tides in alluvial estuaries*, Amsterdam, Elsevier.

SAGA GIS. <http://www.saga-gis.org/en/index.html>

TJITSKE GEERTSEMA, 2013. River discharge and tidal propagation in upstream and downstream parts of the Pearl River region in China. Wageningen: Wageningen University.

T. Schlurmann, W. Kongko N. Goseberg, D. H. Natawidjaja and K. Sieh. 2010. NEAR-FIELD TSUNAMI HAZARD MAP PADANG, WEST SUMATRA: UTILIZING HIGH RESOLUTION GEOSPATIAL DATA AND REASONABLE SOURCE SCENARIOS. COASTAL ENGINEERING 2010.

Teng, J., Vaze, J., Chiew, F.H.S., Wang, B., Perraud, J.M., 2012. Estimating the relative uncertainties sourced from GCMs and hydrological models in modelling climate change impact on runoff. *J. Hydrometeorol.* 13 (1), 122–139.

UNDP/BCPR, 2004: Reducing disaster risk: A challenge for development. United Nations Development Program, Bureau for Crisis Prevention and Recovery, 161 pp. [Available online at [www.undp.org/bcpr/disred/rdr.htm](http://www.undp.org/bcpr/disred/rdr.htm)].

Van der Sande C. (2001), River flood damage assessment using Ikonos imagery, Natural Hazards Project-Floods, Joint Research Centre of the European Commission, S.P.I. 01.147, Ispra, August 2001.

Van der Sande C.J., de Jong S.M., de Roo A.P.J. (2003), A segmentation and classification approach of IKONOS-2 imagery for land cover mapping to assist flood risk and flood damage assessment, *International Journal of Applied Earth Observation and Geoinformation*, pp. 217–229.

William W. Nazaroff, Lisa Alvarez-Cohen. 2001. *Environmental Engineering Science*. Wiley Press, 1st edition. ISBN: 978-0-471-14494-6.

Wu, C.H., Huang, G.R., YU, H.J., 2014. Prediction of extreme floods based on CMIP5 climate models: a case study in the Beijiang River basin, South China. *Hydrol. Earth Syst. Sci. Discuss.* 11, 9643–9669.

Walsh, K J., J McBride, P J Klotzbach, S Balachandran, S J Camargo, G Holland, Thomas R Knutson, J Kossin, T-C Lee, A Sobel, and M Sugi, January 2016: Tropical cyclones and climate change. *Wiley Interdisciplinary Reviews: Climate Change*, 7(1), DOI:10.1002/wcc.371.

White G.F. (1945), "Human Adjustments to Floods: A Geographical approach to the Flood Problem in the United States", Doctoral Dissertation and Research

- paper no. 29. Department of Geography, University of Chicago.
- Xiaoli Ding, D. Z., WT Wong, KW Li, Wu Chen, Ping Zhong. 2004. "recent sea level variations in southern china from tide gauge observations." Proceedings of the Asia-Pacific Space Geodynamics Symposium: p.126-136.
- YEARBOOK OF STATISTICS, Macao, 2010.
- Zhao, H. 1990. The Evolution of the Pearl River Estuary, 357 pp., China Ocean Press, Beijing.
- Zhang, L. M., Y. Xu, et al. 2013. "Assessment of flood risks in Pearl River Delta due to levee breaching." Georisk: Assessment and Management of Risk for Engineered Systems and Geohazards 7(2): 122-133.
- ZHENG GUO HUANG, Y. Z. W. Z. 2004. "Coastal Inundation due to Sea Level Rise in Pearl River Delta." Natural Hazards 33: 247–264.
- Zandbergen, P., 2008. Applications of Shuttle Radar Topography Mission Elevation Data. Geography Compass 2/5 (2008): 1404–1431.
- Zhang, S., X. X. Lu, et al. 2008. "Recent changes of water discharge and sediment load in the Zhujiang (Pearl River) Basin, China." Global and Planetary Change 60(3-4): 365-380.
- ZHENG Jing, FANG Wei Hua, SHI Pei jun, ZHUO Li. 2009. Modelling the impacts of land use change on Hydrological Processes in fast urbanizing Region. A case Study of the Buji Watershed in Shenzhen city, China. JOURNAL OF NATURAL RESOURCES.2009,24(9):1560-1572.

## Appendix 1

### A. Governing Equations in D Flow Flexible Mesh

D-Flow FM model mainly focuses on solving the 2-D shallow-water equations so far. The shallow-water equations express conservation of mass and momentum and can be put into the following form:

$$\frac{\partial h}{\partial t} + \nabla \cdot (h\mathbf{u}) = 0,$$
$$\frac{\partial \mathbf{u}}{\partial t} + \frac{1}{h}(\nabla \cdot (h\mathbf{u}\mathbf{u}) - \mathbf{u}\nabla \cdot (h\mathbf{u})) = -g\nabla\zeta + \frac{1}{h}\nabla \cdot (\nu h(\nabla\mathbf{u} + \nabla\mathbf{u}^T)) + \frac{\boldsymbol{\tau}}{h}$$

where  $\zeta$  is the water level,  $h$  the water depth,  $\mathbf{u}$  the velocity vector,  $g$  the gravitational acceleration,  $\nu$  is the viscosity and  $\mathbf{T}$  is the bottom friction:

$$\boldsymbol{\tau} = -\frac{g}{C^2}\|\mathbf{u}\|\mathbf{u},$$

with  $C$  being the Chézy coefficient. The equations are complemented with appropriate initial conditions and water-level and/or velocity boundary conditions<sup>9</sup>.

---

<sup>9</sup> D-Flow Flexible Mesh manual, 2015

## B. Brief Introduction of Wind Enhance Scheme (WES)

Cyclone wind fields are generated around the given centre positions of the storm, following Holland's method in order to obtain the wind and pressure fields (above sea surface) on a high-resolution grid. The parametric model that has been adopted in WES is based upon Holland (1980). And it has been improved slightly by introducing asymmetry. This asymmetry is brought about by applying the translation speed of the cyclone centre displacement as steering current and by introducing rotation of wind speed due to friction<sup>2</sup>.

This model has basically five parameters:

- 1 the location of the cyclone centre,
- 2 the radius of maximum wind,
- 3 the maximum wind speed,
- 4 the central pressure and
- 5 the current motion vector of the vortex <sup>10</sup>

Here is an example of the output file from WES, which is the forcing input for the hydrodynamic model.

```

FileVersion      = 1.03
filetype         = meteo_on_spiderweb_grid #from TRACK file: 2001_utor.trk
NODATA_value    = -999.000
n_cols          = 36
n_rows         = 500
grid_unit       = degree
spw_radius      = 600000.00
spw_rad_unit    = m
n_quantity      = 3
quantity1       = wind_speed
quantity2       = wind_from_direction
quantity3       = p_drop
unit1           = m s-1
unit2           = degree
unit3           = Pa
TIME            = 0.00 hours since 2001-07-01 14:00:00 +00:00
x_spw_eye       = 138.50
y_spw_eye       = 7.20
p_drop_spw_eye = 1000.00
1.29 1.29 1.29 1.29 1.29 1.29 1.29 1.29 1.29 1.29 1.29 1.29 1.29 1.29 1.29 1.29 1.29 1.29 1.29 1.29 1.29 1.29 1.29 1.29 1.29 1.29 1.29 1.29 1.29 1.29 1.29 1.29 1.29 1.29 1.29 1.29 1.29
1.28 1.28 1.28 1.28 1.28 1.28 1.28 1.28 1.29 1.29 1.29 1.29 1.29 1.29 1.29 1.29 1.29 1.29 1.29 1.29 1.29 1.29 1.29 1.29 1.29 1.29 1.29 1.29 1.29 1.29 1.29 1.29 1.29 1.29 1.29 1.29 1.29
1.29 1.29 1.29 1.29 1.78 1.74 1.69 1.63 1.56 1.48 1.40 1.31 1.21 1.12 1.03 0.94
1.82 1.83 1.82 1.81 1.78 1.74 1.69 1.63 1.56 1.48 1.40 1.31 1.21 1.12 1.03 0.94
0.86 0.80 0.76 0.74 0.76 0.80 0.86 0.94 1.03 1.12 1.21 1.31 1.40 1.48 1.56 1.63
1.69 1.74 1.78 1.81
3.77 3.78 3.77 3.73 3.67 3.58 3.47 3.33 3.17 3.00 2.81 2.60 2.39 2.16 1.94 1.72
1.52 1.36 1.25 1.21 1.25 1.36 1.52 1.72 1.94 2.16 2.38 2.60 2.81 3.00 3.17 3.33
3.47 3.58 3.67 3.73
6.37 6.39 6.37 6.32 6.25 6.14 6.01 5.85 5.67 5.47 5.26 5.04 4.82 4.60 4.39 4.20
4.04 3.92 3.84 3.82 3.84 3.92 4.04 4.20 4.39 4.60 4.82 5.04 5.26 5.47 5.67 5.85
6.01 6.14 6.25 6.32
8.90 8.92 8.90 8.85 8.77 8.65 8.51 8.35 8.16 7.96 7.74 7.51 7.29 7.08 6.87 6.70
6.55 6.44 6.37 6.34 6.37 6.44 6.55 6.70 6.87 7.08 7.29 7.51 7.74 7.96 8.16 8.35
8.51 8.65 8.77 8.85
11.08 11.10 11.08 11.03 10.94 10.83 10.68 10.51 10.32 10.11 9.89 9.67 9.45 9.24 9.04 8.86
8.72 8.61 8.55 8.53 8.55 8.61 8.72 8.86 9.04 9.24 9.45 9.67 9.89 10.11 10.32 10.51
10.68 10.83 10.94 11.03
12.87 12.88 12.87 12.81 12.73 12.61 12.46 12.29 12.10 11.89 11.67 11.45 11.22 11.01 10.82 10.65
10.51 10.40 10.34 10.31 10.34 10.40 10.51 10.65 10.82 11.01 11.22 11.45 11.67 11.89 12.10 12.29

```

<sup>10</sup> WES. Wind Enhance Scheme for cyclone modelling user manual, 2016.

## C. ANUGA model script examples

This is the script for running a tsunami inundation scenario for Shanwei, PRD, China. Source data such as elevation and boundary data are assumed to be available in directories specified by project.py. The output sww file is stored in a directory named after the scenario, i.e., slide or fixed\_wave. The scenario is defined by a triangular mesh created from project.polygon.

```
LI LI, University of Hamburg, From China, 2013-present
#-----
# Import necessary modules
#-----
# Standard modules
import os
import time
import sys

# Related major packages
import anuga
# Application specific imports
import project          # Definition of file names and polygons
#-----
# Preparation of topographic data
# Convert ASC 2 DEM 2 PTS using source data and store result in source data
#-----
# Create DEM from asc data
anuga.asc2dem(project.name_stem+'.asc', use_cache=True, verbose=True)
# Create pts file for onshore DEM
anuga.dem2pts(project.name_stem+'.dem', use_cache=True, verbose=True)
#-----
# Create the triangular mesh and domain based on
# overall clipping polygon with a tagged
# boundary and interior regions as defined in project.py
#-----
domain = anuga.create_domain_from_regions(project.bounding_polygon,
                                          boundary_tags={'top': [0],
                                                         'ocean_east': [1],
                                                         'bottom': [2],
                                                         'onshore': [3]},
                                          maximum_triangle_area=project.default_res,
                                          mesh_filename=project.meshname,
                                          interior_regions=project.interior_regions,
                                          use_cache=True,
                                          verbose=True)
# Print some stats about mesh and domain
print 'Number of triangles = ', len(domain)
print 'The extent is ', domain.get_extent()
print domain.statistics()
#-----
# Setup parameters of computational domain
#-----
domain.set_name('shanwei_' + project.scenario) # Name of sww file
domain.set_datadir('~/.anuga_core/documentation/user_manual/demos/PRD/') # Store sww output
domain.set_minimum_storable_height(0.01)      # Store only depth > 1cm
domain.set_flow_algorithm('tsunami')
```

```

#-----
# Setup initial conditions
#-----
tide = 0.0
domain.set_quantity('stage', tide)
domain.set_quantity('friction', 0.0)
domain.set_quantity('elevation',
                    filename=project.name_stem + '.pts',
                    use_cache=True,
                    verbose=True,
                    alpha=0.1)

#-----
# Setup information for slide scenario (to be applied 1 min into simulation)
#-----
if project.scenario == 'slide':
    # Function for submarine slide
    tsunami_source = anuga.slide_tsunami(length=35000.0,
                                          depth=project.slide_depth,
                                          slope=6.0,
                                          thickness=500.0,
                                          x0=project.slide_origin[0],
                                          y0=project.slide_origin[1],
                                          alpha=0.0,
                                          domain=domain,
                                          verbose=True)

#-----
# Setup boundary conditions
#-----
print 'Available boundary tags', domain.get_boundary_tags()

Bd = anuga.Dirichlet_boundary([tide, 0, 0]) # Mean water level
Bs = anuga.Transmissive_stage_zero_momentum_boundary(domain) # Neutral boundary

if project.scenario == 'fixed_wave':
    # Huge 50m wave starting after 60 seconds and lasting 1 hour.
    Bw = anuga.Transmissive_n_momentum_zero_t_momentum_set_stage_boundary(
        domain=domain,
        function=lambda t: [(60<t<10800)*50, 0, 0])

    domain.set_boundary({'ocean_east': Bw,
                        'bottom': Bw,
                        'onshore': Bs,
                        'top': Bd})

if project.scenario == 'slide':
    # Boundary conditions for slide scenario
    domain.set_boundary({'ocean_east': Bd,
                        'bottom': Bd,
                        'onshore': Bd,
                        'top': Bd})

#-----
# Evolve system through time
#-----
import time
t0 = time.time()

from numpy import allclose

```

```

if project.scenario == 'slide':
    # Initial run without any event
    for t in domain.evolve(yieldstep=10, finaltime=60):
        print domain.timestepping_statistics()
        print domain.boundary_statistics(tags='ocean_east')

    # Add slide to water surface
    if allclose(t, 60):
        domain.add_quantity('stage', tsunami_source)

    # Continue propagating wave
    for t in domain.evolve(yieldstep=10, finaltime=5000,
                          skip_initial_step=True):
        print domain.timestepping_statistics()
        print domain.boundary_statistics(tags='ocean_east')

if project.scenario == 'fixed_wave':
    # Save every two mins leading up to wave approaching land
    for t in domain.evolve(yieldstep=120, finaltime=10000):
        print domain.timestepping_statistics()
        print domain.boundary_statistics(tags='ocean_east')

    # Save every 30 secs as wave starts inundating ashore
    for t in domain.evolve(yieldstep=10, finaltime=10000,
                          skip_initial_step=True):
        print domain.timestepping_statistics()
        print domain.boundary_statistics(tags='ocean_east')
print 'That took %.2f seconds' %(time.time()-t0)

```

## D. D-FLOW FM model set up script examples

### D.1 Dry season of 2002

#### D.1.1 mdu file

# Generated on 17:14:47, 05-11-2014

# Deltares, D-Flow FM Version 1.1.35.22807M, Jun 26 2012, 16:46:00

[model]

Program = D-Flow FM

Version = 1.1.35.22807M

AutoStart = 0 # Autostart simulation after loading MDU or not (0=no, 1=autostart, 2=autostartstop).

[geometry]

NetFile = final\_bathy\_7.7\_latlon\_net.nc # \*\_net.nc

BathymetryFile = # \*.xyb

WaterLevIniFile = # Initial water levels sample file \*.xyz

LandBoundaryFile = # Only for plotting

ThinDamFile = # \*\_thd.pli, Polyline(s) for tracing thin dams.

ThindykeFile = # \*\_tdk.pli, Polyline(s) x,y,z, z = thin dyke top levels

ProflocFile = # \*\_proflocation.xyz) x,y,z, z = profile refnumber

ProfdefFile = # \*\_profdefinition.def) definition for all profile nrs

ManholeFile = # ...

WaterLevIni = 0. # Initial water level

BotLevUni = -5. # Uniform bottom level, (only if Botlevtype>=3, used at missing z values in netfile

BotLevType = 3 # 1 : Bottom levels at waterlevel cells (=flow nodes), like tiles xz, yz, bl , bob = max(bl left, bl right)

# 2 : Bottom levels at velocity points (=flow links), xu, yu, blu, bob = blu,

bl = lowest connected link

# 3 : Bottom levels at velocity points (=flow links), using mean network levels

xk, yk, zk bl = lowest connected link

# 4 : Bottom levels at velocity points (=flow links), using min network levels

xk, yk, zk bl = lowest connected link

# 5 : Bottom levels at velocity points (=flow links), using max network levels

xk, yk, zk bl = lowest connected link

AngLat = 22.3 # Angle of latitude (deg), 0=no Coriolis

Conveyance2D = 3 # -1:R=HU,0:R=H, 1:R=A/P, 2:K=analytic-1D conv, 3:K=analytic-2D conv

[numerics]

CFLMax = 0.7 # Max. Courant nr.

CFLWaveFrac = 0.1 # Wave velocity fraction, total courant vel = u + cflw\*wavevelocity

AdvecType = 3 # Adv type, 0=no, 1= Wenneker, qu-udzt, 2=1, q(ui-o-u), 3=Perot q(ui-o-u), 4=Perot q(ui-u), 5=Perot q(ui-u) without itself

Limtypsa = 0 # Limiter type for salinity transport, 0=no,

1=minmod,2=vanLeer,3=Kooren,4=Monotone Central

Hdam = 0. # Threshold for minimum bottomlevel step at which to apply energy conservation factor i.c. flow contraction

[physics]

UnifFrictCoef = 1.0d-2 # Uniform friction coefficient, 0=no friction

UnifFrictType = 1 # 0=Chezy, 1=Manning, 2=White Colebrook, 3=z0 etc

Vicouv = 0. # Uniform horizontal eddy viscosity

```

Smagorinsky = 0. # Add Smagorinsky horizontal turbulence : vicu = vicu + (
(Smagorinsky*dx)**2)*S, e.g. 0.1
Elder = 0. # Add Elder contribution : vicu = vicu + Elder*kappa*ustar*H/6), e.g.
1.0
Irov = 0 # 0=free slip, 1 = partial slip using wall_ks
wall_ks = 0. # Nikuradse roughness for side walls, wall_z0=wall_ks/30
Vicoww = 0. # Uniform vertical eddy viscosity
TidalForcing = 1 # Tidal forcing (0=no, 1=yes) (only for jsferic == 1)
Salinity = 0 # Include salinity, (0=no, 1=yes)

```

[time]

```

RefDate = 20030112 # Reference date (yyyymmdd)
Tunit = s # Time units in MDU (H, M or S)
DtUser = 3600. # User timestep in seconds (interval for external forcing update)
DtMax = 600. # Max timestep in seconds
DtInit = 1. # Initial timestep in seconds
AutoTimestep = 0 # Use CFL timestep limit or not (1/0)
TStart = 0. # Start time w.r.t. RefDate (in TUnit)
TStop = 2764800. # Stop time w.r.t. RefDate (in TUnit)

```

[restart]

```

RestartFile = # Restart file, only map, hence: *_map.nc
RestartTime = # Restart time (yyyymmddhhmmss)

```

[external forcing]

```

ExtForceFile = dry.ext # *.ext

```

[output]

```

ObsFile = obs_langlon_new.xyn # *.xyn Coords+name of observation stations.
CrsFile = new_cross_1_crs_langlon.pli # *_crs.pli Polyline(s) defining cross section(s).
HisFile = refined_his.nc # *_his.nc History file in NetCDF format.
HisInterval = 3600. # Interval (s) between history outputs
XLSInterval = 0. # Interval (s) between XLS history
FlowGeomFile = # *_flowgeom.nc Flow geometry file in NetCDF format.
MapFile = # *_map.nc Map file in NetCDF format.
MapInterval = 86400. # Interval (s) between map file outputs
RstInterval = 86400. # Interval (s) between map file outputs
WaqFileBase = # Basename (without extension) for all Delwaq files to be written.
WaqInterval = 0. # Interval (in s) between Delwaq file outputs
StatsInterval = 0. # Interval (in s) between simulation statistics output.
SnapshotDir = figures# Directory where snapshots/screen dumps are saved.

```

## C1.2 ext file

```

* QUANTITY: waterlevelbnd, velocitybnd, dischargebnd, tangentialvelocitybnd, normalvelocitybnd
filetype=9 method=2,3
* : salinitybnd filetype=9 method=2,3
* : lowergatelevel, damlevel, pump filetype=9 method=2,3
* : frictioncoefficient, horizontaleddyviscositycoefficient, advectiontype filetype=4,10 method=4
* : initialwaterlevel, initialsalinity filetype=4,10 method=4
* : windx, windy, windxy, rain, atmosphericpressure filetype=1,2,4,7,8 method=1,2,3
*
* kx = Vectormax = Nr of variables specified on the same time/space frame. Eg. Wind
magnitude,direction: kx = 2
* FILETYPE=1 : uniform kx = 1 value 1 dim array uni
* FILETYPE=2 : unimagdir kx = 2 values 1 dim array, uni mag/dir transf to u,v, in index 1,2
* FILETYPE=3 : svwp kx = 3 fields u,v,p 3 dim array nointerpolation
* FILETYPE=4 : arcinfo kx = 1 field 2 dim array bilin/direct
* FILETYPE=5 : spiderweb kx = 3 fields 3 dim array bilin/spw

```

```

* FILETYPE=6 : curvi          kx = ?          bilin/findnm
* FILETYPE=7 : triangulation kx = 1 field    1 dim array  triangulation
* FILETYPE=8: triangulation_magdir kx = 2 fields consisting of Filetype=2 triangulation in (wind)
stations
* FILETYPE=9: poly_tim       kx = 1 field  consisting of Filetype=1 line interpolation in (boundary)
stations
* FILETYPE=10: inside_polygon kx = 1 field    uniform value inside polygon for INITIAL fields
*
* METHOD =0 : provider just updates, another provider that pointers to this one does the actual
interpolation
*   =1 : intp space and time (getval) keep 2 meteofields in memory
*   =2 : first intp space (update), next intp. time (getval) keep 2 flowfields in memory
*   =3 : save weightfactors, intp space and time (getval), keep 2 pointer- and weight sets in memory
*   =4 : only spatial interpolation
*
* OPERAND =+ : Add this provider to forcing value realised by previously defined providers
*           =O : Override
*
* VALUE = : Offset value for this provider
*
* FACTOR = : Conversion factor for this provider
*

```

\*\*\*\*\*

```

QUANTITY=waterlevelbnd
FILENAME=seaeast_langlon.pli
FILETYPE=9
METHOD=3
OPERAND=O

```

```

QUANTITY=waterlevelbnd
FILENAME=seasouth_langlon.pli
FILETYPE=9
METHOD=3
OPERAND=O

```

```

QUANTITY=waterlevelbnd
FILENAME=seawest_langlon.pli
FILETYPE=9
METHOD=3
OPERAND=O

```

```

QUANTITY=dischargebnd
FILENAME=eastdrydis_langlon.pli
FILETYPE=9
METHOD=3
OPERAND=O

```

```

QUANTITY=dischargebnd
FILENAME=northdrydis_langlon.pli
FILETYPE=9
METHOD=3
OPERAND=O

```

```

QUANTITY=dischargebnd
FILENAME=westdrydis_langlon.pli
FILETYPE=9
METHOD=3
OPERAND=O

```

## D.2 Typhoon scenarios: baseline scenario of Dujan

### D2.1 mdu file

# Generated on 17:14:47, 25-01-2015

# Deltares, D-Flow FM Version 1.1.35.22807M, Jun 26 2012, 16:46:00

[model]

Program = D-Flow FM

Version = 1.1.35.22807M

AutoStart = 0 # Autostart simulation after loading MDU or not (0=no, 1=autostart, 2=autostartstop).

[geometry]

NetFile = dongguan\_100\_net.nc # \*\_net.nc

BathymetryFile = # \*.xyb

WaterLevIniFile = # Initial water levels sample file \*.xyz

LandBoundaryFile = # Only for plotting

ThinDamFile = # \*\_thd.pli, Polyline(s) for tracing thin dams.

ThindykeFile = # \*\_tdk.pli, Polyline(s) x,y,z, z = thin dyke top levels

ProflocFile = # \*\_proflocation.xyz x,y,z, z = profile refnumber

ProfdefFile = # \*\_profdefinition.def) definition for all profile nrs

ManholeFile = # \*...

WaterLevIni = 0. # Initial water level

BotLevUni = -5. # Uniform bottom level, (only if Botlevtype>=3, used at missing z values in netfile

BotLevType = 3 # 1 : Bottom levels at waterlevel cells (=flow nodes), like tiles xz, yz, bl , bob = max(bl left, bl right)

# 2 : Bottom levels at velocity points (=flow links), xu, yu, blu, bob = blu, bl = lowest connected link

# 3 : Bottom levels at velocity points (=flow links), using mean network levels xk, yk, zk bl = lowest connected link

# 4 : Bottom levels at velocity points (=flow links), using min network levels xk, yk, zk bl = lowest connected link

# 5 : Bottom levels at velocity points (=flow links), using max network levels xk, yk, zk bl = lowest connected link

AngLat = 22.3 # Angle of latitude (deg), 0=no Coriolis

Conveyance2D = 3 # -1:R=HU,0:R=H, 1:R=A/P, 2:K=analytic-1D conv, 3:K=analytic-2D conv

[numerics]

CFLMax = 0.7 # Max. Courant nr.

CFLWaveFrac = 0.1 # Wave velocity fraction, total courant vel = u + cflw\*wavevelocity

AdvecType = 3 # Adv type, 0=no, 1= Wenneker, qu-udzt, 2=1, q(ui-u), 3=Perot q(ui-u), 4=Perot q(ui-u), 5=Perot q(ui-u) without itself

Limtypsa = 0 # Limiter type for salinity transport, 0=no, 1=minmod,2=vanLeer,3=Kooren,4=Monotone Central

Hdam = 0. # Threshold for minimum bottomlevel step at which to apply energy conservation factor i.c. flow contraction

[physics]

UnifFrictCoef = 2.3d-2 # Uniform friction coefficient, 0=no friction

UnifFrictType = 1 # 0=Chezy, 1=Manning, 2=White Colebrook, 3=z0 etc

Vicouv = 0. # Uniform horizontal eddy viscosity

Smagorinsky = 0. # Add Smagorinsky horizontal turbulence : vicu = vicu + (Smagorinsky\*dx)\*\*2)\*S, e.g. 0.1

Elder = 0. # Add Elder contribution:vicu = vicu + Elder\*kappa\*ustar\*H/6),e.g. 1.0

Irov = 0 # 0=free slip, 1 = partial slip using wall\_ks

wall\_ks = 0. # Nikuradse roughness for side walls, wall\_z0=wall\_ks/30

Vicoww = 0. # Uniform vertical eddy viscosity

```

TidalForcing = 1          # Tidal forcing (0=no, 1=yes) (only for jsferic == 1)
Salinity      = 0          # Include salinity, (0=no, 1=yes)

[time]
RefDate = 20030808      # Reference date (yyyymmdd)
Tunit    = s            # Time units in MDU (H, M or S)
DtUser   = 3600.        # User timestep in seconds (interval for external forcing update)
DtMax    = 600.         # Max timestep in seconds
DtInit   = 1.           # Initial timestep in seconds
AutoTimestep = 1        # Use CFL timestep limit or not (1/0)
TStart   = 0.           # Start time w.r.t. RefDate (in TUnit)
TStop    = 2419200.     # Stop time w.r.t. RefDate (in TUnit)

[restart]
RestartFile =           # Restart file, only map, hence: *_map.nc
RestartTime =           # Restart time (yyyymmddhhmmss)

[external forcing]
ExtForceFile = wet.ext# *.ext

[output]
ObsFile      = langlon_new_obs.xyn # *.xyn Coords+name of observation stations.
CrsFile      = new_cross_1_langlon_crs.pli # *_crs.pli Polyline(s) defining cross section(s).
HisFile      = refined_his.nc # *_his.nc History file in NetCDF format.
HisInterval  = 3600          # Interval (s) between history outputs
XLSInterval  = 0.           # Interval (s) between XLS history
FlowGeomFile =              # *_flowgeom.nc Flow geometry file in NetCDF format.
MapFile      =              # *_map.nc Map file in NetCDF format.
MapInterval  = 3600.        # Interval (s) between map file outputs
RstInterval  = 86400.       # Interval (s) between map file outputs
WaqFileBase  =              # Basename (without extension) for all Delwaq files to be written.
WaqInterval  = 0.           # Interval (in s) between Delwaq file outputs
StatsInterval = 0.          # Interval (in s) between simulation statistics output.
SnapshotDir  = figures      # Directory where snapshots/screen dumps are saved.

[wind]
ICdtyp      = 2            # ( ),1=const, 2=S&B 2 breakpoints, 3= S&B 3 breakpoints,
4=Charnock constantCdbreakpoints
Cdbreakpoints = 6.3d-4 7.23d-3 # ( ), e.g. 0.00063 0.00723
Windspeedbreakpoints = 0. 100. # (m/s), e.g. 0.0 100.0
Rhoair      = 1.20000004768372 # Air density (kg/m3)
PavBnd      = 101325.0000000 # Average air pressure on open boundaries, (N/m2), only applied
if value > 0
PavIni      = 0. # Average air pressure for initial water level correction (N/m2) (only applied if > 0)
Gapres      = 101325.0000000

```

## C2.2 ext file

```
* QUANTITY: waterlevelbnd, velocitybnd, dischargebnd, tangentialvelocitybnd, normalvelocitybnd
filetype=9      method=2,3
*           : salinitybnd                               filetype=9      method=2,3
*           : lowergatelevel, damlevel, pump            filetype=9      method=2,3
*           : frictioncoefficient, horizontaleddyviscositycoefficient, advectiontype filetype=4,10  method=4
*           : initialwaterlevel, initialsalinity        filetype=4,10  method=4
*           : windx, windy, windy, rain, atmosphericpressure filetype=1,2,4,7,8
method=1,2,3
*
```

```
* kx = Vectormax = Nr of variables specified on the same time/space frame. Eg. Wind
magnitude,direction: kx = 2
```

```
* FILETYPE=1 : uniform kx = 1 value 1 dim array uni
* FILETYPE=2 : unimagdir kx = 2 values 1 dim array, uni mag/dir transf to u,v, in index 1,2
* FILETYPE=3 : svwp kx = 3 fields u,v,p 3 dim array nointerpolation
* FILETYPE=4 : arcinfo kx = 1 field 2 dim array bilin/direct
* FILETYPE=5 : spiderweb kx = 3 fields 3 dim array bilin/spw
* FILETYPE=6 : curvi kx = ? bilin/findnm
* FILETYPE=7 : triangulation kx = 1 field 1 dim array triangulation
* FILETYPE=8 : triangulation_magdir kx = 2 fields consisting of Filetype=2 triangulation in (wind)
stations
* FILETYPE=9 : poly_tim kx = 1 field consisting of Filetype=1 line interpolation in (boundary)
stations
* FILETYPE=10 : inside_polygon kx = 1 field uniform value inside polygon for INITIAL fields
*
```

```
* METHOD=0: provider just updates, another provider that pointers to this one does the actual
interpolation
```

```
* =1 : intp space and time (getval) keep 2 meteofields in memory
* =2 : first intp space (update), next intp. time (getval) keep 2 flowfields in memory
* =3 : save weightfactors, intp space and time (getval), keep 2 pointer- and weight sets in memory
* =4 : only spatial interpolation
*
```

```
* OPERAND =+ : Add this provider to forcing value realised by previously defined providers
*           =O : Override
*
```

```
* VALUE= : Offset value for this provider
*
```

```
* FACTOR = : Conversion factor for this provider
*
```

```
*****
```

```
wQUANTITY=frictioncoefficient
FILENAME=frcf.pol
FILETYPE=10
METHOD=4
OPERAND=O
VALUE=.08
```

```
QUANTITY=waterlevelbnd
FILENAME=seaeast_langlon.pli
FILETYPE=9
METHOD=3
OPERAND=O
```

```
QUANTITY=waterlevelbnd
FILENAME=seasouth_langlon.pli
FILETYPE=9
METHOD=3
```

OPERAND=O

QUANTITY=waterlevelbnd  
FILENAME=seawest\_langlon.pli  
FILETYPE=9  
METHOD=3  
OPERAND=O

QUANTITY=dischargebnd  
FILENAME=eastwetdis\_langlon.pli  
FILETYPE=9  
METHOD=3  
OPERAND=O

QUANTITY=dischargebnd  
FILENAME=northwetdis\_langlon.pli  
FILETYPE=9  
METHOD=3  
OPERAND=O

QUANTITY=dischargebnd  
FILENAME=westwetdis\_langlon.pli  
FILETYPE=9  
METHOD=3  
OPERAND=O

wQUANTITY=windxy  
FILENAME=2010.wnd  
FILETYPE=2  
METHOD=1  
OPERAND=O

QUANTITY =airpressure\_windx\_windy  
FILENAME =Dajuan\_0.spw  
FILETYPE =5  
METHOD =1  
OPERAND =O

## Appendix 2 About the Author

LI Li is born in Heilongjiang Province, China. She obtained her undergraduate education at Northeast Petroleum University. Then she continued her master program in Sichuan Agriculture University. She became a Doctoral candidate at the University of Hamburg after the master program. She dived into a completed new but exciting field, coastal research and climate change. During the Ph.D. study, she went to Deltares and Technical University of Delft in Netherlands for the visiting study.

### Publishing

Li L. Q.H. YE, A van Dam, BOEHNER J. (2015) Application of 2D hydrodynamic model suites for Pearl River Delta. Proc. of 3rd Hydrospace conference, Rome, Italy.

Li L. Q.H. YE, A van Dam, BOEHNER J., GÖNNERT G. (2015): 2D hydrodynamics of Pearl River Estuary using D-Flow Flexible Mesh, Proc. of the 36th IAHR World Congress, The Hague, the Netherlands.

Li L., Zeng W.Z., (2010): A Review of Land Ecological Security Evaluation China. Journal of Geography and Geology, Vol. 2, No. 1; 48-57.

Zeng W.Z., Li L., Cai X.,(2010): Analysis of Coordinated Development between Urban Land Intensive Use and Urban Land Ecological Security: A Case of Chengdu City. Journal of Sustainable Development, Vol. 3, No. 2; 201-209.

## Research and Conference Experience

- 2011.10 - 2016.7 University of Hamburg, Hamburg, Germany, Ph.D. Candidate
- 2014.7 -2015.3 Deltares, and Technical University of Delft, Delft, Netherlands,  
Visiting Study  
Project: 2D hydrodynamics of Pearl River Estuary using D-Flow Flexible Mesh
- 2015.9 Third Hydro Space Conference, 'Surface Water Storage and Runoff: Modelling, In-Situ data and Remote Sensing', ESA-ESRIN, Rome, Italy
- 2015.6 The 8th RainGain Project meeting, Paris, France (Presentation)
- 2015.7 The 36th IAHR World Congress, The Hague, Netherlands.  
(Presentation)
- 2015.4 European Geosciences Union General Assembly 2015, Vienna.  
(Presentation)
- 2014.10 Delft Software Days 2014, Deltares, Delft, the Netherlands
- 2014.9 11th International Conference on Hydro science & Engineering, Hamburg, Germany (presentation)
- 2014.8 World Weather Open Science Conference, Montreal, Canada.  
(Presentation)
- 2014.4 Workshop on Hydrodynamic Modelling in Delft3D, Deltares, Delft, the Netherlands
- 2013.9 Interdisciplinary Conference of Young Earth System Scientists 2013, Hamburg, Germany (Presentation)
- 2013.7 2nd Young Scientists Meeting of the Helmholtz Water Network, Leipzig, Germany (workshop)
- 2013.4 17th Pacific Asian Marginal Sea (PAMS/JECSS) Conference, Hangzhou, China (Presentation)
- 2012.10 Workshop 'Coast and Sea- Current Research and Future Challenges' in Helmholtz-Zentrum Geesthacht (Institute of Coastal Research), Hamburg, Germany (Poster)
- 2012.7 Gene Golub SIAM Summer School, Simulation and Super Computing in the Geosciences, Monterey, California, USA

## **Acknowledgements**

Here are a few of remarkable moments in life, finishing the Ph.D. work is one of them. I am so excited with the final point approaching, then I would have the opportunity to thank all who walked with me on this journey.

Firstly, the unique, special thanks to my parents. They always support me unconditionally. The luxurious freedom gives me a broad sky to fly. Thank you for all your understanding these years.

I would like to express my appreciations to my 'Doktorvater', Prof. Dr. Jürgen Böhner. He opened this new research field to me and gave me the support no matter how tough it is. With his encouragement, I have participated in many international conferences, USA, Canada and the visiting study in Netherlands. These blissful experiences enriched my visions of the science and definitely become my admirable asset in the future. Thank you for allowing me to be a part of your journey. Your leadership, your vision and your resolute working style have cleared every dilemma during my study.

I also would like to take this opportunity to thank Prof. Gabriele Gönnert. She suggested me to work on the Deflt3D model and encouraged me to make the exchange study at Deltares. Moreover, I would like to thank the support from the colleagues and friends during the study in Netherlands. Special thanks to Dr. Qinghua Ye and Dr. Arthur van Dam, they lighted me up in the field of hydrodynamic modelling, from basic to advance, we made a stirring mile stone in the new generation of the Deltares software application in China.

I also would like to express the credits to CliSAP. They supported me several times for the scientific conference and workshops during my Ph.D. study. The workshops and seminars organized by CliSAP provided me a unique international working environment and platform, which helps me make a group of colleagues from all over the world.

An appreciated express to the data support from Dr. Xiaoqing Song, Dr. Xinli Ke, Ting Zhou and the colleague from Hong Kong Technical University. Special thanks to the research team 'Landscape ecology and human habitat of south China', which is led by

Prof. Zhifeng Wu in Guangdong Institute of Eco-environment and Soil Science. They provided the land use dataset in Chapter 4.

I appreciated so much to my working group. Thank you for the daily concerns and greeting on my final stage of writing, all the happy time to work together will be part of my unforgettable memory. Special thanks go to Dr. Olaf Conrad, who have supported me with the SAGA GIS data progressing. The last thanks go to all my best friends. Wenfeng Zhu, Mrs. Hanna Stadelhofer, Tara, John, I am deeply grateful to you for assisting me revising my English with your valuable time. Dr. Chuanyu Liu, a special thank you to your guidance at the beginning of my Ph.D. study. Dr. Kesheng Shu. Dr. Feifei Liu, Qian Jiang, BingZhao, Anqi Wang, Qiqi Li, all the encouragement from you make me a pleasant life in Hamburg.

Finally, I would express the special acknowledge the financial support of China Scholarship Council (CSC). Prof. Weizhong Zeng, my supervisor in the master program, my study fellows, Yonghe, Xiulan Chen, my uncle Bin Shao, they gave me the incredible support for the application of CSC.

Again thanks to my parents at the last few meter to the finish this Ph.D. marathon!

Yours Sincerely,

Li Li

April, 2016